Antibody Responses to HIV-1 Immunogens and Viruses

Thesis by

Andrew T. DeLaitsch

In Partial Fulfillment of the Requirements for
the Degree of
Doctor of Philosophy

CALIFORNIA INSTITUTE OF TECHNOLOGY
Pasadena, California

2026
(Defended November 21, 2025)

Andrew T. DeLaitsch
ORCID: 0000-0002-3458-3449

ACKNOWLEDGEMENTS

Thank you to all my family, friends, and mentors. I am incredibly grateful to so many people for their support, guidance, and friendship along the way. The impact of the people in my life far exceeds that of the science presented in this thesis, and for that, I feel truly lucky.

Above all, thank you to my parents for supporting me through every idea and adventure, including the particularly wild one of deciding to go to graduate school. This thesis is dedicated to them.

ABSTRACT

The Envelope (Env) trimer mediates fusion of the HIV-1 viral membrane with that of the target cell. As such, it is the sole target for neutralizing antibodies against the virus. Broadly neutralizing antibodies (bnAbs) that are capable of blocking entry of diverse viral strains hold therapeutic potential for people living with HIV-1 and may be utilized for prophylaxis, either through passive immunization or as templates for immunogen design. Chapter 1 of this thesis introduces relevant background to the HIV-1 virus, the Env trimer, antibodies, and antibody-antigen interactions, with an emphasis on bivalent antibody binding to enveloped viruses. Chapter 2 then describes the results of a preclinical sequential immunization study aimed at eliciting, and subsequently boosting, antibodies directed to the V3 glycan patch on Env. Electron microscopy-based polyclonal epitope mapping demonstrated initial V3-targeting, followed by an increase in off-target responses with boosting that was associated with the disassociation of trimeric Env immunogens. Nonetheless, monoclonal antibodies that competed with the V3-targeting bnAb 10-1074 and exhibited weak, heterologous neutralizing activity were isolated after the third boost. Cryo-electron microscopy structures of two of these monoclonal antibodies, reported in Chapter 3, revealed targeting of altered Env conformations. The results presented in Chapters 2 and 3 provide insight into Env structural dynamics and inform strategies for improved immunogen design.

Chapters 4 and 5 of this thesis present new best-in-class human bnAbs targeting the CD4-binding site and V3 glycan patch on Env, respectively. These antibodies were identified from top elite neutralizers out of an international cohort of over 2,300 people living with HIV-1. Multiple, distinct VRC01-class, CD4-binding site bnAbs were identified from one of these individuals. These bnAbs differed in the presence and length of framework region insertions and CDRH3 lengths. One bnAb, 04_A06, exhibited an 11-amino acid long insertion, and structural analyses demonstrated this resulted in a protruding CDRH1 loop that recognized highly conserved residues on the adjacent gp120, contributing to the near pan-neutralizing breadth and resilience to escape mutations by 04_A06. Chapter 5 then presents 007, a highly broad and potent V3 bnAb that binds Env independently of the gp120 N332 glycan. 007 exhibited weak monovalent binding affinity, and pseudovirus neutralization assays demonstrated antibody bivalency contributes to potency. Structures of 007 IgG in complex with engineered, soluble Env ectodomains revealed a dimer of Env trimers, crosslinked by three IgG molecules. The results presented in Chapters 4 and 5 advance our mechanistic understanding of Env recognition and neutralization by bnAbs and inform the development of antibody therapy and vaccines for HIV-1.

PUBLISHED CONTENT AND CONTRIBUTIONS

*Denotes equal contributions

1. Skelly, A.N., Gristick, H.B., Li, H., Gavor, E., Connell, A.J., Kreider, E.F., Marchitto, L., Hogarty, M.P., Newby, M.L., Allen, J.D., Liu, W., West., A.P., Ayyanathan, K., Campion, M.S., Winters, K., Gordon, C.G., Osbaldeston, R.A., Akeley, M.J., Li, Y., Singh, A., Cruickshank, K., Park, Y., Zhao, C., Li, X., Van Itallie, E., Carey, J.W., Albertus, A., **DeLaitsch, A.T.,** Keeffe, J.R., Lituchy, M.G., Morris, D.J., Habib, R., Bibollet-Ruche, F., Koranda, N.S., Plante, S.J., Martella, C.L., Lora, J., Wang, E.J.D., Lewis, M.G., Martin, M.A., Nussenzweig, M.C., Seaman, M.S., Irvine, D.J., Wiehe, K.J., Haynes, B.F., Wagh, K., Korber, B.T., Andrabi, R., Crispin, M., Weissman, D., Bjorkman, P.J., Hahn, B.H., Shaw, G.M. Consistent induction of broadly neutralizing HIV antibodies by a novel two-step mechanism informs immunogen design. (*Science - in review*).

A.T.D. helped support structural analyses, reviewed, and edited the manuscript.

2. Gieselmann, L.*, **DeLaitsch, A.T.***, Rohde, M.*, Radford, C., Worczinski, J., Momot, A., Ahmadov, E., Burger, J.A., Havenar-Daughton, C., Deshpande, S., Giovannoni, F., Corti, D., Kreer, C., Ercanoglu, M.S., Schommers, P., Georgiev, I.S., West Jr., A.P., Knufer, J., Stumpf, R., Kroidl, A., Geldmacher, C., Maganga, L., William, W., Ntinginya, N.E., Hoelscher, M., Yang, Z., Wei, Q., Renfrow, M., Green, T.J., Novak, J., van Gils, M.J., Gristick, H.B., Gruell, H.B., Gruell, H., Bloom, J.D., Seaman, M.S., Bjorkman, P.J., Klein, F. Identification of a broad and potent V3 glycan site bNAb targeting an N332 glycan-independent epitope. *bioRxiv (accepted at Nat Immunol).*

A.T.D. contributed to the conceptualization of the study, performed cryo-EM analyses, and contributed to surface plasmon resonance, molar neutralization assays, and glycan analysis experiments. ATD wrote a portion of the manuscript and was involved in reviewing and editing.

3. Gieselmann, L.*, **DeLaitsch, A.T.***, Gruell, H., Kreer, C., Ercanoglu, M.S., Gristick, H.B., Schommers, P., Ahmadov, E., Radford, C., Mazzolini, A., Rohde, M., Zhang, L., West., A.P., Reichwein, M.L., Knüfer, J., Stumpf, R., Mkhize, N.N., Kaldine, H., Bhebhe, S., Kroidl, A., Adhikari, A., Nanfack, A.J., Ambada, G.E., Duerr, R., Maganga, L., William, W. , Ntinginya, N.E., Wolf, T., Geldmacher, C., Hoelscher, M., Lehmann, C., Moore, P.L., Mora, T., Walczak, A.M., Gilbert, P.B., Doria-Rose, N.A., Huang, Y., Bloom, J.D., Seaman, M.S., Bjorkman, P.J., Klein, F. Profiling of HIV-1 elite neutralizer cohort reveals CD4bs bNAb for HIV-1 prevention and therapy. *Nat Immunol* 1-14 (2025).

A.T.D. contributed to the conceptualization of the study, performed structural analyses, wrote a portion of the manuscript, and was involved in reviewing and editing.

4. **DeLaitsch, A.T.**, Keeffe, J.R., Gristick, H.B., Lee, J.A., Ding, W., Liu, W., Skelly, A.N., Shaw, G.M., Hahn, B.H., Björkman, P.J. Neutralizing antibodies elicited in sequentially immunized

macaques recognize V3 residues on altered conformations of HIV-1 Env trimer. *NPJ Vaccines* **9**, 240 (2024).

A.T.D. led the study design, experimentation, and writing of the manuscript.

5. Yang, Z., Dam, K.-M.A., Bridges, M.D., Hoffmann, M.A.G., **DeLaitsch, A.T.,** Gristick, H.B., Escolano, A., Gautam, R., Martin, M.A., Nussenzweig, M.C., Hubbell, W.L., Bjorkman, P.J. Neutralizing antibodies induced in immunized macaques recognize the CD4-binding site on an occluded-open HIV-1 envelope trimer. *Nat Commun* **13,** 732 (2022).

A.T.D. contributed to processing and analyzing crystallography data, as well as reviewing and editing the manuscript.

6. Escolano, A.*, Gristick, H.B.*, Gautam, R.*, **DeLaitsch, A.T.***, Abernathy, M.E., Yang, Z., Wang, H., Hoffmann, M.A.G., Nishimura, Y., Wang, Z., Koranda, N., Kakutani, L.M., Gao, H., Gnanapragasam, P.N.P., Raina, H., Gazumyan, A., Cipolla, M., Oliveira, T.Y., Ramos, V., Irvine, D.J., Silva, M., West, A.P., Keeffe, J.R., Barnes, C.O., Seaman, M.S., Nussenzweig, M.C., Martin, M.A., Bjorkman, P.J. Sequential immunization of macaques elicits heterologous neutralizing antibodies targeting the V3-glycan patch of HIV-1 Env. *Sci Transl Med* **13,** eabk1533 (2021).

A.T.D. led nsEMPEM experiments and contributed to the writing and editing of the manuscript.

7. Muecksch, F., Weisblum, Y., Barnes, C.O., Schmidt, F., Schaefer-Babajew, D., Wang, Z., Lorenzi, J.C.C., Flyak, A.I., **DeLaitsch, A.T.**, Huey-Tubman, K.E., Hou, S., Schiffer, C.A., Gaebler, C., Da Silva, J., Poston, D., Finkin, S., Cho, A., Cipolla, M., Oliveira, T.Y., Millard, K.G., Ramos, V., Gazumyan, A., Rutkowska, M., Caskey, M., Nussenzweig, M.C., Bjorkman, P.J., Hatziioannou, T., Bieniasz, P.D. Affinity maturation of SARS-CoV-2 neutralizing antibodies confers potency, breadth, and resilience to viral escape mutations. *Immunity* **54,** 1853-1868.e7 (2021).

A.T.D. contributed to the cryo-EM experiments and structure analysis.

TABLE OF CONTENTS

Chapter 1

INTRODUCTION

Human immunodeficiency virus 1 (HIV-1) is a virus that, when left untreated, can decimate the immune system and lead to acquired immunodeficiency syndrome, or AIDS[1, 2, 3]. Since the start of the epidemic, ~91 million people have been infected with HIV-1 and ~44 million have died from AIDS-related illnesses[4]. Despite the availability of effective treatments since the mid-1990s, the epidemic continues to be a major global health concern, with approximately 1.3 million new HIV-infections and 630,000 AIDS-related deaths occurring in 2024 alone[4].

The HIV-1 Virus

HIV-1 is an enveloped virus, ~110 nm in diameter[5]. Inside a mature virion is a cone-shaped capsid core, which encases two copies of the virus's single-stranded, positive-sense RNA genome. The ~10 kilobase genome encodes three main genes, Gag (Group-specific antigen), Pol (Polymerase), and Env (Envelope), which are discussed in more detail in the following sections. Numerous regulatory and accessory elements are also encoded, which are critical for the viral life cycle, but are not a focus of this thesis. As part of its retroviral life cycle, the viral enzyme reverse transcriptase (RT) is responsible for reverse transcribing the RNA genome of HIV into DNA, which is subsequently integrated into the host cell's DNA via the viral enzyme integrase (IN). This establishes a latent reservoir, severely complicating efforts to design an effective vaccine or cure for HIV. A more complete review of the HIV-1 virus and its genome can be found elsewhere[6].

The Envelope Glycoprotein

HIV-1 targets host immune cells bearing the chemokine receptor CD4, known as $CD4^+$ T-cells[7]. To infect a $CD4^+$ T-cell, an HIV-1 virion must first fuse its viral membrane with that of the target cell, a process that requires considerable energy[8]. The energy required for membrane fusion is stored within the trimeric Env glycoproteins on the viral surface, which must trigger at the correct time and place to lead to an infection (i.e., when the virus is bound to its target cell). The elegant mechanism by which Env accomplishes this tightly controlled fusion event is a consequence of structural features of the glycoprotein itself.

In its native context, Env is first synthesized in the rough endoplasmic reticulum (ER) of a virally infected cell as a glycoprotein of approximately 160 kDa (gp160) in mass. Protein folding, signal peptide cleavage, glycosylation, and oligomerization of the gp160s occurs in the ER[9, 10]. Additionally, the Envs of certain viral strains can be further modified by the addition of lipid moieties to one or more free cysteine residues (i.e., palmitoylation) present on the cytoplasmic tail[11]. Further modifications are then made during trafficking to the cell membrane: high-mannose glycans can be enzymatically processed (reviewed in [12]), and furin proteases cleave gp160 polypeptides into heterodimers of soluble gp120 and membrane-bound gp41 subunits[13]. These subunits remain non-covalently attached in the pre-fusion Env conformation to create a trimer of gp120-gp41 heterodimers, which can then be incorporated into new viruses as they bud from the cell surface.

Within this metastable trimeric assembly, the gp120 subunits act as a fusion-suppressive cap and provide specificity for the receptor, CD4, and co-receptor, either CCR5 or CXCR4[14, 15]. Sequential binding of multiple copies of receptor and co-receptor, which occurs when the virus encounters a target $CD4^+$ T-cell, shepherd the trimer through a series of conformational changes, which ultimately leads to gp120 subunits being shed from the virus and gp41-mediated fusion of viral and host cell

membranes[15]. An HIV Env trimer can bind up to three copies of CD4 (one copy per gp120 subunit), and recent structural studies have revealed distinct open conformations for trimers bound by different numbers of CD4 molecules[16, 17, 18, 19]. These open trimer conformations exhibit an outward rotation of their gp120 subunits and, for gp120 subunits bound by CD4, large-scale rearrangements of variable loops 1 and 2 (V1V2) at the trimer apex which exposes the underlying co-receptor binding site consisting of variable loop 3 (V3) residues[20, 21] (Fig. 1). Co-receptor binding is thought to promote the insertion of the hydrophobic fusion peptide, located at the N-terminus of gp41, into the target cell membrane. This leads to a highly unstable gp41 conformation, referred to as the pre-hairpin intermediate[22, 23, 24], which ultimately collapses on itself into a post-fusion six-helix bundle [22, 25], releasing the energy required to bring the two membranes together and form the fusion pore.

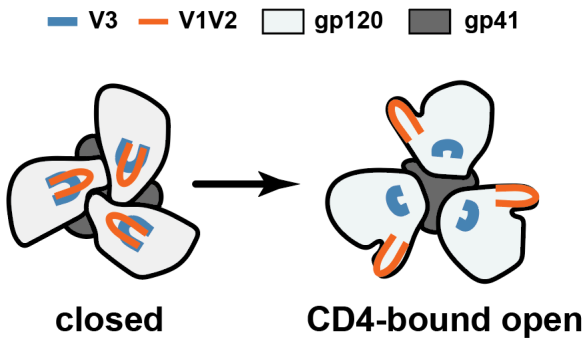

Figure 1: Env structural rearrangements associated with CD4 binding.
A schematic showing top-down views of a closed Env trimer (left) and a CD4-bound open Env trimer (right). The CD4-bound open Env exhibits outwardly rotated gp120 subunits and large-scale structural rearrangements of the V1V2 loops exposing underlying V3 residues for co-receptor binding.

Gag, Pol, and the Incorporation of Env

Gag and Pol are HIV-1 polyproteins encoded at the 5' end of the HIV genome. The ratio of Gag to Pol expression is dictated by a conserved ribosomal frameshift signal at the 3' end of the *gag* RNA, which causes a -1-nucleotide frameshift at a certain frequency leading to the continued translation of

pol[26]. *Gag*, which is capable of producing immature virus-like particles when expressed alone, encodes the protein domains matrix, capsid, nucleocapsid, and p6 which are interspaced by spacer peptides SP1 and SP2. *Pol* encodes the viral enzymes protease, reverse transcriptase, ribonuclease H, and integrase. During translation, the N-terminal glycine of the matrix domain is myristoylated. The myristate moiety, along with a highly basic region also located in the N-terminus of matrix, promotes the association of Gag and GagPol polyproteins with the inner leaflet of the plasma membrane[27]. At the plasma membrane, matrix exists as a hexameric lattice of trimers[28, 29]. Initially this lattice remains tethered to a hexameric lattice of capsid domains[29], which form the proteinaceous core of the virus. As Gag molecules accumulate, the plasma membrane begins to curve, forming spherical immature virions. Facilitating membrane scission are the ESCRT (endosomal sorting complexes required for transport) associated proteins TSG101 and ALIX, which bind amino acid motifs located in the C-terminal p6 domain of Gag[30].

Although it is not fully understood how Env trimers are coordinated into newly formed viruses, the ~150 residue long cytoplasmic tail of Env appears to be implicated. When reconstituted in lipid bicelles, the cytoplasmic tail of Env forms a trimeric baseplate comprising amphipathic alpha helices that wrap around the transmembrane domain of Env[31, 32]. This baseplate stabilizes the Env ectodomain, as evidenced by the observation that C-terminal tail truncations change the antigenicity of Env[33]. In the majority of human T-cell lines, which are highly relevant for studying HIV-1 replication, the Env cytoplasmic tail is essential for efficient viral replication and spread[34]. In these cell types, deemed non-permissive, Env incorporation into viruses is linked to its endocytosis and recycling through tubular endosomes, which is mediated by endocytosis motifs located in the Env C-terminal tail[35]. In addition to the cell-type-specific importance of the endocytic recycling of Env, interactions between the Env cytoplasmic tail and the matrix domain of Gag may also play a role in proper Env incorporation into viruses[36]. Although a complete structural description of this interaction

remains elusive, recent experiments support a direct interaction between the trimeric matrix domain and the cytoplasmic tail of Env[37, 38], possibly acting to trap Env at the site of viral budding.

Newly formed immature virions contain Env, Gag, and, to a lesser extent, Gag-Pol. The viral protease becomes active upon dimerization, cleaving Gag and GagPol polyproteins into successively smaller fragments[39]. Proteolytic cleavage of Gag triggers structural maturation of CA[40], which involves the reorganization of an incompletely closed sphere of CA hexamers to a fully closed, fullerene cone of CA hexamers and exactly 12 CA pentamers[40, 41]. Meanwhile, proteolytic release of the SP2 peptide encoded by *gag* triggers Matrix maturation, which is correlated with increased fusion kinetics of viral particles[42]. The mature matrix lattice is rearranged relative to the immature lattice and is bound by SP2[29, 42].

Antibodies and their Molecular Architecture

Antibodies are immune recognition molecules that can take on numerous forms, called isotypes. This thesis focuses on the IgG isotype of antibodies, and their related membrane bound B-cell receptors. During B-cell development a single type of B-cell receptor is used from a large pool of possible B-cell receptors via processes that will be discussed in the following section. B-cells that bind antigen proliferate and differentiate into cells that secrete antibodies, which are soluble forms of the B-cell receptor.

IgG antibodies consist of two identical heavy chains, with masses of ~50kDa, and two identical light chains, with masses of ~25kDa (Fig. 2). Each heavy chain comprises four protein domains: one variable domain (V_H) and three constant domains (C_H1, C_H2, and C_H3). Each light chain comprises two domains: one variable domain (V_L) and one constant domain (C_L). Often critical to their function, IgG molecules take on a “Y”-shaped architecture. The stalk of the “Y”, known as the crystallizable

fragment, or Fc, includes the homodimeric interface between the C_H2 and C_H3 domains of the two heavy chains. Meanwhile, the arms of the "Y" make up two identical antigen binding fragments, or Fabs, which include the antibody light chain and the N-terminal V_H and C_H1 domains of the heavy chain. The precise location for antigen binding, referred to as the antibody combining site, is located at the tips of the "Y" within the variable domains. As the name implies, this region varies is sequence across different antibodies, thereby conferring this class of molecules the ability to recognize diverse targets.

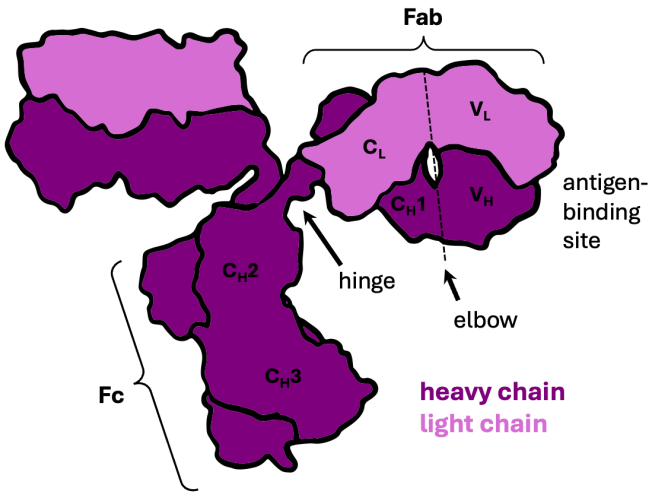

Figure 2: Architecture of an IgG antibody.
Figure based on PDB 1IGT (ref [43]).

The domains of an antibody each adopt a signature immunoglobulin fold consisting of a sandwich of two beta sheets covalently linked by a disulfide bond. Within the constant domains, one beta-sheet is made up of four antiparallel beta-strands, and the other is made up of three. Within the variable domains, two additional beta-strands give rise to a five-stranded beta-sheet that folds onto the four-stranded sheet. Each variable domain also contains three predominant loops, referred to as complementary determining regions (CDRs), which are formed between pairs of sequence-adjacent beta-strands and are important for contacting antigen[44].

Importantly, flexibility is inherent to the structure of antibodies[45]. A flexible region connecting the Fabs to the Fc, known as the antibody hinge, allows the Fabs to occupy different configurations relative to each other. Additionally, a flexible "elbow" links the V_H-V_L domains to the C_H1-C_L domains within the Fab region[46, 47] (Fig. 2). Flexibility is consequential to bivalent antibody binding, a topic discussed in a later section.

Diversity is a Key Feature of Antibodies

The mammalian immune system must produce an immense diversity of immune recognition molecules to account for the many chemical structures that can be associated with pathogens. In 1957, Burnet noted that a requirement for his newfound clonal selection theory was "a genetic process for which there is no available precedent[48]." As it turns out, not one, but several processes contribute to antibody diversity, including V(D)J recombination, junctional diversity, and somatic hypermutation.

Unsurprisingly, antibody sequence diversity is concentrated within the antibody variable domains, the location of antigen binding. The variable region of an antibody heavy chain is encoded by variable (V), diversity (D), and joining (J) gene segments, which are assembled in early B-cell development in a process known as V(D)J recombination. In human, the germline encodes 38-46 productive V, 23 D, and 6 J gene segments than can be assembled to form approximately 6000 combinations[49]. In a similar fashion, the light chain variable region is encoded by its own sets of V and J gene segments that combine to produce several hundred light chains. Heavy and light chain pairing can then give rise to millions of combinations of assembled gene segments.

Additional diversity arises from enzymatic processes that stitch the V, D, and J gene segments together (reviewed in [50]). The V-D-J and the V-J junction regions encode the CDR3 loops of the

heavy and light chains, respectively. This added diversity, collectively referred to as junctional diversity, results in the CDR3 loops being the most variable part of the antibody combining site and therefore important determinants in antigen specificity[51].

During V(D)J recombination, DNA hairpins are formed at the coding ends of the gene segments and are subsequently opened, which can form short palindromic sequences of P-nucleotides. Non-templated N-nucleotides can then also be added to the 3' ends, primarily during heavy chain rearrangement. Exonucleases further modify junctions by trimming away nucleotides, including the P- and N- additions. Following these modifications, complementary base pairing occurs between the gene segments, and DNA repair machinery completes the formation of a double-stranded DNA joint. Notably, these processes, which occur at the nucleotide level, can shift the open reading frame and lead to non-productive rearrangements. While the J-gene must always be read in a specific frame, the D-gene can often form a productive heavy chain in two or three of its reading frames, further contributing to the diversity of the heavy chain CDR3 loop.

V(D)J recombination gives rise to an incredibly diverse repertoire of what are referred to as “germline” antibody sequences. However, these sequences, initially expressed as B-cell receptors, undergo even further modifications in response to antigen stimulation (reviewed in [52]). In this process, referred to as affinity maturation, B-cell clones, each encoding a unique B-cell receptor sequence, compete for the ability to bind antigen. The B-cell clone that binds is selected for and subsequently undergoes an increased rate of cellular division, at which point the enzyme activation induced cytidine deaminase (AID) initiates a mutational process called somatic hypermutation, ultimately leading to mutated daughter cells[53]. The daughter cells continue to compete for limited antigen, giving rise to progeny that express high-affinity (i.e., affinity-matured) antibody sequences.

The Interactions between Antibody and Antigen

A focus of this thesis is on the biologically relevant interactions that occur between bivalent IgG antibodies and multivalent antigens. For clarity, this section first describes the binding of monovalent antibodies with antigens to provide a conceptual framework. Monovalent antibodies include Fab fragments and monovalent IgG molecules engineered to have only one functional Fab binding arm. Together with antigen, these antibodies form one-to-one binding interactions. The strength of the interaction, referred to as affinity (K_D), is a consequence of the association rate (k_a or k_{on}) and dissociation rate (k_d or k_{off}) of the antibody (Ab) with antigen (Ag) (Equations 1 and 2).

Equation 1:

$$Ab + Ag \underset{k_{\text{off}}}{\overset{k_{\text{on}}}{\rightleftharpoons}} Ab - Ag$$

Equation 2:

$$K_D = \frac{k_{\text{off}}}{k_{\text{on}}}$$

In contrast to monovalent antibodies, bivalent IgG molecules possess two identical Fab binding arms that are physically tethered at the antibody hinge region. The bivalent nature of an IgG molecule raises the possibility that both arms simultaneously bind two copies of an antigen in close enough proximity. The cumulative strength of a multivalent binding interaction, such as a bivalent interaction between an IgG and a multivalent antigen, is referred to as apparent affinity or avidity, and is discussed at the end of this section.

Monovalent Antibody Binding

The likelihood an antibody encounters its target antigen in solution depends on the concentrations of both the antibody and antigen and is time-dependent; as a consequence, the association rate has units of $M^{-1}s^{-1}$. A theoretical upper limit for the association rate is set by the rates of diffusion of the antibody and antigen. Since smaller antibody formats such as Fabs diffuse faster than larger formats like monovalent IgGs, they could in theory have enhanced association rates. However, measured association rates for antibody-antigen interactions are typically lower than would be expected if limited by diffusion[54]. Rather, conformational selection and induced-fit mechanisms of binding are thought to limit the association rate of most antibody-antigen complexes[55]. In the context of an Ab-Ag interaction, conformational selection describes how a binding event selects for pre-existing states of structurally dynamic antibody and antigen, while induced fit refers to the structural adjustments that may occur upon binding. These mechanisms are not mutually exclusive and may work in tandem to facilitate binding (reviewed in [55]). As an example, a flexible CDR loop on an antibody or a flexible glycan on an antigen may become ordered upon Ag-Ab binding as a result of conformational selection and structural rearrangement. These mechanisms are distinct from a 'lock-and-key' mechanism of binding, in which the Ab and Ag are pre-configured for binding. Of note, Ab-Ag interactions that exhibit a 'lock-and-key' mechanism of binding suffer less of an entropic cost of binding and thus have enhanced association rates.

The dissociation of an antibody-antigen complex is concentration-independent and has units of s^{-1}. The antibody dissociation rate can be interpreted as the fraction of Ab-Ag complex that dissociates per unit of time. Mathematically equivalent, the inverse of the dissociation rate is the mean retention time, or the average amount of time an Ab-Ag complex stays together. As an example, for an Ab-Ag complex with a dissociation rate of $0.01s^{-1}$, 1% of Ab-Ag complexes will dissociate per second and

the average amount of time an Ab will stay bound is 100s. Together, the on- and off-rates of antibody with antigen give rise to the antibody affinity (K_D).

Bivalent IgG Binding

Bivalent IgG molecules can interact with antigens either monovalently or bivalently, depending on the nature of the antigen. If a bivalent IgG molecule interacts monovalently (i.e., engaging only one of its Fab arms), the association rate of the IgG is expected to be at most 2-fold enhanced relative to a size-matched monovalent IgG, as every free bivalent IgG molecule in solution contains twice the number of binding arms as a monovalent IgG.

In the case of a bivalent IgG, after one Fab arm is bound, the ability of the second Fab arm to bind depends entirely on the availability of free antigen within reach of the tethered IgG. If no antigen is present within ~15 nm of the bound IgG[56], the effective local concentration of antigen is zero, and a second [specific] binding event will not occur. However, if another copy of the antigen is within reach and is compatible with bivalent binding, there is an extremely high effective local concentration of Fab and antigen, and the second binding event occurs rapidly. In addition, since the first binding event involves the association of two previously separated molecules, it incurs a greater entropic penalty than the second binding event. As a result, the second Fab arm to bind is expected to have a faster association rate than the first.

Bivalent Binding to Enveloped Viruses

Enveloped viruses typically present repeating structures that can serve as targets for antibody recognition. Against such targets, neutralizing antibodies can be raised that are capable of binding with both arms simultaneously. The appreciation for the importance of antibody bivalency for viral neutralization dates back to the early 1960s[57, 58], over a decade before the development of hybridoma

technology for monoclonal antibody production[59]. At that time, polyclonal mixtures of bivalent IgG molecules were already known to be cleavable into monovalent fragments (now termed Fabs) by papain digestion[60]. In experiments performed by Lafferty[57], rabbit antiserum raised against influenza virus was first digested with papain to form Fabs. While both intact IgGs and monovalent Fabs were capable of neutralizing influenza, only the IgGs retained potent neutralizing activity upon dilution, demonstrating that antibody bivalency was essential for stabilization of the antibody-antigen complex. Complementary electron microscopy studies revealed that this stabilization reflected bivalent binding to repeating antigenic structures that densely coated influenza[58]. Depending on the concentrations of antibodies and viral particles, antibodies could also be observed bridging antigenic structures on separate virions, leading to their aggregation (i.e., inter-virion crosslinking).

At the time of Lafferty's work, little was known about the proteins that stud the surface of enveloped viruses or their oligomeric nature. It was later discovered that HA exists as a trimer[61]. Similarly, other class 1 fusion proteins were found to be trimeric, including the glycoproteins present on HIV, RSV, Lassa, Ebola, SARS-CoV-2, and other related viruses (reviewed in [62]). One implication of the oligomeric nature of these glycoproteins is that an IgG molecule could bind bivalently to adjacent protomers of a single trimeric assembly (i.e., intra-spike crosslinking), in addition to crosslinking nearby trimers (i.e., inter-spike crosslinking). Indeed, intra-spike, inter-spike, and inter-virion crosslinking are all mechanisms by which an IgG could bind bivalently.

Numerous factors are expected to influence the likelihood and nature of bivalent IgG binding. For example, the probability a monovalently bound IgG-virus complex encounters and crosslinks another virion increases with virus concentration. Additionally, certain reaction conditions and binding kinetics may cause available epitopes to become saturated by monovalent IgG binding before bivalent binding can occur. Factors that affect the probability of inter-spike crosslinking include the density,

distribution (e.g., clustered v. dispersed), and mobility of spikes within the membrane. If spikes can move laterally, rotate, or tilt relative to the membrane, epitopes on neighboring spikes may transiently align in positions that can be captured by bivalent IgG binding. In contrast, if spikes are immobile in the membrane, the feasibility of inter-spike crosslinking by a given IgG is largely determined by spike positions and epitope geometry. The likelihood that an antibody can form an intra-spike crosslink depends on where that antibody's epitope is on the trimer. For certain antigens, conformational plasticity can further shift these positions; for example, the receptor binding domains (RBDs) of the various human coronaviruses sample up conformations[63, 64, 65], and bivalent binding by a particular IgG may be compatible only with certain configurations of up and down RBDs within the trimer.

Structures with intact IgGs provide the most direct evidence for bivalent binding mechanisms in action. As examples, cryo-electron tomography (cryo-ET) of IgGs in complex with either influenza or SARS-CoV-2 virus revealed both inter-spike and inter-virion crosslinking[66, 67]. Additionally, structures of IgGs in complex with soluble SARS-CoV-2 Spike trimers demonstrated intra-spike crosslinking[68, 69, 70]. Bivalent binding has also been inferred from Spike-Fab structures[71, 72]. An important caveat, however, is that IgGs may bind trimers in a different manner than their corresponding Fabs; in one study that compared structures of SARS-CoV-2 Spike complexed with either the Fab or IgG formats of the same antibodies, differences in binding stoichiometries, Fab angles of approach, and Spike conformations were observed[68]. Although less direct than structural characterization, single particle mass analysis techniques such as mass photometry and charge-detection native mass spectrometry can also reveal useful insights into antibody bivalency by unveiling binding stoichiometries[73]. Finally, beyond biophysical characterization, functional assays comparing monovalent and bivalent antibody formats can provide crucial evidence for bivalency

effects, for example in viral neutralization of influenza[57, 66, 74], SARS-CoV-2[67, 68, 69, 72], RSV[75], and other viruses.

Although bivalent binding and neutralization mechanisms appear common for antibodies against many enveloped viruses, HIV is believed to have evolved to largely evade such binding[76]. The relatively few Envs on the surface of the virus and the positioning of conserved bnAb epitopes are expected to limit potential inter- and intra-Env crosslinking, respectively. Additionally, broadly neutralizing antibodies to HIV typically exhibit similar potencies whether formatted as an IgG or Fab (reviewed in [76]). Antibodies PGT128 and EPTC112, which both target a similar epitope on HIV-1 Env, are notable exceptions, as they are both more potent as IgGs than as Fabs[77, 78]. Despite this functional data, a mechanism explaining the enhanced IgG neutralization was not determined and was only speculated to be a result of inter-spike crosslinking.

In contrast to the aforementioned homotypic bivalent binding (i.e., both Fab arms bind identical epitopes), an alternative mechanism for antibodies to bind bivalently is enabled by the antibody-intrinsic property of polyreactivity. Despite strong negative selection during B-cell development[79], antibodies nevertheless emerge that react broadly to diverse targets. These polyreactive antibodies may bind completely unrelated structures, or they may bind with high specificity to an epitope with broad distribution, rendering them functionally polyreactive (e.g., an *N*-linked glycan structure). It was previously suggested that polyreactive antibodies can bind HIV with increased apparent affinity via heteroligation, a process that involves the IgG simultaneously binding to two distinct epitopes with varying monovalent affinities[80]. While fascinating, this mechanism is likely not important for the neutralization mechanism of two polyreactive HIV-1 antibodies, 4E10 and 2F5, as suggested by the observation that their Fab and IgG formats exhibited similar potencies[81, 82].

Bivalent binding is a defining feature of antibody function. Despite this, our understanding of antibody bivalency remains limited, particularly for IgG antibodies that neutralize HIV through bivalent mechanisms. Further study in this area will help guide the design of next-generation vaccines, enhance therapeutic strategies, engineer more effective antibodies, and enable the creation of bispecific IgGs with novel functions.

Antibodies to HIV-1 Envelope

In 1984, Margaret Heckler, then Secretary of Health and Human Services, stated, "We hope to have a vaccine ready for testing in about two years… Yet another terrible disease [HIV] is about to yield to patience, persistence, and outright genius." HIV has since proven to be a formidable foe and the fact that over four decades later there remains no effective vaccine serves as a reflection on the many unique challenges the field has uncovered in our attempts to target the virus and its Env trimer.

By binding to HIV-1 Env, certain antibodies can block fusion and thereby neutralizing the virus. To be broadly effective, these antibodies must neutralize a wide range of circulating HIV-1 strains. Antibodies that achieve such breadth are referred to as broadly neutralizing antibodies (bnAbs). bnAbs hold promise to be used therapeutically to control viral replication in people living with HIV or for prophylactic administration to prevent viral acquisition. Correspondingly, immunogens that elicit such antibodies are likely a necessary component of a prophylactic vaccine. Because Env is the only viral target of neutralizing antibodies, anti-Env antibodies are central to antibody-mediated therapy, prophylaxis, and vaccine responses.

The search for HIV-1 bnAbs and strategies to elicit them through vaccination started over 30 years ago when the antibody b12, which targets the CD4 binding site (CD4bs) on gp120, was isolated from a phage display library prepared using the bone marrow of a person living with HIV[83]. Subsequent

studies showed that b12 effectively neutralizes diverse HIV-1 strains[84], highlighting the potential for eliciting bnAbs through vaccination. In the ensuing decades, numerous additional HIV-1 bnAbs were identified from people living with HIV, targeting the CD4bs as well as other conserved features on Env. Collectively, bnAbs have been shown to target much of the Env surface, including regions such as the V1V2 apex, V3 glycan patch, CD4bs, silent face, gp120/gp41 interface, fusion peptide, and the membrane-proximal external region (MPER)[85] (Fig. 3).

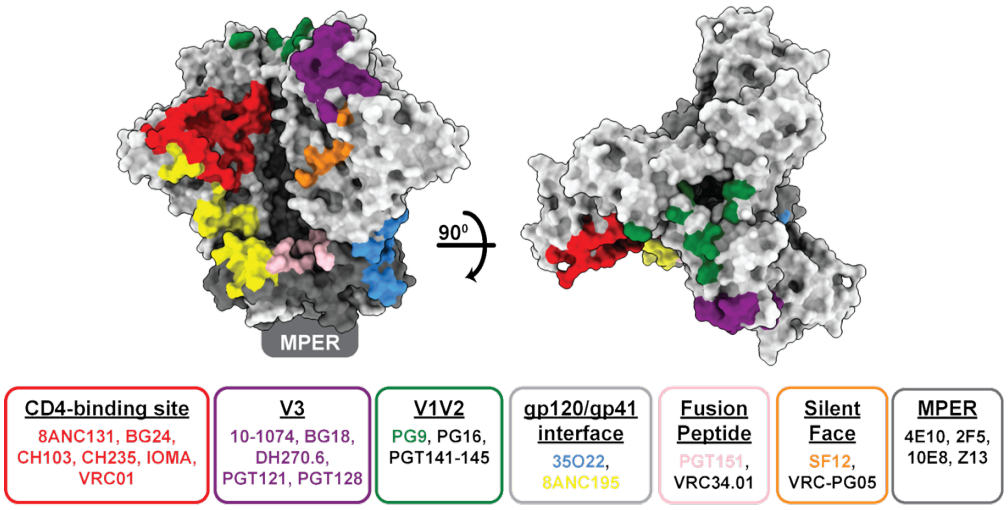

Figure 3: Broadly neutralizing antibody epitopes on HIV-1 Env.
A side view (left) and a top-down view (right) of a BG505 Env trimer (PDB ID: 9D8V) shown as a surface representation. Colored surface patches indicate bnAb epitope regions on Env, including the CD4-binding site, V3, V1V2, gp120/gp41 interface, fusion peptide, silent face, and membrane-proximal external region (MPER). For clarity, each epitope region is highlighted once per trimer. Env residues contacted by one or more bnAbs listed in colored text are similarly colored on the surface representation, with additional bnAbs listed for some epitope regions in black text. Surfaces not part of a bnAb epitope region are colored light or dim grey for gp120 and gp41, respectively.

bnAbs to HIV-1 have been described at length in various published reviews[86, 87, 88, 89, 90]. Briefly, b12 and other first generation bnAbs were identified from hybridoma screens or using phage display technologies and exhibited only modest levels of breadth and potency. Single B-cell cloning, along with the identification of people with broadly neutralizing serum, led to a new generation of bnAbs being isolated in the late 2000s, which exhibited greatly enhanced properties[91, 92, 93, 94]. In the years

that followed, additional bnAbs were isolated, including antibodies targeting the CD4bs that are nearly pan-neutralizing[95, 96, 97]. This thesis describes several newly identified bnAbs, including the current best-in-class bnAbs to the CD4bs and V3 epitopes. It also describes the characterization of antibody responses in rabbits and non-human primates (NHPs) that were sequentially immunized with engineered V3-targeting Env immunogens.

Challenges in Antibody-Targeting of HIV-1 Env

As described below, the dense glycan shield, high sequence and structure variability across strains, and the limited potential for bivalent antibody engagement of Env pose major obstacles to the development of broad and potent neutralizing antibodies. Furthermore, because HIV is a retrovirus capable of establishing a latent reservoir shortly after infection, the virus likely must be neutralized before integration occurs. This imposes a particularly high bar for antibody-based targeting of Env in a prophylactic setting, as an effective therapy or vaccine would need to confer sterilizing immunity.

bnAbs against HIV often exhibit unusual structural and genetic features including long CDRH3 loops, insertions and/or deletions (indels), and high levels of somatic hypermutation that can extend into framework regions, which are often required for broad and potent neutralization[98]. However, because such features are rare and difficult to reproducibly elicit through vaccination, they also represent major obstacles for HIV-1 vaccine design.

Challenge 1: The Glycan Shield

HIV-1 Env is extensively glycosylated, containing on average ~93 potential *N*-linked glycosylation sites per trimer across viral strains[99]. This dense glycan shield poses a significant challenge to the immune system, as the host cell-derived glycans are poorly immunogenic[100]. Notably, only the PNGS sequon (N-x-S/T, where x is any amino acid besides proline) is directly encoded; the appended glycan

structures depend on the accessibility of the glycosylation and glycan-processing enzymes within the ER and Golgi. Consequently, Env can exhibit highly heterogeneous glycosylation patterns, as glycans at a single site can vary not only between viral strains, but also among different trimers of the same strain, and among protomers within a single trimer. As a result, certain classes of HIV-1 bnAbs must tolerate or recognize multiple glycoforms at a given *N*-linked glycosylation site[101].

Challenge 2: A Highly Variable Target

The error-prone reverse transcriptase of HIV allows for rapid viral evolution in response to antibody pressure in people living with HIV, contributing to the immense global diversity of Env across circulating strains. As protein sequences change, PNGS sequons are also introduced, altered, or removed, resulting in a constantly shifting glycan shield. Oftentimes, glycan holes exist on the trimer, presenting strain-specific, immunodominant epitopes for immune recognition. However, these strain-specific antibodies are quickly rendered ineffective upon the introduction of a glycan within the epitope.

Despite extensive variability, evolutionary constraints maintain certain conserved features on Env that can be targeted by bnAbs. Viruses must retain their ability to bind both receptor and co-receptor and to mediate membrane fusion. As a result, the CD4bs on Env, which is framed by surrounding glycans, presents a relatively conserved proteinaceous surface. However, the CD4bs lies within a recessed crevice formed between two gp120 protomers. Because antibody Fabs are sterically bulkier than the CD4 receptor, this creates a barrier to antibody access, particularly against closed trimer conformations. Antibodies that manage this steric restriction are often encoded by the highly similar V_H1-2 or V_H1-46 germline genes, or alternatively, utilize CDRH3-mediated binding modes. Similar to the CD4bs, the V3 region also contains conserved features that are important for co-receptor

binding. V3 bnAbs can target slightly different epitopes within this region and do so with markedly different angles of approach.

Challenge 3: Limited Potential for Bivalent Antibody Engagement

As discussed earlier in this chapter, antibodies are capable of binding viruses bivalently through a variety of mechanisms including inter- and intra-spike crosslinking. Notably, germline versions of antibodies that bind with bivalent mechanisms could benefit from slower effective off rates giving rise to improved apparent affinities, even before affinity maturation shapes the antibody combining site. As a result, it may be quicker and easier to elicit broad and potent responses by targeting the elicitation of antibodies that engage bivalently. However, such efforts would require a thorough understanding of the different manners in which natural antibodies are capable of engaging targets bivalently.

Against HIV-1 Env, there remains a near-complete lack of understanding of the potential bivalent binding mechanisms employed by natural antibodies. While the relative sparsity of Env trimers on the virion surface and the spatial positioning of conserved bnAb epitopes have been proposed to limit the ability of antibodies to engage Env bivalently[76], antibodies PGT128 and EPTC112 were each shown to be more potent as bivalent IgG molecules than as monovalent Fabs[77, 78]. Despite these findings, first reported over a decade ago for PGT128[77], the underlying mechanisms remain elusive, limiting our ability to leverage this knowledge for vaccine design or therapeutic intervention.

Thesis Summary

This thesis first presents the characterization of rabbit and non-human primate antibodies elicited in response to sequential immunization in Chapters 2 and 3, followed by detailed structural and

biophysical characterizations of human broadly neutralizing antibodies targeting the CD4bs and V3-epitopes in Chapters 4 and 5, respectively.

Chapter 2 presents the evaluation of immune responses in sequentially immunized rabbits and non-human primates using negative stain, electron microscopy-based polyclonal epitope mapping (nsEMPEM). These experiments revealed the important finding that antibody responses went from being on-target after the initial V3-targeting priming immunogen to being progressively more off-target after boosting. This shift to progressively off-target responses was likely exacerbated by the elicitation of antibodies that caused the trimeric Env immunogens to dissociate into protomers. Chapter 2 also describes the isolation of heterologous neutralizing monoclonal antibodies isolated after the third or fourth boost. Seven of nine antibodies reported competed for Env binding with the V3-directed bnAb 10-1074, indicating targeting of the intended V3 epitope.

Chapter 3 presents cryo-EM structures of two of the 10-1074-competing monoclonal antibodies first described in Chapter 2. These structures revealed targeting of V3 residues, but on altered conformations of Env. Together, the findings reported in Chapters 2 and 3 provide insight into Env structural dynamics and inform strategies for improved immunogen design.

Chapters 4 and 5 describe human monoclonal antibodies isolated from two individuals whose serum neutralization profiles ranked first and second out of a large cohort of over 2,300 people living with HIV-1. Chapter 4 focuses on the numerous V_H1-2-encoded, VRC01-class bnAbs that were isolated from one of these individuals. These antibodies likely originated from multiple clonally distinct naïve B-cell precursors that varied in framework region insertions and CDRH3 lengths. One antibody, 04_A06, contained an 11-amino acid insertion in the heavy chain framework region 1 and exhibited high breadth and potency against multiclade pseudovirus panels (geometric mean half-maximal

inhibitory concentration (GeoMean IC_{50}) = 0.059 μg/mL, breadth = 98.5%, 332 strains). Structural analyses of this antibody and two additional bnAbs from the same individual are presented.

Chapter 5 describes the structural, functional, and biophysical characterizations of another new antibody, 007, isolated from a second individual. 007 also exhibited high breadth and potency against multiclade pseudovirus panels (GeoMean IC_{50} = 0.012 μg/mL; breadth = 69%, 217 virus strains). Structural characterizations of this antibody revealed targeting of an $N332_{gp120}$ glycan-independent V3 epitope on Env. Surprisingly, 007 demonstrated a weak monovalent binding affinity for Env, first observed by EM analysis and later confirmed by surface plasmon resonance. This unexpected finding led to the discovery that antibody bivalency is critical to 007's neutralization potency. Finally, possible mechanisms underlying this requirement were further explored and discussed.

References

1. Barre-Sinoussi, F. *et al.* Isolation of a T-lymphotropic retrovirus from a patient at risk for acquired immune deficiency syndrome (AIDS). *Science* **220**, 868-871 (1983).

2. Gallo, R.C. *et al.* Isolation of human T-cell leukemia virus in acquired immune deficiency syndrome (AIDS). *Science* **220**, 865-867 (1983).

3. Gallo, R.C. & Montagnier, L. The discovery of HIV as the cause of AIDS. *N Engl J Med* **349**, 2283-2285 (2003).

4. UNAIDS. Global HIV & AIDS statistics - Fact sheet; 2025.

5. Zhu, P. *et al.* Distribution and three-dimensional structure of AIDS virus envelope spikes. *Nature* **441**, 847-852 (2006).

6. Votteler, J. & Schubert, U. Human Immunodeficiency Viruses: Molecular Biology. In: Mahy, B.W.J. & Van Regenmortel, M.H.V. (eds). *Encyclopedia of Virology (Third Edition).* Academic Press: Oxford, 2008, pp 517-525.

7. Klatzmann, D. *et al.* Selective tropism of Lymphadenopathy Associated Virus (LAV) for helper-inducer T lymphocytes. *Science* **225**, 59-63 (1984).

8. Rand, R.P. & Parsegian, V.A. Hydration forces between phospholipid bilayers. *Biochimica et Biophysica Acta (BBA) - Reviews on Biomembranes* **988**, 351-376 (1989).

9. McCaul, N. *et al.* Intramolecular quality control: HIV-1 envelope gp160 signal-peptide cleavage as a functional folding checkpoint. *Cell Rep* **36**, 109646 (2021).

10. Earl, P.L., Moss, B. & Doms, R.W. Folding, interaction with GRP78-BiP, assembly, and transport of the human immunodeficiency virus type 1 envelope protein. *J Virol* **65**, 2047-2055 (1991).

11. Bhattacharya, J., Peters, P.J. & Clapham, P.R. Human immunodeficiency virus type 1 envelope glycoproteins that lack cytoplasmic domain cysteines: Impact on association with membrane lipid rafts and incorporation onto budding virus particles. *J Virol* **78**, 5500-5506 (2004).

12. Behrens, A.J. & Crispin, M. Structural principles controlling HIV envelope glycosylation. *Curr Opin Struct Biol* **44**, 125-133 (2017).

13. McCune, J.M. *et al.* Endoproteolytic cleavage of gp160 is required for the activation of human immunodeficiency virus. *Cell* **53**, 55-67 (1988).

14. Wilen, C.B., Tilton, J.C. & Doms, R.W. HIV: Cell binding and entry. *Cold Spring Harb Perspect Med* **2** (2012).

15. Harrison, S.C. Viral membrane fusion. *Virology* **479-480**, 498-507 (2015).

16. Wang, H. *et al.* Cryo-EM structure of a CD4-bound open HIV-1 envelope trimer reveals structural rearrangements of the gp120 V1V2 loop. *Proc Natl Acad Sci U S A* **113**, E7151-E7158 (2016).

17. Ozorowski, G. *et al.* Open and closed structures reveal allostery and pliability in the HIV-1 envelope spike. *Nature* **547**, 360-363 (2017).

18. Dam, K.A., Fan, C., Yang, Z. & Bjorkman, P.J. Intermediate conformations of CD4-bound HIV-1 Env heterotrimers. *Nature* **623**, 1017-1025 (2023).

19. Li, W. *et al.* HIV-1 Env trimers asymmetrically engage CD4 receptors in membranes. *Nature* **623**, 1026-1033 (2023).

20. Shaik, M.M. *et al.* Structural basis of coreceptor recognition by HIV-1 envelope spike. *Nature* **565**, 318-323 (2019).

21. Zhang, Z. *et al.* CXCR4 mediated recognition of HIV envelope spike and inhibition by CXCL12. *Nat Commun* **16**, 8653 (2025).

22. Chan, D.C., Fass, D., Berger, J.M. & Kim, P.S. Core structure of gp41 from the HIV envelope glycoprotein. *Cell* **89**, 263-273 (1997).

23. Furuta, R.A., Wild, C.T., Weng, Y. & Weiss, C.D. Capture of an early fusion-active conformation of HIV-1 gp41. *Nat Struct Biol* **5**, 276-279 (1998).

24. Ladinsky, M.S. *et al.* Electron tomography visualization of HIV-1 fusion with target cells using fusion inhibitors to trap the pre-hairpin intermediate. *Elife* **9** (2020).

25. Weissenhorn, W., Dessen, A., Harrison, S.C., Skehel, J.J. & Wiley, D.C. Atomic structure of the ectodomain from HIV-1 gp41. *Nature* **387**, 426-430 (1997).

26. Jacks, T. *et al.* Characterization of ribosomal frameshifting in HIV-1 gag-pol expression. *Nature* **331**, 280-283 (1988).

27. Murphy, R.E. & Saad, J.S. The interplay between HIV-1 gag binding to the plasma membrane and Env incorporation. *Viruses* **12** (2020).

28. Alfadhli, A., Barklis, R.L. & Barklis, E. HIV-1 matrix organizes as a hexamer of trimers on membranes containing phosphatidylinositol-(4,5)-bisphosphate. *Virology* **387**, 466-472 (2009).

29. Qu, K. *et al.* Maturation of the matrix and viral membrane of HIV-1. *Science* **373**, 700-704 (2021).

30. Votteler, J. & Sundquist, W.I. Virus budding and the ESCRT pathway. *Cell Host Microbe* **14**, 232-241 (2013).

31. Piai, A. *et al.* Structural basis of transmembrane coupling of the HIV-1 envelope glycoprotein. *Nat Commun* **11**, 2317 (2020).

32. Piai, A. *et al.* NMR model of the entire membrane-interacting region of the HIV-1 fusion protein and its perturbation of membrane morphology. *J Am Chem Soc* **143**, 6609-6615 (2021).

33. Chen, J. *et al.* Effect of the cytoplasmic domain on antigenic characteristics of HIV-1 envelope glycoprotein. *Science* **349**, 191-195 (2015).

34. Murakami, T. & Freed, E.O. The long cytoplasmic tail of gp41 is required in a cell type-dependent manner for HIV-1 envelope glycoprotein incorporation into virions. *Proc Natl Acad Sci U S A* **97**, 343-348 (2000).

35. Lerner, G., Ding, L., Candor, K. & Spearman, P. Incorporation of the HIV-1 envelope glycoprotein into viral particles is regulated by the tubular recycling endosome in a cell type-specific manner. *bioRxiv* (2023).

36. Checkley, M.A., Luttge, B.G. & Freed, E.O. HIV-1 envelope glycoprotein biosynthesis, trafficking, and incorporation. *J Mol Biol* **410**, 582-608 (2011).

37. Alfadhli, A. *et al.* Analysis of HIV-1 matrix-envelope cytoplasmic tail interactions. *J Virol* **93**, 10.1128/jvi.01079-01019 (2019).

38. Chaubey, M. *et al.* Specific interactions between HIV-1 Env cytoplasmic tail and gag matrix domain probed by NMR. *J Am Chem Soc* (2025).

39. Pettit, S.C., Everitt, L.E., Choudhury, S., Dunn, B.M. & Kaplan, A.H. Initial cleavage of the human immunodeficiency virus type 1 GagPol precursor by its activated protease occurs by an intramolecular mechanism. *J Virol* **78**, 8477-8485 (2004).

40. Mattei, S. *et al.* High-resolution structures of HIV-1 Gag cleavage mutants determine structural switch for virus maturation. *Proc Natl Acad Sci U S A* **115**, E9401-E9410 (2018).

41. Ganser, B.K., Li, S., Klishko, V.Y., Finch, J.T. & Sundquist, W.I. Assembly and analysis of conical models for the HIV-1 core. *Science* **283**, 80-83 (1999).

42. Stacey, J.C.V. *et al.* The conserved HIV-1 spacer peptide 2 triggers matrix lattice maturation. *Nature* **640**, 258-264 (2025).

43. Harris, L.J., Larson, S.B., Hasel, K.W. & McPherson, A. Refined structure of an intact IgG2a monoclonal antibody. *Biochemistry* **36**, 1581-1597 (1997).

44. Padlan, E.A., Abergel, C. & Tipper, J.P. Identification of specificity-determining residues in antibodies. *FASEB J* **9**, 133-139 (1995).

45. Zhang, X. *et al.* 3D structural fluctuation of IgG1 antibody revealed by individual particle electron tomography. *Sci Rep* **5**, 9803 (2015).

46. Lesk, A.M. & Chothia, C. Elbow motion in the immunoglobulins involves a molecular ball-and-socket joint. *Nature* **335**, 188-190 (1988).

47. Bailey, L.J. *et al.* Locking the elbow: Improved antibody fab fragments as chaperones for structure determination. *J Mol Biol* **430**, 337-347 (2018).

48. Burnet, F.M. A modification of Jerne's theory of antibody production using the concept of clonal selection. *The Australian Journal of Science* **20**, 67-69 (1957).

49. Lefranc, M.-P. & Lefranc, G. *The Immunoglobulin FactsBook*. Elsevier Science: Burlington, 2001.

50. Schatz, D.G. & Ji, Y. Recombination centres and the orchestration of V(D)J recombination. *Nat Rev Immunol* **11**, 251-263 (2011).

51. Xu, J.L. & Davis, M.M. Diversity in the CDR3 region of V(H) is sufficient for most antibody specificities. *Immunity* **13**, 37-45 (2000).

52. Victora, G.D. & Nussenzweig, M.C. Germinal centers. *Annu Rev Immunol* **30**, 429-457 (2012).

53. Muramatsu, M. *et al.* Class switch recombination and hypermutation require Activation-Induced Cytidine Deaminase (AID), a potential RNA editing enzyme. *Cell* **102**, 553-563 (2000).

54. Tummino, P.J. & Copeland, R.A. Residence time of receptor-ligand complexes and its effect on biological function. *Biochemistry* **47**, 5481-5492 (2008).

55. Csermely, P., Palotai, R. & Nussinov, R. Induced fit, conformational selection and independent dynamic segments: An extended view of binding events. *Trends Biochem Sci* **35**, 539-546 (2010).

56. Saphire, E.O. *et al.* Crystal structure of a neutralizing human IgG against HIV-1: A template for vaccine design. *Science* **293**, 1155-1159 (2001).

57. Lafferty, K.J. The interaction between virus and antibody II. Mechanism of the reaction. *Virology* **21**, 76-90 (1963).

58. Lafferty, K.J. & Oertelis, S. The interaction between virus and antibody III. Examination of virus-antibody complexes with the electron microscope. *Virology* **21**, 91-99 (1963).

59. Kohler, G. & Milstein, C. Continuous cultures of fused cells secreting antibody of predefined specificity. *Nature* **256**, 495-497 (1975).

60. Porter, R.R. The hydrolysis of rabbit γ-globulin and antibodies with crystalline papain. *Biochem J* **73**, 119-127 (1959).

61. Wiley, D.C., Skehel, J.J. & Waterfield, M. Evidence from studies with a cross-linking reagent that the haemagglutinin of influenza virus is a trimer. *Virology* **79**, 446-448 (1977).

62. Rey, F.A. & Lok, S.-M. Common features of enveloped viruses and implications for immunogen design for next-generation vaccines. *Cell* **172**, 1319-1334 (2018).

63. Yuan, Y. *et al.* Cryo-EM structures of MERS-CoV and SARS-CoV spike glycoproteins reveal the dynamic receptor binding domains. *Nat Commun* **8**, 15092 (2017).

64. Wrapp, D. *et al.* Cryo-EM structure of the 2019-nCoV spike in the prefusion conformation. *Science* **367**, 1260-1263 (2020).

65. Tsai, Y.-X., Chien, Y.-C., Hsu, M.-F., Khoo, K.-H. & Hsu, S.-T.D. Molecular basis of host recognition of human coronavirus 229E. *Nat Commun* **16**, 2045 (2025).

66. Williams, J.A., Gui, L., Hom, N., Mileant, A. & Lee, K.K. Dissection of epitope-specific mechanisms of neutralization of influenza virus by intact IgG and fab fragments. *J Virol* **92** (2018).

67. Yao, H. *et al.* Cryo-ET of IgG bivalent binding on SARS-CoV-2 provides structural basis for antibody avidity. *bioRxiv*, 2025.2002.2028.640788 (2025).

68. Yan, R. *et al.* Structural basis for bivalent binding and inhibition of SARS-CoV-2 infection by human potent neutralizing antibodies. *Cell Res* **31**, 517-525 (2021).

69. Callaway, H.M. *et al.* Bivalent intra-spike binding provides durability against emergent Omicron lineages: Results from a global consortium. *Cell Rep* **42**, 112014 (2023).

70. Patel, A. *et al.* Molecular basis of SARS-CoV-2 Omicron variant evasion from shared neutralizing antibody response. *Structure* **31**, 801-811.e805 (2023).

71. Barnes, C.O. *et al.* SARS-CoV-2 neutralizing antibody structures inform therapeutic strategies. *Nature* **588**, 682-687 (2020).

72. Jette, C.A. *et al.* Broad cross-reactivity across sarbecoviruses exhibited by a subset of COVID-19 donor-derived neutralizing antibodies. *Cell Rep* **36**, 109760 (2021).

73. Yin, V. *et al.* Probing affinity, avidity, anticooperativity, and competition in antibody and receptor binding to the SARS-CoV-2 spike by single particle mass analyses. *ACS Cent Sci* **7**, 1863-1873 (2021).

74. Schofield, D.J., Stephenson, J.R. & Dimmock, N.J. Variations in the neutralizing and haemagglutination-inhibiting activities of five influenza A virus-specific IgGs and their antibody fragments. *J Gen Virol* **78**, 2431-2439 (1997).

75. Wu, H. *et al.* Ultra-potent antibodies against respiratory syncytial virus: Effects of binding kinetics and binding valence on viral neutralization. *J Mol Biol* **350**, 126-144 (2005).

76. Klein, J.S. & Bjorkman, P.J. Few and far between: How HIV may be evading antibody avidity. *PLOS Pathog* **6**, e1000908 (2010).

77. Pejchal, R. *et al.* A potent and broad neutralizing antibody recognizes and penetrates the HIV glycan shield. *Science* **334**, 1097-1103 (2011).

78. Molinos-Albert, L.M. *et al.* Anti-V1/V3-glycan broadly HIV-1 neutralizing antibodies in a post-treatment controller. *Cell Host Microbe* (2023).

79. Wardemann, H. *et al.* Predominant autoantibody production by early human B cell precursors. *Science* **301**, 1374-1377 (2003).

80. Mouquet, H. *et al.* Polyreactivity increases the apparent affinity of anti-HIV antibodies by heteroligation. *Nature* **467**, 591-595 (2010).

81. Klein, J.S. *et al.* Examination of the contributions of size and avidity to the neutralization mechanisms of the anti-HIV antibodies b12 and 4E10. *Proc Natl Acad Sci U S A* **106**, 7385-7390 (2009).

82. Ofek, G. *et al.* Structure and mechanistic analysis of the anti-human immunodeficiency virus type 1 antibody 2F5 in complex with its gp41 epitope. *J Virol* **78**, 10724-10737 (2004).

83. Burton, D.R. *et al.* A large array of human monoclonal antibodies to type 1 human immunodeficiency virus from combinatorial libraries of asymptomatic seropositive individuals. *Proc Natl Acad Sci U S A* **88**, 10134-10137 (1991).

84. Burton, D.R. *et al.* Efficient neutralization of primary isolates of HIV-1 by a recombinant human monoclonal antibody. *Science* **266**, 1024-1027 (1994).

85. Sievers, S.A., Scharf, L., West, A.P. & Bjorkman, P.J. Antibody engineering for increased potency, breadth and half-life. *Curr Opin HIV AIDS* **10**, 151-159 (2015).

86. Caskey, M. Broadly neutralizing antibodies for the treatment and prevention of HIV infection. *Curr Opin HIV AIDS* **15**, 49-55 (2020).

87. Sok, D. & Burton, D.R. Recent progress in broadly neutralizing antibodies to HIV. *Nat Immunol* **19**, 1179-1188 (2018).

88. Burton, D.R. & Hangartner, L. Broadly neutralizing antibodies to HIV and their role in vaccine design. *Annu Rev Immunol* **34**, 635-659 (2016).

89. Gruell, H. & Klein, F. Antibody-mediated prevention and treatment of HIV-1 infection. *Retrovirology* **15**, 73 (2018).

90. McCoy, L.E. & Burton, D.R. Identification and specificity of broadly neutralizing antibodies against HIV. *Immunol Rev* **275**, 11-20 (2017).

91. Walker, L.M. *et al.* Broad and potent neutralizing antibodies from an African donor reveal a new HIV-1 vaccine target. *Science* **326**, 285-289 (2009).

92. Wu, X. *et al.* Rational design of envelope identifies broadly neutralizing human monoclonal antibodies to HIV-1. *Science* **329**, 856-861 (2010).

93. Walker, L.M. *et al.* Broad neutralization coverage of HIV by multiple highly potent antibodies. *Nature* **477**, 466-470 (2011).

94. Scheid, J.F. *et al.* Sequence and structural convergence of broad and potent HIV antibodies that mimic CD4 binding. *Science* **333**, 1633-1637 (2011).

95. Cale, E.M. *et al.* Antigenic analysis of the HIV-1 envelope trimer implies small differences between structural states 1 and 2. *J Biol Chem* **298**, 101819 (2022).

96. Sajadi, M.M. *et al.* Identification of near-pan-neutralizing antibodies against HIV-1 by deconvolution of plasma humoral responses. *Cell* **173**, 1783-1795.e1714 (2018).

97. Schommers, P. *et al.* Restriction of HIV-1 escape by a highly broad and potent neutralizing antibody. *Cell* **180**, 471-489.e422 (2020).

98. Klein, F. *et al.* Somatic mutations of the immunoglobulin framework are generally required for broad and potent HIV-1 neutralization. *Cell* **153**, 126-138 (2013).

99. Stewart-Jones, Guillaume B.E. *et al.* Trimeric HIV-1-Env structures define glycan shields from clades A, B, and G. *Cell* **165**, 813-826 (2016).

100. Newby, M.L., Allen, J.D. & Crispin, M. Influence of glycosylation on the immunogenicity and antigenicity of viral immunogens. *Biotechnol Adv* **70**, 108283 (2024).

101. Mouquet, H. *et al.* Complex-type N-glycan recognition by potent broadly neutralizing HIV antibodies. *Proc Natl Acad Sci U S A* **109**, E3268-E3277 (2012).

C h a p t e r 2

SEQUENTIAL IMMUNIZATION OF MACAQUES ELICITS HETEROLOGOUS NEUTRALIZING ANTIBODIES TARGETING THE V3-GLYCAN PATCH OF HIV-1 ENV

Escolano, A.*, Gristick, H.B.*, Gautam, R.*, **DeLaitsch, A.T.***, Abernathy, M.E., Yang, Z., Wang, H., Hoffmann, M.A.G., Nishimura, Y., Wang, Z., Koranda, N., Kakutani, L.M., Gao, H., Gnanapragasam, P.N.P., Raina, H., Gazumyan, A., Cipolla, M., Oliveira, T.Y., Ramos, V., Irvine, D.J., Silva, M., West, A.P., Keeffe, J.R., Barnes, C.O., Seaman, M.S., Nussenzweig, M.C., Martin, M.A., Bjorkman, P.J. Sequential immunization of macaques elicits heterologous neutralizing antibodies targeting the V3-glycan patch of HIV-1 Env. *Sci Transl Med* **13,** eabk1533 (2021). doi: 10.1126/scitranslmed.abk1533

*** *Equal Contributions***

Abstract: Broadly neutralizing antibodies (bnAbs) against HIV-1 develop after prolonged virus and antibody coevolution. Previous studies showed that sequential immunization with a V3-glycan patch germline-targeting HIV-1 envelope trimer (Env) followed by variant Envs can reproduce this process in mice carrying V3-glycan bnAb precursor B cells. However, eliciting bnAbs in animals with polyclonal antibody repertoires is more difficult. We used a V3-glycan immunogen multimerized on virus-like particles (VLPs), followed by boosting with increasingly native-like Env-VLPs, to elicit weak broadly neutralizing antibodies in nonhuman primates (NHPs). Structures of antibody/Env complexes after prime and boost vaccinations demonstrated target epitope recognition with apparent maturation to accommodate glycans. However, we also observed increasing off-target antibodies with boosting. Eight vaccinated NHPs were subsequently challenged with simian-human immunodeficiency virus (SHIV), and seven of eight animals became infected. The single NHP that remained uninfected after viral challenge exhibited one of the lowest neutralization titers against the challenge virus. These results demonstrate that more potent heterologous neutralization resulting from sequential immunization is necessary for protection in this animal model. Thus, improved prime-boost regimens to increase bnAb potency and stimulate other immune protection mechanisms are essential for developing anti-HIV-1 vaccines.

Introduction

Nearly 40 years after the emergence of the acquired immunodeficiency syndrome (AIDS) pandemic, there is no vaccine or cure. However, preclinical models have shown that broadly neutralizing antibodies (bnAbs) against the HIV-1 envelope trimer (Env), the only viral protein on the surface of virions, can prevent HIV-1 infection[1, 2, 3, 4, 5, 6, 7, 8, 9, 10, 11, 12, 13], suggesting that a vaccination regimen that elicits bnAbs would be protective. In contrast to most human antibodies, anti-HIV-1 bnAbs are extensively hypermutated[14, 15, 16, 17] and develop after prolonged periods of virus and antibody coevolution in infected humans and nonhuman primates (NHPs)[18, 19, 20]. These observations led to the proposal that a vaccine regimen recapitulating this process would require a series of sequential immunogens[21, 22], a hypothesis that was validated in knock-in mice that carried V3-glycan bnAb precursor B cells[23]. However, knock-in mice that carry a specific bnAb precursor have a limited B cell antibody repertoire, which is not representative of the complexity of genetically intact mammalian immune systems.

An obstacle to initiating bnAb responses is that the inferred germline (iGL) precursors of most bnAbs do not bind to HIV-1 envelopes present on circulating HIV-1 strains[24, 25, 26, 27, 28, 29]. A goal of HIV-1 vaccine development has therefore been to design iGL-targeting immunogens to recruit B cells that express bnAb precursors. Nonetheless, the low frequency of bnAb precursors within a polyclonal repertoire can be circumvented using transgenic iGL knock-in animals.

Previous studies in wild-type (wt) animals have shown that initiation of B cell responses depends in part on a specific B cell receptor's affinity for antigen and on the bnAb precursor frequency[30, 31, 32, 33, 34]. Thus, protein engineers have focused on producing immunogens that bind with high affinity to specific bnAb precursors. However, optimizing binding to a unique iGL precursor antibody can limit the repertoire of recruited B cells qualitatively and quantitatively. Moreover, it does not take

into account observations indicating that, when B cells clonally expand within each germinal center, there are multiple founder B cells with a wide range of affinities, and that entry into the germinal center is limited by competition and not absolute affinity[34, 35]. To date, no one has consistently elicited heterologously neutralizing serum in wt animals with a polyclonal repertoire, with one exception in which anti-HIV-1 bnAbs were elicited by a fusion peptide-based immunogen in NHPs[36]. In that case, however, the elicited antibodies were of limited breadth and potency.

We recently described RC1 and RC1-4fill, low-affinity priming Env trimer immunogens engineered to elicit antibody responses that target the V3-glycan patch[37] at the apex of the HIV-1 Env trimer. We showed that immunization of wt animals with RC1-4fill multimerized on virus-like particles (VLPs) elicited antibodies that recognized the V3-glycan patch[38]. Here, we report the results of boosting experiments in wt animals primed with RC1-4fill-VLPs designed, based in part, on iGL knock-in mouse experiments that succeeded in eliciting bnAbs targeting the V3-glycan patch[23]. Although boosting antigens designed to shepherd bnAb development elicited antibody evolution to avoid potential clashes with the gp120 N156 glycan, modified native-like Env gp140 trimer (SOSIP) antigen administration produced off-target responses. Here, we present analyses of post-boost serum and monoclonal antibodies (mAbs) cloned from vaccinated animals, finding both on- and off-target heterologously neutralizing antibodies.

Results

Design of V3-glycan patch immunogens used for sequential immunization

The gp120 V3-glycan patch includes a group of nine high-mannose and complex-type N-glycans surrounding the V3 loop of Env (attached to gp120 residues N133, N137, N156, N295, N301, N332, N339, N385, and N392)[37]. Human donor-derived bnAbs targeting this site, including PGT121[39], 10-1074[28], and BG18[40], reach through these glycans using elongated heavy (H) and light

(L) chain complementarity-determining region (CDR) loops; in particular, CDRH3 and portions of CDRL1 and CDRL3 contact the highly conserved Env GDIR motif (G324-D325-I326-R327) in gp120 at the base of V3[41]. 11MUTB includes substitutions in V1 and lacks potential N-linked glycosylation sites (PNGSs) at gp120 positions N133 and N137[42]. We previously described immunogens, RC1 and RC1-4fill, that were derived from a soluble version of the clade A BG505 native-like Env trimer (SOSIP.664)[43] and designed to bind germline versions of V3-glycan patch bnAbs. RC1 and RC1-4fill were based on a V3-glycan patch-targeting immunogen 11MUTB[42], which is related to the 10MUT initial immunogen in a series that elicited V3-glycan patch bnAbs in iGL knock-in mice[23].

To construct RC1, we modified 11MUTB to include an additional mutation (N156Q) to remove the N156 glycan, which we reasoned would increase accessibility of V1 residues that interact with V3-glycan patch bnAbs[44, 45] and produce a more electrostatically neutral Env surface that could facilitate the binding of largely neutral V3-glycan patch iGLs[46]. RC1-4fill contains four additional PNGSs at gp120 positions 230, 241, 289, and 344 to cover an immunogenic hole in the BG505 glycan shield[47] with added N-glycans. Prime immunizations with soluble RC1- and RC1-4fill induced V3-glycan-specific antibody responses in PGT121/10-1074 iGL knock-in mice and wt mice[38]. For other immunizations, both immunogens were multimerized on VLPs derived from the AP205 bacteriophage using the SpyTag-SpyCatcher system[48, 49] to enhance potential avidity effects and limit exposure to off-target epitopes at the Env base[47, 50].

Serum and mAbs derived from wt animals immunized with soluble and multimerized RC1-based immunogens were nonneutralizing, as expected after only a prime immunization[38]. We therefore designed a boosting regimen for immunized NHPs and rabbits starting with an RC1-4fill-VLP prime (Fig. 1A) to guide neutralizing antibody responses against the V3-glycan patch. For boosting

immunizations, purified SOSIP immunogens or "wt" SOSIPs were covalently attached to VLPs (Fig. 1A). To evaluate antibody responses, we constructed HIV-1 pseudoviruses, including strains with RC1 and 11MUTB Envs (table S1), to map targeted epitopes and determine neutralization potencies using an in vitro neutralization assay[51].

Antibody-RC1 structures solved using Fabs from mAbs isolated after the prime suggested potential clashes with the gp120 N156 glycan when present on an HIV Env[38]. Thus, 11MUTB, which includes the N156 glycan, was a logical choice for the first boosting immunogen. We attached a SpyTagged version of 11MUTB[42] with 4fill mutations[38] to VLPs to create 11MUTB-4fill-VLPs, which were used for boost 1 (B1) (Fig. 1A). The clade A BG505-based 5MUT immunogen[42] was the third in a series of antigens that elicited bnAbs in immunized knock-in mice[23]. For boost 2 (B2), we used this immunogen but attempted to avoid BG505 strain-specific responses by engineering the clade B B41 SOSIP trimer[52] to include the 5MUT mutations[42] and an introduced PNGS at gp120 position 289. SpyTagged versions of B41-5MUT and wt B41 were attached to VLPs to create B41-5MUT-VLPs and B41wt-VLPs, respectively, which were used for B2 in two cohorts of four NHPs each (tables S1 and S2). For boost 3 (B3), we diverged from the knock-in mouse experimental protocol to try to increase breadth and further avoid strain-specific responses by making mosaic VLPs to which we coupled two different wt SOSIPs from clade B (AMC011)[53] and clade C (Du422)[54] (AMC011/Du422-VLPs) (Fig. 1A). These Envs were chosen because their native glycan shields cover immunodominant regions of HIV-1 Env, and the corresponding viruses are highly susceptible to neutralization by V3-glycan patch-specific bnAbs[28, 53]. An additional shielding glycan was added to AMC011 by introducing a PNGS at gp120 position 230. For boost 4 (B4), we attempted to further diversify the V3-glycan patch epitope presented on Env trimers, seeking to avoid strain-specific epitopes by constructing a mosaic VLP that was conjugated with consensus group M and consensus clade C SOSIPs (ConM/ConC-VLPs) (Fig. 1A)[55, 56].

Serum samples from prime-boosted wt animals targeted the V3-glycan patch and showed weak, heterologous neutralizing activity

To map epitope(s) recognized by serum antibodies elicited in NHPs, we used an automated competition enzyme-linked immunosorbert assay (ELISA) in which a randomly biotinylated RC1 trimer was immobilized on an ELISA plate, incubated with a Fab from a potential competitor mAb of known epitope on Env trimer, and probed with serum containing a polyclonal mixture of antibodies (Fig. S1A). Controls involved using monoclonal IgG antibodies of known epitopes instead of NHP serum. The following competitor Fabs or control IgG antibodies were used: 10-1074 and PGT128, representative V3-glycan patch bnAbs[28, 39]; PGT145 and PG16, V1V2 bnAb[57, 58]; 3BNC117 and IOMA, CD4bs bnAbs[26, 45]; SF12, a bnAb against the glycan-dominated silent face[59]; VRC34, a gp41 fusion peptide-directed bnAb[60], 8ANC195, a bnAb against the gp120-g41 interface[61]; 3BC315, a bnAb that binds between adjacent gp41 protomers and neutralizes by promoting Env trimer decay[62]; and 10A and 12N, nonneutralizing antibodies that bind to distracting epitopes on BG505 Env: 10A binds to the glycan hole surrounding gp120 residue 241, and 12N binds to the trimer base[47].

Results from the competition ELISAs were fairly uniform across the samples from NHPs 1 to 8, showing competition with the V3-glycan patch bnAbs 10-1074 and PGT128 after the prime (Fig. S1A). The amount of competition with the V3-glycan patch bnAbs diminished with boosting, especially for the PGT128 competition (Fig. S1A). Although these results indicate targeting of the desired epitope, we did not observe 100% competition with 10-1074/PGT128 for any of the samples, consistent with elicitation of antibodies that recognize off-target Env epitopes. Off-target responses increased with boosting as evidenced by increased serum responses against RC1 and proportionally decreased V3-glycan patch binding (Fig. S1B).

We also evaluated post-prime and post-boost serum samples by neutralization assays against RC1, 11MUTB, $SHIV_{DH12\text{-}V3AD8}$, and $SHIV_{AD8EO}$ pseudoviruses (PV)[51] and against a replication-competent (RC) $SHIV_{DH12\text{-}V3AD8}$ constructed as described (Fig. 1B and table S1)[63]. The RC1 and 11MUTB pseudoviruses represent autologous strains for our immunogens (RC1 for prime and boost immunizations; 11MUTB for boost immunizations). The heterologous tier 2 $SHIV_{DH12\text{-}V3AD8}$ and $SHIV_{AD8EO}$ viruses were chosen to assess responses against potential viral strains that could be used in later challenge experiments, with $SHIV_{AD8EO}$ representing a highly pathogenic strain[64] and $SHIV_{DH12\text{-}V3AD8}$ being a $SHIV_{AD8EO}$ derivative with less pathogenicity in NHPs[63].

Two weeks after the prime, serum samples from NHPs 1 to 8 exhibited autologous neutralization against RC1 ranging from 50% inhibitory doses (ID_{50}s) of 200 to 1000, and undetectable neutralization of 11MUTB, $SHIV_{DH12\text{-}V3AD8}$, and $SHIV_{AD8EO}$ except for neutralization of 11MUTB in NHP 4 serum (ID_{50} = 400) (table S1). By 8-week post-prime, autologous neutralization of RC1 had risen to ID_{50}s of 6500 to 75,000 and responses to 11MUTB ranged from ID_{50}s of 350 to 8000, demonstrating neutralization of a pseudovirus containing the N156 glycan. Concurrently, we observed low titers of heterologous neutralization of $SHIV_{DH12\text{-}V3AD8}$ pseudovirus or replication-competent viruses (ID_{50}s < 60) in three of the primed NHPs (table S1).

Three weeks after the first boost with 11MUTB-4fill-VLPs, autologous neutralization of RC1 rose again to ID_{50}s of 80,000 to 300,000 and 11MUTB titers also rose to ID_{50}s of 50,000 to 300,000 (Fig. 1B and table S1). At this time point, titers against $SHIV_{DH12\text{-}V3AD8}$ pseudovirus and replication-competent viruses were barely detectable in all eight NHPs. By 3 weeks post-B2 with B41 wt-VLPs or B41-5MUT-VLPs, neutralization potencies against RC1 and 11MUTB remained high, but titers against the heterologous $SHIV_{DH12\text{-}V3AD8}$ pseudovirus rose to values ranging from 584 to 3378,

with detectable neutralization against the replication-competent $SHIV_{DH12\text{-}V3AD8}$ in all 8 NHPs (ID_{50}s from 36 to 92). The mean titers after boost 2 against the $SHIV_{DH12\text{-}V3AD8}$ pseudovirus were significantly higher in the four NHPs that received the B41-5MUT-VLP boost (NHPs 1, 2, 5, and 6) compared with the four NHPs that received the B41wt-VLP boost (NHPs 3, 4, 7, and 8) (mean $ID_{50} = 2445 \pm 809$ versus 1027 ± 283; $P = 0.046$). We conclude that the immunization series starting with RC1-4fill-VLPs, followed by 11MUTB-4fill-VLPs and B41-5MUT-VLPs, elicited antibodies that neutralized autologous strains and also exhibited weak activity against a heterologous SHIV pseudovirus.

Two weeks after B3, we observed relatively steady titers against RC1 and 11MUTB. Importantly, serum neutralization titers against pseudotyped $SHIV_{DH12\text{-}V3AD8}$ rose to values above 2000 in seven of eight animals (mean $ID_{50} = 3671 \pm 2004$) with an ID_{50} greater than 8000 observed in NHP 4 (table S1). Similarly, the titers against replication-competent $SHIV_{DH12\text{-}V3AD8}$ rose in most of the NHPs and ranged from 47 to 164, with NHP 4 again exhibiting the highest titer. Samples collected two weeks after B4 showed relatively steady neutralization titers in most NHPs against RC1, 11MUTB, and the $SHIV_{DH12\text{-}V3AD8}$ pseudovirus. Titers against replication-competent $SHIV_{DH12\text{-}V3AD8}$ rose or fell in NHPs 1 to 8, with a range from 39 to 256. As expected, no serum neutralization activity was ever detected against $SHIV_{AD8EO}$, as this virus is less sensitive than $SHIV_{DH12\text{-}V3AD8}$ to PGT121, a V3-targeting bnAb[63]. Overall, the trends across NHPs 1 to 8 (Fig. 1B) suggested that (*i*) neutralization titers against autologous RC1 and 11MUTB pseudotype viruses increased after the prime and first boost, remaining relatively constant after the remaining boosts with heterologous immunogens; (*ii*) neutralization titers against the heterologous $SHIV_{DH12\text{-}V3AD8}$ pseudovirus remained at baseline until after B1, rose after B2 and B3, but then remained relatively constant; and (*iii*) neutralization titers against the replication-competent $SHIV_{DH12\text{-}V3AD8}$ virus were lower than titers against the homologous pseudotype viruses[65, 66].

We next evaluated serum neutralization in immunized NHPs against a panel of heterologous tier 1 and tier 2 pseudotyped viruses (Fig. 1C and table S2). Neutralization against these viruses was very weak or undetectable after the prime and B1. Sequential boosting with B41wt-VLPs or B41-5MUT-VLPs elicited weakly neutralizing activity against the heterologous HIV-1 strain JRCSF.JB (B2; table S2). The heterologous neutralizing responses were maintained or, in some cases, improved, by the boost of Du422/AMC011-VLPs (B3), but were reduced after the ConC/ConM-VLP boost (B4) (Fig. 1C and table S2). Serum neutralization assays for rabbits immunized with the same prime-boost regimen as the NHPs (Fig. S2A) showed qualitatively similar results. No neutralization against heterologous viruses was observed after the prime or B1, weak neutralization against JRCSF.JB was observed after B2 and B3, and no neutralization was observed after the ConC/ConM-VLP boost (Fig. S2B).

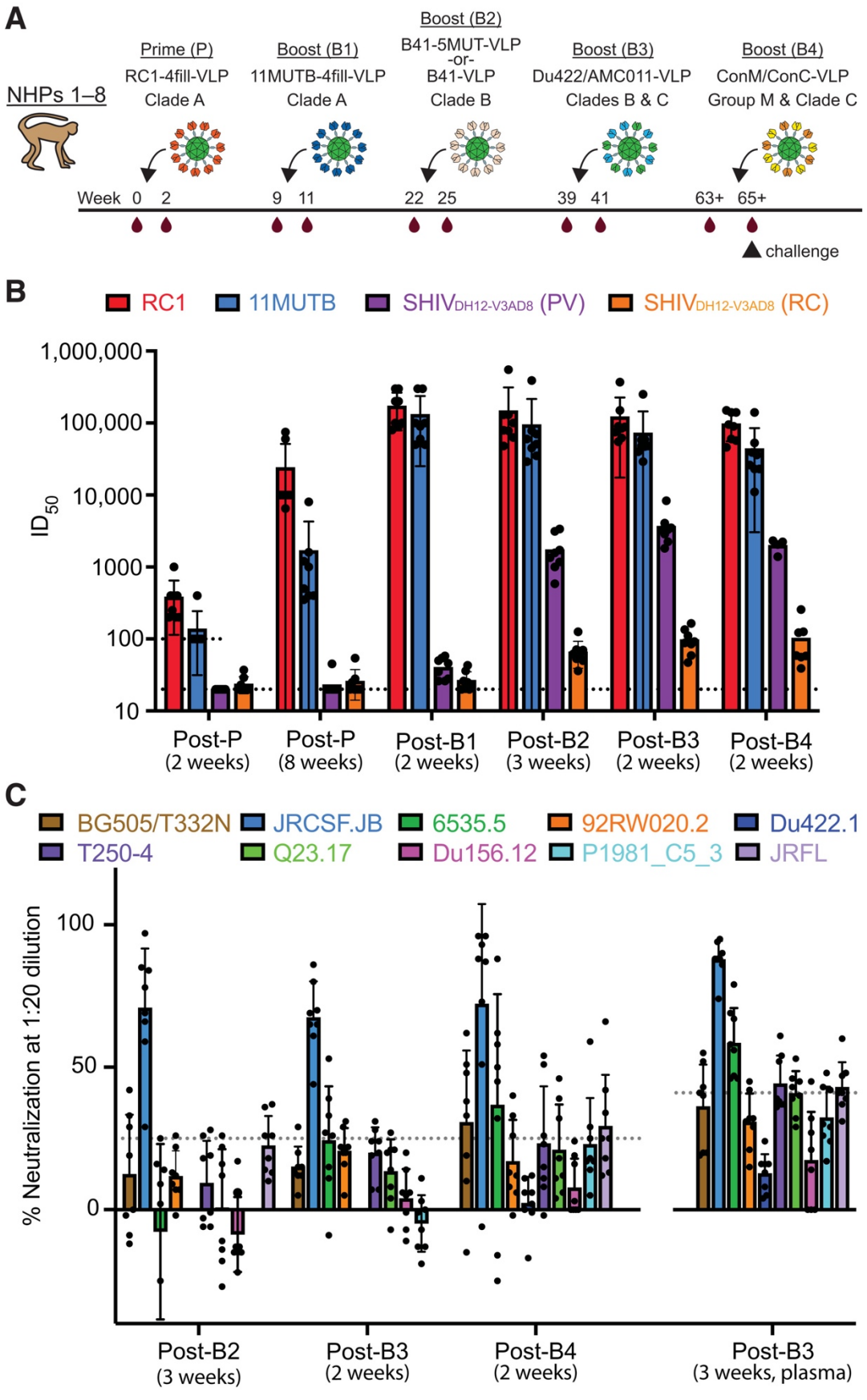
A
Prime (P)
RC1-4fill-VLP
Clade A
Boost (B1)
11MUTB-4fill-VLP
Clade A
Boost (B2)
B41-5MUT-VLP
-or-
B41-VLP
Clade B
Boost (B3)
Du422/AMC011-VLP
Clades B & C
Boost (B4)
ConM/ConC-VLP
Group M & Clade C
NHPs 1–8
Week 0 2 9 11 22 25 39 41 63+ 65+
challenge
B
RC1
11MUTB
SHIVDH12-V3AD8 (PV)
SHIVDH12-V3AD8 (RC)
ID50
1,000,000
100,000
10,000
1000
100
10
Post-P (2 weeks)
Post-P (8 weeks)
Post-B1 (2 weeks)
Post-B2 (3 weeks)
Post-B3 (2 weeks)
Post-B4 (2 weeks)
C
BG505/T332N
JRCSF.JB
6535.5
92RW020.2
Du422.1
T250-4
Q23.17
Du156.12
P1981_C5_3
JRFL
% Neutralization at 1:20 dilution
100
50
0
Post-B2 (3 weeks)
Post-B3 (2 weeks)
Post-B4 (2 weeks)
Post-B3 (3 weeks, plasma)

Figure 1. NHPs were immunized with a prime and four boosts. (**A**) The sequential immunization regimen is shown. NHPs were bled at the indicated times and other times noted in tables S1 and S2. The NHP (NHP 1) used for nsEMPEM (Fig. 2) was immunized with B41-5MUT-VLPs for boost 2. (**B**) ID_{50} values are shown for serum neutralization of viruses at the indicated time points (table S1). Individual dots represent each NHP. The dotted line at 100 indicates the lowest dilution for the 11MUTB and RC1 pseudoviruses (PVs). The dotted line at 20 indicates the lowest dilution for SHIVDH12-V3AD8 PV and replication-competent (RC) viruses. The arithmetic mean for each entry is indicated by the height of the bar, with the standard deviation shown as a vertical line. (**C**) Percent neutralization at a 1:20 dilution is shown against heterologous HIV-1 strains at the indicated time points. Individual dots represent each NHP. Samples are serum except for the 3-week post-B3 sample, which was plasma. Dotted lines indicate the highest background neutralization value for the murine leukemia virus (MuLV) control for serum samples (25%) and plasma samples (41%; post-B3, 3 weeks) (table S2). The arithmetic mean for each entry is indicated by the height of the bar, with the standard deviation shown as a vertical line.

Polyclonal negative-stain EM demonstrated antibody targeting of the V3-glycan patch

We also used negative stain EM-based polyclonal epitope mapping (nsEMPEM)[50, 67] to map the epitopes of elicited antibodies on HIV-1 Envs. In this method, polyclonal Fabs that bind to an antigen are purified from unbound Fabs by size exclusion chromatography (SEC), imaged by electron microscopy (EM), and antibody epitopes are identified in two-dimensional (2D) class averages or 3D classes. A caveat of nsEMPEM is that some antibody epitopes in a polyclonal mixture are not visualized in 2D or 3D classes. For example, nsEMPEM mapping of epitopes in plasmas from coronavirus disease 2019 (COVID-19) convalescent donors revealed less epitope diversity than apparent from single B cell cloning of antibody genes or competition experiments[68]. We therefore refer to the nsEMPEM-visualized epitopes as “predominant” or “primary” epitopes and acknowledge that other epitopes may exist.

After demonstrating that RC1-4fill-VLP priming elicited similar RC1 and 11MUTB pseudotype virus neutralizing responses in rabbits and NHPs (Fig. S2C), we did initial nsEMPEM studies to evaluate polyclonal responses in a rabbit for which we had serum samples in sufficient quantities

for Fab isolations after the same prime/boosting regimen used in NHPs (Fig. 1A, Fig. S2A, and table S3). 3D reconstructions of RC1 bound to polyclonal Fabs derived from rabbit serum after the prime and boosts 1 to 3 showed a primary epitope in the vicinity of the V3-glycan patch of the RC1 trimer after a priming immunization (Fig. 2A), demonstrating targeting of the desired Env epitope. In addition, Fabs that target the base of the trimer were identified in all 2D class averages, with their prevalence gradually increasing after each boost (Fig. 2A and Fig. S3). Trimer base-binding Fabs also appeared in concurrence with the observation of dissociated Env trimers (Figs. S3 and S4A), consistent with observations by others[69]. In contrast to previous EMPEM analyses of serum from BG505-immunized animals[50, 67], we did not observe Fabs binding to the region of the residue 241 "glycan hole" in serum Fab complexes with RC1 Env trimer (Fig. 2, A and B, and Fig. S3). This indicates that the 4fill mutations designed to block access to this site in BG505-derived immunogens[38] prevented detectable elicitation of these types of nonneutralizing antibodies.

We next employed nsEMPEM to evaluate serum from NHP 1 (immunized using the regimen that included B41-5MUT-VLPs as B2) after the prime and the first boost, time points for which we had sufficient NHP serum for Fab isolation. After the prime, we observed V3-targeting Fabs, with few to no detectable base-binding Fabs (Fig. 2B and Fig. S4B). After B1 with 11MUTB-4fill, we observed an increase in Fabs that targeted both the V3 region and the trimer base (Fig. 2B and Fig. S4B). As also observed in the rabbit serum nsEMPEM results, we did not find detectable anti-glycan hole antibodies in 3D reconstructions (Fig. 2B) or 2D class averages of serum Fabs bound to RC1 (Fig. S4B).

It is noteworthy that the nsEMPEM results for the NHP serum Fabs, as well as rabbit serum Fabs, showed a primary epitope in the V3 region (Fig. 2, A to C), demonstrating successful focusing of the anti-Env antibody response to the desired epitope in two different species of immunized wt

animals. Comparison of the binding poses of the V3-directed rabbit and NHP Fabs showed similar V3 targeting, but different orientations of the Fab V_H-V_L domains (Fig. 2C). In addition, the trimer base-binding Fabs observed in serum from NHP 1 exhibited different characteristics than those boosted in the rabbit: the NHP base-binding Fabs adopted a distinct binding orientation compared to the rabbit Fabs and the predominant class appeared to bind three per trimer, versus one per trimer for the rabbit Fabs (Fig. 2, A and B).

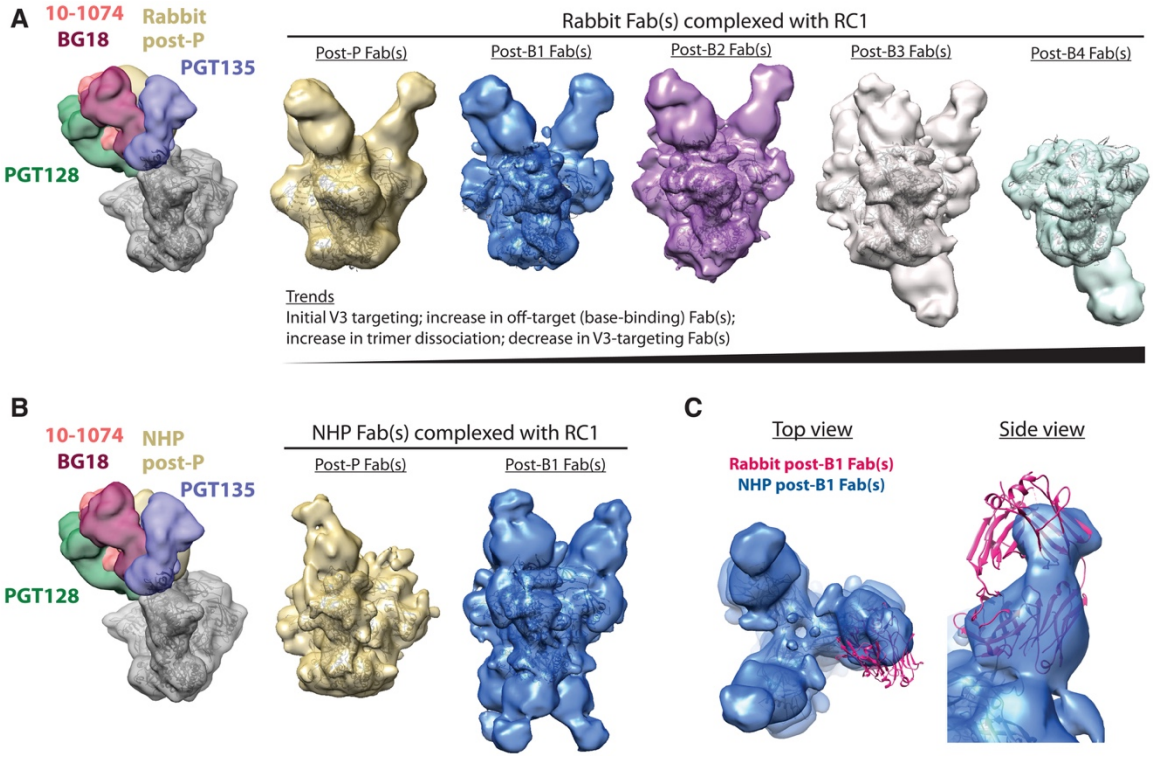

Figure 2. nsEMPEM shows predominant V3 targeting after the prime and initial boosts. (**A**) Left: A low-pass filtered structure of representative HIV-1 SOSIP Env trimer is shown complexed with V3-glycan patch bnAb Fabs (PDB codes: 5T3Z, 6CH8, 5C7K, and 4JM2; colors as indicated) and post-P rabbit Fabs (gold) bound to one Env protomer. Polyclonal Fabs were isolated from Rabbit 2249 (Fig. S2B), which received B41-5MUT-VLPs as B2. Right: 3D reconstructions of Fabs from antibodies isolated from a rabbit 2 weeks after P, B1, B2, B3, and B4 in complex with RC1 are shown. The predominant states for each time point are shown. See also Figs. S3 and S4 for 2D classes, including bottom-binding Fabs after P, B1, and B2 and Fabs bound to dissociated protomers. Coordinates of RC1 (PDB 6ORN) were independently docked into EM density maps. (**B**) Left: A low-pass filtered structure of representative HIV-1 SOSIP Env trimer is shown

complexed with V3-glycan patch bnAb Fabs (colors as indicated) and post-P NHP Fabs (gold) bound to one protomer. Polyclonal Fabs were isolated from NHP 1, which received B41-5MUT-VLPs as B2 (Fig. 1A). Right: 3D reconstructions of Fabs from antibodies isolated from an immunized NHP 2 weeks after P and B1 are shown. See also Fig. S4 for 2D classes showing bottom-binding Fabs. (**C**) Comparison of Fabs binding poses for rabbit and NHP nsEMPEM reconstructions is shown. Rabbit post-B1 Fabs are shown as a pink cartoon of PDB 5UD9 that was docked into the nsEMPEM 3D reconstruction; NHP post-B1 Fabs indicated by the density from the 3D reconstruction.

The binding pose adopted by the rabbit Fabs after the prime was distinct from the binding poses of V3-glycan patch bnAb Fabs and from the poses of mAbs cloned after the RC1-4fill-VLP prime in wt mice ($Ab275_{mur}$) and NHPs ($Ab874_{NHP}$ and $Ab897_{NHP}$) (Fig. 3, A and B)[38]. However, a new cryo-electron microscopy (cryo-EM) structure (Figs. S5 and S6 and table S3) of an RC1 complex with the prime-elicited mAb $Ab1170_{NHP}$[38] showed that the $Ab1170_{NHP}$ Fab matched the rabbit nsEMPEM Fabs binding pose more closely (Fig. 3B), providing a higher-resolution structure resembling the Fabs revealed by nsEMPEM. In addition, although a distinct pose, our previous structure of RC1 complexed with $Ab275_{mur}$ also showed a Fab binding pose more similar to the rabbit Fabs (Fig. 3B).

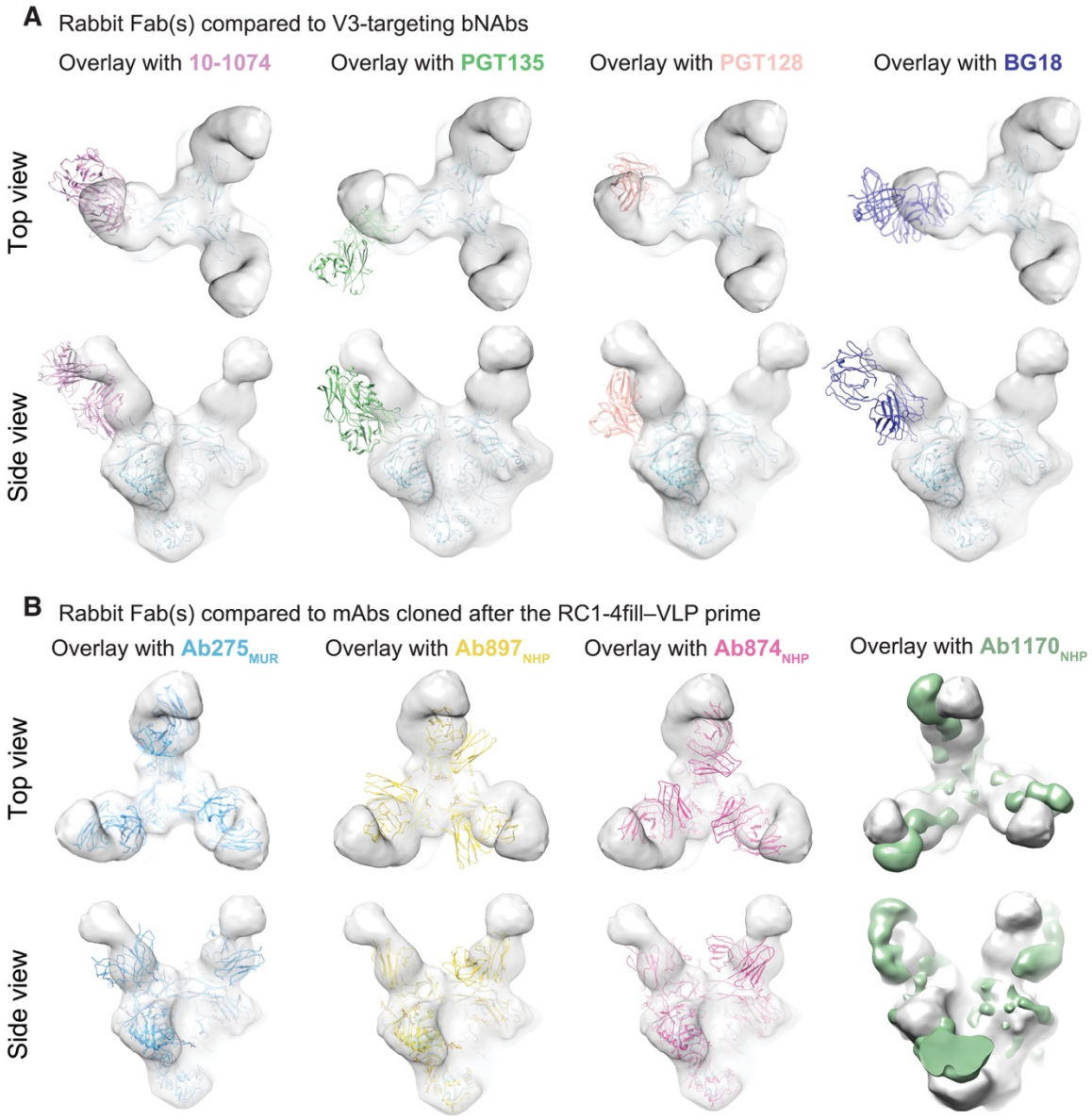

Figure 3. Elicited antibodies adopt binding poses similar to V3 bnAbs. (**A** and **B**) EM density maps for 3D reconstruction of RC1 bound to rabbit Fabs elicited after the RC1-4fill-VLP prime are overlaid with coordinates for the indicated bnAbs (PDB codes 5T3Z, 6CH8, 5C7K, and 4JM2) aligned on Env trimer (A) or overlaid with coordinates for mAbs elicited from a primed wt mouse (Ab275mur; PDB 6ORQ), or a primed NHP (Ab897NHP: PDB 6ORP, Ab874NHP: PDB 6ORO, and Ab1170NHP: this study, shown as an EM density map) (B).

We extended our previous analysis of the $Ab275_{mur}$-RC1 cryo-EM structure [Protein Data Bank (PDB) 6ORQ] to include a comparison with a new structure of RC1 complexed with $Ab283_{mur}$ (Fig.

4A, Fig. S5, and table S3). Ab283$_{mur}$ was isolated after an RC1 prime followed by sequential boosting in a wt mouse. After aligning on the RC1 trimer coordinates of both structures, we observed a shift in the mAb pose in a direction that would better accommodate the gp120 N156 glycan, which was present on the boosting immunogen, but not the priming immunogen (Fig. 4B).

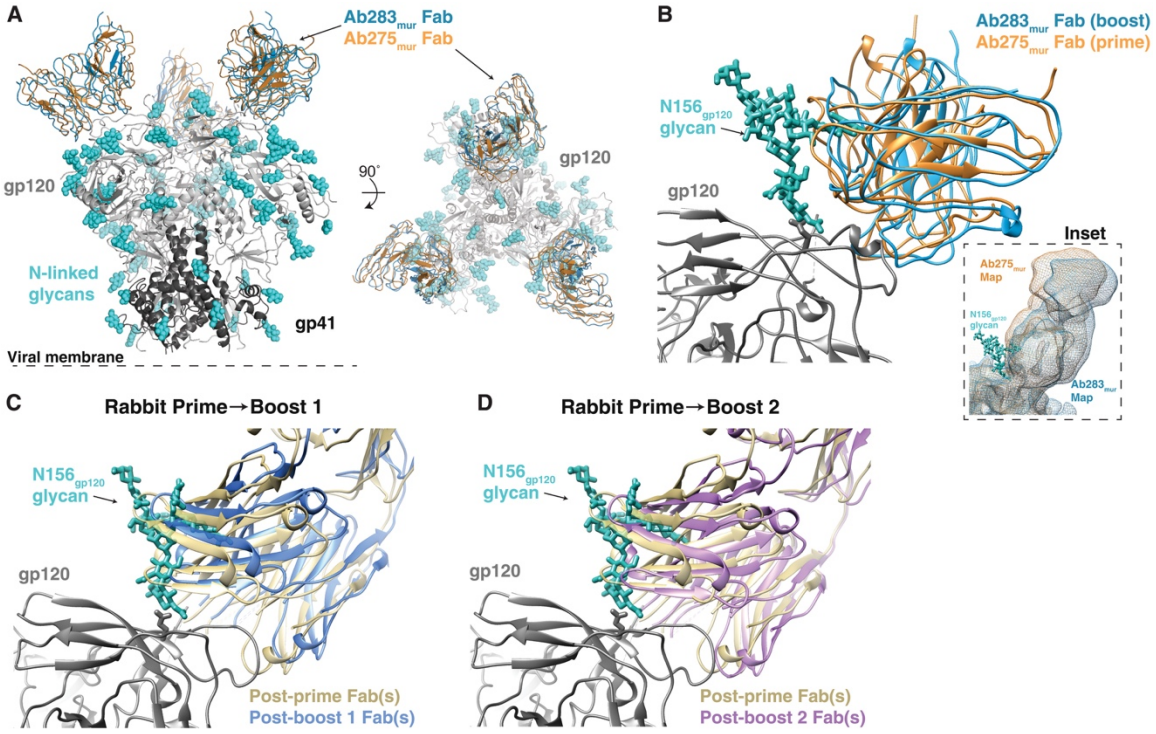

Figure 4. Cryo-EM and nsEMPEM Fab-Env structures show apparent accommodation of gp120 N156 glycan after boosting. (**A**) A comparison of Ab275mur-RC1 (PDB 6ORQ) and Ab283mur-RC1 structures is shown. (**B**) A comparison of binding poses of two mouse monoclonal antibodies, Ab275mur and Ab283mur, isolated from wt mice after a prime only (Ab275mur) or prime plus sequential boost (Ab283mur) is shown. After aligning the Ab283mur-RC1 structure reported here and the Ab275mur-RC1 structure (PDB 6ORQ) on the RC1 coordinates, the pose of Ab283mur was shifted relative to that of Ab275mur in a direction that might better accommodate the gp120 N156 glycan (blue sticks from PDB 5T3X), which was present on boosting immunogens but not the priming immunogen. Inset: Overlay of low-pass filtered single-particle cryo-EM maps of the Fab-RC1 structures. (**C** and **D**) Coordinates docked into Fabs-Env nsEMPEM reconstructions (Fig. 2A) (C3 symmetry constraints applied) were aligned on the RC1 trimer and displayed as a close-up view of the antibody interaction site with the VH-VL domains of the post-P and post-B1 Fabs (C) or the post-P and post-B2 Fabs (D). The post-B1 Fabs and post-B2 Fabs

appear to shift in a direction that might better accommodate the gp120 N156 glycan (blue sticks from PDB 5T3X).

To address whether the V3-targeting Fabs revealed by nsEMPEM after the prime and first two boosts in rabbits also underwent a shift to accommodate the gp120 N156 glycan, we examined the orientations of the Fabs after aligning on RC1 coordinates fit to the trimer densities. Fab coordinates fit to the densities after B1 and B2 (11MUTB-4fill-VLPs and B41-5MUT-VLPs, respectively) indicated a slightly different binding pose relative to the V3-glycan patch compared with the predominant Fabs after the prime, with the Fabs after boosting being translated in a direction that might more easily accommodate the gp120 N156 glycan (Fig. 4, C and D).

We conclude from these structural studies that, as designed, the RC1-4fill-VLP immunogen elicited V3-targeting antibodies. In addition, the initial boosting immunogens elicited antibodies that can better accommodate the gp120 N156 glycan, a potential roadblock in our vaccination regimen. However, the results also demonstrated that the immunization regimen requires further optimization to reduce the elicitation of off-target antibodies that increased upon boosting.

EM of RC1-4fill-VLPs revealed incomplete conjugation and free Env trimers

The observation of increased antibodies against the Env trimer base (Fig. 2, A and B, and Figs. S3 and S4B) after boosting suggested accessibility of the SOSIP base to antibodies. To investigate the mechanism by which antibodies could gain access to the Env base in a covalently coupled VLP in which the trimer base should be inaccessible, we examined SOSIP-coupled VLPs by negative stain EM (nsEM). These imaging studies revealed two relevant findings. First, SpyTagged RC1, but not SpyTagged RC1-4fill, conjugated efficiently to VLPs, as revealed by densities corresponding to closely packed trimers on RC1-VLPs (Fig. S7A, second and third images from left) compared with

the relatively sparse trimer densities for RC1-4fill-VLPs (Fig. S7A, left). Notably, the epitope for the anti-trimer base antibody 12N[47] was not accessible on densely-packed RC1-VLPs (Fig. S7B). As assessed biochemically, with the exception of RC1-4fill, all SpyTagged SOSIP Env trimers, including 11MUTB-4fill, conjugated efficiently to VLPs (Fig. S7C). Thus, the RC1-4fill immunogen trimer exhibited unique undesirable properties compared to the other immunogen-VLPs. Second, although the SEC protocol efficiently separated free SOSIP trimers from VLP-coupled SOSIP trimers when evaluated at relatively small scales (Fig. S7D), the same protocol did not completely isolate free SOSIP trimers when scaled up to make the quantities of SOSIP-VLPs required for NHP and rabbit immunizations (Fig. S7E, black trace). Thus the RC1-4fill-VLPs used for the primes in NHPs and rabbits[38] and the SOSIP-VLPs used for B1 to B3 included free Env trimers in addition to VLP-conjugated trimers. We worked out an alternative SEC protocol for separating SOSIP-VLPs from free trimers in time for B4 (Fig. S7E, red trace). These characterizations revealed two potential reasons to explain the presence of the off-target, anti-trimer base antibodies: (*i*) sparse conjugation of the priming immunogen RC1-4fill and (*ii*) the presence of unconjugated Env trimers in the prime and first three boosts.

Single B cell cloning revealed heterologous weakly neutralizing antibodies with epitopes that competed with V3-glycan patch bnAbs and other bnAbs

Env-specific B cells were isolated using a multibait strategy including Avitagged-biotinylated RC1-glycanKO[38] or an irrelevant, non-HIV-1-based, biotinylated bait and two or three Avitagged-biotinylated SOSIP Env-based baits: RC1, BG505 and B41[20, 70] (Fig. 5). We screened about 30 IgG mAbs produced from these sequences against a panel of seven tier 1 and tier 2 HIV-1 pseudoviruses (Fig. 5A, screening panel), finding nine that neutralized four or more strains (Fig. 5A and table S4). These were further evaluated against 12 strains from a global HIV-1 reference panel (Fig. 5A, 12-strain panel)[71]. Although most of the 50% inhibitory concentrations (IC_{50} values) indicated extremely

low potencies, the nine mAbs showed neutralization breadth across this 19-virus panel. In particular, selected mAbs neutralized the heterologous $SHIV_{DH12\text{-}V3AD8}$ pseudovirus with IC_{50}s of <0.020 μg/ml (Ab1456, Ab1457, Ab1415, and Ab1461); these mAbs also exhibited IC_{50}s of ≤1.1 μg/mL against replication-competent $SHIV_{DH12\text{-}V3AD8}$ (Fig. 5A).

A

	Competed by			10-1074 (V3-glycan patch)							3BNC117 (CD4bs)	
	NHP mAb			Ab1456	Ab1457	Ab1271	Ab1415	Ab1289	Ab1368	Ab1461	Ab1303	Ab1573
	NHP number and ID			NHP 1 DGJI	NHP 1 DGJI	NHP 4 T15	NHP 4 T15	NHP 4 T15	NHP 6 HAA	NHP 1 DGJI	NHP 4 T15	NHP 1 DGJI
	Boost			B3	B3	B3	B3	B3	B3	B3	B3	B4
	Virus	Clade	Tier	IC_{50} (μg/ml)								
Screening	BG505/T332N	A	2	466	>500	28	57	29	61	>500	15	71
	6535.5	B	1	0.72	0.17	0.8	1.5	60	139	1.2	2.3	2.8
	92RW020.2	A	2	76	201	11	66	37	68	347	84	>500
	Du422.1	C	2	>500	>500	298	492	354	>500	>500	>500	>500
	T250-4	AG	2	31	40	13	15	14	50	23	>500	383
	Q23.17	A	1	403	247	33	64	45	52	289	437	>500
	JRCSF	B	2	0.11	0.22	13	0.47	2.2	47	0.26	57	47
12 strain	246F3	AC	2	279	>500	220	294	205	429	447	226	>500
	25710	C	1	>500	>500	49	144	113	160	>500	10	11
	398F1	A	1	68	440	33	46	26	57	113	98	455
	BJOX2000	BC	2	124	108	41	65	53	168	51	2.6	>500
	CE1176	C	2	161	128	35	53	40	109	148	70	>500
	CE0217	C	2	229	>500	114	175	154	190	>500	12	>500
	CH119	BC	2	>500	>500	71	144	93	236	>500	>500	>500
	CNE55	AE	2	>500	>500	328	>500	274	498	>500	492	>500
	CNE8	AE	2	>500	>500	401	>500	454	>500	>500	>500	>500
	TRO11	B	2	>500	93	54	96	65	126	>500	70	>500
	X1632	G	2	1.1	10	6.9	1.6	60	142	1.2	68	173
	X2278	B	2	>500	78	32	26	41	81	>500	40	32
SHIVs	$SHIV_{AD8EO}$ (PV)		2	108	150	198	117	170	367	194	332	>500
	$SHIV_{DH12\text{-}V3AD8}$ (PV)		2	0.014	0.018	0.19	0.041	0.076	11	0.012	13	>50
	$SHIV_{DH12\text{-}V3AD8}$ (RC)		2	0.61	1.1	16	4.0	6.0	75	0.78	222	>500

0.1–9.9 μg/ml | 10–99 μg/ml | 100–500 μg/ml | NN

B

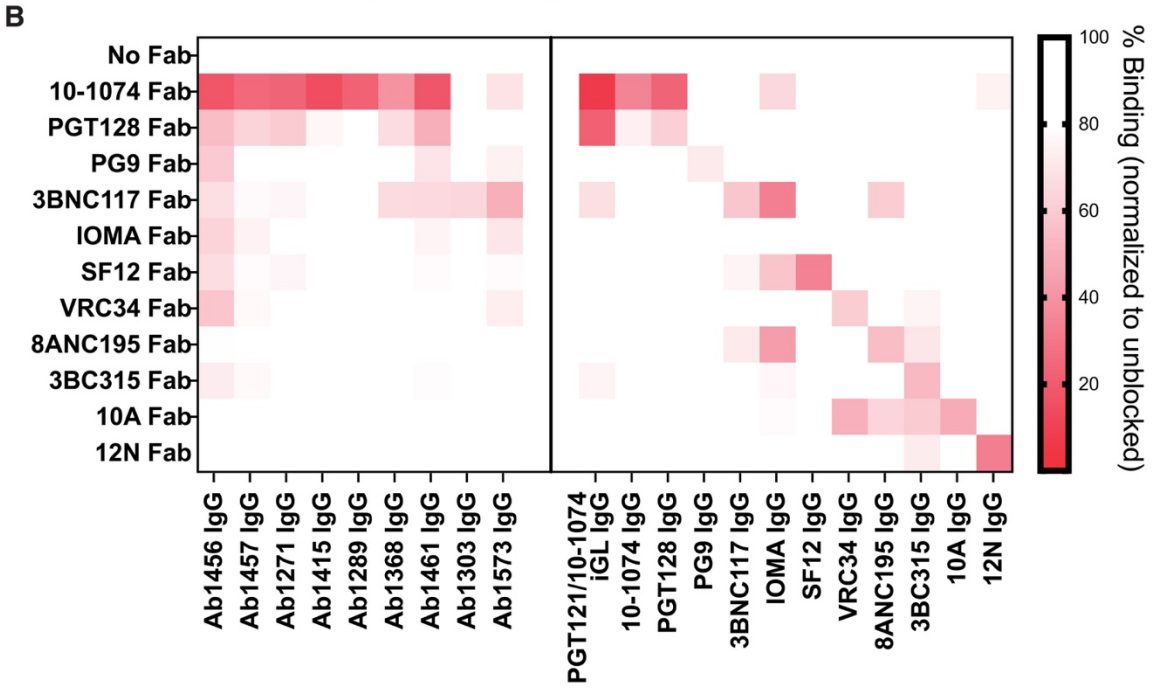

Figure 5. mAbs isolated from prime-boosted NHPs show weak, but heterologous, neutralization and target epitopes that compete with V3-glycan patch bnAbs. (**A**) IC_{50} values against the indicated pseudoviruses are shown for nine selected mAbs cloned from immunized

NHPs for neutralization. NN, non-neutralizing. **(B)** The heatmap shows results of competition ELISAs to map epitopes of mAbs derived from immunized NHPs. Results represent one experiment of two independent replicates. Randomly biotinylated RC1 was bound to a Streptavidin ELISA plate. Each well was then incubated with a potential competitor Fab for 2 hours and then an IgG was added. Bound IgG was detected using an anti-Fc antiserum. The percent binding observed after addition of a competitor Fab was normalized to the binding in the absence of a competitor Fab. NHP IgG results are shown on the left; control bnAb or non-neutralizing IgG antibody (10A and 12N) results are shown on the right.

To map epitope(s) recognized by the NHP mAbs, we adapted the competition ELISA for mAb epitope mapping. For these experiments, we incubated immobilized RC1 with a Fab from a potential competitor mAb and then probed with an NHP IgG or control IgG (Fig. 5B). We used the same competitor Fabs and control IgG antibodies as in the serum competition assay with the addition of PGT121/10-1074 iGL, the iGL sequence for the PGT121 and 10-1074 V3-glycan patch bnAbs[28], and the substitution of PG9[58] as the representative V1V2 bnAb.

Results from the competition ELISA (Fig. 5B) mapped seven mAbs (Ab1456, Ab1457, Ab1271, Ab1415, Ab1289, Ab1368, and Ab1461) as targeting epitopes on Env that were blocked by the V3-glycan patch bnAbs 10-1074 and PGT128[28, 39] and two mAbs (Ab1303 and Ab1573) as targeting a CD4bs epitope blocked by 3BNC117 (Fig. 5B)[26]. Verification of the competition ELISA methodology was provided by experiments using control bnAbs targeting known HIV-1 Env epitopes (Fig. 5B). Although its epitope was not intentionally targeted in our prime-boost protocol, the CD4bs Ab1303 exhibited neutralization activity against almost every strain it was tested against (Fig. 5A), demonstrating that our prime-boost regimen elicited neutralizing antibodies against more than one epitope on HIV-1 Env.

SHIV infection was observed after challenge in seven of eight of immunized NHPs

Using a "high-dose" challenge regimen (Fig. 6A), four immunized macaques (NHPs 1 to 4) were challenged a single time intrarectally (IR) with 1000 median tissue culture infectious dose ($TCID_{50}$) of $SHIV_{DH12\text{-}V3AD8}$ and three of the four became infected (Fig. 6B), including NHP 4 (T15), which had generated the highest antivirus neutralization titers against $SHIV_{DH12\text{-}V3AD8}$ (1:9953) after the fourth boost in the pseudotyped virus assay (table S1). By contrast, NHP 1 (DGJI), which did not become infected after the challenge, showed the lowest $SHIV_{DH12\text{-}V3AD8}$ pseudovirus neutralization titers (1:1687) of the four animals. The other four immunized macaques (NHPs 5 to 8) were inoculated using a repeated low-dose (RLD; 10 $TCID_{50}$) challenge regimen. In this case, the immunized monkeys (pseudovirus $SHIV_{DH12\text{-}V3AD8}$ titers ranging from 1:1393 to 1:2314; table S1) and control monkeys both rapidly became infected (median times = 5.5 and 5.2 weeks, respectively) (Fig. 6C), indicating no protection as a result of vaccination.

A

Animal number and ID		Contains soluble Env trimer: Prime (P) Day 0	Boost (B1) Week 9	Boost (B2) Week 22	Boost (B3) Week 39	Boost (B4) Week 63	Challenge IR (single high dose) Week 65
1	DGJI	RC1-4fill-VLP	11MUTB-4fill-VLP	B41-5MUT-VLP	DU422/AMC011-VLP	ConM/ConC-VLP	√
2	DGPE	RC1-4fill-VLP	11MUTB-4fill-VLP	B41-5MUT-VLP	DU422/AMC011-VLP	ConM/ConC-VLP	√
3	T10	RC1-4fill-VLP	11MUTB-4fill-VLP	B41-WT-VLP	DU422/AMC011-VLP	ConM/ConC-VLP	√
4	T15	RC1-4fill-VLP	11MUTB-4fill-VLP	B41-WT-VLP	DU422/AMC011-VLP	ConM/ConC-VLP	√
Animal number and ID		Prime (P) Day 0	Boost (B1) Week 9	Boost (B2) Week 22	Boost (B3) Week 39	Boost (B4) Week 63	Challenge IR (RLD) weekly Starting week 71
5	DGNB	RC1-4fill-VLP	11MUTB-4fill-VLP	B41-5MUT-VLP	DU422/AMC011-VLP	ConM/ConC-VLP	√
6	HAA	RC1-4fill-VLP	11MUTB-4fill-VLP	B41-5MUT-VLP	DU422/AMC011-VLP	ConM/ConC-VLP	√
7	DGMK	RC1-4fill-VLP	11MUTB-4fill-VLP	B41-WT-VLP	DU422/AMC011-VLP	ConM/ConC-VLP	√
8	HMK	RC1-4fill-VLP	11MUTB-4fill-VLP	B41-WT-VLP	DU422/AMC011-VLP	ConM/ConC-VLP	√

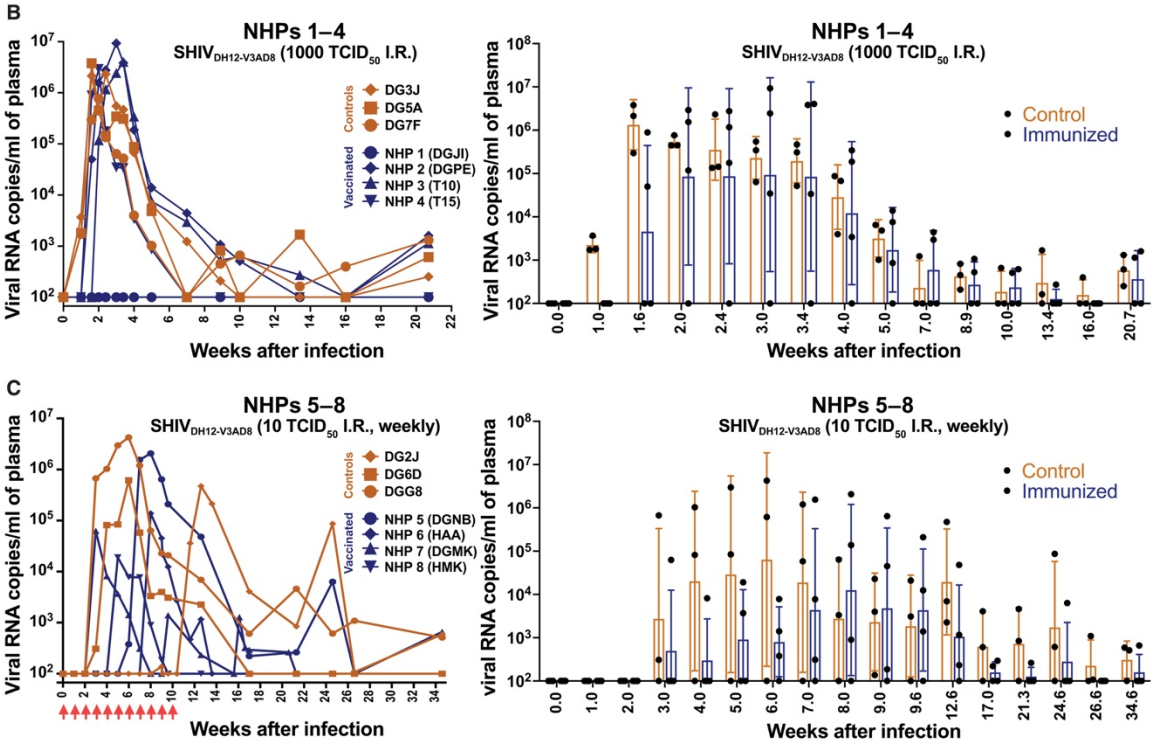

Figure 6. Immunization conferred minimal protection against intrarectal challenge of a heterologous SHIV in NHPs. (**A**) The schedule for prime, boosting, and SHIV$_{DH12-V3AD8}$ challenge for NHPs is shown, including NHP numbers and IDs. (**B**) Left: Plasma viral loads are shown for macaques challenged intrarectally with a single high dose (1000 TCID$_{50}$) of SHIV$_{DH12-V3AD8}$ 2 weeks after receiving the final boost. Controls are shown in orange and immunized animals are shown in blue. Right: A comparison of viral loads in control versus immunized NHPs is shown as a function of time after infection presented as geometric means with standard deviations. Values for individual NHPs are shown as dots. (**C**) Left: Plasma viral loads are shown for macaques challenged intrarectally with repeated low doses (10 TCID$_{50}$) of SHIV$_{DH12-V3AD8}$ weekly, beginning 2 weeks after the final boost. Controls are shown in orange and immunized animals are shown in blue. Right: A comparison of viral loads in control versus immunized NHPs is shown as a function

of time after infection presented as geometric means with standard deviations. Values for individual NHPs are shown as dots. Time points were plotted when all animals were tested.

The results of minimal to no protection in SHIV-challenged animals can be evaluated with reference to in vitro neutralization assay results. When pseudotyped $SHIV_{DH12\text{-}V3AD8}$ was used to monitor neutralization activity in the serum of the immunized macaques at the time of virus challenge, neutralization titers were measured in the 1:1393 to 1:9953 range (table S1). By contrast, against replication-competent virus, the titers were much lower (1:39 to 1:256) (table S1). Similarly, high neutralization titers were observed against pseudotyped $SHIV_{SF162.LS}$, but not against replication-competent SF162P3 (table S1). Last, no neutralization activity was detected against the highly pathogenic $SHIV_{AD8EO}$[64], even in an assay using a pseudovirus readout (table S1). Thus, the prime-boost immunization regimen did not achieve protection from SHIV challenge, despite high titers against the heterologous $SHIV_{DH12\text{-}V3AD8}$ in the in vitro pseudovirus assay.

This lack of protection after immunization contrasts with previously reported results obtained after the administration of bnAbs to macaques before high-dose challenges with $SHIV_{DH12\text{-}V3AD8}$[63]. On the day of challenge, two animals that received the V3-glycan patch bnAb 10-1074[28] generated serum neutralization titers in pseudovirus assays of 1:420 and 1:376, respectively, and both were protected from infection. Similarly, two monkeys that were administered the CD4-binding site bnAb 3BNC117[26] produced neutralization titers in pseudovirus assays of 1:143 and 1:142, respectively, and also resisted $SHIV_{DH12\text{-}V3AD8}$ infection[63]. Although the vaccine regimen used in our study generated much higher polyclonal neutralizing titers against $SHIV_{DH12\text{-}V3AD8}$ (table S1), it failed to prevent infection in all but one of eight NHPs. We also note that serum neutralization titers against BG505 pseudovirus elicited in BG505-vaccinated NHPs that were protected against autologous BG505 SHIV challenge[72, 73] were much lower than the $SHIV_{DH12\text{-}V3AD8}$ titers measured

here. However, it should be noted that the autologous neutralizing antibody response to BG505 largely consists of antibodies directed against the glycan hole in the vicinity of gp120 residue 241[47, 50, 67]. Thus, the autologous anti-BG505 neutralizing antibodies, like the administered bnAbs, appear to protect at lower potencies than the more heterogeneous responses (Fig. 5A) produced after the vaccination regimen described here. Achieving protection from heterologous SHIV challenge will likely require higher neutralizing titers, measured using replication-competent virus, than exhibited in bnAb-administered or autologously vaccinated NHPs.

Discussion

To date, no HIV-1 vaccination protocol designed to elicit neutralizing antibodies has elicited protective serum responses against heterologous HIV-1 or SHIV challenge in animals with a polyclonal antibody repertoire. Here, we report strategies that elicited consistent, although weakly, heterologous neutralizing serum (all immunized NHPs) and mAbs (from representative NHPs). A main hurdle in the elicitation of bnAbs by immunization in wt animals with polyclonal antibody repertoires is the activation and expansion of distracting antibody responses that target nonconserved epitopes of Env. Immunization experiments in rabbits and NHPs have shown that holes in the Env glycan shield, the base of the trimer, and epitopes exposed upon trimer dissociation into protomers represent distracting, nonneutralizing epitopes elicited by SOSIP Env trimers[47, 50, 67]. Moreover, additional interference to the bnAb development process may come from antibody responses to conserved epitopes of Env that show poor potential to become bnAbs[21, 22]. The design of Env immunogens and immunization strategies to focus the antibody responses to conserved epitopes of Env while preventing off-target responses is crucial for the success of a vaccine protocol in humans.

In this study, we aimed to focus the antibody responses to conserved epitopes of Env by using a series of engineered SOSIP Env trimers followed by native-like SOSIPs in an attempt to gradually induce the maturation of bnAb precursors as previously reported in knock-in mice[23, 74]. To mask potentially immunodominant and distracting regions of Env, we introduced extra potential N-linked glycans to the glycan shields of the immunogens and conjugated them to VLPs. To minimize boosting of antibody responses to HIV-1 strain-specific epitopes, we used a series of multiclade Env immunogens derived from different HIV-1 strains that we conjugated individually or in combinations to VLPs.

Both nsEMPEM and competition ELISA analyses suggest that the predominant antibodies elicited in rabbits and NHPs, both representing animals with polyclonal repertoires, bind an epitope at or near the V3-glycan patch, as targeted by our immunogen. Although these results are encouraging, both methods of analysis include caveats related to their interpretation. For nsEMPEM, kinetic and affinity properties of the polyclonal Fabs can influence which Fab-Env complexes are observed. Kinetic and affinity differences could also affect results of competition ELISAs. In addition, a specific mAb used as competitor against a particular epitope, such as the trimer base, may not block all antibodies in that class, and the competitor mAbs do not cover all possible Env epitopes. With these caveats, our results showed that our immunogen design was successful at primarily recruiting antibodies against the desired region of Env in wt animals despite the many neutralizing and non-neutralizing epitopes on HIV-1 Env, a more difficult endeavor compared with previous studies that used modified animals expressing the relevant germline B cell receptor[23, 74]. This is in contrast to structural studies of animals immunized with BG505, which predominantly developed antibodies against non-conserved epitopes and did not consistently elicit antibodies with breadth and potency against heterologous Envs[75]. In addition, our results showed slight differences in the orientation of Fabs observed by nsEMPEM after the prime and first boosts that were consistent with

accommodating the gp120 N156 glycan (which had been removed in our priming immunogen), consistent with higher-resolution cryo-EM structures of Env trimers bound to prime and boost mouse mAbs and with serum neutralization data demonstrating potent neutralization of both RC1 and 11MUTB pseudoviruses as well as weaker, but relatively broad, neutralization of a diverse panel of HIV-1 strains. Thus, our prime-boost strategy elicited antibodies that targeted the desired epitope and exhibited neutralization of heterologous strains.

We previously reported cryo-EM structures of mAbs cloned from primed NHPs and wt mice complexed with RC1, revealing recognition of the V3-glycan patch[38]. A recent report suggested that the Env interactions of two of our prime-elicited NHP mAbs, $Ab874_{NHP}$ and $Ab897_{NHP}$, resembled those of 43A, a nonneutralizing V1/V3 antibody identified from a rabbit immunized with soluble BG505 SOSIP.664[76], suggesting that antibodies induced by RC1-4fill-VLP could not mature to become neutralizing. However, table S2 of that paper[76] showed more $Ab874_{NHP}$ and $Ab897_{NHP}$ interactions with residues within the conserved V3-glycan patch GDIR motif and fewer interactions with V1 as compared with 43A, implying that the NHP antibodies elicited after priming with RC1-4fill-VLPs could represent a different class than the nonneutralizing 43A antibody. In addition, $Ab874_{NHP}$ (and $Ab1170_{NHP}$) showed interactions with the gp120 N332 glycan, another desirable property for a bnAb precursor that targets the V3-glycan patch.

Here, we demonstrated that at least a subset of the antibodies induced after a RC1-4fill-VLP prime[38] did mature to become neutralizing, both with respect to polyclonal serum neutralization and as individual mAbs isolated after boosting. Indeed, all three NHPs from which mAbs were isolated produced neutralizing antibodies that showed V3-glycan patch targeting. Although the observed antibody potencies were weak compared with human donor-derived bnAb potencies, the induced responses were heterologously neutralizing, including neutralization of strains representing the

global HIV-1 pandemic[71], suggesting that these mAbs recognize a conserved epitope on HIV-1 Env. It is also noteworthy that nsEMPEM showed that the RC1-4fill and subsequent boosting immunogens induced predominant responses that mapped to the Env trimer at the targeted epitope, at or near the V3-glycan patch. Because V3-glycan patch bnAbs adopt different poses, a successful V3-glycan patch immunogen need not elicit antibodies that bind the V3 region of Env in the same way as known V3-glycan patch bnAbs. Our results suggest it is possible to elicit different classes of V3-targeting bnAbs using an RC1-based immunogen, which is potentially a more desirable property in a vaccine than inducing antibodies derived from only one V gene segment lineage.

Although the elicited antibodies were at least partially specific for the V3-glycan patch, nsEMPEM demonstrated that our boosting regimen needs further optimization to minimize off-target responses. In particular, we observed increased antibodies against nonneutralizing epitope(s) at the Env trimer base after repeated boosts and the presence of dissociated Env trimers. Biochemical and biophysical characterization of our immunogen nanoparticles indicated that improved purification methods can be used to ensure that the immunization does not include free Env trimer to prevent access to the trimer base. In addition, off-target responses to the Env base might be eliminated by using a modified version of RC1-4fill that conjugates efficiently to SpyCatcher nanoparticles (RC1-3fill, with one fewer introduced PNGS in the vicinity of the glycan hole in BG505). Last, immunogens could incorporate mutations to prevent trimers from dissociating into protomers that will induce off-target nonneutralizing antibodies, such as SOSIPs with introduced disulfide bonds (DS-SOSIPs)[77, 78].

The analysis of the neutralization activity elicited by our sequential immunization protocol revealed an important caveat in the preclinical methods commonly used to evaluate vaccine candidates. We observed a discrepancy between the serum neutralization activity in assays involving pseudoviruses

versus replication-competent viruses, with the activity against the latter being lower. These results are in agreement with previous observations showing higher IC_{50} values for antibodies against peripheral blood mononuclear cell (PBMC)-derived HIV-1 viruses compared with pseudoviruses produced in human embryonic kidney (HEK) cells[72, 79, 80, 81, 82] and with the finding that differences in the cells used to produce viruses can affect the virus' neutralization sensitivities[79].

A recent study demonstrated that comparable or lower pseudovirus antibody titers to those seen in our study provided protective responses in NHPs[72]; however, the animals in those studies were challenged with a BG505 SHIV that was autologous to the BG505 immunogen. Comparison of our results with those studies suggests that protection from heterologous HIV-1 or SHIV infection will require higher in vitro neutralization potencies than exhibited by the heterologously neutralizing antibodies elicited in our study. For example, recent clinical trials to evaluate bnAb-mediated protection from HIV-1 infection in humans demonstrated a lack of protection from infection by HIV-1 strains against which the administered bnAb VRC01 exhibited weak in vitro potencies (HVTN 704/HPTN 085 and HVTN 703/HPTN 081). This finding, when considered in combination with our results and with studies of the limited ability of weakly neutralizing anti-HIV-1 bnAbs to delay viral rebound after cessation of antiretroviral therapy[83], suggests that high titers of broadly-active serum neutralizing activity will be required for a protective vaccine against HIV-1. As a potential way around an absolute requirement for eliciting highly potent neutralizing antibody activity for protection after vaccination, a recent study evaluating protection from an autologous SHIV challenge in BG505-immunized NHPs showed that low serum neutralizing titers (<1:300 in a pseudovirus assay) were sufficient for protection when anti-Gag T cell responses were simultaneously induced[73]. Thus, even weakly neutralizing antibody responses, if sufficiently broad, might be protective if combined with an optimal T cell-inducing vaccination regimen.

As discussed above, our study has several limitations including the use of immunogens that allow off-target antibody elicitation. Thus, other vaccination regimes may further improve neutralization activity. For example, future efforts to use immunogens designed to target two or more epitopes could be beneficial to prevent resistance to antibodies against a single Env epitope, a strategy that should be possible by vaccination because antibodies are elicited against multiple epitopes on HIV-1 Env during natural infection[18, 40, 84, 85, 86]. Our results combined with other studies suggest that using prime and boost immunogens targeting multiple epitopes that circumvent the problems identified in this study in a sequential vaccination strategy, perhaps in combination with T cell-inducing immunization regimens, may elicit protective immune responses against HIV-1 infection.

Methods

Study Design

The objective of this study was to investigate whether an immunization regimen with RC1 as a priming immunogen can elicit anti-HIV bnAbs and protect against heterologous SHIV challenge in NHPs. RC1 was selected as a prime based on a previous study[38], which demonstrated RC1 could elicit antibody precursors to the V3 epitope in both wild-type mice and NHPs. NHPs (n=8) were primed and boosted four times and serum isolated after each immunization was tested for neutralization against a panel of HIV and SHIV strains. We used ELISAs and nsEMPEM to map the epitopes of elicited antibodies on HIV-1 Envs and single-cell sorting of antigen-positive memory B cells from immunized macaques identified multiple mAbs that demonstrated breadth and potency against a panel of heterologous HIV strains, including the challenge strain $SHIV_{DH12\text{-}V3AD8}$. Two of these mAbs were then structurally characterized using cryo-EM, which revealed their mode of binding to HIV-1 Env. Following immunization, NHPs were challenged with high-dose rectal challenge (n=4) or repeated low-dose rectal challenge (n=4) and viral loads were assessed

over 21 to 35 weeks. The study was not blinded and all data were included except where specified in the text or figure legends. All NHP experiments were carried out in strict accordance with the recommendations in the Guide for the Care and Use of Laboratory Animals of the National Institutes of Health.

Immunogen expression and purification

Env immunogens were expressed as soluble SOSIP.664 native-like gp140 trimers[43] as described[38]. For SpyTagged trimers, a C-terminal SpyTag sequence (13 residues) was added to allow formation of an irreversible isopeptide bond to SpyCatcher protein[49]. We also produced AviTagged BG505 and clade B B41 SOSIPS for B cell sorting experiments, and untagged and SpyTagged versions of 11MUTB-4fill (a version of the BG505-related 11MUTB SOSIP[42] containing PNGSs to add glycans to gp120 positions N230, N241, N289, and N344), B41-5MUT (a B41 version of the BG505-related 5MUT SOSIP[42] including a PNGS at gp120 position 289, B41wt (a B41 SOSIP with an introduced PNGS at position 289), clade C Du422, clade B AMC011 with an introduced PNGS at gp120 position 230, consensus C SOSIP (ConC)[56], and a consensus M SOSIP (ConM)[55]. Amino acid sequences of SpyTagged SOSIP immunogens are shown in table S5.

Soluble SOSIP Envs were expressed by transient transfection in HEK293-6E cells (National Research Council of Canada) or Expi293 cells (Life Technologies) and purified from transfected cell supernatants by 2G12 or NIH45-46 immunoaffinity chromatography and size exclusion chromatography (SEC) as described[87]. Soluble Envs were stored at 4°C in 20 mM Tris pH 8.0, and 150 mM sodium chloride (TBS) (untagged and AviTagged versions) or 20 mM sodium phosphate pH 7.5, 150 mM NaCl (PBS) (SpyTagged versions).

VLP preparation and conjugation

SpyCatcher-AP205 VLPs were expressed in bacteria and purified as described[48, 88]. SpyTagged SOSIP immunogens were incubated at a 2 to 3–fold molar excess with SpyCatcher-VLPs for 12 to 24 hours at room temperature in phosphate-buffered saline (PBS). Conjugated VLPs were separated from free Env trimers by SEC on a Superdex 200 (Fig. S7D) or Superose 6 (Fig. S7E) column. Conjugation of Env trimers was verified by SDS-PAGE (Fig. S7C). Immunogen concentrations for immunizations were estimated by comparing to known amounts of the analogous unconjugated Env trimer on an SDS-PAGE gel.

Conjugated VLPs were examined by nsEM (Fig. S7A and D). Purified VLPs were diluted to about 10 μg/mL immediately before adding 3 μL to a glow-discharged ultrathin C film on a holey carbon support film, 400 mesh, Cu grid (Ted Pella). After blotting, the grids were stained by uranyl acetate and then imaged using a FEI Tecnai T12 transmission electron microscope operating at 120 keV with a Gatan Ultrascan 2k × 2k CCD camera. Each image was collected using a 1 second exposure at about 2 μm defocus and 42,000× magnification, resulting in 2.5 Å per pixel.

SPR binding studies

SPR experiments were performed using a T200 (Biacore). To determine if the Env trimer base was accessible for antibody binding on a densely-conjugated VLP, we covalently immobilized 12N IgG[47] on a CM5 chip using primary amine chemistry according to manufacturer's instructions to a coupling density of about 3000 resonance units (RUs). 0.1 mg/mL RC1 SOSIP or 0.1 mg/mL RC1-VLPs (based on SOSIP concentration) were then injected at a flow rate of 30μL/min for 60 seconds, followed by monitoring of the dissociation phase for 300 seconds. Flow cells were regenerated with 10 mM glycine pH 3.0 at a flow rate of 90 μl/min. Sensorgrams were processed and plotted using the Biacore Evaluation Software.

Animal immunizations

Eight rhesus macaques (*Macaca mulatta*) of Indian genetic origin, two-to-four years of age, were housed in a biosafety level 2 NIAID facility and cared for in accordance with Guide for Care and Use of Laboratory Animals Report number NIH 82-53 (Department of Health and Human Services, Bethesda, 1985). All animal procedures and experiments were performed according to protocols approved by the IACUC of NIAID, NIH. The NHPs used in this study did not express the MHC class I Mamu-A*01, Mamu-B*08 and Mamu-B*17 alleles. NHPs were immunized subcutaneously in the medial inner forelegs and hind legs (total of 4 sites per animal) with approximately 100 μg of the indicated SOSIP-VLPs adjuvated in IscoMPLA (375 U/animal) as described[38]. Animals were immunized and blood samples were drawn from naïve and immunized macaques at the time points indicated in Fig. 1A, tables S1 and S2, and Fig. 6. Blood samples were processed to serum or plasma by centrifugation in serum separating tubes or EDTA-treated tubes, respectively. Serum and plasma samples were frozen and stored at -80ºC. Lymph node biopsies for single B cell cloning were obtained after boost 3 and boost 4 (Fig. 1A).

Four six-month-old New Zealand White rabbits (Covance) were used for immunizations. Rabbits were immunized subcutaneously with ~22 μg of a SOSIP-VLP in an ISCOMs-like saponin adjuvant as described[38, 89]. Blood from immunized rabbits was collected from the medial ear artery on weeks 0 and 2 following immunization (test and production bleeds) or the jugular vein/carotid artery after the final boost (terminal exsanguination) by Covance. Serum was processed by Covance laboratory technicians by centrifugation in serum separating tubes and shipped frozen. Procedures in rabbits were approved by the Denver PA IACUC Committee.

In vitro neutralization assays

RC1 and 11MUTB pseudoviruses were generated by transfection of HEK293 cells with a codon-optimized gp160 construct containing RC1[38] or 11MUTB[42] mutations in gp120 and a wild-type BG505 gp41 as previously described[51, 90]. Pseudovirus neutralization assays were conducted using TZM-bl reporter cells as described[51, 90], either in house (table S1) or at the Collaboration for AIDS Vaccine Discovery (CAVD) core neutralization facility (table S2, Fig. 5A). IgG mAbs were evaluated in duplicate with an 8-point, 5-fold dilution series starting at a top concentration of 500 μg/mL. RC1 and 11MUTB pseudovirus assays were repeated at least twice for each value reported in table S1. For polyclonal neutralizations, serum or plasma samples were heat inactivated at 56 ºC for 1 hour before being added to the neutralization assays, and then neutralization was evaluated in duplicate with an 8-point, 4-fold dilution series starting at a dilution of 1:20 (heterologous strains) or 1:100 (RC1 and 11MUTB strains). The dilution at which 50% of virus was neutralized (ID_{50}) and the percent of neutralization at a 1:20 dilution (% 1:20) are reported (table S2). The panel of global HIV-1 Env reference clones were obtained through the NIH HIV Reagent Program (ARP-12670) as contributed by Dr. David Montefiori.

For neutralization assays to evaluate NHP serum for neutralization against SHIVs, we used two types of assays[91]: (i) a TZM-bl entry assay with a pseudotyped $SHIV_{DH12\text{-}V3AD8}$ and (ii) a TZM-bl infection assay using replication-competent $SHIV_{DH12\text{-}V3AD8}$ virus. The pseudotyped virus expressed the $SHIV_{DH12\text{-}V3AD8}$ Env was conducted as described above. The replication-competent $SHIV_{DH12\text{-}V3AD8}$ virus was made as described[63, 92] by first transfecting HEK293T cells with $SHIV_{DH12\text{-}V3AD8}$ cloned DNA, infecting rhesus PBMCs with the transfected HEK293T cell supernatant, and then collecting the infected rhesus PBMC cell supernatant at 48 hours as the SHIV DH12-V3AD8 replication competent virus stock. For replication-competent virus assays, the protease inhibitor,

indinavir (Merck), was added to the medium (final concentration of 1 μM) to prevent a second round of viral replication.

Isolation and purification of rabbit and NHP polyclonal IgG antibodies

Rabbit and NHP polyclonal IgG antibodies were purified from serum samples using 5-mL HiTrap MabSelect SuRe columns (Cytiva). Serum samples were diluted 10-fold with cold PBS, and applied to prepacked columns at 1 mL/min. Bound IgG antibodies were washed with 5 column volumes PBS and eluted with 5 column volumes 0.1M glycine pH 3.0, 100 mM NaCl. Samples were then immediately neutralized with 2M Tris-HCl, pH 8. To produce polyclonal Fab fragments, IgG antibodies were buffer exchanged into PBS and cleaved by papain digestion using activated crystallized papain (Sigma-Aldrich) for 30 to 60 min at 37°C at a 1:100 enzyme:IgG ratio. To remove undigested IgG antibodies and Fc fragments, digested products were applied to a 1 mL HiTrap MabSelect SuRe column (Cytiva) and the flowthrough containing cleaved Fabs was collected. Fabs were further purified by SEC using a Superdex 200 Increase 10/300 column (GE Healthcare Life Sciences) in TBS, before concentrating and storage at 4°C.

nsEMPEM data collection and processing

nsEMPEM methods were adapted from[50, 67]. Polyclonal rabbit Fab-Env complexes were formed by incubating 25 μg of a SOSIP.664 trimer with 2-3 mg of polyclonal Fabs in 100 μL total volume either overnight (post-Prime and post-boost 1) or for 30 minutes (all others) at room temperature. NHP Fab-Env complexes were formed by incubating 12.5 μg of Env SOSIP.664 trimers with 1.25 mg of polyclonal Fabs in 50 μL total volume for 30 minutes at room temperature. Fab-Env complexes were purified by SEC on a Superose 6 increase 10/300 GL column (Cytiva). Fractions containing complexes were pooled and concentrated to 5 to 10 μg/mL before deposition on a freshly

glow-discharged 300 mesh carbon-coated copper grid (Ted Pella) and stained with 1.5% (w/v) uranyl formate (Electron Microscopy Sciences).

All Fab-Env complexes were imaged on a 200 kV Talos Arctica transmission electron microscope (Thermo Fisher Scientific) operating at room temperature, equipped with a K3 direct electron detector (Gatan) using SerialEM 3.7[93], except for the Rabbit 2249 RC1-post-Prime complex, which was imaged on a 120 kV Tecnai T12 equipped with a CCD camera. Images were processed in cryoSPARC v 2.14, and a reference-free particle stack was generated using a Gaussian blob picker[94] or by EMAN2[95] for the rabbit post-boost 4 – RC1 dataset. Particles corresponding to Fab-Env complexes were identified by iterative rounds of 2D classification. 2D class averages that displayed structural elements interpreted as Fabs bound to an intact Env trimer or dissociated gp140 protomer were selected for further 2D and 3D classification. Ab initio models generated in cryoSPARC were either reported directly or used for heterogeneous or homogenous refinement. Figures were prepared using UCSF Chimera[96, 97], and Fabs were highlighted in selected 2D classes using IMOD[98].

Isolation of mAbs from immunized NHPs

Single HIV-1 Env-specific B cells were isolated from NHP lymph nodes from lymph nodes[20, 70]. Antibody cloning from immunized NHPs and production of the NHP mAbs in Fig. 5 was done as described[20, 70]. Additional mAbs were either previously reported ($Ab1170_{NHP}$, $Ab275_{mur}$)[38] or isolated from an RC1-primed and sequentially-boosted wt mouse ($Ab283_{mur}$) using similar methods. V(D)J gene assignments of NHP and murine antibodies were done using IMGT/V-QUEST[99]. Sequence alignments were done using Clustal Omega[100].

Epitope mapping by competition ELISAs

Competition ELISAs were performed using a Tecan Evo liquid handling robot. RC1 was randomly biotinylated at primary amines using EZ-link NHS-PEG4 Biotinylation Kit according to the manufacturer's protocol (Thermo Fisher Scientific), resulting in about 5 biotins per protomer. Randomly biotinylated SOSIP trimers coated on streptavidin plates were verified to exhibit similar properties as counterpart site-specifically immobilized SOSIPs (by a C-terminal tag recognized by an anti-tag antibody) and evaluated for binding to anti-Env antibodies by ELISA. By contrast, SOSIP trimers directly coated onto ELISA plates exhibited aberrant behaviors such as binding to CD4-induced antibodies in the absence of CD4, which was not observed for counterpart experiments using randomly biotinylated or site-specifically immobilized SOSIPs. Biotinylated RC1 (1 □g/mL) was bound overnight at 4ºC to a 384-well ELISA plate coated with streptavidin (Thermo Fisher Scientific). The plate was washed with TBS-T, incubated with 10 □g/mL Fab for 2 hours, and then 1:100 dilution of serum, 1 µg/mL IgG (controls in serum competition ELISA), or 10 ug/mL mAb IgG (controls and NHP mAbs; mAb competition ELISA) was added and incubated for 2 hours at room temperature. Bound IgG was detected using an horseradish peroxidase-conjugated anti-human IgG Fc secondary antibody (Southern Biotech Cat # 2014-05; 1 hour, room temperature) and developed with SuperSignal ELISA Femto Substrate (Thermo Fisher Scientific). Relative light units (RLU) were measured and the signal for each Fab-IgG pair was normalized to the signal for the IgG when no blocking Fab was present. Measurements were performed in technical quadruplicates and the data presented are representative of two independent experiments.

Antibody production and purification

IgG mAbs were expressed by transient transfection in Expi293 cells or HEK293-6E cells and purified from cell supernatants using MabSelect SURE (Cytiva) or protein A or G columns (GE

Healthcare) as described[38, 61]. 6xHis-tagged Fabs were purified by Ni-NTA chromatography (Cytiva) and SEC[61]. The $Ab283_{mur}$ mouse Fab for structural studies was obtained by digesting $Ab283_{mur}$ IgG at 1-5 mg ml^{-1} with ficin (Sigma Aldrich) and purified by protein G (GE Healthcare) and SEC chromatography[101], followed by monoQ 5/50 (GE Healthcare) ion exchange chromatography. The common iGL of the PGT121 and 10-1074 bnAbs[28] was expressed as an IgG.

Single-particle cryo-EM

For the $Ab283_{MUR}$–RC1–8ANC195 complex structure, purified $Ab283_{mur}$ Fab, 8ANC195 Fab, derived from a bnAb directed against the gp120-gp41 interface[61], and RC1 SOSIP trimer were incubated at a 3:1 molar ratio of Fab per protomer overnight at room temperature. For the $Ab1170_{NHP}$–RC1–8ANC195 complex structure, purified $Ab1170_{NHP}$ Fab, 8ANC195 Fab, and RC1 SOSIP trimer were incubated at a 3:1 molar ratio of Fab per protomer overnight at room temperature.

The complexes were subjected to SEC on a Superdex 200 column (GE Life Sciences), and 3 µL of purified complex (0.4 mg/mL for $Ab1170_{NHP}$–RC1–8ANC195 and 1.35 mg/mL for $Ab283_{mur}$–RC1–8ANC195) was added to freshly glow-discharged 300 mesh, 1.2/1.3 Quantifoil copper grids and then blotted for either 2 or 3.5 seconds with Whatman no. 1 filter paper at 22˚C and 100% relative humidity using a Mark IV Vitrobot. Samples were then vitrified in 100% liquid ethane. Micrographs were collected on a Talos Arctica TEM (Thermo Fisher Scientific) operating at 200 kV and processed in Relion[102, 103] for both complexes (table S3).

For the $Ab283_{mur}$–RC1–8ANC195 complex, automated data collection was carried out using EPU 2 software (Thermo Fisher Scientific) with a Falcon 3EC direct electron detector (Thermo Fisher Scientific). Micrographs were motion-corrected including dose-weighting using MotionCorr2

within Relion[102]. The non-dose-weighted micrographs were used for contrast transfer function (CTF) estimation in CTFFind-4.1[104]. After discarding micrographs with poor CTF fits and signs of visible ice, particles were auto-picked, extracted, and 2D classified. Particles from selected 2D classes were used for an initial refinement with an initial map that was created by 60 Å-low-pass-filtering a map created from a model of BG505–10-1074–8ANC195 complex using molmap in UCSF Chimera[96, 105]. This model was then used as an input model for 3D classification. Particles from selected 3D classes were refined again into a 3D model, which was calculated using C3 symmetry applied and a mask that did not include Fab C_HC_L domains. From there, particles were polished and movie-refined before a final 3D refinement that resulted in a map with a gold standard Fourier shell coefficient (FSC) calculation of 5.2 Å.

For the Ab1170$_{NHP}$–RC1–8ANC195 complex, automated data collection was carried out using SerialEM software[93, 106] with a Gatan K3 camera. Micrographs were motion-corrected including dose-weighting using MotionCorr2 within Relion[102]. The non-dose-weighted micrographs were used for CTF estimation in CTFFind-4.1[104]. After discarding micrographs with poor CTF fits and signs of visible ice, particles were auto-picked, extracted, and 2D classified. Particles from selected 2D classes were used for 3D classification with an initial map that was created by 50 Å-low-pass-filtering a map created from a model of the BG505–8ANC195 complex[61] using molmap in UCSF Chimera[96, 105]. Selected particles were then 3D refined using C1 symmetry into a map with a gold standard FSC calculation of 4.5 Å. Coordinates for the Ab283mur–RC1 portion of the Ab283mur–RC1–8ANC195 complex were generated by docking chains from reference structure (PDB 6ORQ) into the map using UCSF Chimera[96, 105]. The model was then modified to the correct sequence. Subsequently, the model was refined iteratively in Phenix[107, 108] and Coot[109]. Structure figures were made using UCSF Chimera[96] or PyMol[110].

NHP challenge experiments

The origin and preparation of the $SHIV_{DH12\text{-}V3AD8}$ stock used for virus challenge in NHPs was previously described[63]. In "high dose" virus challenges, NHPs were inoculated intrarectally with 1000 $TCID_{50}$ of $SHIV_{DH12\text{-}V3AD8}$ 2 weeks following boost 4. For "repeated low dose challenges," animals were also challenged intrarectally 2 weeks following the boost 4, but with 10 $TCID_{50}$ of $SHIV_{DH12\text{-}V3AD8}$ and every week thereafter, until infection was established, as described[91]. Viral RNA amounts in plasma were determined by quantitative reverse transcriptase polymerase chain reaction (qRT-PCR) (ABI Prism 7900HT sequence detection system; Applied Biosystems) as described[111].

Statistical analyses

All raw, individual level data are shown in data file S1. For the statistical analysis of the mean titers after boost 2 against the $SHIV_{DH12\text{-}V3AD8}$ pseudovirus in comparisons of the four NHPs that received the B41-5MUT-VLP boost with the four NHPs that received the B41wt-VLP boost, we performed a two-tailed t-test assuming unequal variances using Excel. For both of these groups of NHPs, the Shapiro-Wilk test on their titer measurements does not reject the null hypothesis of normal distribution, so this t-test was applicable. For analyzing the Kaplan-Meier curves indicating the fraction of NHPs (immunized versus control) with viral loads below the limit of detection following challenge, two methods were used: the Log-rank (Mantel-Cox) test and the Gehan-Breslow-Wilcoxon test. Geometric means were calculated for the viral loads presented in Fig. 6B and C since the values varied over many orders of magnitude.

Acknowledgements

We thank members of the Bjorkman, Martin, and Nussenzweig laboratories for discussions, M. Howarth (Oxford) for providing plasmids and advice for VLP expression and purification, J. Moore

(Weill Cornell Medical College), R.W. Sanders and M.J. van Gils (Amsterdam UMC) for SOSIP expression plasmids, J. Vielmetter, P. Hoffman, and the Protein Expression Center in the Beckman Institute at Caltech for expression assistance, T. Eisenreich and S. Tittley for animal husbandry, and K. Gordon for flow cytometry. Electron microscopy was performed in the Caltech Cryo-EM Center with assistance from S. Chen and A. Malyutin.

Funding: This work was supported by the National Institute of Allergy and Infectious Diseases (NIAID) Grant HIVRAD P01 AI100148 (to P.J.B. and M.C.N.), the Bill and Melinda Gates Foundation Collaboration for AIDS Vaccine Discovery (CAVD) grant INV-002143 (to P.J.B., M.C.N., and M.A.M.), a Bill and Melinda Gates Foundation grant #OPP1146996 (to M.S.S.), the Intramural Research Program of the NIAID (to M.A.M.), NIH P50 AI150464 (to P.J.B.), and NIH grants UM1 AI144462 and P01 AI048240 (to D.J.I.). A.E. was supported by a NIH K99/R00 grant, A.T.D. and M.E.A. were supported by NSF Graduate Research Fellowships, and C.O.B. was supported by the Hanna Gray Fellowship Program from the Howard Hughes Medical Institute and the Postdoctoral Enrichment Program from the Burroughs Wellcome Fund. M.C.N. is an HHMI investigator.

Author contributions: H.B.G., J.R.K., A.E., R.G., A.T.D., A.P.W., C.O.B., M.C.N., M.A.M., and P.J.B. conceived experiments. Immunogens were selected and designed by H.B.G., A.E., and J.R.K.; proteins were expressed by N.K., H.G., A.G., and M.C. Pseudovirus production and neutralization assays were performed and analyzed by M.S.S., R.G., H.R., M.A.G.H., L.M.K., and P.N.P.G. Adjuvants were provided by D.J.I. and M.S. NHP experiments were conducted and interpreted by R.G., Y.N., and M.A.M. nsEMPEM and other structural studies were performed by A.T.D., C.O.B., M.A.E., Z.Y., and H.W. Single B cell cloning and isolation of mAbs was done by A.E., Z.W., and M.C.N. Sequence and statistical analyses were done by A.P.W. Bioinformatics was done by T.Y.O.

and V.R. The paper was written by P.J.B., H.B.G., A.T.D., C.O.B., J.R.K., A.E., M.C.N., and M.A.M. with assistance from other authors.

Competing interests: H.B.G., P.J.B., A.E., and M.C.N. are coinventors on a patent (*HIV Vaccine Immunogens*; PCT/US2019/063619) covering RC1 immunogens. All other authors have no competing interests.

Data and materials availability: All data associated with this study are in the paper or supplementary materials. nsEMPEM and cryo-EM reconstructions were deposited in the Electron Microscopy Data Bank (EMDB, https://www.emdataresource.org/) and the associated accession numbers are listed in table S3. ISCOMs-like saponin adjuvant is available from Darrell Irvine under a materials transfer agreement with MIT.

Supplementary Figures and Tables

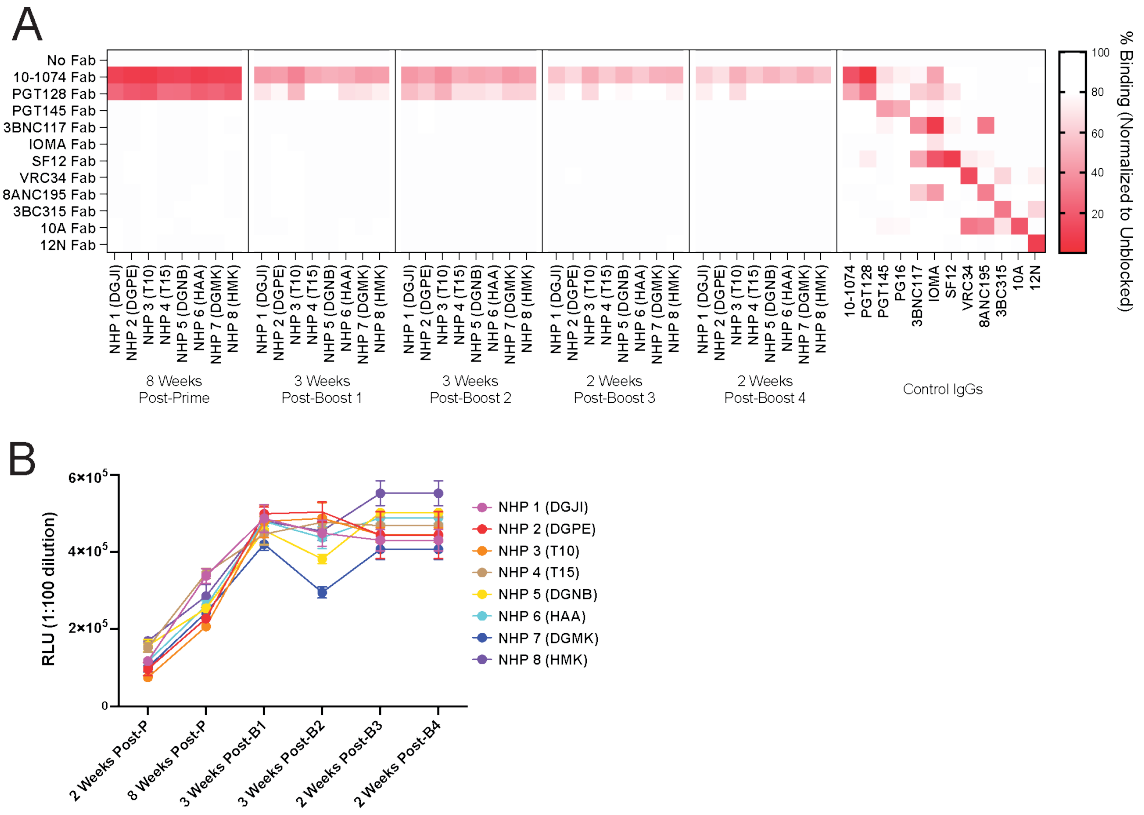

Figure S1. Serum from immunized non-human primates (NHPs) competes with V3-glycan patch broadly neutralizing antibodies (bnAbs) by enzyme-linked immunoassays (ELISAs). **(A)** A heat map shows results of competition experiments to map epitopes of serum IgGs derived from immunized NHPs. Randomly biotinylated RC1 was bound to a Streptaidin ELISA plate. Each well was then incubated with a potential competitor Fab for 2 hours and then a 1:100 dilution of serum or 2 µg/mL control monoclonal Ab was added. Bound IgGs were detected using an anti-Fc antiserum. The percent binding observed after addition of a competitor Fab was normalized to the binding in the absence of a competitor Fab. NHP serum results are shown on the left at different time points in the immunization regimen; control broadly neutralizing (bnAb) or non-neutralizing IgG (10A and 12N) results are shown on the right. **(B)** ELISA serum responses against RC1 are shown at the indicated time points.

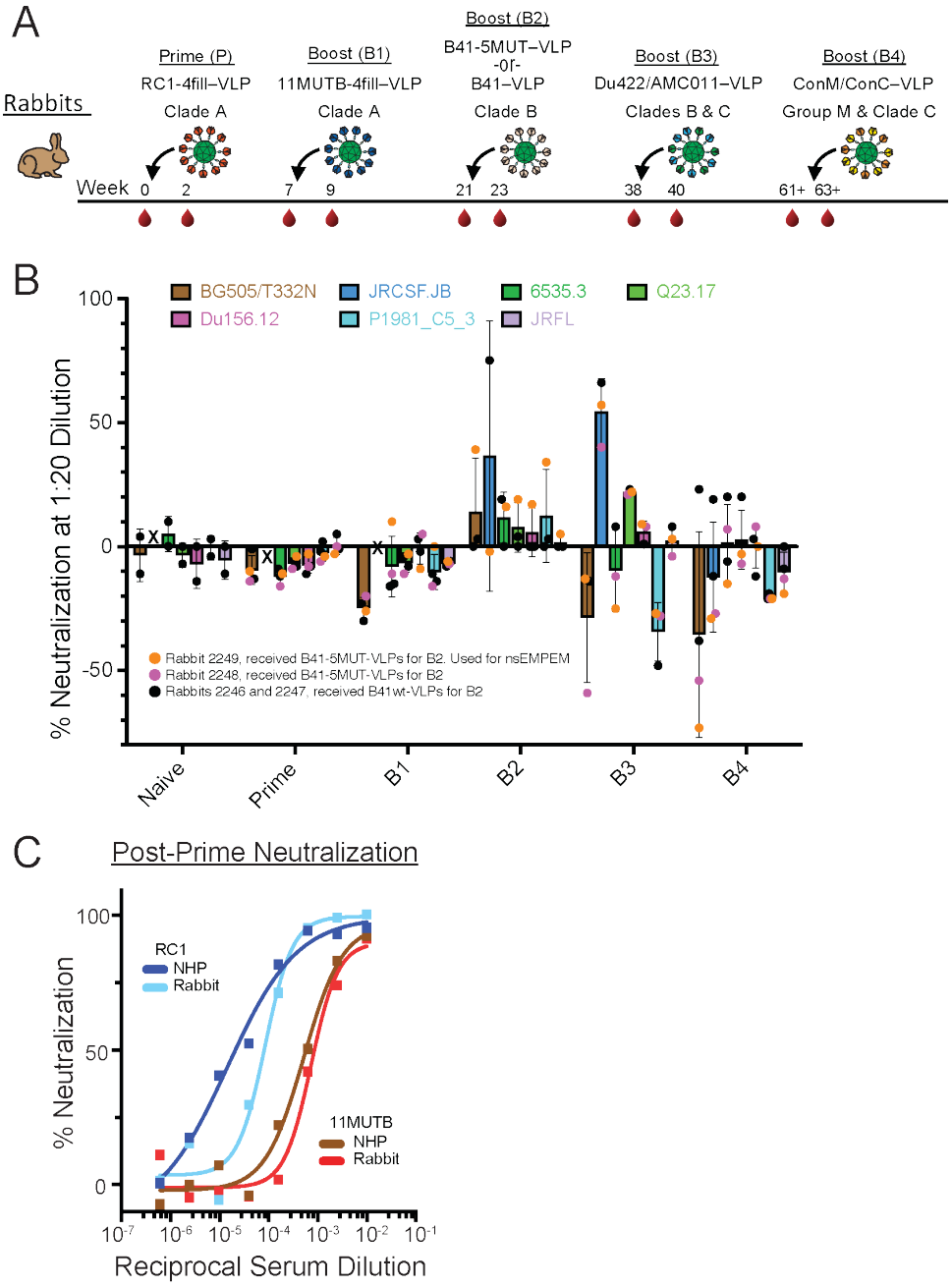

Figure S2. Rabbits were immunized with a prime and four boosts and antibody responses were compared to NHP responses.

(A) The sequential immunization regimen is shown. Rabbits were bled at the indicated times and other times noted in tables S1 and S2. **(B)** Percent neutralization of rabbit serum samples at a 1:20 dilution against heterologous HIV-1 strains are shown for the indicated time points. Neutralization data for samples that exhibited >15% neutralization of the control MLV or substantial cell toxicity/stress at a 1:20 dilution were excluded from analysis (rabbit 2248 B2, rabbit 2246 B3).

Neutralization results were not available for the naïve, B1, and B2 samples (indicated by an X). **(C)** Neutralization activities against RC1 and 11MUTB pseudoviruses of serum samples from an NHP and a rabbit after an RC1-4fill-VLP prime are shown. Both animals exhibited stronger neutralizing antibody responses to RC1 than to 11MUTB.

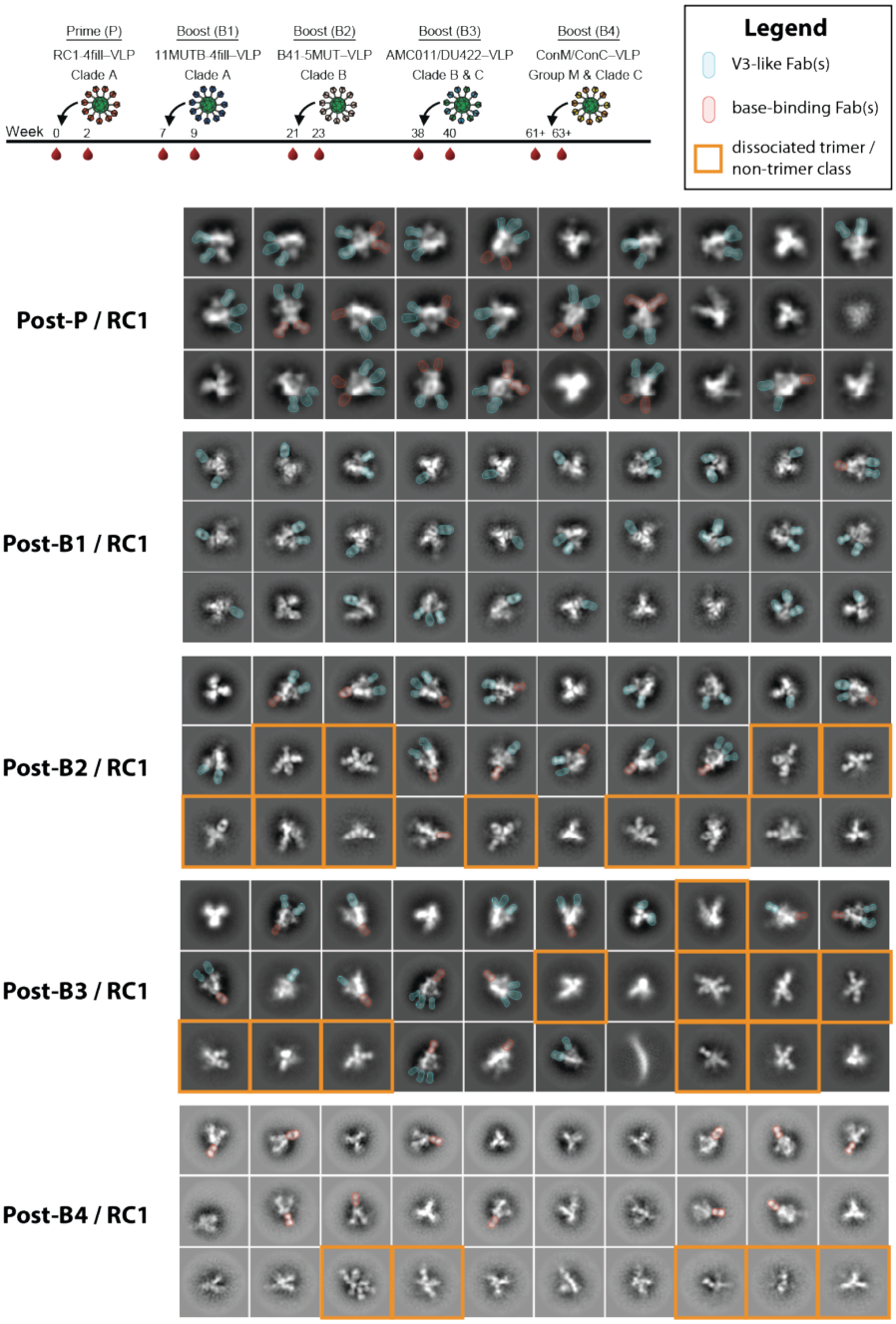

Figure S3. 2D classes of Rabbit 2249 serum Fabs in complex with RC1 SOSIP.664 trimer show V3- and base-targeting Fab(s) as well as trimer dissociation.

Top: The immunization schedule for Rabbit 2249 is shown. Bottom: The most populated negative stain 2D classes are shown for polyclonal Fabs collected 2-weeks post-P, post-B1, post-B2, post-B3, and post-B4 in complex with a RC1 SOSIP.664 trimer. Fabs targeting the V3-glycan patch (cyan) and the base of the trimer (red) are highlighted in select 2D classes. Disassociated gp140

protomer classes bound to Fabs identified in 2D classes after post-B2, post-B3, and post-B4 are boxed in orange.

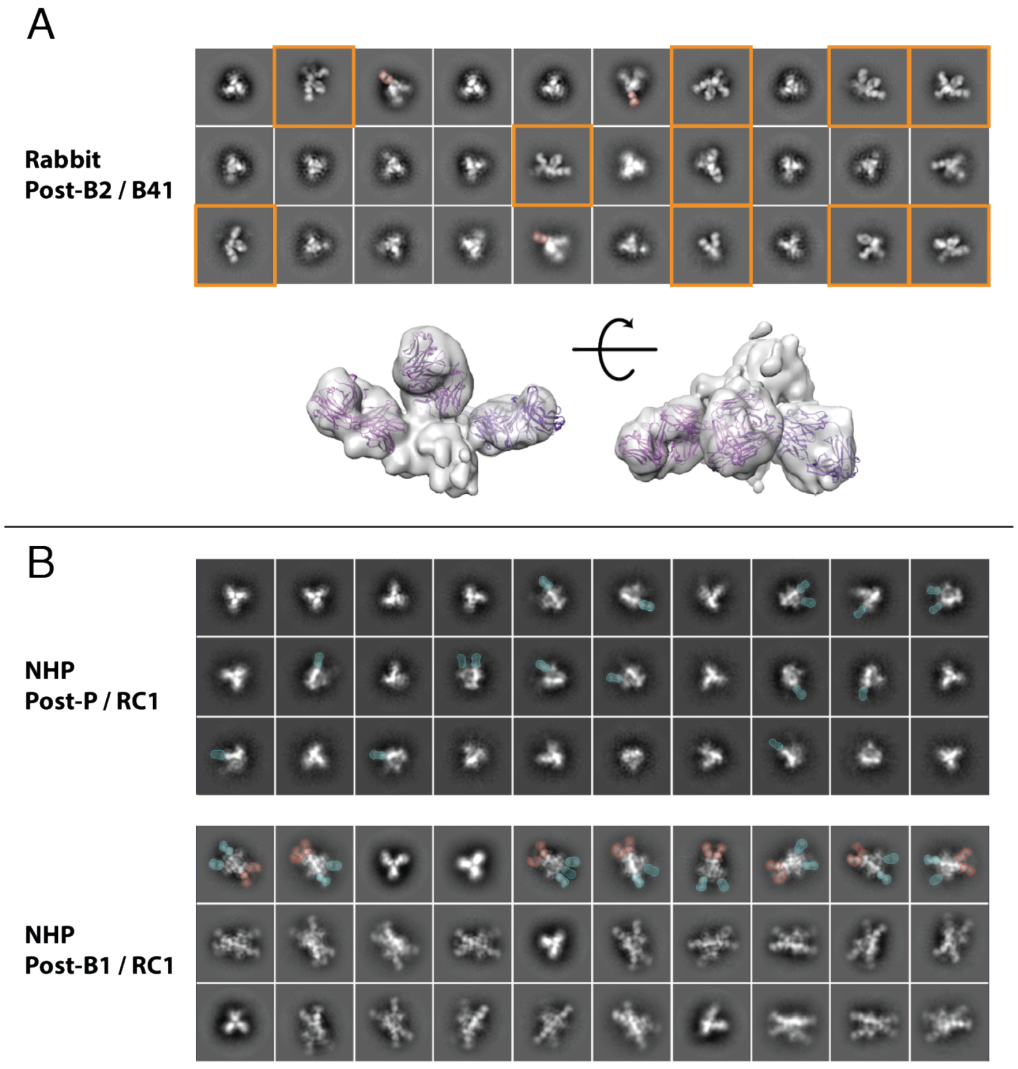

Figure S4. Negative stain EM-based polyclonal epitope mapping (nsEMPEM) characterizations of rabbit Fabs bound to dissociated trimers and NHP 2D classes.
(A) Negative stain 2D classes classes of rabbit post-B2 Fab(s) complexed with B41 SOSIP.664 v4.2 trimer are shown. Base-binding Fab(s) were observed bound to Env trimers (red), in addition to Fabs bound to disassociated protomers (orange boxes). A low-resolution 3D reconstruction of a Fab-protomer class is shown. Fab coordinates (PDB 5UD9) (purple cartoon) were docked into the EM density. **(B)** Negative stain 2D classes of NHP 1 (DGJI) polyclonal Fabs bound to RC1 SOSIP.664 trimers 2 weeks post-P and post-B1 are shown. Fabs targeting the V3-glycan patch (cyan) and the base of the trimer (red) are highlighted in select 2D classes.

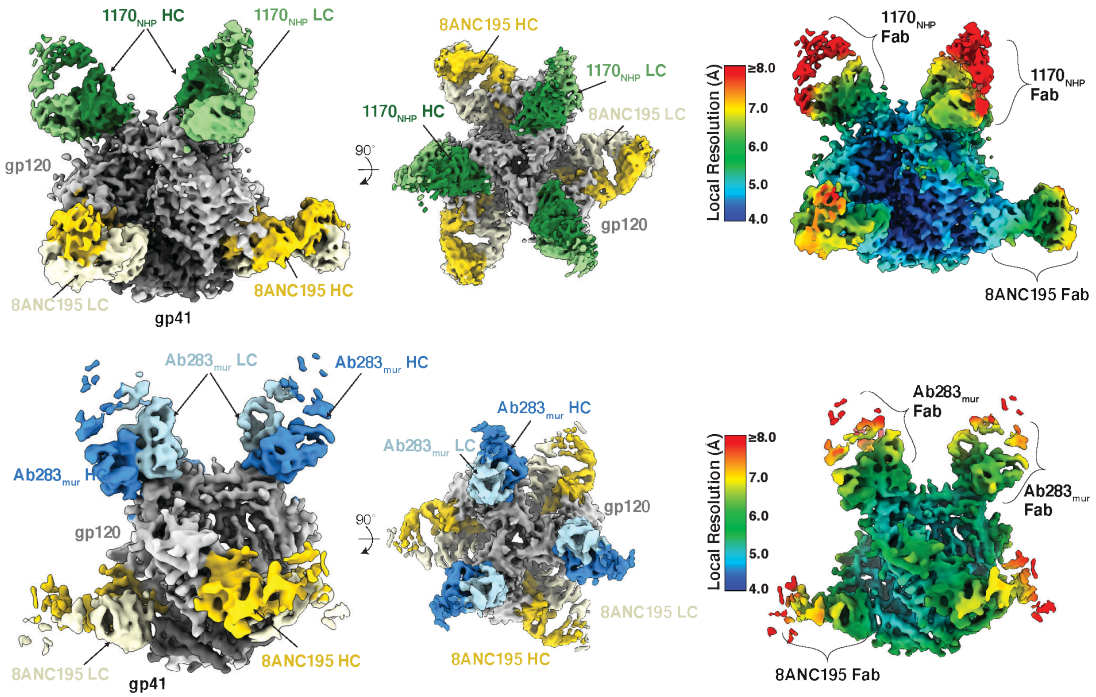

Figure S5. Cryo-EM reconstructions and local resolution estimates for $Ab283_{mur}$-RC1 and 1170_{NHP}-RC1 complexes.

Cryo-EM density and local resolution estimations were calculated in RELION v3.1[102, 103] for (top) 1170_{NHP} - RC1 and (bottom) $Ab283_{mur}$ - RC1 trimer complexes.

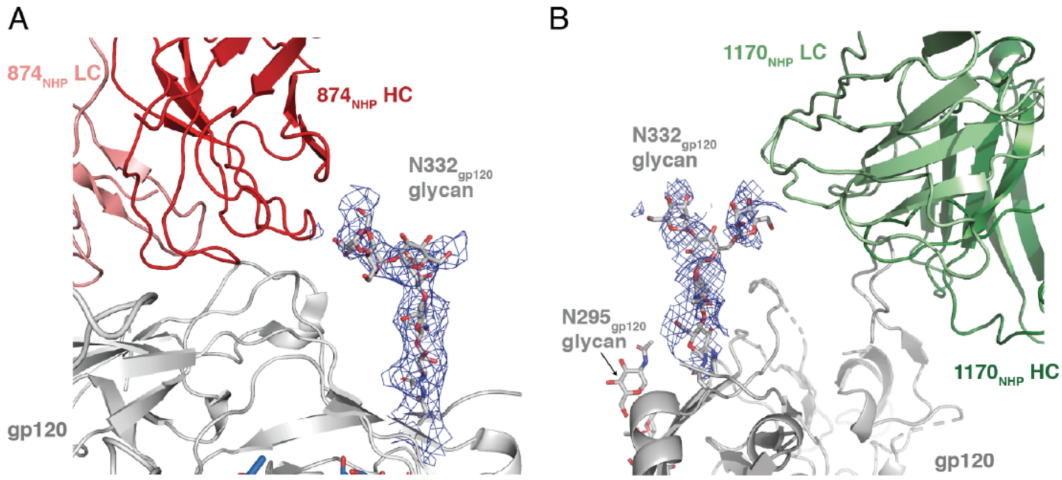

Figure S6. Antibodies Ab874$_{NHP}$ and Ab1170$_{NHP}$ interact with the N332$_{gp120}$ glycan. Antibodies **(A)** Ab874$_{NHP}$ and **(B)** Ab1170$_{NHP}$ elicited in NHPs after priming with RC1-4fill-VLPs[38] contact the high-mannose N-glycan attached to gp120 residue N332 (modeled from PDB 6ORO) (Ab874$_{NHP}$) and this study (Ab1170$_{NHP}$). Cryo-EM density for the N332$_{gp120}$ glycan is shown as blue mesh contoured at 4σ.

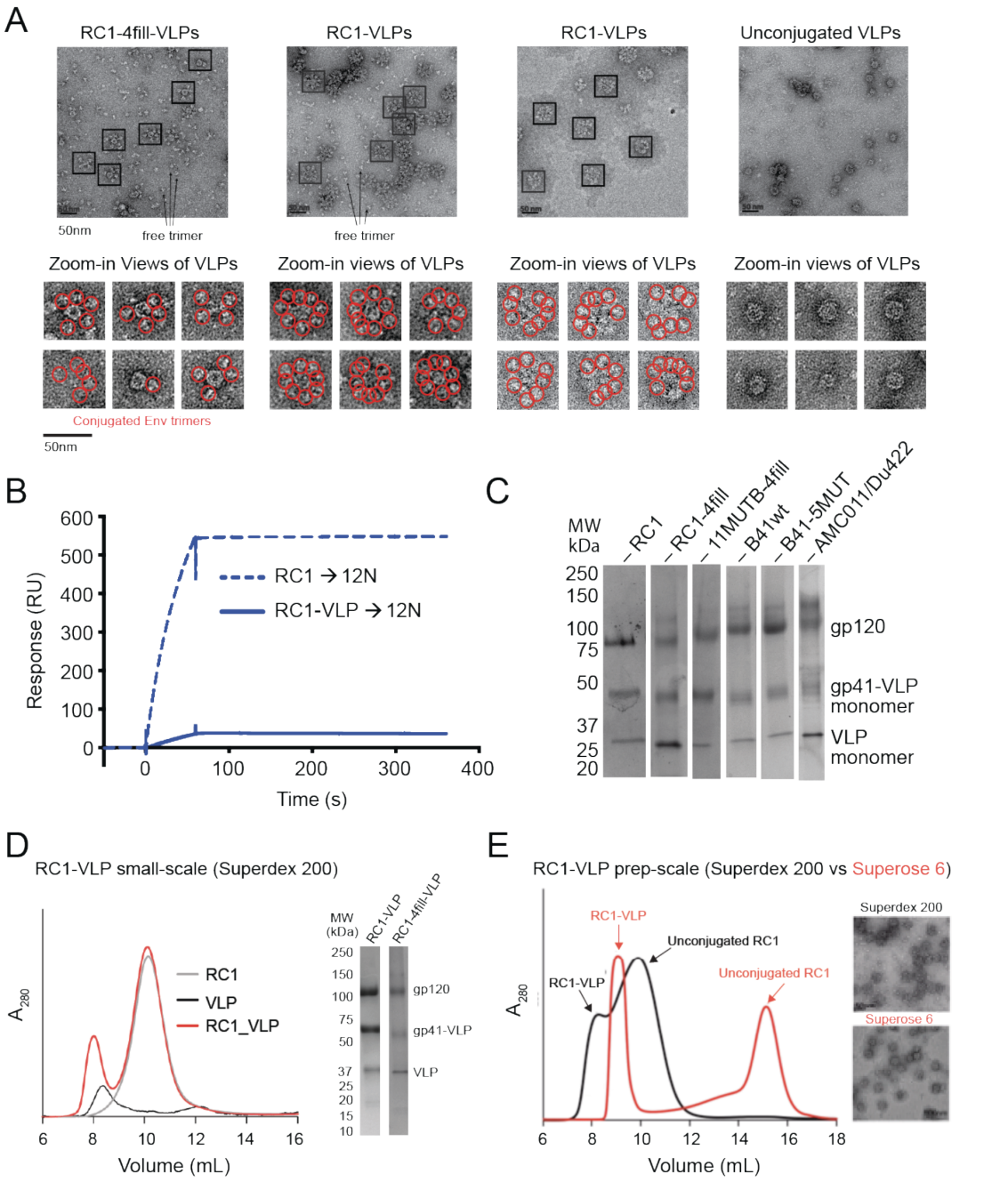

Figure S7. Native-like Env trimer (SOSIP)-conjugated virus-like particles (VLPs) are characterized biochemically and by negative stain electron microscopy (nsEM).
(A) Negative stain electron microscopy (nsEM) images comparing RC1-4fill-VLPs (left), RC1-VLPs with free trimer (second from left), RC1-VLPs without free trimer (third from left), and unconjugated VLPs (right) are shown. Bottom panels show zoom-in views with conjugated Env trimers indicated by red circles. **(B)** Surface plasmon resonance (SPR) demonstration that 12N, a rabbit mAb against the base of the BG505 SOSIP trimer, accesses its epitope on free RC1, but not

on RC1-VLPs. RC1 or RC1-VLPs were injected over 12N IgG that was immobilized on a biosensor chip. **(C)** A commassie-stained SDS-PAGE gel of conjugations of different immunogens to VLPs is shown. Note that the ratio of gp120 and gp41 to the VLP monomer subunit is lower in the RC1-4fill conjugation than the other conjugations. **(D)** Left: Separation by size-exclusion chromatography (SEC) on Superdex 200 column of RC1-VLPs from unconjugated RC1 at small scale (100 μg SOSIP) is shown. The RC1-VLP peak is distinct from the peak for unconjugated RC1 trimer. Right: Coomassie-stained SDS-PAGE of SEC-purified RC1-VLP and RC1-4fill-VLP preps are shown. **(E)** Left: Black trace: Separation by SEC on Superdex 200 column of RC1-VLPs from unconjugated RC1 at preparation scale of about 2 mg of SOSIP. The RC1-VLP peak is not distinct from the peak for unconjugated RC1 trimer. Red trace: Separation by SEC on Superose 6 column of RC1-VLPs from unconjugated RC1 at preparation scale ~2 mg. The RC1-VLP peak is distinct from the peak for unconjugated RC1 trimer. Right: nsEM images of RC1-VLPs purified using the Superdex 200 or the Superose 6 column are shown. Free RC1 trimer was observed in the RC1-VLP prep purified on the Superdex 200 column, but not in the prep purified on the Superose 6 column.

			RC1	11MUTB	$SHIV_{DH12-v3AD8}$ (PV)	$SHIV_{DH12-v3AD8}$ (RC)	$SHIV_{AD8EO}$ (PV)	$SHIV_{SF162.LS}$ (PV)	$SHIV_{SF162P3}$ (RC)
NHP 1 (DGJI)	Week 2 (P, RC1-4fill-VLP)	2 weeks Post Prime	400	<100	<20	<20	<20		
	Week 8 (P, RC1-4fill-VLP)	8 weeks Post Prime	60,000	1,600	45	28	NT		
	Week 11 (B1, 11MUTB-4fill-VLP)	2 weeks Post B1	100,000	60,000	50	36	<20		
	Week 25 (B2, B41-5MUT-VLP)	3 weeks Post B2	48,000	29,000	1,568	53	NT		
	Week 41 (B3, Du422/AMC011-VLP)	2 weeks Post B3	62,000	29,000	3,502	59	21	>4860	<20
	Week 65 (B4, ConM/ConC-VLP)	2 weeks Post B4	57,000	11,000	1,687	59	NT		
	Week 67 (Challenge)	2 weeks Post Challenge			815	26			
	Week 72 (Challenge)	7 weeks Post Challenge			328	20			
	Week 75 (Challenge)	10 weeks Post Challenge			516	27			
NHP 2 (DGPE)	Week 2 (P, RC1-4fill-VLP)	2 weeks Post Prime	200	<100	<20	<20	<20		
	Week 8 (P, RC1-4fill-VLP)	8 weeks Post Prime	10,000	1,200	<20	<20	NT		
	Week 11 (B1, 11MUTB-4fill-VLP)	2 weeks Post B1	300,000	300,000	46	25	<20		
	Week 25 (B2, B41-5MUT-VLP)	3 weeks Post B2	550,000	390,000	3,373	126	NT		
	Week 41 (B3, Du422/AMC011-VLP)	2 weeks Post B3	370,000	250,000	3,302	92	<20	>4860	<20
	Week 65 (B4, ConM/ConC-VLP)	2 weeks Post B4	140,000	140,000	5,215	126	NT		
	Week 67 (Challenge)	2 weeks Post Challenge			1,369	63			
	Week 72 (Challenge)	7 weeks Post Challenge			>43,740	648			
	Week 75 (Challenge)	10 weeks Post Challenge			28,917	1,157			
NHP 3 (T10)	Week 2 (P, RC1-4fill-VLP)	2 weeks Post Prime	250	<100	<20	29	<20		
	Week 8 (P, RC1-4fill-VLP)	8 weeks Post Prime	6,500	350	<20	25	NT		
	Week 11 (B1, 11MUTB-4fill-VLP)	2 weeks Post B1	100,000	50,000	54	43	<20		
	Week 25 (B2, B41wt-VLP)	3 weeks Post B2	100,000	60,000	1,003	70	NT		
	Week 41 (B3, Du422/AMC011-VLP)	2 weeks Post B3	90,000	59,000	2,864	85	<20	>4860	<20
	Week 65 (B4, ConM/ConC-VLP)	2 weeks Post B4	90,000	36,000	3,106	122	NT		
	Week 67 (Challenge)	2 weeks Post Challenge			792	21			
	Week 72 (Challenge)	7 weeks Post Challenge			10,169	621			
	Week 75 (Challenge)	10 weeks Post Challenge			16,258	2,125			
NHP 4 (T15)	Week 2 (P, RC1-4fill-VLP)	2 weeks Post Prime	400	400	<20	<20	<20		
	Week 8 (P, RC1-4fill-VLP)	8 weeks Post Prime	75,000	8,000	<20	<20	NT		
	Week 11 (B1, 11MUTB-4fill-VLP)	2 weeks Post B1	300,000	300,000	28	<20	<20		
	Week 25 (B2, B41wt-VLP)	3 weeks Post B2	130,000	70,000	1,345	58	NT		
	Week 41 (B3, Du422/AMC011-VLP)	2 weeks Post B3	150,000	58,000	8,308	164	<20	>4860	<20
	Week 65 (B4, ConM/ConC-VLP)	2 weeks Post B4	140,000	39,000	9,953	256	NT		
	Week 67 (Challenge)	2 weeks Post Challenge			14,096	98			
	Week 72 (Challenge)	7 weeks Post Challenge			>43,740	588			
	Week 75 (Challenge)	10 weeks Post Challenge			>43,740	1,597			
NHP 5 (DGNB)	Week 2 (P, RC1-4fill-VLP)	2 weeks Post Prime	400	<100	<20	<20	<20		
	Week 8 (P, RC1-4fill-VLP)	8 weeks Post Prime	10,000	400	<20	54	NT		
	Week 11 (B1, 11MUTB-4fill-VLP)	2 weeks Post B1	200,000	90,000	26	21	<20		
	Week 25 (B2, B41-5MUT-VLP)	3 weeks Post B2	63,000	35,000	1,717	50	NT		
	Week 41 (B3, Du422/AMC011-VLP)	2 weeks Post B3	84,000	48,000	2,245	47	<20	>4860	<20
	Week 71 (B4, ConM/ConC-VLP)	2 weeks Post B4	46,000	23,000	2,314	NT	NT		
	Week 73 (Challenge)	2 weeks Post Challenge			1,248	67			
NHP 6 (HAA)	Week 2 (P, RC1-4fill-VLP)	2 weeks Post Prime	200	<100	<20	23	<20		
	Week 8 (P, RC1-4fill-VLP)	8 weeks Post Prime	10,000	1,000	<20	<20	NT		
	Week 11 (B1, 11MUTB-4fill-VLP)	2 weeks Post B1	90,000	100,000	35	26	<20		
	Week 25 (B2, B41-5MUT-VLP)	3 weeks Post B2	79,000	78,000	3,121	71	NT		
	Week 41 (B3, Du422/AMC011-VLP)	2 weeks Post B3	75,000	47,000	4,070	135	<20	>4860	<20
	Week 71 (B4, ConM/ConC-VLP)	2 weeks Post B4	95,000	26,100	2,229	56	NT		
	Week 73 (Challenge)	2 weeks Post Challenge			2,157	87			
NHP 7 (DGMK)	Week 2 (P, RC1-4fill-VLP)	2 weeks Post Prime	200	<100	<20	<20	<20		
	Week 8 (P, RC1-4fill-VLP)	8 weeks Post Prime	10,000	400	<20	<20	NT		
	Week 11 (B1, 11MUTB-4fill-VLP)	2 weeks Post B1	80,000	50,000	26	<20	<20		
	Week 25 (B2, B41wt-VLP)	3 weeks Post B2	130,000	51,000	584	36	NT		
	Week 41 (B3, Du422/AMC011-VLP)	2 weeks Post B3	88,000	40,000	1,814	88	<20	1239	<20
	Week 71 (B4, ConM/ConC-VLP)	2 weeks Post B4	60,000	23000	1,393	39	NT		
	Week 73 (Challenge)	2 weeks Post Challenge			1,461	57			
NHP 8 (HMK)	Week 2 (P, RC1-4fill-VLP)	2 weeks Post Prime	1000	<100	<20	37	<20		
	Week 8 (P, RC1-4fill-VLP)	8 weeks Post Prime	10,000	500	<20	<20	NT		
	Week 11 (B1, 11MUTB-4fill-VLP)	2 weeks Post B1	200,000	100,000	58	21	<20		
	Week 25 (B2, B41wt-VLP)	3 weeks Post B2	78,000	45,000	1,174	62	NT		
	Week 41 (B3, Du422/AMC011-VLP)	2 weeks Post B3	55,000	48,000	3,264	111	<20	>4860	<20
	Week 71 (B4, ConM/ConC-VLP)	2 weeks Post B4	150,000	53,000	2,047	58	NT		
	Week 73 (Challenge)	2 weeks Post Challenge			1,931	59			

Table S1. Serum neutralization from immunized NHPs against RC1, 11MUTB, and indicated pseudovirus (PV) and replication competent virus (RC) simian-human immunodeficiency virus (SHIV) strains.

			Neutralization ID50 and % Neutralization at 1:20 dilution															
			NHP 1 (DGJI)								NHP 2 (DGPE)							
			Week 25 (B2)		Week 41 (B3)		Week 42 (B3)		Week 65 (B4)		Week 25 (B2)		Week 41 (B3)		Week 42 (B3)		Week 65 (B4)	
			3 weeks Post B2		2 weeks Post B3		3 weeks Post B3		2 weeks Post B4		3 weeks Post B2		2 weeks Post B3		3 weeks Post B3		2 weeks Post B4	
Virus	Clade	Tier	ID_{50}	% 1:20	ID_{50}	% 1:20	ID_{50}	% 1:20	ID_{50}	% 1:20	ID_{50}	% 1:20	ID_{50}	% 1:20	ID_{50}	% 1:20	ID_{50}	% 1:20
BG505/T332N	A	2	<20	-12	<50	15	<20	19	<20	-15	<20	-2	<50	5	<20	20	34	62
JRCSF.JB	B	2	180	84	165	69	169	88	<20	-6	352	97	152	70	228	90	236	96
6535.5	B	1B	<20	14	<50	33	38	58	<20	-25	<20	2	<50	11	<20	46	45	62
92RW020.2	A	2	<20	7	<50	5	<20	21	<20	6	<20	13	<50	16	<20	15	<20	33
Du422.1	C	2					<20	4	<20	2					<20	5	<20	12
T250-4	AG	2	<20	18	<50	24	<20	38	<20	-2	<20	-1	<50	7	<20	37	50	54
Q23.17	A	1B	<20	-14	<50	20	<20	29	<20	4	<20	-27	<50	-7	<20	45	<20	39
Du156.12	C	2	<20	-13	<50	5	<20	0	<20	0	<20	-13	<50	-11	<20	0	<20	0
P1981_C5_3	G				<50	-19	<20	24	<20	25			<50	-13	<20	17	28	59
JRFL	B	2	<20	26			<20	31	<20	18	<20	37			<20	39	<20	42
0815.v3.c3	A						<20	0	<20	-63					<20	0	<20	-4
928-28	A	2					<20	47	<20	-4					<20	40	<20	37
MuLV			<20	25	<50	23	<20	24	<20	-2			<50	-1	<20	16	<20	5

			Neutralization ID50 and % Neutralization at 1:20 dilution															
			NHP 3 (T10)								NHP 4 (T15)							
			Week 25 (B2)		Week 41 (B3)		Week 42 (B3)		Week 65 (B4)		Week 25 (B2)		Week 41 (B3)		Week 42 (B3)		Week 65 (B4)	
			3 weeks Post B2		2 weeks Post B3		3 weeks Post B3		2 weeks Post B4		3 weeks Post B2		2 weeks Post B3		3 weeks Post B3		2 weeks Post B4	
Virus	Clade	Tier	ID_{50}	% 1:20	ID_{50}	% 1:20	ID_{50}	% 1:20	ID_{50}	% 1:20	ID_{50}	% 1:20	ID_{50}	% 1:20	ID_{50}	% 1:20	ID_{50}	% 1:20
BG505/T332N	A	2	<20	29	<50	13	22	52	<20	33	<20	42	<50	29	28	55	48	48
JRCSF.JB	B	2	23	59	99	65	108	88	45	73	43	66	440	86	343	95	257	96
6535.5	B	1B	<20	-25	<50	27	<20	47	<20	45	<20	9	73	53	122	79	129	88
92RW020.2	A	2	<20	-2	<50	20	<20	32	<20	12	<20	7	<50	31	<20	42	<20	40
Du422.1	C	2					<20	16	<20	6					<20	16	<20	0
T250-4	AG	2	<20	-3	<50	24	22	54	<20	26	<20	-6	<50	19	64	61	21	51
Q23.17	A	1B	<20	-11	<50	8	<20	43	<20	18	<20	-18	<50	14	24	53	<20	32
Du156.12	C	2	<20	-15	<50	-7	<20	0	<20	0	<20	-15	<50	14	<20	27	<20	0
P1981_C5_3	G				<50	-1	<20	29	<20	17			<50	11	<20	42	<20	29
JRFL	B	2	<20	10			<20	41	<20	13	<20	13			29	60	65	66
0815.v3.c3	A						<20	0	<20	-55					<20	24	<20	40
928-28	A	2					<20	49	<20	18					42	60		
MuLV			<20	5	<50	10	<20	34	<20	8	<20	6	<50	10	<20	36	<20	5

			Neutralization ID50 and % Neutralization at 1:20 dilution															
			NHP 5 (DGNB)								NHP 6 (HAA)							
			Week 25 (B2)		Week 41 (B3)		Week 42 (B3)		Week 71 (B4)		Week 25 (B2)		Week 41 (B3)		Week 42 (B3)		Week 71 (B4)	
			3 weeks Post B2		2 weeks Post B3		3 weeks Post B3		2 weeks Post B4		3 weeks Post B2		2 weeks Post B3		3 weeks Post B3		2 weeks Post B4	
Virus	Clade	Tier	ID_{50}	% 1:20	ID_{50}	% 1:20	ID_{50}	% 1:20	ID_{50}	% 1:20	ID_{50}	% 1:20	ID_{50}	% 1:20	ID_{50}	% 1:20	ID_{50}	% 1:20
BG505/T332N	A	2	<20	33	<50	15	<20	41	21	51	<20	-9	<50	12	<20	43	<20	38
JRCSF.JB	B	2	84	78	102	65	167	86	121	88	96	85	208	80	266	94	143	93
6535.5	B	1B	<20	25	<50	39	90	69	35	58	<20	-48	<50	15	41	56	<20	32
92RW020.2	A	2	<20	12	<50	20	<20	31	<20	13	<20	9	<50	22	<20	32	<20	8
Du422.1	C	2					<20	8	<20	-1					<20	16	<20	-17
T250-4	AG	2	<20	11	<50	7	<20	36	<20	15	<20	19	<50	28	<20	39	<20	11
Q23.17	A	1B	<20	26	<50	4	<20	32	<20	1	<20	16	<50	27	<20	46	<20	12
Du156.12	C	2	<20	23	<50	-1	<20	14	<20	19	<20	6	<50	6	<20	21	<20	3
P1981_C5_3	G				<50	0	<20	43	<20	5			<50	3	<20	26	<20	18
JRFL	B	2	<20	18			<20	41	<20	25	<20	26			<20	48	<20	34
0815.v3.c3	A						<20	0							<20	0		
928-28	A	2					<20	46							<20	46		
MuLV			<20	18	<50	16	<20	16	<20	-2	<20	22	<50	23	<20	29	<20	5

			Neutralization ID50 and % Neutralization at 1:20 dilution															
			NHP 7 (DGMK)								NHP 8 (HMK)							
			Week 25 (B2)		Week 41 (B3)		Week 42 (B3)		Week 71 (B4)		Week 25 (B2)		Week 41 (B3)		Week 42 (B3)		Week 71 (B4)	
			3 weeks Post B2		2 weeks Post B3		3 weeks Post B3		2 weeks Post B4		3 weeks Post B2		2 weeks Post B3		3 weeks Post B3		2 weeks Post B4	
Virus	Clade	Tier	ID_{50}	% 1:20	ID_{50}	% 1:20	ID_{50}	% 1:20	ID_{50}	% 1:20	ID_{50}	% 1:20	ID_{50}	% 1:20	ID_{50}	% 1:20	ID_{50}	% 1:20
BG505/T332N	A	2	<20	0	<50	12	<20	20	<20	10	<20	19	<50	20	<20	40	<20	19
JRCSF.JB	B	2	<20	29	<50	44	60	74	20	51	80	69	85	61	118	88	96	87
6535.5	B	1B	<20	-55	<50	-9	<20	46	<20	-16	<20	16	<50	26	143	67	20	50
92RW020.2	A	2	<20	22	<50	22	<20	29	<20	-2	<20	26	<50	29	<20	45	<20	26
Du422.1	C	2					<20	13	<20	6					<20	24	<20	11
T250-4	AG	2	<20	28	<50	20	<20	37	<20	8	<20	26	<50	31	26	52	<20	23
Q23.17	A	1B	<20	22	<50	21	<20	39	<20	6	<20	12	<50	21	<20	40	<20	11
Du156.12	C	2	<20	17	<50	6	<20	32	<20	24	<20	-22	<50	20	<20	45	<20	16
P1981_C5_3	G				<50	-13	<20	48	<20	14			<50	-7	<20	30	<20	17
JRFL	B	2	<20	14			<20	37	<20	12	<20	36			<20	47	<20	25
0815.v3.c3	A						<20	0							<20	6		
928-28	A	2					<20	40					<50	6	28	62		
MuLV			<20	5	<50	20	<20	19	<20	8			<50	21	<20	41	<20	5

Table S2. Neutralization 50% inhibitory dose (ID50) and percent neutralization at a 1:20 dilution of serum from immunized NHPs against a panel of heterologous HIV strains.

	Ab283$_{mur}$-RC1-8ANC195	Ab1170$_{NHP}$-RC1-8ANC195	NHP post-P / RC1	NHP post-B1 / RC1	Rabbit post-B2 / B41
EMD	**24853**	**24854**	**24860**	**24861**	**-**
Data collection conditions					
Sample	cryo	cryo	negative stain	negative stain	negative stain
Microscope	Talos Arctica	Talos Arctica	Talos Arctica	Talos Arctica	Talos Arctica
Camera	Falcon 3EC	Gatan K3 Summit	Gatan K3 Summit	Gatan K3 Summit	Gatan K3 Summit
Magnification	92,000x	45,000x	28,000x	28,000x	28,000x
Voltage (kV)	200	200	200	200	200
Recording mode	counting	counting	counting	counting	counting
Dose rate (e^-/pixel/s)	1.06	12.7			
Electron dose (e^-/Å^2)	39.2	60	10	10	15
Defocus range (μm)	1.2 – 3.0	1.0 – 2.5	1.0 - 1.5	1.0 - 1.5	0.5 - 2.0
Pixel size (Å)	1.145	0.8972	1.437	1.437	1.437
Micrographs collected	365	1,151	483	1,399	1,329
Micrographs used	346	1,079	423	1,260	1,329
Total extracted particles	92,225	170,550	180,049	909,046	633,617
Refined particles	41,961	91,166			
Particles in final reconstruction	8,469	91,166	9,757	55,890	42,248
Symmetry imposed	C3	C1	C1	C3	C1
FSC=0.143 Resolution (Å)	5.2	4.5	-	-	-

	Rabbit post-P / RC1	Rabbit post-B1 / RC1	Rabbit post-B2 / RC1	Rabbit post-B3 / RC1	Rabbit post-B4 / RC1
EMD	**24855**	**24856**	**24857**	**24858**	**24859**
Data collection conditions					
	negative stain	negative stain	negative stain	negative stain	negative stain
Microscope	Tecnai T12	Talos Arctica	Talos Arctica	Talos Arctica	Talos Arctica
Camera	Gatan Ultrascan 2k X 2k CCD	Gatan K3 Summit	Gatan K3 Summit	Gatan K3 Summit	Gatan K3 Summit
Magnification	56,000x	28,000x	28,000x	28,000x	28,000x
Voltage (kV)	120	200	200	200	200
Recording mode	linear	counting	counting	counting	counting
Dose rate (e^-/pixel/s)					
Electron dose (e^-/Å^2)	10	15	15	15	15
Defocus range (μm)	1.0-1.5	0.5 - 3.5	0.5 - 3.5	0.5 - 2.0	0.5 - 2.0
Pixel size (Å)	2.06	1.437	1.437	1.437	1.437
Micrographs collected	265	1,186	822	1,745	877
Micrographs used	172	357	593	1,138	252
Total extracted particles	18,290	259,911	624,021	820,444	61,022
Refined particles					
Particles in final reconstruction	12,842	20,549	8,871	14,876	9,854
Symmetry imposed	C3	C1	C1	C1	C1
FSC=0.143 Resolution (Å)	-	-	-	-	-

Table S3. Electron microscopy (EM) data collection and processing statistics.

	Heavy chain VDJ genes (IGH)						VH Protein Sequence
Sequence ID	V-GENE	D-GENE	J-GENE	CDR3-IMGT	CDRH3 Length	---CDRH1--- ---CDRH2--- -------CDRH3--------	
Ab12771	V4-92*01	D2-15*01	J4*01	AAPDCSGPDCSPGFDY	16	QVQLVESGPGLVKPSETLSLTCAVSGDSISSTNWWIRQPPGKGLEWIGRISGDGQNTDYSPSLKSRVTISTDTSKNQLSLRLTSVAAADTAVYFCAAPDCSG---PDCSPGFDYWGPGVLVTVSS	
Ab12891	V5-43*01	D3-9*01	J4*01	SKARYEDEYGYYYSGDYGY	18	QVQLVQSGAEVKRAGESLRISCKTSGYIFSDSWIDWVRQMPGRGLEWMGSIYPGDSETRYNPSFQGHVTISADKSISTIYLQWSSLKASDTAIYYCSKARYEDEYGYYYSGDYGYWGQGVLVTVSS	
Ab13031	V4-160*01	D2-27*01	J4*01	ARRDTDFWRGIYYFEF	16	QVLQESGPGLVKPSETLSLTCAVSGGSISGNYWSWIRQSPGKGLEWIGHINDYSGRTDYNPSLKSRVTISTDTSTNQFFLTLSSVSAADTAVYYCARRDTDF---WRGIYYFEFWGQGVLVTVSS	
Ab13681	V4-143*01	D6-31*01	J4*01	ARCIVAAGTFYFDY	14	EVQLVESGPAVVKPSETLSLTCAVSGGSISGNYWSWIRQPPGKGLEWIGSIYGSSGSTYNNPSLKTRVTISKDTSKNQLSLKLSSVTAADTAVYYCARCIVAA----GTFYFDYWGQGVLVTVSS	
Ab14151	V5-43*01	D5-12*01	J4*01	TIPDADNFNSPYFDY	15	EVQLVQSGAEVKRPGESLHISCKTSGYSFTDTWIGWVRQTPGKGLEWIGSIYPGDSDTRYNPSFQGHVTISADKSISTTYLQWSDLKAPDTAIYYCTIPDADN----FNSPYFDYWGQGVLVTVSS	
Ab14561	V5-43*02	D2-33*01	J6*01	AKWGVDCSDGSCGSS4FDS	18	EVQLVQSGAEVKRPGDSLKISCKTSGDVFTSTWIGWVRQMPGKGLEMMAIYLDDSDTQYNPSFQGHVTISADKSINTTYLQLSSLKVSDTAIYYCAKWGVDCSDGSCGSS4FDSWGQGVLVTVSS	
Ab14571	V4-147*01	D3-3*01	J4*01	ASPFCSTTSCHPSFDY	16	QVQLVESGPGLVKPSETLSLTCAVSGDSINNYWNWIRQPPGEGLEWIGRIYVGDGCTTTWNPSLQSRVTFSTDTSKNQFSLRLTSVTAADTAVYYCASPFCST--TSCHPSFDYWGQGVLVTVSS	
Ab14611	V5-43*01	D5-24*01	J4*01	GRIDGDNGSFDD	12	QVQLVESGGEVKRPGESLRISCETSEYTFTNWITWVRQVPGKGLEMMGNIFPDDSDTIYSPAFQGHVTFSADKSITTYLQWRSLRASDTAIYYCGRIDGDN----GSFDDWGQGVLVTVSS	
Ab15731	V1-198*02	D4-29*01	J5-2*02	ARVGDRFGSGYAMDV	15	QVQLVQSGAEVKKPGASVKVSCKASGFTFGRYSFTWVRQAPGQGLEWVGVIVPLVGVTNSAKKFQGRVTITADTSTNTVYMDLSSLRSEDTAVYYCARVGDRF---GSGYAMDVWGRGALVTVSS	
Ab874NHP	V3-103*01	D6-43*01	J1*01	AKSPWGQSTSFEYFEF	16	EVQLVETGGGLVQPGGSLKLSCAASGFTFSSYGMNWVRQAPGKGLEWVSGINSGGGTKYYADSVKGRFTISRDNSKNTLSLQMNSLRAEDTAVYYCAKSPWGQ---STSFEYFEFWGQGALVTVSS	
Ab1170NHP	V1-111*02	D2-39*02	J4*01	ARGGGHSSFDF	11	QVQLVQSGAEVKKPGASVKISCKASGYTFTDHFLHWVRQAPGKGLEWMGGVDPEDGEADYAQKFQDRVALTADMSTDTAYMELSSLRPEDTAVYHCARGG----------GHSSFDFWGQGVLVTVSS	
Ab2751mur	VH5-6*01	D1-1*01	J4*01	ARHGITTYGVAMDY	14	EVQLQESGGDLVKPGGSLKLSCAASGFTFSRYGMSWVRQTPDKRLEWVATISSGGSYTYYPDSVKGRFTISRDNAKNTLYLQMSSLKSEDTAMYYCARHGITT-----VGVAMDYWGQGTTVSHVSS	
Ab2839mur	VH5-6*01	D1-1*01	J3*01	ARHEHYFGSSSHFAY	15	EVKLVESGGDLVHPGGSLKLSCAASGFTFNSYGMSWVRQTPDKRLEWVATISSGGGYTYYPDSVKGRFTISRDNAENTLYLQMNSLKSEDTAMYFCARHEHYF---G-SSSHFAYWGQGTLVTVSS	

	Light chain VJ genes					VL Protein Sequence	
Sequence ID	V-GENE	J-GENE	CDR3-IMGT	CDRL3 Length	------CDRL1------	----CDRL2----	----CDRL3-----
Ab12771	LV1-85*01	LJ3*01	QSYDSSNSWVL	12	-QPVLTQPPSVSVSPGQRVTISCTGSSS-DIGR-FYVQWYQQLPGTAPKLLIYEN------TKRPSGISDRFSGSKSGPSASLTITGLQSEDEADYYCQSYDSSNSWVLFGGGTRLTVL	
Ab12891	LV1-85*01	LJ3*01	QSYDSSNSWVL	11	-QSVLTQPPSVSVSPGQRVTISCSGSSS-NIET-NYYYWYQQVPGTAPKLLIYDN------DQRPSGVPDRFSGSTSGTSASLAISGLQSEDEADYYCSAWDNGLSGPV-FGGGTRLTVL	
Ab13031	LV4-97*01	LJ1*01	QTWTTGIYI	9	-QSVLTQSPSASASLGASVKLTCTLSSG-LRS-YTIAWYQRQRQAPRYLLRLDSYGSHTKYDQIPDRFSGSSSGTERYLTISNLQSEDEADYFCQTWTTGI----YIFGGGTRLSVL	
Ab13681	LV2-32*01	LJ2A*01	CSYAGSYTWV	10	-QSALTQPRSVSGSPGQSVTISCTGTSS-DIGGYNYVSWYQQHPGTAPKLHIYAV------SKRPSGVSDRFSGSKSGNTASLTISGLQAEDEADYYCCSYAGSYT-WVFGGGTRLTVL	
Ab1415	LV1-85*01	LV2-32*01	QSYDSTLVAHV	11	-QLVLTQPPSVSGAPGQRVTFSCTGSSS-NIGP-YFVQWYQQYPGTAPKVLIYEN------NKRPSGVSDRFSGSLSDTSASLTITGLQAEDEADYYCQSYDSTLVAHV-FGSGTKLTVL	
Ab1456	LV1-85*01	LJ6*01	QSYDDSLSAHV	11	-QSVLTQPPSVSGAPGQRVTISCTGTS-NIGN-YYVQWYQQLPGTAPKLLIYEN------NKRPSGISDRFSGSDSGTSGSLTITGLQSEDEADYFCQSYDDSLSAHV-FGSGTKVTIL	
Ab1457	LV1-85*01	LJ2*01	QSFDNSPSAHVL	12	-NFMLTQPPSVSGAPGQRVTISCTGSNS-NMGD-YYVQWYQQPPGTAPKLLIYEN------TKRPSGVSDRFSGSLSGSSASLTITGLQSEDEADYYCQSFDNSPSAHVL-FGGGTRLTVL	
Ab1461	LV1-64*02	LV1-64*02	LSYDSSLSGWL	11	-QSVLTQPPSVSGAPGQTVTISCTGSSS-NIGN-YFVSWYQHLPGAPPKVLIYQY------NKRPSGVSDRFSGSKSGDTSASLTITGLQTEDEADYYCLSYDSSLSGWL-FGGGTRLTVL	
Ab1573	LV1-64*01	LJ2A*01	QSYDSSLTVWV	11	-QSALTQPPSVSVSPGAPGERVTISCSGSSS-NFEY-SFVYWYQQVPGTAPKLLIYDN------YKRPSGVSDRFSGSRSGTSASLTITGLQTEDESDYYCQSYDSSLTVWV-FGGGTRLTVL	
Ab874NHP	LV3-34*01	LJ3*01	QVWDSSSDHPL	11	-QSVLTQPRSVSVSQGQTARITCGGDN----IGS-EAVQWYQQKPAQAPVLVIYDD------SERPSGIPDRFSGSKSGNTATLTISGVEAGDEADYYCQVWDSSSD-HPLFGGGTRLTVL	
Ab1170NHP	LV2-32*02	LJ2A*01	SSYAGINTLV	10	-QSVLTQPRSVSGSPGQSVTISCTGTSS-DIGGYNYVSWYQQHPGTAPKLMIYEV------SKRPSGVSDRFSGSKSGNTASLTISGLQAEDEADYYCSSYAGINT-LVFGGGTRLTVL	
Ab275mur	KV3-4*01	KJ5*01	QQSNEDPYT	9	DIVMTQSPASLAVSLGQRATISCKASQSVDYDGDSYMNWYQQKPGQPPKLLIYAA------SNLESGIPARFSGSGSGTDFTLNIHPVEEEDAATYYCQQSNEDP----YTFGAGTKLELK	
Ab283mur	KV3-4*01	KJ4*01	HQSYEDPFT	9	QIVLTQSPVSLAVSLGQRATISCKASQSVDYDGDSYMNWYQLKPGQPPKLLIYAA------SNLESGIPARFSGSGSGTDFTLNIHPVEEEDAATYYCHQSYEDP----FTFGAGTKLELK	

Table S4. VDJ assignments and sequences of antibodies from immunized NHPs and mice.

Immunogen Name	Sequence
RC1-4fill-Spytag	MDAMKRGLCCVLLLCGAVFVSPAGAGSNLWVTVYYGVPVWKDAETTLFCASDAKAYETEKHNVWATHACVPTDPNPQEIHLENVTEEFNM WKNNMVEQMHEDIISLWDQSLKPCVKLTPLCVTLQCTNYAPNLLSNMRGELKQCSFNMTTELRDKKQKVYSLFYRLDVVQINENQGNRSNN SNKEYRLINCNTSAITQACPKVSFEPIPIHYCAPAGFAILKCKNKTFNGTGPCPNVSTVQCTHGIKPVVSTQLLLNGSLAEEEVIIRSENITNNAKNI LVQLNTSVQINCTRPNNNTVKSIRIGPGQAFYYFGDIIGDIRMAHCNVSKATWNETLGNVSKQLRKHFGNNTIIRFAQSSGGDLEVTTHSFNC GGEFFYCNTSGLFNSTWISNTSVQGSNSTGSNDSIVLPCRIKQIINMWQRIGQAMYAPPIQGVIRCVSNITGLILTRDGGSTNSTTETFRPGG GDMRDNWRSELYKYKVVKIEPLGVAPTRCKRRVVGRRRRRRAVGIGAVSLGFLGAAGSTMGAASMTLTVQARNLLSGIVQQQSNLLRAPE PQQHLLKDTHWGIKQLQARVLAVEHYLRDQQLLGIWGCSGKLICCTNVPWNSSWSNRNLSEIWDNMTWLQWDKEISNYTQIIYGLLEESQ NQQEKNEQDLLALDGGGGSGGGSGGGSGSGAHIVMVDAYKPTK
11MUTB-4fill-Spytag	MDAMKRGLCCVLLLCGAVFVSPAGAGSNLWVTVYYGVPVWKDAETTLFCASDAKAYETEKHNVWATHACVPTDPNPQEIHLENVTEEFNM WKNNMVEQMHEDIISLWDQSLKPCVKLTPLCVTLQCTNYAPNLLSNMRGELKNCSFNMTTELRDKKQKVYSLFYRLDVVQINENQGNRSNN SNKEYRLINCNTSAITQACPKVSFEPIPIHYCAPAGFAILKCKNKTFNGTGPCPNVSTVQCTHGIKPVVSTQLLLNGSLAEEEVIIRSENITNNAKNI LVQLNTSVQINCTRPNNNTVKSIRIGPGQAFYYFGDIIGDIRMAHCNVSKATWNETLGNVSKQLRKHFGNNTIIRFAQSSGGDLEVTTHSFNC GGEFFYCNTSGLFNSTWISNTSVQGSNSTGSNDSIVLPCRIKQIINMWQRIGQAMYAPPIQGVIRCVSNITGLILTRDGGSTNSTTETFRPGG GDMRDNWRSELYKYKVVKIEPLGVAPTRCKRRVVGRRRRRRAVGIGAVSLGFLGAAGSTMGAASMTLTVQARNLLSGIVQQQSNLLRAPE PQQHLLKDTHWGIKQLQARVLAVEHYLRDQQLLGIWGCSGKLICCTNVPWNSSWSNRNLSEIWDNMTWLQWDKEISNYTQIIYGLLEESQ NQQEKNEQDLLALDGGGGSGGGSGGGSGSGAHIVMVDAYKPTK
B41wt-Spytag	MDAMKRGLCCVLLLCGAVFVSPSQEIHARFRRGARAAKKWVTVYYGVPVWKEATTTLFCASDAKAYDTEVHNVWATHACVPTDPNPQEIVL GNVTENFNMWKNNMVEQMHEDIISLWDQSLKPCVKLTPLCVTLNCNNVNTNNTNNSTNATISDWEKMETGEMKNCSFNVTTSIRDKIKKE YALFYKLDVVPLENKNNININNTNITNYRLINCNTSVITQACPKVSFEPIPIHYCAPAGFAILKCNSKTFNGSGPCTNVSTVQCTHGIRPVVSTQLLLN GSLAEEEIVIRSENITDNAKTIIVQLNESVEINCTRPNNNTRKSIHIGPGRAFYATGDIIGNIRQAHCNISKARWNETLGQIVAKLEEQFPNKTIIF NHSSGGDPEIVTHSFNCGGEFFYCNTTPLFNSTWNNTRTDDYPTGGEQNITLQCRIKQIINMWQGVGKAMYAPPIRGQIRCSSNITGLLLTR DGGRDQNGTETFRPGGGNMRDNWRSELYKYKVVKIEPLGIAPTACKRRVVQRRRRRRAVGLGAFILGFLGAAGSTMGAASMALTVQARL LLSGIVQQQNNLLRAPEAQQHMLQLTVWGIKQLQARVLAVERYLRDQQLLGIWGCSGKIICCTNVPWNDSWSNKTINEIWDNMTWMQW EKEIDNYTQHIYTLLEVSQIQQEKNEQELLELDGGGGSGGGSGGGSGSGAHIVMVDAYKPTK
B41-5MUT-Spytag	MDAMKRGLCCVLLLCGAVFVSPSQEIHARFRRGARAAKKWVTVYYGVPVWKEATTTLFCASDAKAYDTEVHNVWATHACVPTDPNPQEIVL GNVTENFNMWKNNMVEQMHEDIISLWDQSLKPCVKLTPLCVTLNCNNYNPNLTNDMRNATISDWEKMETGEMKNCSFNVTTSIRDKIKKE YALFYKLDVVPLENKNNININNTNITNYRLINCNTSVITQACPKVSFEPIPIHYCAPAGFAILKCNSKTFNGSGPCTNVSTVQCTHGIRPVVSTQLLLN GSLAEEEIVIRSENITDNAKTIIVQLNESVEINCTRPNNNTRKSIHIGPGRWFYATGDIIGNIRQAHCNISKARWNETLGQIVAKLEEQFPNKTIIF NHSSGGDPEIVTHSFNCGGEFFYCNTTPLFNSTWNNTRTDDYPTGGEQNITLQCRIKQIINMWQGVGKAMYAPPIRGQIRCSSNITGLLLTR DGGRDQNGTETFRPGGGNMRDNWRSELYKYKVVKIEPLGIAPTACKRRVVQRRRRRRAVGLGAFILGFLGAAGSTMGAASMALTVQARL LLSGIVQQQNNLLRAPEAQQHMLQLTVWGIKQLQARVLAVERYLRDQQLLGIWGCSGKIICCTNVPWNDSWSNKTINEIWDNMTWMQW EKEIDNYTQHIYTLLEVSQIQQEKNEQELLELDGGGGSGGGSGGGSGSGAHIVMVDAYKPTK
AMC011-Spytag	MDAMKRGLCCVLLLCGAVFVSPSQEIHARFRRGARAEQLWVTVYYGVPVWKEATTTLFCASDARAYDTEVRNVWATHCCVPTDPNPQEVV LENVTENFNMWKNNMVEQMHEDIISLWDQSLKPCVKLTPLCVTLNCTDLRNATNTNATNTTSSSRGTMEGGEIKNCSFNITTSMRDKVQKE YALFYKLDVVPIKNDNTSYRLISCNTSVITQACPKVSFEPIPIHYCAPAGFAILKCNNKTFNGTGPCTNVSTVQCTHGIRPVVSTQLLLNGSLAEEE VVIRSANFTDNAKIIIVQLNKSVEINCTRPNNNTRKSIHIGPGRWFYTTGEIIGDIRQAHCNISGTKWNDTLKQIVVKLKEQFGNKTIVFNHSSG GDPEIVMHSFNCGGEFFYCNSTQLFNSTWNDTTGSNYTGTIVLPCRIKQIVNMWQEVGKAMYAPPIKGQIRCSSNITGLILIRDGGKNRSEN TEIFRPGGGDMRDNWRSELYKYKVVKIEPLGIAPTKCKRRVVQRRRRRRAVGIGAVFLGFLGAAGSTMGAASMTLTVQARQLLSGIVQQQ NNLLRAPECQQHLLKLTVWGIKQLQARVLAVERYLKDQQLLGIWGCSGKLICCTAVPWNTSWSNKSYNQIWNNMTWMEWEREIDNYTSLI YTLIEDSQNQQEKNEQELLELDGGGGSGGGSGGGSGSGAHIVMVDAYKPTK
Du422-Spytag	MDAMKRGLCCVLLLCGAVFVSPSQEIHARFRRGARNLDLWVTVYYGVPVWKEAKTTLFCASDAKAYDKEVRNVWATHACVPTDPNPQEIVL ENVTENFNMWKNDMVDQMHEDIISLWDQSLKPCVKLTPLCVTLNCKNVNISANANATATLNSSMNGEIKNCSFNTTTELRDKKQKVYALFY KPDVVPLNGGEHNETGEYILINCNSSTITQACPKVSFDPIPIHYCAPAGYAILKCNNKTFNGTGPCNNVSTVQCTHGIKPVVSTQLLLNGSLAEEE IIVRSENLTNNIKTIIVHLNKSVEINCTRPNNNTRKSVRIGPGQWFYATGEIIGDIREAHCNISRETWNSTLIQVKEKLREHYNKTIKFEPSSGGDL EVTTHSFNCRGEFFYCNTTKLFNETKLFNESEYVDNKTIILPCRIKQIINMWQEVGRAMYAPPIEGNITCKSNITGLLLTWDGGENSTEGVFRP GGGNMKDNWRSELYKYKVVEIKPLGVAPTKCKRKVVGRRRRRRAVGLGAVLLGFLGAAGSTMGAASMTLTVQARQLLSGIVQQQSNLLR APEAQQHLLQLTVWGIKQLQTRVLAIERYLKDQQLLGLWGCSGKLICCTAVPWNSSWSNKSLGDIWDNMTWMQWDREISNYTNTIFRLLE DSQNQQEKNEKDLLALDGGGGSGGGSGGGSGSGAHIVMVDAYKPTK
ConM-Spytag	MDAMKRGLCCVLLLCGAVFVSPSQEIHARFRRGARAENLWVTVYYGVPVWKDAETTLFCASDAKAYDTEKRNVWATHCCVPTDPNPQEIVL ENVTENFNMWKNNMVEQMHTDIISLWDQSLKPCVKLTPLCVTLNCTDVNATNNTTNNEEIKNCSFNITTELRDKKKKVYALFYKLDVVPIDDN NSYRLINCNTSAITQACPKVSFEPIPIHYCAPAGFAILKCNDKKFNGTGPCKNVSTVQCTHGIKPVVSTQLLLNGSLAEEEIIIRSENITNNAKTIIVQ LNESVEINCTRPNNNTRKSIRIGPGQWFYATGDIIGDIRQAHCNISRTKWNKTLQQVAKKLREHFNKTIIFNPSSGGDLEITTHSFNCGGEFFYC NTSELFNSTWNGTNNTITLPCRIKQIINMWQRVGQAMYAPPIEGKIRCTSNITGLLLTRDGGNNNTETFRPGGGDMRDNWRSELYKYKVVK IEPLGVAPTRCKRRVVERRRRRRAVGIGAVFLGFLGAAGSTMGAASMTLTVQARNLLSGIVQQQSNLLRAPECQQHLLQLTVWGIKQLQAR VLAVERYLKDQQLLGIWGCSGKLICCTNVPWNSSWSNKSQDEIWDNMTWMEWDKEINNYTDIIYSLIEESQNQQEKNEQELLALDGGGGS GGGSGGGSGSGAHIVMVDAYKPTK
ConC-Spytag	MRVRGILRNWQQWWIWGILGFWMLMICNVVGNLWVTVYYGVPVWKEAKTTLFCASDAKAYEKEVHNVWATHACVPTDPNPQEMVLE NVTENFNMWKNDMVDQMHEDIISLWDQSLKPCVKLTPLCVTLNCTNVNVTNTNNNNMKEEMKNCSFNTTTEIRDKKQKEYALFYRLDIVPL NENSSEYRLINCNTSTITQICPKVSFDPIPIHYCAPAGYAILKCNNKTFNGTGPCNNVSTVQCTHGIKPVVSTQLLLNGSLAEEEIIIRSENLTDNAK TIIVHLNESVEINCTRPNNNTRKSIRIGPGQTFYATGDIIGDIRQAHCNISEAKWNKTLQRVKKKLKEHFPNKTIKFAPSSGGDLEITTHSFNCRGE FFYCNTSKLFNSTYNNTTSNSTITLPCRIKQIINMWQEVGRAMYAPPIAGNITCKSNITGLLLTRDGGNNNNNTETFRPGGGDMRDNWRSEL YKYKVVEIKPLGIAPTKCKRRVVERRRRRRAVGIGAVFLGFLGAAGSTMGAASNTLTVQARQLLSGIVQQQSNLLRAPEAQQHMLQLTVWG FKQLQARVLAIERYLEVQQLLGIWGCSGKLICCTAVPWNSSWSNKSQEDIWDNMTWMQWDREISNYTDTIYRLLEESQFQQEINEKDLLAL DGGGGSGGGSGGGSGSGAHIVMVDAYKPTK

Table S5. SOSIP immunogen sequences.

Data File S1 is available online with DOI: 10.1126/scitranslmed.abk1533.

References

1. Baba, T.W. *et al.* Human neutralizing monoclonal antibodies of the IgG1 subtype protect against mucosal simian-human immunodeficiency virus infection. *Nat Med* **6**, 200-206 (2000).

2. Balazs, A.B. *et al.* Antibody-based protection against HIV infection by vectored immunoprophylaxis. *Nature* **48**, 81-88 (2012).

3. Eichberg, J.W., Murthy, K.K., Ward, R.H. & Prince, A.M. Prevention of HIV infection by passive immunization with HIVIG or CD4-IgG. *AIDS Res Hum Retroviruses* **8**, 1515 (1992).

4. Emini, E.A. *et al.* Prevention of HIV-1 infection in chimpanzees by gp120 V3 domain-specific monoclonal antibody. *Nature* **355**, 728-730 (1992).

5. Hessell, A.J. *et al.* Broadly neutralizing monoclonal antibodies 2F5 and 4E10 directed against the human immunodeficiency virus type 1 gp41 membrane-proximal external region protect against mucosal challenge by simian-human immunodeficiency virus SHIVBa-L. *J Virol* **84**, 1302-1313 (2010).

6. Hessell, A.J. *et al.* Effective, low-titer antibody protection against low-dose repeated mucosal SHIV challenge in macaques. *Nat Med* **15**, 951-954 (2009).

7. Hessell, A.J. *et al.* Broadly neutralizing human anti-HIV antibody 2G12 is effective in protection against mucosal SHIV challenge even at low serum neutralizing titers. *PLoS Pathog* **5**, e1000433 (2009).

8. Mascola, J.R. *et al.* Protection of macaques against vaginal transmission of a pathogenic HIV-1/SIV chimeric virus by passive infusion of neutralizing antibodies. *Nat Med* **6**, 207-210 (2000).

9. Mascola, J.R. *et al.* Protection of Macaques against pathogenic simian/human immunodeficiency virus 89.6PD by passive transfer of neutralizing antibodies. *J Virol* **73**, 4009-4018 (1999).

10. Moldt, B. *et al.* Highly potent HIV-specific antibody neutralization in vitro translates into effective protection against mucosal SHIV challenge in vivo. *Proc Natl Acad Sci U S A* **109**, 18921-18925 (2012).

11. Parren, P.W. *et al.* Antibody protects macaques against vaginal challenge with a pathogenic R5 simian/human immunodeficiency virus at serum levels giving complete neutralization in vitro. *J Virol* **75**, 8340-8347 (2001).

12. Pietzsch, J. *et al.* A mouse model for HIV-1 entry. *Proc Natl Acad Sci U S A* **109**, 15859-15864 (2012).

13. Shibata, R. *et al.* Neutralizing antibody directed against the HIV-1 envelope glycoprotein can completely block HIV-1/SIV chimeric virus infections of macaque monkeys. *Nat Med* **5**, 204-210 (1999).

14. Bonsignori, M. *et al.* Antibody-virus co-evolution in HIV infection: Paths for HIV vaccine development. *Immunol Rev* **275**, 145-160 (2017).

15. Kwong, P.D. & Mascola, J.R. HIV-1 vaccines based on antibody identification, B cell ontogeny, and epitope structure. *Immunity* **48**, 855-871 (2018).

16. McCoy, L.E. & Burton, D.R. Identification and specificity of broadly neutralizing antibodies against HIV. *Immunol Rev* **275**, 11-20 (2017).

17. West, A.P., Jr. *et al.* Structural insights on the role of antibodies in HIV-1 vaccine and therapy. *Cell* **156**, 633-648 (2014).

18. Liao, H.X. *et al.* Co-evolution of a broadly neutralizing HIV-1 antibody and founder virus. *Nature* **496**, 469-476 (2013).

19. Roark, R.S. *et al.* Recapitulation of HIV-1 Env-antibody coevolution in macaques leading to neutralization breadth. *Science* **371**, eabd2638 (2021).

20. Wang, Z. *et al.* A broadly neutralizing macaque monoclonal antibody against the HIV-1 V3-Glycan patch. *eLife* **9** (2020).

21. Escolano, A., Dosenovic, P. & Nussenzweig, M.C. Progress toward active or passive HIV-1 vaccination. *J Exp Med* **214**, 3-16 (2017).

22. Haynes, B.F. & Mascola, J.R. The quest for an antibody-based HIV vaccine. *Immunol Rev* **275**, 5-10 (2017).

23. Escolano, A. *et al.* Sequential immunization elicits broadly neutralizing anti-HIV-1 antibodies in Ig knockin mice. *Cell* **166**, 1445-1458 e1412 (2016).

24. Xiao, X. *et al.* Germline-like predecessors of broadly neutralizing antibodies lack measurable binding to HIV-1 envelope glycoproteins: implications for evasion of immune responses and design of vaccine immunogens. *Biochem Biophys Res Commun* **390**, 404-409 (2009).

25. Bonsignori, M. *et al.* Analysis of a clonal lineage of HIV-1 envelope V2/V3 conformational epitope-specific broadly neutralizing antibodies and their inferred unmutated common ancestors. *J Virol* **85**, 9998-10009 (2011).

26. Scheid, J.F. *et al.* Sequence and structural convergence of broad and potent HIV antibodies that mimic CD4 binding. *Science* **333**, 1633-1637 (2011).

27. Klein, F. *et al.* Somatic mutations of the immunoglobulin framework are generally required for broad and potent HIV-1 neutralization. *Cell* **153**, 126-138 (2013).

28. Mouquet, H. *et al.* Complex-type N-glycan recognition by potent broadly neutralizing HIV antibodies. *Proc Natl Acad Sci U S A* **109**, E3268-3277 (2012).

29. Zhou, T. *et al.* Structural basis for broad and potent neutralization of HIV-1 by antibody VRC01. *Science* **329**, 811-817 (2010).

30. Abbott, R.K. *et al.* Precursor frequency and affinity determine B cell competitive fitness in germinal centers, tested with germline-targeting HIV vaccine immunogens. *Immunity* **48**, 133-146 e136 (2018).

31. Dal Porto, J.M., Haberman, A.M., Shlomchik, M.J. & Kelsoe, G. Antigen drives very low affinity B cells to become plasmacytes and enter germinal centers. *J Immunol* **161**, 5373-5381 (1998).

32. Dosenovic, P. *et al.* Anti-HIV-1 B cell responses are dependent on B cell precursor frequency and antigen-binding affinity. *Proc Natl Acad Sci U S A* **115**, 4743-4748 (2018).

33. Shih, T.A., Meffre, E., Roederer, M. & Nussenzweig, M.C. Role of BCR affinity in T cell dependent antibody responses in vivo. *Nat Immunol* **3**, 570-575 (2002).

34. Tas, J.M. *et al.* Visualizing antibody affinity maturation in germinal centers. *Science* **351**, 1048-1054 (2016).

35. Schwickert, T.A. *et al.* A dynamic T cell-limited checkpoint regulates affinity-dependent B cell entry into the germinal center. *J Exp Med* **208**, 1243-1252 (2011).

36. Kong, R. *et al.* Antibody lineages with vaccine-induced antigen-binding hotspots develop broad HIV neutralization. *Cell* **178**, 567-584.e519 (2019).

37. Kong, L. *et al.* Supersite of immune vulnerability on the glycosylated face of HIV-1 envelope glycoprotein gp120. *Nat Struct Mol Biol* **20**, 796-803 (2013).

38. Escolano, A. *et al.* Immunization expands B cells specific to HIV-1 V3 glycan in mice and macaques. *Nature* **570**, 468-473 (2019).

39. Walker, L.M. *et al.* Broad neutralization coverage of HIV by multiple highly potent antibodies. *Nature* **477**, 466–470 (2011).

40. Freund, N.T. *et al.* Coexistence of potent HIV-1 broadly neutralizing antibodies and antibody-sensitive viruses in a viremic controller. *Sci Transl Med* **9** (2017).

41. Sok, D. *et al.* A prominent site of antibody vulnerability on HIV envelope incorporates a motif associated with CCR5 binding and its camouflaging glycans. *Immunity* **45**, 31-45 (2016).

42. Steichen, J.M. *et al.* HIV vaccine design to target germline precursors of glycan-dependent broadly neutralizing antibodies. *Immunity* **45**, 483-496 (2016).

43. Sanders, R.W. *et al.* A next-generation cleaved, soluble HIV-1 Env trimer, BG505 SOSIP.664 gp140, expresses multiple epitopes for broadly neutralizing but not non-neutralizing antibodies. *PLOS Pathog* **9**, e1003618 (2013).

44. Garces, F. *et al.* Structural evolution of glycan recognition by a family of potent HIV antibodies. *Cell* **159**, 69-79 (2014).

45. Gristick, H.B. *et al.* Natively glycosylated HIV-1 Env structure reveals new mode for antibody recognition of the CD4-binding site. *Nat Struct Mol Biol* **23**, 906-915 (2016).

46. Scharf, L. *et al.* Structural basis for germline antibody recognition of HIV-1 immunogens. *eLife* **5** (2016).

47. McCoy, L.E. *et al.* Holes in the glycan shield of the native HIV envelope are a target of trimer-elicited neutralizing antibodies. *Cell Rep* **16**, 2327-2338 (2016).

48. Brune, K.D. *et al.* Plug-and-display: Decoration of virus-like particles via isopeptide bonds for modular immunization. *Sci Rep* **6**, 19234 (2016).

49. Zakeri, B. *et al.* Peptide tag forming a rapid covalent bond to a protein, through engineering a bacterial adhesin. *Proc Natl Acad Sci U S A* **109**, E690-697 (2012).

50. Bianchi, M. *et al.* Electron-microscopy-based epitope mapping defines specificities of polyclonal antibodies elicited during HIV-1 BG505 envelope trimer immunization. *Immunity* **49**, 288-300 e288 (2018).

51. Montefiori, D.C. Evaluating neutralizing antibodies against HIV, SIV, and SHIV in luciferase reporter gene assays. *Curr Protoc Immunol* **Chapter 12**, Unit 12.11 (2005).

52. Pugach, P. *et al.* A native-like SOSIP.664 trimer based on an HIV-1 subtype B env gene. *J Virol* **89**, 3380-3395 (2015).

53. van Gils, M.J. *et al.* An HIV-1 antibody from an elite neutralizer implicates the fusion peptide as a site of vulnerability. *Nat Microbiol* **2** (2016).

54. Li, M. *et al.* Genetic and neutralization properties of subtype C human immunodeficiency virus type 1 molecular env clones from acute and early heterosexually acquired infections in Southern Africa. *J Virol* **80**, 11776-11790 (2006).

55. Rutten, L. *et al.* A universal approach to optimize the folding and stability of prefusion-closed HIV-1 envelope trimers. *Cell Rep* **23**, 584-595 (2018).

56. Sliepen, K. *et al.* Structure and immunogenicity of a stabilized HIV-1 envelope trimer based on a group-M consensus sequence. *Nat Commun* **10** (2019).

57. Lee, J.H. *et al.* A broadly neutralizing antibody targets the dynamic HIV envelope trimer apex via a long, rigidified, and anionic beta-hairpin structure. *Immunity* **46**, 690-702 (2017).

58. Walker, L.M. *et al.* Broad and potent neutralizing antibodies from an African donor reveal a new HIV-1 vaccine target. *Science* **326**, 285-289 (2009).

59. Schoofs, T. *et al.* Broad and potent neutralizing antibodies recognize the silent face of the HIV envelope. *Immunity* **50**, 1513-1529 e1519 (2019).

60. Kong, R. *et al.* Fusion peptide of HIV-1 as a site of vulnerability to neutralizing antibody. *Science* **352**, 828-833 (2016).

61. Scharf, L. *et al.* Broadly neutralizing antibody 8ANC195 recognizes closed and open states of HIV-1 Env. *Cell* **162**, 1379-1390 (2015).

62. Lee, J.H. *et al.* Antibodies to a conformational epitope on gp41 neutralize HIV-1 by destabilizing the Env spike. *Nat Commun* **6**, 8167 (2015).

63. Shingai, M. *et al.* Passive transfer of modest titers of potent and broadly neutralizing anti-HIV monoclonal antibodies block SHIV infection in macaques. *J Exp Med* **211**, 2061-2074 (2014).

64. Nishimura, Y. *et al.* Generation of the pathogenic R5-tropic simian/human immunodeficiency virus SHIVAD8 by serial passaging in rhesus macaques. *J Virol* **84**, 4769-4781 (2010).

65. Lorenzi, J.C.C. *et al.* Neutralizing activity of broadly neutralizing anti-HIV-1 antibodies against primary African isolates. *J Virol* **95** (2020).

66. Cohen, Y.Z. *et al.* Neutralizing activity of broadly neutralizing anti-HIV-1 antibodies against clade B clinical isolates produced in peripheral blood mononuclear cells. *J Virol* **92** (2018).

67. Nogal, B. *et al.* Mapping polyclonal antibody responses in non-human primates vaccinated with HIV Env trimer subunit vaccines. *Cell Rep* **30**, 3755-3765 e3757 (2020).

68. Barnes, C.O. *et al.* Structures of human antibodies bound to SARS-CoV-2 spike reveal common epitopes and recurrent features of antibodies. *Cell* **182**, 828-842 e816 (2020).

69. Turner, H.L. *et al.* Disassembly of HIV envelope glycoprotein trimer immunogens is driven by antibodies elicited via immunization. *Sci Adv* **7** (2021).

70. Wang, Z. *et al.* Isolation of single HIV-1 Envelope specific B cells and antibody cloning from immunized rhesus macaques. *J Immunol Methods* **478**, 112734 (2020).

71. deCamp, A. *et al.* Global panel of HIV-1 Env reference strains for standardized assessments of vaccine-elicited neutralizing antibodies. *J Virol* **88**, 2489-2507 (2014).

72. Pauthner, M.G. *et al.* Vaccine-induced protection from homologous tier 2 SHIV challenge in nonhuman primates depends on serum-neutralizing antibody titers. *Immunity* **50**, 241-252.e246 (2019).

73. Arunachalam, P.S. *et al.* T cell-inducing vaccine durably prevents mucosal SHIV infection even with lower neutralizing antibody titers. *Nat Med* **26**, 932-940 (2020).

74. Steichen, J.M. *et al.* A generalized HIV vaccine design strategy for priming of broadly neutralizing antibody responses. *Science* **366** (2019).

75. Antanasijevic, A. *et al.* Polyclonal antibody responses to HIV Env immunogens resolved using cryoEM. *bioRxiv* (2021).

76. Nogal, B. *et al.* HIV envelope trimer-elicited autologous neutralizing antibodies bind a region overlapping the N332 glycan supersite. *Sci Adv* **6**, eaba0512 (2020).

77. Joyce, M.G. *et al.* Soluble prefusion closed DS-SOSIP.664-Env trimers of diverse HIV-1 strains. *Cell Rep* **21**, 2992-3002 (2017).

78. Antanasijevic, A. *et al.* Structural and functional evaluation of de novo-designed, two-component nanoparticle carriers for HIV Env trimer immunogens. *PLOS Pathog* **16**, e1008665 (2020).

79. Provine, N.M., Cortez, V., Chohan, V. & Overbaugh, J. The neutralization sensitivity of viruses representing human immunodeficiency virus type 1 variants of diverse subtypes from early in infection is dependent on producer cell, as well as characteristics of the specific antibody and envelope variant. *Virology* **427**, 25-33 (2012).

80. Muecksch, F. *et al.* Development of potency, breadth and resilience to viral escape mutations in SARS-CoV-2 neutralizing antibodies. *Immunity* (2021).

81. Wieczorek, L. *et al.* Mitigation of variation observed in a peripheral blood mononuclear cell (PBMC) based HIV-1 neutralization assay by donor cell pooling. *Virology* **447**, 240-248 (2013).

82. Mascola, J.R. *et al.* Recommendations for the design and use of standard virus panels to assess neutralizing antibody responses elicited by candidate human immunodeficiency virus type 1 vaccines. *J Virol* **79**, 10103-10107 (2005).

83. Trkola, A. *et al.* Delay of HIV-1 rebound after cessation of antiretroviral therapy through passive transfer of human neutralizing antibodies. *Nat Med* **11**, 615-622 (2005).

84. Bonsignori, M. *et al.* Maturation pathway from germline to broad HIV-1 neutralizer of a CD4-mimic antibody. *Cell* **165**, 449-463 (2016).

85. Gao, F. *et al.* Cooperation of B cell lineages in induction of HIV-1-broadly neutralizing antibodies. *Cell* **158**, 481-491 (2014).

86. Medina-Ramirez, M. *et al.* Design and crystal structure of a native-like HIV-1 envelope trimer that engages multiple broadly neutralizing antibody precursors in vivo. *J Exp Med* **214**, 2573-2590 (2017).

87. Wang, H. *et al.* Asymmetric recognition of HIV-1 Envelope trimer by V1V2 loop-targeting antibodies. *eLife* **6** (2017).

88. Tissot, A.C. *et al.* Versatile virus-like particle carrier for epitope based vaccines. *PLoS One* **5**, e9809 (2010).

89. Lövgren-Bengtsson, K. & Morein, B. The ISCOM(TM) Techology. In: O'Hagan, D.T. (ed). *Vaccine Adjuvants: Preparation Methods and Research Protocols*. Humana, 2000, pp 239-258.

90. Montefiori, D.C. Measuring HIV neutralization in a luciferase reporter gene assay. *Methods Mol Biol* **485**, 395-405 (2009).

91. Gautam, R. *et al.* A single injection of anti-HIV-1 antibodies protects against repeated SHIV challenges. *Nature* **533**, 105-109 (2016).

92. Shingai, M. *et al.* Most rhesus macaques infected with the CCR5-tropic SHIV(AD8) generate cross-reactive antibodies that neutralize multiple HIV-1 strains. *Proc Natl Acad Sci U S A* **109**, 19769-19774 (2012).

93. Mastronarde, D.N. Automated electron microscope tomography using robust prediction of specimen movements. *J Struct Biol* **152**, 36-51 (2005).

94. Punjani, A., Rubinstein, J.L., Fleet, D.J. & Brubaker, M.A. cryoSPARC: algorithms for rapid unsupervised cryo-EM structure determination. *Nat Methods* **14**, 290-296 (2017).

95. Tang, G. *et al.* EMAN2: an extensible image processing suite for electron microscopy. *J Struct Biol* **157**, 38-46 (2007).

96. Goddard, T.D., Huang, C.C. & Ferrin, T.E. Visualizing density maps with UCSF Chimera. *J Struct Biol* **157**, 281-287 (2007).

97. Pettersen, E.F. *et al.* UCSF Chimera--a visualization system for exploratory research and analysis. *J Comput Chem* **25**, 1605-1612 (2004).

98. Kremer, J.R., Mastronarde, D.N. & McIntosh, J.R. Computer visualization of three-dimensional image data using IMOD. *J Struct Biol* **116**, 71-76 (1996).

99. Brochet, X., Lefranc, M.P. & Giudicelli, V. IMGT/V-QUEST: The highly customized and integrated system for IG and TR standardized V-J and V-D-J sequence analysis. *Nucleic Acids Res* **36**, W503-508 (2008).

100. Sievers, F. *et al.* Fast, scalable generation of high-quality protein multiple sequence alignments using Clustal Omega. *Mol Syst Biol* **7**, 539 (2011).

101. Diskin, R., Marcovecchio, P.M. & Bjorkman, P.J. Structure of a clade C HIV-1 gp120 bound to CD4 and CD4-induced antibody reveals anti-CD4 polyreactivity. *Nat Struct Mol Biol* **17**, 608-613 (2010).

102. Scheres, S.H. RELION: Implementation of a Bayesian approach to cryo-EM structure determination. *J Struct Biol* **180**, 519-530 (2012).

103. Zivanov, J. *et al.* New tools for automated high-resolution cryo-EM structure determination in RELION-3. *eLife* **7** (2018).

104. Rohou, A. & Grigorieff, N. CTFFIND4: Fast and accurate defocus estimation from electron micrographs. *J Struct Biol* **192**, 216-221 (2015).

105. Goddard, T.D. *et al.* UCSF ChimeraX: Meeting modern challenges in visualization and analysis. *Protein Sci* **27**, 14-25 (2018).

106. Hagen, W.J.H., Wan, W. & Briggs, J.A.G. Implementation of a cryo-electron tomography tilt-scheme optimized for high resolution subtomogram averaging. *J Struct Biol* **197**, 191-198 (2017).

107. Afonine, P.V. *et al.* Real-space refinement in PHENIX for cryo-EM and crystallography. *Acta Crystallogr D Struct Biol* **74**, 531-544 (2018).

108. Terwilliger, T.C., Adams, P.D., Afonine, P.V. & Sobolev, O.V. A fully automatic method yielding initial models from high-resolution cryo-electron microscopy maps. *Nat Methods* **15**, 905-908 (2018).

109. Emsley, P., Lohkamp, B., Scott, W.G. & Cowtan, K. Features and development of Coot. *Acta Crystallogr D Biol Crystallogr* **66**, 486-501 (2010).

110. Schrödinger, L. The PyMOL Molecular Graphics System. 1.2r3pre ed: The PyMOL Molecular Graphics System; 2011.

111. Endo, Y. *et al.* Short- and long-term clinical outcomes in rhesus monkeys inoculated with a highly pathogenic chimeric simian/human immunodeficiency virus. *J Virol* **74**, 6935-6945 (2000).

C h a p t e r 3

NEUTRALIZING ANTIBODIES ELICITED IN MACAQUES RECOGNIZE V3 RESIDUES ON ALTERED CONFORMATIONS OF HIV-1 ENV TRIMER

DeLaitsch, A.T., Keeffe, J.R., Gristick, H.B., Lee, J.A., Ding, W., Liu, W., Skelly, A.N., Shaw, G.M., Hahn, B.H., Björkman, P.J. Neutralizing antibodies elicited in sequentially immunized macaques recognize V3 residues on altered conformations of HIV-1 Env trimer. *npj Vaccines* **9,** 240 (2024). doi: https://doi.org/10.1038/s41541-024-01038-0

Abstract: Eliciting broadly neutralizing antibodies that protect against diverse HIV-1 strains is a primary goal of AIDS vaccine research. We characterized Ab1456 and Ab1271, two heterologously-neutralizing antibodies elicited in non-human primates by priming with an engineered V3-targeting SOSIP Env immunogen and boosting with increasingly native-like SOSIP Envs derived from different strain backgrounds. Structures of Env trimers in complex with these antibodies revealed V3 targeting, but on conformational states of Env distinct from the typical closed, prefusion trimeric SOSIP structure. Env trimers bound by Ab1456 adopted conformations resembling CD4-bound open Env states in the absence of soluble CD4, whereas trimers bound by Ab1271 exhibited a trimer apex-altered conformation to accommodate antibody binding. The finding that elicited antibodies cross-neutralized by targeting altered, non-closed, prefusion Env trimer conformations provides important information about Env dynamics that is relevant for HIV-1 vaccine design aimed at raising antibodies to desired epitopes on closed pre-fusion Env trimers.

Introduction

The HIV-1 envelope glycoprotein (Env) on the virion surface is responsible for fusing viral and host cell membranes during infection[1]. Env, a heavily glycosylated trimer of gp120-gp41 heterodimers, functions via a dynamic mechanism initiated upon engaging one or more copies of the host cell receptor CD4[1]. CD4 binding leads to open conformational states of Env trimer in which gp120s undergo an outward rotation[2], and protomers bound by CD4 exhibit a large-scale rearrangement in the V1V2 region of gp120 that exposes the binding site for the HIV-1 co-receptor, CCR5 or CXCR4[3]. This conformation can be described as a CD4-bound open state, as it is typically observed in the presence of CD4 or a CD4 mimetic small molecule[3, 4, 5, 6]. After co-receptor binding, gp41-mediated fusion of viral and host cell membranes allows the HIV-1 genetic material to enter the host cell to establish an infection[1].

Neutralizing antibodies against HIV-1 solely target Env, where they act to prevent fusion of the viral and host cell membranes. As such, Env comprises a key target of HIV-1 vaccine strategies[7, 8]. Because the rapid mutation rate of HIV-1 creates high levels of sequence diversity both within and between hosts, an effective prophylactic vaccine will need to induce broadly neutralizing antibodies (bNAbs) capable of recognizing not one, but many, circulating strains[7, 8]. bNAbs isolated from people living with HIV-1 target conserved features on Env, including the CD4 binding-site (CD4bs) and the V3-loop at the Env trimer apex involved in co-receptor binding[9]. Structures of bNAb-Env complexes mainly reveal targeting of pre-fusion closed Env trimers[3] with the exception of b12, one of the first characterized bNAbs[10]. b12 targets an Env conformation in which the gp120s undergo an outward rotation, but V1V2 remains on top of V3, thereby occluding access to the co-receptor binding site and distinguishing this occluded-open conformation from the CD4-bound open conformation[11, 12, 13].

In an attempt to produce bNAbs in wildtype animals with polyclonal antibody repertoires, we previously described an immunization protocol that involved priming with a V3 germline-targeting Env immunogen[14] followed by sequential boosting with increasingly "native" Env trimers[15]. After boosts 3 and 4, we isolated heterologous, but weakly neutralizing, monoclonal antibodies (mAbs) from immunized non-human primates (NHPs). Seven of nine NHP mAbs elicited after the prime-boost regimen targeted the V3-glycan patch, as demonstrated by competition with the V3-targeting bNAb 10-1074[15]. However, the remaining two mAbs, Ab1303 and Ab1573, competed with the CD4bs bNAb 3BNC117[15] and were shown by single-particle cryo-electron microscopy (cryo-EM) to target the CD4bs of Env trimers in an occluded-open, rather than a CD4-bound open, conformation[12].

Here, we report cryo-EM structures of two of the 10-1074-competing NHP mAbs from the prime-boost sequential immunization regimen[15] in complex with stabilized, soluble Env trimeric ectodomains (SOSIPs)[16]. In common with Ab1303 and Ab1573, which were also elicited in this immunization regimen, neither of the V3-targeting NHP mAbs recognized the pre-fusion closed Env conformation. Instead, Ab1456 interacted with the V3-epitope on Env trimers adopting various CD4-bound open conformations although neither soluble CD4 (sCD4) nor a CD4 mimetic was included in the complex. The other antibody, Ab1271, also interacted with the V3 region of an Env trimer but recognized a distinct Env conformation in which V1V2 was displaced but the gp120s did not exhibit outward rotation. The discovery of apparently preferential targeting of non-closed Env conformations by antibodies elicited by sequential immunization with SOSIP-based immunogens has important implications for HIV/AIDS vaccine design.

Results

Ab1456 and Ab1271 are heterologously-neutralizing mAbs elicited in sequentially immunized NHPs

Ab1456 and Ab1271 were isolated from NHPs after sequential immunizations with engineered or wildtype SOSIP-based immunogens designed to target the V3-glycan patch on the gp120 subunit of Env and characterized as weak, but heterologously-neutralizing mAbs[14, 15]. NHPs were primed with RC1-4fill, a low affinity V3-glycan patch germline-targeting immunogen conjugated to virus-like particles (VLPs) using the SpyCatcher-SpyTag system[17, 18]. RC1-4fill is a modification of the clade A BG505-based 11MUTB SOSIP immunogen[19], in which the $N156_{gp120}$ glycan was removed (N156Q) and potential N-linked glycosylation sites (PNGSs) to block BG505 strain-specific responses to an immunodominant glycan hole in the vicinity of residue 241_{gp120}[20] were added. A series of boosts consisting of VLPs presenting 11MUTB-4fill[15], a clade B B41[21] or B41-5MUT[15], a mosaic of a clade B (AMC011)[22] and clade C (Du422)[23], and a mosaic of consensus Envs from Group M and clade C (ConM/ConC)[24, 25] were given to try to shepherd antibody responses towards broader reactivities and avoid strain-specific responses (Fig. 1a).

Using single B-cell cloning techniques, Ab1456 and Ab1271 were isolated after the third boost in the same two NHPs as the Ab1573 and Ab1303 CD4bs mAbs[15] (Fig. 1a). In contrast to the Ab1573 and Ab1303 competition results, Ab1456 and Ab1271 each competed with the V3 bNAb 10-1074, suggesting on-target binding specificities for these mAbs[15]. However, structural characterizations of Ab1456 and Ab1271 remained elusive. Both mAbs displayed heterologous neutralization when tested against a panel of 19 pseudoviruses including the 12-strain global HIV-1 panel[26] and two SHIVs, neutralizing 6 of 19 (Ab1456) or 14 of 19 (Ab1271) HIV-1 pseudoviruses with IC_{50} values < 100 μg/mL[15]. While neutralization potencies were generally weak, Ab1271 in particular exhibited breadth, neutralizing all viruses tested at IC_{50} values < 500 μg/mL. Ab1456 was derived

from macaque IGHV5-43*02 and IGLV1-81*01 germline V gene segments, exhibiting 14.3% (heavy chain; HC) and 7.1% (light chain; LC) amino acid changes due to somatic hypermutation. Ab1271, derived from the IGHV4-92*01 and IGLV1-85*01 germline V gene segments, exhibited 15.5% (HC) and 8.2% (LC) changes from somatic hypermutation (Fig. 1b). Of note, there is a one-residue deletion in the HC framework region 1 (FWRH1) of Ab1271.

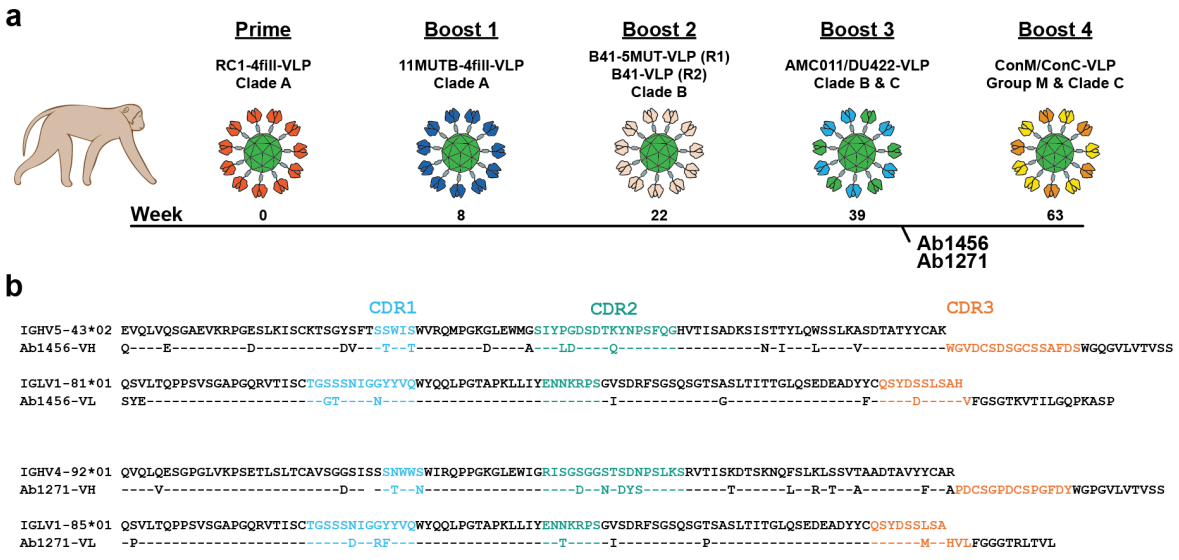

Figure 1: Characterization of Ab1456 and Ab1271. a, Schematic describing the sequential immunization of NHPs that gave rise to Ab1456 (Regimen 1 in boost 2; R1) and Ab1271 (Regimen 2 in boost 2; R2)[15]. Ab1456 was isolated from NHP DGJI, and Ab1271 was isolated from NHP T15. **b**, Alignments of Ab1456 and Ab1271 to their presumptive germline VH gene precursors, as identified by IMGT/V-QUEST[27, 28]. CDRs are defined according to Kabat[29].

Ab1456 recognizes CD4-bound open Env trimer conformations

For structural studies of Ab1456 recognition of Env, we formed Fab-Env complexes using a chimeric SOSIP Env containing a gp120 derived from JRCSF.JB, an HIV-1 strain that was potently neutralized by Ab1456[15], and a gp41 derived from BG505[30]. Fab-SOSIP complexes isolated by size-exclusion chromatography (SEC) were used for EM analysis. Initial processing in cryoSPARC[31] yielded a 6.6 Å resolution structure that showed targeting of the trimer apex of an

open Env conformation with an apparent stoichiometry of one Fab per trimer (Fig. 2a, b). In this structure, two of three protomers in the trimer appeared to adopt a CD4-bound open conformation as indicated by rearranged V1V2 densities, while the third protomer exhibited an outward rotation, but lacked the V1V2 rearrangement[32]. Overall, this state of the Env trimer resembled the conformation of HT2, a SOSIP heterotrimer in complex with two, rather than three, copies of soluble CD4[6]; hence, we refer to this Ab1456-bound Env conformation as HT2-like, noting, however, that the Ab1456-Env structure was determined in the absence of CD4 and with a homotrimeric SOSIP (Fig. 2a, b). Unexplained density was present at the trimer apex (Supplementary Fig. 1a), suggesting that this consensus structure included particles from distinct 3D classes. Indeed, 3D classification in RELION[33] revealed extensive heterogeneity. Structural classes were identified that differed in the conformational state of the trimer, the number of bound Fabs per trimer, the relative positioning of the bound protomers, and the approach angles of the Fabs (Fig. 2). Sorting of approximately 80,000 particles allowed us to determine eight structural classes with resolutions ranging from 8.8 Å to 14 Å (Supplementary Fig. 2). Given the high degree of heterogeneity, additional states could exist. In addition, imperfect separation of particles may bias some of the reported structures.

Two different three Fab-bound HT2-like trimer classes were identified. In these classes, the Fab bound to protomer B was wedged either in front, or behind, of the Fab bound to protomer C, resulting in distinct angles of approach (Classes 1 and 2) (Fig. 2c).

Multiple structural classes of Env trimers with two bound Fabs were also found. Two distinct classes of two Fab-bound HT2-like trimers were identified with the Ab1456 Fabs binding to different configurations of the Env A, B, and C protomers. In one configuration, both Fab-bound protomers (protomers A and B) adopted the CD4-bound open conformation (Class 3) (Fig. 2d). In

another structural class, both the protomer that lacked apparent V1V2 rearrangements (protomer C) and an adjacent protomer in the CD4-bound open conformation (protomer A) exhibited bound Ab1456 Fabs (Class 4) (Fig. 2d). Another structural class showed two Ab1456 Fabs bound to a fully-open trimer in which all three protomers displayed V1V2 rearrangements (Class 5) (Fig. 2d).

In Env structures exhibiting a single bound Fab, three different trimer conformational states were identified (Fig. 2a, e). In one state, only the Fab-bound protomer adopted a CD4-bound open conformation (as defined by a V1V2 rearrangement), and the other protomers exhibited neither an outward gp120 rotation nor V1V2 rearrangement (Class 6) (Fig. 2e). Another class was found in which the Env trimer adopted an HT2-like state, and only protomer A was bound (Class 7) (Fig. 2e). Finally, a structure of a single Ab1456 Fab bound to a trimer in which all three protomers adopted a CD4-bound open conformation was identified (Class 8) (Fig. 2e).

At the resolutions of our EM structures, we are mostly limited to analyzing the Ab1456 epitope through docking of previously-determined EM and X-ray structures. Docking of protomer A from the HT2 trimer[6] (Env heterotrimer bound by 2 copies of soluble CD4; PDB 8FYJ) into the consensus structure revealed qualitative agreement with protomer A density in the EM map (Supplementary Fig. 1b). The docked protomer showed apparent Ab1456 targeting of V3 residues that were not built in the HT2 structure as a consequence of being disordered in PDB 8FYJ. To account for additional Ab1456 and Env V3 density in the Ab1456-JRCSF Env structure, we docked a crystal structure of the human mAb 3074 in complex with a V3 peptide spanning gp120 residues 301-324 (PDB 3MLX; residues 305-320 were ordered in the crystal structure). We chose this peptide/V3-antibody structure because 3074 neutralizes viruses in common with Ab1456 (e.g., both neutralized JRCSF, 6535.3, and X1632 to a greater extent than other strains[15, 34]) and preferentially

binds Env in the presence of CD4[35]. While these properties may indicate that 3074 and Ab1456 make similar contacts with Env, such interactions could be mediated by different antibody features (e.g., different complementarity-determining regions, different specific Fab-Env interactions, different Fab binding orientations, etc.). The docked Fab-bound V3 peptide fit the EM density well, providing support for the interpretation that Ab1456 and mAb 3074 contact similar V3 residues that are exposed on open states of the trimer (Fig. 2f). Ab1456 targeting of the V3 epitope is consistent with it competing for Env binding with the human V3-directed bNAb 10-1074[15].

To further characterize the stoichiometry of Ab1456 Fab binding to Env trimer, we performed mass photometry, a technique that detects binding interactions in solution via mass measurements of individual molecules[36, 37]. Unlike the Ab1456-JRCSF SOSIP complex used for cryo-EM, the Fab-Env sample for mass photometry was not purified by SEC, and mass photometry was performed at a more dilute final concentration (diluted from ~ 1 mg/mL to < 1 μg/mL for measurement) than what was imaged by cryo-EM (~ 1.1 mg/mL). By mass photometry, the JRCSF trimer appeared at ~ 300 kDa, whereas a second population of approximately one third the mass (experimentally measured as ~ 80 kDa) is assumed to be JRCSF monomer, which was also observed in the SEC profile of this SOSIP (Supplementary Fig. 3). In agreement with observations by cryo-EM, the Ab1456-JRCSF sample showed particles with increased mass relative to the trimer alone control (Fig. 2g). Although distinct populations could not be unambiguously identified, the masses of the complexes were consistent with a mixture of Fab-Env particles containing either 0, 1, 2, or 3 bound Fabs per trimer (Fig. 2g).

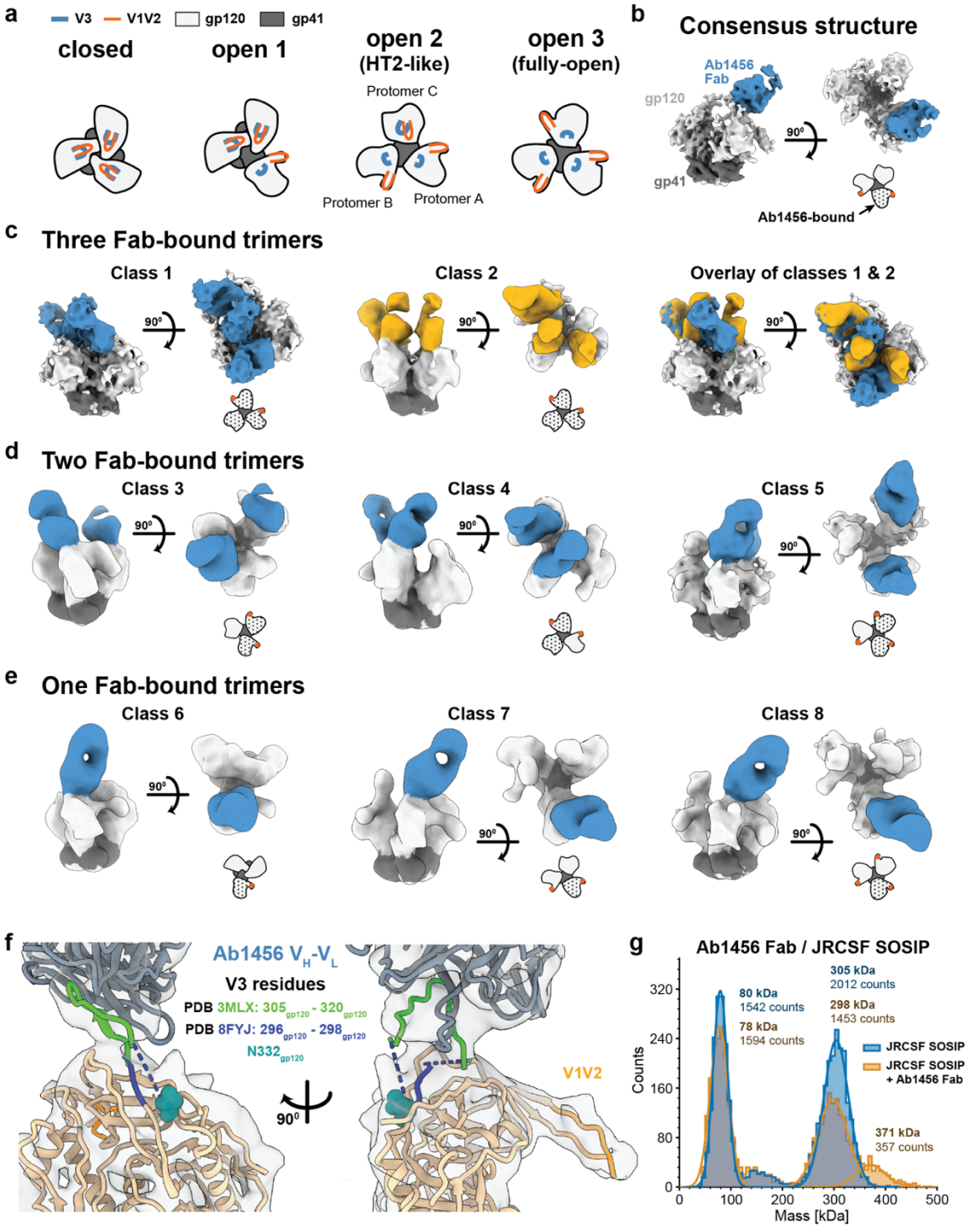

Figure 2: Ab1456 Fab binds open forms of HIV-1 Env. a, Schematic of top-down views of Env trimers showing a potential pathway from a closed (left) to a fully-open (right) trimer. The three open Env states were identified in structural classes with bound Ab1456 Fab(s). **b**, Results of a non-

uniform refinement of Ab1456 Fab-bound JRCSF SOSIP particles prior to 3D classification. A schematic representation of the top-down view of the trimer conformation is shown in this and subsequent panels with the Ab1456-bound protomer(s) indicated by a black dotted pattern and displaced V1V2 loop(s) indicated by orange dot(s). **c**, Left and middle: Two structural classes showing three Ab1456 Fabs bound. Right: An overlay of the two structural classes. **d**, Three structural classes showing two Ab1456 Fab-bound trimers. **e**, Three structural classes showing one Ab1456 Fab-bound trimers. **f**, Analysis of the Ab1456 epitope. Protomer A from PDB 8FYJ (HT2 Env heterotrimer complexed with two CD4s) and 3MLX (human mAb 3074 complexed with a V3 peptide; ordered residues 305-320) were independently docked into the density corresponding to protomer A and Ab1456 Fab/V3 peptide in the consensus map, respectively. **g**, Mass photometry of JRCSF SOSIP (blue) and JRCSF SOSIP in complex with Ab1456 Fab (gold).

Ab1271 recognizes a conformation distinct from pre-fusion closed Env trimers

We next focused on Ab1271, which exhibits a broader neutralization profile than Ab1456[15]. For these structural studies, we formed Fab-Env complexes using a chimeric SOSIP with a gp120 derived from 6535.3, a tier 1 virus that was potently neutralized by Ab1271[15], and a gp41 derived from BG505[30]. Cryo-EM analysis revealed trimers that were not complexed with Ab1271 Fab, yielding a 4.6 Å structure of the unliganded 6535.3 SOSIP trimer (Fig. 3a, Supplementary Fig. 4). Although the 6535.3 Env conformation generally resembled a typical closed prefusion trimer in that gp120s were not outwardly rotated and the V1V2 regions were not displaced to the trimer sides as seen in the CD4-bound open Env conformation[11, 32, 38], the trimer apex in 6535.3 Env differed from those of BG505 and other SOSIP Env structures. Docking of a closed BG505 SOSIP (PDB 6UDJ) into the 6535.3 SOSIP density showed differences in the presumptive locations of the V1V2 regions at the trimer apex for two of the three 6535.3 protomers, and density for V1V2 on the third protomer was not observed (Fig. 3a).

In addition to the unbound 6535.3 trimer structure, we determined a 6.3 Å structure of a 6535.3 SOSIP bound by a single Ab1271 Fab (Fig. 3b). In this structure, the Env portion of the density closely matched the density for the unbound 6535.3 SOSIP (Fig. 3a, b), with Ab1271 interacting with the V3 region of the protomer lacking apparent V1V2 density. The apex of a docked closed

BG505 trimer (PDB 6UDJ) clashed with density corresponding to the Ab1271 Fab, suggesting that V1V2 must be in a position distinct from its position in BG505 in order to accommodate Ab1271 binding (Fig. 3c). Unlike the occluded-open Env conformations found in the Ab1303-Env and Ab1573-Env complex structures[12] or the CD4-bound open structures with Ab1456 (Fig. 2), the Env trimer in the Ab1271-Env complex did not exhibit an outward rotation of its gp120s, in common with conventional pre-fusion closed SOSIP trimer structures[3]. However, as the form of the Env trimer in the Ab1271-6535.3 SOSIP complex is distinct from previously-determined closed trimer structures[3], we refer to its conformation as apex-altered closed. While low resolution limited our analysis of antibody epitope details, the docked structure revealed apparent Ab1271 targeting at or near the conserved GDIR motif within the V3 loop of gp120[39] ($gp120_{324-327}$) (Fig. 3c).

To further investigate the stoichiometry of Ab1271 Fab binding to the Env trimer, we evaluated Ab1271 Fab-6535.3 SOSIP complex formation using mass photometry. Similar to the JRCSF SOSIP, the 6535.3 SOSIP also included multiple populations, predominantly corresponding to SOSIP trimers and protomers (Fig. 3d; Supplementary Fig. 3). Although a majority of the trimers remained unbound in the presence of Ab1271 Fab, a small shoulder with a mass ~ 50 kDa greater than the trimer alone control appeared in the experimental histogram of the Ab1271-6535.3 SOSIP sample, consistent with a population of one Fab-bound trimers (Fig. 3d). Additionally, excess Fab (~ 50 kDa) likely contributes to the large increase in the size of the peak experimentally measured at ~ 70 kDa. As mass photometry experiments were conducted at more dilute final concentrations (diluted from ~ 1 mg/mL to < 1 µg/mL) compared to cryo-EM (~ 1.9 mg/mL), this result suggests a weak affinity and/or fast off-rate of Ab1271 Fab for the 6535.3 SOSIP trimer.

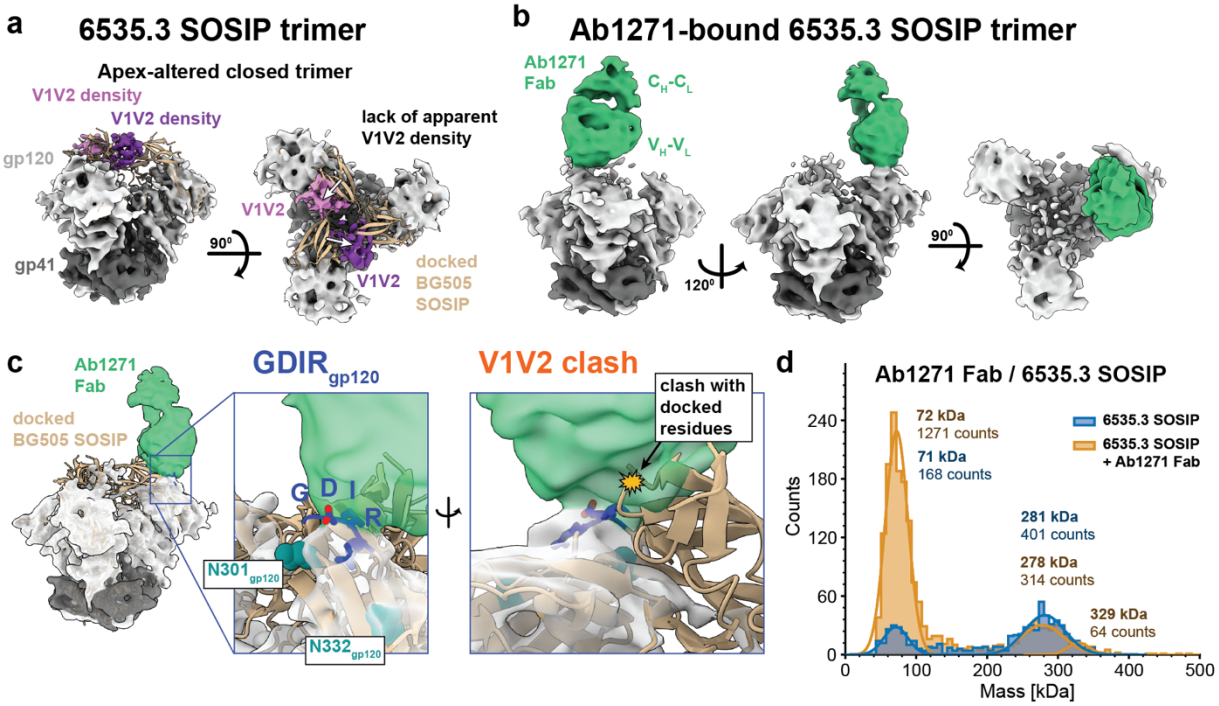

Figure 3: Ab1271 recognizes a closed 6535.3 Env trimer with an altered apex. a, Side and top-down views of a structural class of unliganded 6535.3 SOSIP. BG505 SOSIP (PDB 6UDJ) (tan cartoon representation) was docked into 6535.3 density. Presumptive V1V2 density for two of the three 6535.3 protomers (pink and purple) is shifted relative to the BG505 V1V2, as indicated by white arrows in the top-down view on the right. **b**, A structural class of Ab1271-Env complex with a single copy of Ab1271 Fab bound to the 6535.3 SOSIP. **c**, Left: Ab1271-6535.3 complex. Middle: Close-up of Fab-Env interaction showing apparent targeting of Ab1271 Fab towards the V3 GDIR motif ($G324_{gp120}$ – $R327_{gp120}$). Right: Close-up of Fab-Env interaction showing apparent clash with V1V2 residues of the docked BG505 SOSIP. **d**, Mass photometry of 6535.3 SOSIP (blue) and 6535.3 SOSIP in complex with Ab1271 Fab (gold).

Antibody-virus pre-incubation is not necessary for in vitro neutralization by Ab1456

Based on the cryo-EM structures of the weakly neutralizing NHP mAb Ab1456 that revealed recognition of open Env conformations, we reasoned that Ab1456 targeting could be limited by the conformational availability of the epitope on virion-bound Env trimers. Standard TZM-bl neutralization assays provide a time window, typically 1 hour, in which an antibody is incubated at 37 °C with the virus prior to the addition of target cells[40, 41]. We hypothesized that this incubation

could allow sampling of open trimer conformations, which could then be captured, permitting antibody binding to virion Envs to achieve neutralization. The antibody-virus co-incubation step is distinct from how antibodies neutralize HIV-1 in vivo, where antibodies and viruses are not pre-incubated in a small volume and where there might only be a limited time window for an antibody to recognize Env on a virus prior to encountering a target cell. We therefore reasoned that pre-incubation of antibody and virus might artificially inflate the neutralization potencies of antibodies that target an epitope on an open Env trimer.

To test this possibility, we compared the 50% inhibitory concentrations (IC_{50}s) of Ab1456 and other weakly and broadly neutralizing mAbs in the standard TZMbl assay, in which virus and antibodies were preincubated for 1 hour[40, 41], and in a modified assay, in which antibodies were first added to the cells followed by virus addition in a separate step. Selecting a set of both sensitive and more resistant viruses[15], we found that the neutralization potencies of Ab1456 were very similar regardless of whether the standard or modified assay was used (Fig. 4a). This was true for HEK293T-derived pseudoviruses and replication-competent simian-human immunodeficiency viruses (SHIVs) as well as a SHIV challenge stock that was propagated in rhesus macaque peripheral blood mononuclear cells (PBMCs)[15, 42]. Preincubation also had no effect on the neutralization potencies of other antibodies known to target open Env conformations, such as the CD4-induced antibody 17b[2] and the linear V3 mAb 3074[43] (Fig. 4b). The slopes of the 17b and 3074 neutralization curves, like those of Ab1456, were more shallow than the slopes of potent bNAbs, such as the V3 bNAb 10-1074[44] and the CD4bs bNAb VRC01[45] that recognize closed Env conformations (Supplementary Fig. 5). Since shallow dose-response curves are associated with less favorable therapeutic potentials[46], these results imply limited in vivo protection efficacy for Ab1456.

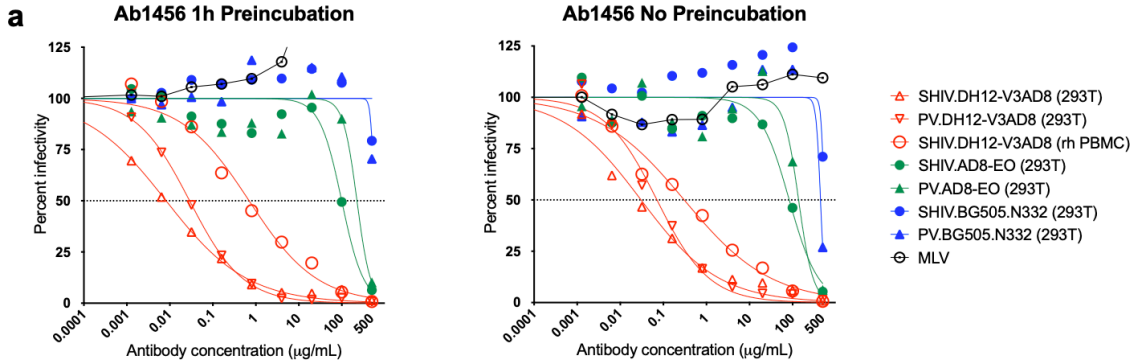

b

	1 hour preincubation					No preincubation				
	Ab1456	VRC01	10-1074	3074	17b	Ab1456	VRC01	10-1074	3074	17b
SHIV.DH12-V3AD8 (293T)	0.008	0.734	0.016	0.220	0.918	0.030	0.806	0.015	0.233	1.86
PV.DH12-V3AD8 (293T)	0.029	0.784	0.021	0.297	11.9	0.071	1.00	0.035	0.477	11.8
SHIV.DH12-V3AD8 (rh PBMC)	0.699	3.85	0.035	3.50	>100	0.306	1.90	0.054	3.54	>100
SHIV.AD8-EO (293T)	99.5	0.297	0.041	>100	>100	83.7	0.320	0.050	>100	>100
PV.AD8-EO (293T)	225	0.360	0.057	>100	>100	138	0.471	0.072	>100	>100
SHIV.BG505.N332 (293T)	>500	0.085	0.063	>100	>100	>500	0.071	0.063	>100	>100
PV.BG505.N332 (293T)	>500	0.080	0.060	>100	>100	445	0.067	0.069	>100	>100

IC50 (μg/mL)
>100
100-50
50-10
10-1
1-0.1
<0.1

Figure 4: Preincubation of antibody and virus during in vitro neutralization does not affect neutralization potency. a, Sensitivity of viruses expressing the DH12-V3AD8 ($SHIV_{DH12\text{-}V3AD8}$; red), AD8-EO ($SHIV_{AD8EO}$; green) and BG505.N332 (blue) Envs to neutralization by Ab1456 using a TZMbl assay with (left) and without (right) a 1 hour antibody and virus preincubation step. Neutralization curves are shown for pseudovirus (PV) and replication-competent forms of SHIVs derived either by HEK293T transfection (293T) or following propagation in rhesus macaque PBMCs (rh PBMC). Dotted lines indicate 50% reduction in virus infectivity. **b**, Sensitivity of the viruses shown in a (listed on the left) to neutralization by other mAbs (listed on top) with (left panel) and without (right panel) a 1 hour antibody and virus preincubation step. 50% inhibitory concentrations (IC_{50}) are shown in μg/mL (coloring indicates relative neutralization potency).

Discussion

The results reported here provide potentially valuable information for the design of immunogens to elicit bNAbs that target closed, prefusion HIV-1 Env trimers rather than antibodies such as Ab1456, which recognize non-closed Env conformations, neutralize heterologous HIV-1 strains only weakly, and lack breadth against difficult-to-neutralize tier 2 HIV-1 strains. Here, we show from cryo-EM structures that our RC1-based prime-boost regimen successfully elicited antibodies against the V3 glycan patch, as previously predicted from competition with the human V3 bNAb 10-1074[15]. As there are no available structures showing 10-1074 recognition of the altered states of the trimer observed here, we cannot conclude whether 10-1074 directly competes with Ab1456 and Ab1271, or rather competes allosterically (i.e., by trapping a closed conformation that is not accessible to Ab1456 or Ab1271). We note the human linear V3 mAb 3074[47] exhibited a similar neutralization profile as that of Ab1456[15]: e.g., both neutralized 6535.3, JRCSF, and X1632 strains to a greater degree than other strains[47]. Given that mAb 3074 recognizes linear V3 peptides[43] and preferentially binds Env trimers in the presence of soluble CD4[35], the finding of a vaccine-elicited monoclonal or polyclonal antibody response with a mAb 3074/Ab1456-like neutralization profile suggests targeting of undesirable open Env conformations, which is supported by our cryo-EM structures of Ab1456 in complex with open Env trimer conformations.

SOSIP Env trimer immunogens were designed to elicit antibodies that recognize the closed, prefusion Env state[16]. However, at least four [Ab1303[12], Ab1573[12], Ab1456 (this study), and Ab1271 (this study)] of the mAbs that we isolated after boosts 3 and 4 from NHPs immunized sequentially with SOSIP-VLP immunogens[15] do not target conventional closed, prefusion Env trimer conformations, in contrast to the closed Env conformations in Fab-Env complexes involving mAbs isolated after the prime and first boost[14, 15]. Thus, it is interesting to consider how such antibodies were elicited. One possibility is that these antibodies were raised in response to SOSIP

trimers with a propensity to sample open conformations. Consistent with this idea, heterologous serum neutralization titers from the animals that produced Ab1456 and Ab1271 spiked after receiving boost 2 with a B41-based SOSIP Env[15], a SOSIP that has been characterized as exhibiting more lability than BG505-based SOSIPs[48, 49]. Additionally, the B41 SOSIP Env from boost 2 is less thermostable (T_m = 57 °C)[48] than 11MUTB (T_m = 71 °C)[19], the SOSIP Env on which the priming and boost 1 immunogens are based, the related BG505 SOSIP (T_m = 68 °C)[16], or SOSIP Envs involved in the subsequent boost 3 (AMC011 = 63 °C[22], Du422 = 63 °C[50]). Importantly, neutralization activity following the B41 boost increased against JRCSF, a strain that is neutralized by linear V3 antibodies[34], suggesting that the B41-based boost 2 was responsible for eliciting Ab1456 / Ab1271-like responses. Alternatively, contaminating Env protomers may have elicited these antibodies, and only through the ability of these antibodies to also bind intact trimers, albeit in non-conventional closed conformations, can they neutralize a virus. In support of this idea, we previously showed by negative stain electron microscopy-based polyclonal epitope mapping (nsEMPEM)[51] that antibodies elicited by our vaccine regimen caused SOSIP trimers to dissociate into protomers[15]. Preventing SOSIP trimer immunogens from opening through the incorporation of an engineered disulfide (e.g., DS-SOSIPs) should limit exposure of epitopes exposed on open Env conformations[52, 53] but SOSIPs that have dissociated into protomers could also present Ab1456-like epitopes to the immune system. Therefore, preventing both Env trimer opening and trimer dissociation in vivo seems critical for avoiding Ab1456-like responses. The extent to which attempts to avoid such responses in vivo using full-length membrane-embedded Env immunogens (e.g., using EABR technology[54]), and/or engineered disulfides that prevent Env opening to sample the CD4-bound open conformation[52, 53], engineered disulfides that cross-link adjacent protomers[55], or chemically crosslinked Envs[56] warrants further investigation.

Antibody feedback mechanisms[57, 58, 59, 60, 61] could also skew immune responses towards targeting non-closed conformations. While antibody feedback is typically thought of in terms of elicited antibodies forming immune complexes that shield targeted epitopes[57, 58, 59, 60, 61], some antibodies may also trap particular Env conformations; e.g., open Envs, and thereby facilitate further responses to non-closed Env conformations. Indeed, in each of the two NHPs from which these antibodies were isolated, we identified both a CD4bs mAb (Ab1573 or Ab1303) and a V3-targeting mAb (Ab1456 or Ab1271) that recognize non-closed Env conformations: Ab1573 and Ab1456 were isolated from NHP DGJI; Ab1303 and Ab1271 were isolated from NHP T15[15]. Transitions of Env from closed to open conformations, Env trimer dissociation, and antibody feedback need not be mutually exclusive ways to elicit antibodies against non-closed Env conformations; thus, future studies to better understand mechanisms by which anti-Env antibodies are elicited are warranted.

The conformations of Env recognized by Ab1456 also raise questions regarding Env dynamics. For example, even in the absence of CD4, SOSIPs can sample open Env states and conformations other than that of a closed, prefusion trimer[12, 62]. SOSIP trimers, as well as Env trimers on virions, may transiently sample states such as the one observed in which only one of the three constituent protomers adopted a CD4-bound open conformation or an HT2-like state in which two of three protomers adopted a CD4-bound open conformation in the absence of a bound ligand (Fig. 2a). When a mAb such as Ab1456 recognizes one of these states, the trimer likely cannot return to a closed conformation without the antibody first dissociating. With Ab1456 Fab bound to an open protomer, the trimer may then transiently sample more “fully-open” states in which all three protomers adopt CD4-bound open conformations (Fig. 2a). Our multiple structural classes of the JRCSF SOSIP in complex with Ab1456 Fab(s) hint at different pathways for progressive trimer opening. Of note, we identified a single structural class of one Fab-bound JRCSF Env in which the

trimer adopted an HT2-like state. In this conformation, protomer A (the bound protomer) as well as a neighboring unbound protomer (protomer B, clockwise to protomer A) both adopted a CD4-bound open conformation. Notably, we did not observe a structural class in which protomer B, but not protomer A, was bound by Ab1456 Fab, potentially suggesting that protomers on an HIV-1 Env trimer open in a clockwise fashion.

Previous studies showed that the duration of virus and antibody preincubation can influence the IC_{50} values of antibodies that neutralize HIV-1 by particular mechanisms; e.g., increasing preincubation times resulted in increasing potencies (decreasing IC_{50} values) of antibodies that neutralized by accelerating trimer decay[63]. Here, we tested whether omitting virus and antibody preincubation would reduce the potency (i.e., increase IC_{50} values) of antibodies that recognize open Env conformations. This was not the case, however, suggesting that such antibodies do not have to wait for, and then capture, trimers as they sample various open conformations. Instead, it seems likely that viruses that are sensitive to Ab1456 and antibodies with similar recognition properties are already displaying their Envs in open conformations and that the neutralization profile of Ab1456, which mostly neutralizes tier 1 viruses with the exception of the tier 2 virus JRCSF[15], is an indicator of the conformational flexibility of these Envs.

The 6535.3 SOSIP Env trimer structures, both bound by Ab1271 and unliganded, raise further questions. For example, it will be important to determine whether the apex-altered conformation that we observed with the 6535.3 SOSIP is related to this Env being derived from a tier 1 HIV-1 and/or whether this state can also be seen in native, virion-embedded Envs. In any case, this unusual apex conformation may result from Env protomers that are transitioning to a CD4-bound conformation. Finally, it will be important to ascertain to what extent Envs from different HIV-1

strains exhibit differing dynamics at the trimer apex since this may influence their utility as potential immunogens.

Our structural analyses of Ab1456 and Ab1271 highlight the value of single-particle cryo-EM for deciphering underlying heterogeneities that can be present in antibody-antigen interactions. For example, Ab1456 Fab bound to the JRCSF SOSIP with varying stoichiometries, recognized different structural states of the trimer, bound to different configurations of protomers on a trimer, and even bound Env trimers with different angles of approach, all of which were resolved as different structural classes by cryo-EM. Although understanding this degree of heterogeneity is important for understanding the many ways in which Ab1456 can recognize Env, it limited the resolution of our 3D reconstructions, in part by reducing the number of particles in each class. Despite extensive classification, it is likely that heterogeneity persisted within the constituent particles of a given 3D class. By collecting larger datasets, it might be possible to determine higher-resolution structures and potentially even identify different structural classes. However, our reported structures were of sufficient resolution for observing V1V2 rearrangements and outward gp120 rotations, providing important insights into the Env conformations being targeted, as well as revealing epitope information.

Both Ab1456 and Ab1271 appear to recognize epitopes that are not available on closed Env trimers; therefore, both Env dynamics and recognition of specific epitope residues may influence antibody binding. For example, an Env trimer may include residues recognized by the antibody, but rarely, if ever, sample Env conformations that expose these epitopes for recognition. Conversely, an Env may sample the conformation recognized by an antibody (e.g., a CD4-bound open conformation for Ab1456), but lack sequence and or structure requirements for antibody recognition. The complex interplay between these factors likely limits the utility of antibodies whose binding is

constrained by the conformational availability of the epitope; thus, consideration should be given to whether immunogens could be designed to avoid eliciting such antibodies.

In summary, here we examined the structure and function of two NHP mAbs that were elicited in a sequential SOSIP-based immunization approach, yielding results that rationalize the limited ability of heterologously neutralizing antibodies induced by this vaccine regimen to protect from a SHIV challenge[15]. Although both mAbs exhibited heterologous neutralization breadth and targeted the V3 region of HIV-1 Env as intended[14, 15], the mAbs also bound Env trimers in conformational states distinct from a typical closed, prefusion trimeric SOSIP conformation. Thus, an important finding of our present and previous analyses[14, 15] is that the appearance of heterologous neutralization breadth does not necessarily predict the presence of emerging bNAb lineages. Instead, we suggest that heterologous breadth elicited by a vaccine regimen should be examined in comparison to neutralization profiles of undesirable anti-Env antibodies to determine whether the stimulated antibody lineages represent a dead end or have the potential to mature along desired pathways. Of particular relevance to immunogen design efforts, the appearance of a neutralization profile consistent with CD4i or linear V3 antibodies, involving heterologous activity only against tier 1 HIV-1 strains and/or JRCSF, may indicate recognition of an undesirable epitope and consequently the inability to mature into a functional bNAb capable of robust protection from HIV-1 infection.

Methods

Protein expression and purification

JRCSF (JRCSF.JB) and 6535.3 Envs were expressed as soluble chimeric SOSIP trimers[16] (i.e., comprising a gp120 from JRCSF or 6535.3 paired with a BG505 gp41 and including stabilizing MD39 substitutions in gp41[30]). Relevant gp120 genes were synthesized (IDT gBlocks™) and subcloned into a pcDNA3.1 expression plasmid backbone containing a gene encoding the stabilized BG505 gp41. SOSIPs were expressed via transient transfection of Expi293F cells with a 4:1 ratio of SOSIP- and soluble furin-encoding plasmids and then purified from transfected cell supernatants by immunoaffinity chromatography using immobilized mAbs (PGT145 for JRCSF or 2G12 for 6535.3) followed by SEC as described[64]. Soluble Env trimers were stored at 4 °C in 20 mM Tris pH 8.0, 150 mM NaCl (TBS).

Previously-reported IgG mAbs[15] used in this study were expressed via transient transfection of Expi293 cells as chimeric IgGs with NHP V_H-V_L domains and human IgG1 constant regions and purified by MabSelect SuRe chromatography (Cytiva). To produce Fabs for structural and biochemical experiments, IgG antibodies in phosphate-buffered saline (PBS) were cleaved by papain digestion using activated crystallized papain (Sigma-Aldrich) for 30 to 60 min at 37 °C at a 1:100 enzyme:IgG ratio. Digested protein was applied to a 1 mL HiTrap MabSelect SuRe column (Cytiva) and flowthrough containing Fabs was collected. Fabs were further purified by SEC in TBS using a Superdex 200 Increase 10/300 column (GE Healthcare Life Sciences) before concentrating and storage at 4 °C.

Single-particle cryo-EM

For single-particle cryo-EM, SOSIP was complexed with Fab at room temperature, overnight with an approximate 1.3:1 molar excess Fab: SOSIP protomer. Samples were purified on a Superose 6

Increase 10/300 column (GE Healthcare Life Sciences) operating in TBS and leading SEC fractions were further concentrated to ~1.1 mg/mL (JRCSF/Ab1456 sample) or ~1.9 mg/mL (6535.3/Ab1271 sample) using 10 kDa spin concentrators (Millipore). The samples were supplemented with octyl-maltoside, fluorinated solution (Anatrace) to a final concentration of 0.02% (JRCSF/Ab1456 sample) or 0.01% (6535.3/Ab1271 sample) immediately before deposition of 3 μL onto a 300 Cu mesh, Quantifoil R1.2/1.3 grid (Electron Microscopy Sciences) that had been glow discharged for 1 min at 20 mA using a PELCO easiGlow (Ted Pella). Using a Mark IV Vitrobot (Thermo Fisher), the samples were blotted with a blot force of 0 for 3 s using Whatman No. 1 filter paper at 22 °C and 100% humidity and vitrified in liquid ethane.

Data collection and processing

40-frame movies were collected in super-resolution at a pixel size of 0.416 Å (105,000x magnification) using SerialEM[65] on a 300 kV Titan Krios microscope (Thermo Fisher Scientific). Movies were collected using a 3x3 beam image shift with 3 shots per hole using beam-tilt compensation. The microscope was equipped with a K3 6k x 4k direct electron detector (Gatan) and a BioQuantum Energy Filter (Gatan) with a slit width of 10 eV. Collection parameters are described in Supplementary Table 1 and the data processing workflow is shown in Supplementary Fig. 2 and Supplementary Fig. 4. Briefly, movies were binned and patch motion corrected using CryoSPARC Live[31]. The final particle stack used was picked using Topaz[66]. Ab1271/6535.3 SOSIP data were initially processed by ab initio reconstruction and refinement in CryoSPARC[31]. Particles were imported to RELION[33] and subjected to 3D classification using the low-pass filtered, refined map as a reference model. Particles from select 3D classes were re-extracted in CryoSPARC[31] and subject to ab initio reconstruction and non-uniform refinement[67] to produce final maps. A similar workflow, but including iterative rounds of 3D classification, was used to process the Ab1456/JRCSF SOSIP dataset.

Structural analysis

Structure figures were prepared in ChimeraX[68]. EM density corresponding to antibody Fab(s) was selected and colored by segmenting the map and gp41 density was colored corresponding to SOSIP coordinates that were docked into the low resolution maps.

Mass photometry

Mass photometry was performed on a OneMP (Refeyn). Glass coverslips (VWR) were pre-cleaned in water and isopropanol prior to use. Fab-SOSIP complexes were formed at room temperature in TBS overnight, at 4 μM trimer concentration and a 1.05 molar excess of Fab to SOSIP protomer. Fab-SOSIP complexes were diluted to 8 nM (trimer concentration) and diluted 10-fold (6535.3 SOSIP and 6535.3 SOSIP + Ab1271 Fab) or 4-fold (JRCSF SOSIP and JRCSF SOSIP + Ab1456 Fab) on the instrument. Movies were recorded for two minutes using Acquire^{MP} (Refeyn, v2023 R1.1) and analyzed using Discover^{MP} software (Refeyn, v2023 R1.2). A mass standard curve was prepared using beta amylase from sweet potato (dimer and tetramer) and bovine serum albumin (monomer and dimer). Figures were prepared on the Discover^{MP} software.

Neutralization assays

The neutralization capacities of Ab1456 and other mAbs were assessed using TZM-bl reporter cells as described[15], including or not including the standard 1 h antibody-virus incubation step. Briefly, 96-well plates were seeded with TZM-bl cells (15,000 cells per well) overnight in Dulbecco's modified Eagle's medium (DMEM) containing 10% fetal bovine serum (FBS) and 100 U/mL Penicillin-Streptomycin-Glutamine (Gibco). For the standard assay, serial 5-fold dilutions of mAbs (e.g., 500, 100, 20, 4, 0.8, 0.16, 0.032, 0.0064, 0.00128 μg/mL) were incubated with transfection-derived or PBMC propagated virus at a multiplicity of infection (MOI) of 0.3 in a total volume of

100 µL in the presence of DEAE-dextran (40 µg/mL) for 1 hour at 37 °C, and this mixture was then added to TZM-bl cells. For the modified test, mAb dilutions were first added to the cells in a volume of 50 µL, followed by the addition of virus in a volume of 50 µL, both in the presence of DEAE-dextran (40 µg/mL). TZM-bl cells were analyzed for luciferase expression 48 hours after virus addition using a Synergy Neo2 Multimode Microplate reader (Bio-Tek) with Gen5 version 1.11 software. Uninfected cells were used to correct for background luciferase activity. The infectivity of each virus without antibodies was set at 100%. The 50% inhibitory concentration (IC_{50}) is the antibody concentration that reduces by 50% the relative light units (RLUs) compared with the no antibody control wells after correction for background. Nonlinear regression curves were determined and IC_{50} values calculated by using the variable slope (four parameters) function in Prism software (v8.0).

Pseudoviral and SHIV stocks were generated by transfection of HEK293T cells. Briefly, 100-mm tissue culture dishes were seeded with 4 x 10^6 HEK293T cells overnight in DMEM containing 10% FBS and 100 U/mL Penicillin-Streptomycin-Glutamine. Cells were transfected by adding 0.5 mL of a preincubated DMEM solution containing 4.5 µg of HIV-1 (SG3Δenv) backbone plasmids and 1.5 µg of HIV-1 Env plasmids or 6 µg of SHIV DNA, and 18 µL of FuGENE 6 transfection reagent (Promega), according to manufacturer's recommendations. The cells were incubated at 37 °C in a CO_2 incubator for 48-72 h, and the supernatant was harvested and stored at −80 °C in 0.5 mL aliquots. The generation of the rhesus PBMC-propagated $SHIV_{DH12\text{-}V3AD8}$ challenge stock used for in vitro neutralization assays has been described[42].

mAbs tested for neutralization were produced by co-transfecting paired heavy and light chain expression plasmids into Expi293F cells using ExpiFectamine 293 transfection reagents

(ThermoFisher Scientific), purified from culture supernatants using the Protein A/Protein G GraviTrap kit (GE Healthcare), and buffer-exchanged into PBS as described[69].

Acknowledgements

We thank Songye Chen and the Caltech Cryo-EM Center, Anastasiya Oguienko, Morgan Abernathy, Welison Floriano, and Jost Vielmetter and the Caltech Protein Expression Center for experimental and technical support, and Malcolm Martin (NIH) for providing $SHIV_{DH12\text{-}V3AD8}$ and $SHIV_{AD8\text{-}EO}$ proviral DNA and the rhesus macaque PMBC-derived $SHIV_{DH12\text{-}V3AD8}$ challenge stock. This work was supported by the National Institute of Allergy and Infectious Diseases (NIAID) Grant HIVRAD P01 AI100148 (P.J.B., G.B.S., B.H.H.), R37 AI 150590 (B.H.H.), P01 AI 131251 (G.M.S.), NIH P50 1U54AI170856 (P.J.B.). This work was supported, in whole or in part, by the Bill & Melinda Gates Foundation grant INV-002143 (P.J.B.). Under the grant conditions of the Foundation, a Creative Commons Attribution 4.0 Generic License has already been assigned to the Author Accepted Manuscript version that might arise from this submission. A.T.D. was supported by an NSF Graduate Research Fellowship.

Author contributions

Conceptualization, A.T.D., J.R.K., H.B.G., G.M.S., B.H.H., P.J.B.; Methodology, A.T.D., W.D., W.L.; Investigation, A.T.D., J.A.L., W.D., W.L., A.N.S.; Writing – Original Draft, A.T.D., B.H.H., P.J.B.; Writing – Review & Editing, A.T.D., J.R.K., H.B.G., J.A.L., A.N.S., B.H.H., P.J.B.; Visualization, A.T.D., W.D.; Supervision and Project Administration, J.R.K., G.M.S., B.H.H., P.J.B.; Funding Acquisition, G.M.S., B.H.H., P.J.B.

Competing interests

The authors declare no competing interests.

Data availability

Cryo-EM maps of Ab1456 Fab/JRCSF SOSIP were deposited to the Electron Microscopy Data Bank (EMDB) and have accession codes: EMD-45944 (consensus structure), EMD-45945 (Class 1), EMD-45946 (Class 2), EMD-45947 (Class 3), EMD-45948 (Class 4), EMD-45949 (Class 5), EMD-45950 (Class 6), EMD-45951 (Class 7), EMD-45952 (Class 8). Ab1271/6535.3 SOSIP structures have accession codes: EMD-45942 (unbound) and EMD-45943 (bound). This paper does not report atomic models or original code. Additional information can be made available upon request.

References

1. Harrison, S.C. Viral membrane fusion. *Virology* **479-480**, 498-507 (2015).

2. Liu, J., Bartesaghi, A., Borgnia, M.J., Sapiro, G. & Subramaniam, S. Molecular architecture of native HIV-1 gp120 trimers. *Nature* **455**, 109-113 (2008).

3. Ward, A.B. & Wilson, I.A. The HIV-1 envelope glycoprotein structure: Nailing down a moving target. *Immunol Rev* **275**, 21-32 (2017).

4. Jette, C.A. *et al.* Cryo-EM structures of HIV-1 trimer bound to CD4-mimetics BNM-III-170 and M48U1 adopt a CD4-bound open conformation. *Nat Commun* **12**, 1950 (2021).

5. Li, W. *et al.* HIV-1 Env trimers asymmetrically engage CD4 receptors in membranes. *Nature* **623**, 1026-1033 (2023).

6. Dam, K.A., Fan, C., Yang, Z. & Bjorkman, P.J. Intermediate conformations of CD4-bound HIV-1 Env heterotrimers. *Nature* **623**, 1017-1025 (2023).

7. Korber, B. *et al.* Evolutionary and immunological implications of contemporary HIV-1 variation. *Br Med Bull* **58**, 19-42 (2001).

8. Kim, J., Vasan, S., Kim, J.H. & Ake, J.A. Current approaches to HIV vaccine development: a narrative review. *J Int AIDS Soc* **24 Suppl 7**, e25793 (2021).

9. Gruell, H. & Schommers, P. Broadly neutralizing antibodies against HIV-1 and concepts for application. *Curr Opin Virol* **54**, 101211 (2022).

10. Roben, P. *et al.* Recognition properties of a panel of human recombinant Fab fragments to the CD4 binding site of gp120 that show differing abilities to neutralize human immunodeficiency virus type 1. *J Virol* **68**, 4821-4828 (1994).

11. Ozorowski, G. *et al.* Open and closed structures reveal allostery and pliability in the HIV-1 envelope spike. *Nature* **547**, 360-363 (2017).

12. Yang, Z. *et al.* Neutralizing antibodies induced in immunized macaques recognize the CD4-binding site on an occluded-open HIV-1 envelope trimer. *Nat Commun* **13**, 732 (2022).

13. Saunders, K.O. *et al.* Vaccine induction of CD4-mimicking HIV-1 broadly neutralizing antibody precursors in macaques. *Cell* **187**, 79-94 e24 (2024).

14. Escolano, A. *et al.* Immunization expands B cells specific to HIV-1 V3 glycan in mice and macaques. *Nature* **570**, 468-473 (2019).

15. Escolano, A. *et al.* Sequential immunization of macaques elicits heterologous neutralizing antibodies targeting the V3-glycan patch of HIV-1 Env. *Sci Transl Med* **13**, eabk1533 (2021).

16. Sanders, R.W. *et al.* A next-generation cleaved, soluble HIV-1 Env trimer, BG505 SOSIP.664 gp140, expresses multiple epitopes for broadly neutralizing but not non-neutralizing antibodies. *PLoS Pathogens* **9**, e1003618-1003620 (2013).

17. Brune, K.D. *et al.* Plug-and-Display: Decoration of Virus-Like Particles via isopeptide bonds for modular immunization. *Sci Rep* **6**, 19234 (2016).

18. Zakeri, B. *et al.* Peptide tag forming a rapid covalent bond to a protein, through engineering a bacterial adhesin. *Proc Natl Acad Sci U S A* **109**, E690-697 (2012).

19. Steichen, J.M. *et al.* HIV vaccine design to target germline precursors of glycan-dependent broadly neutralizing antibodies. *Immunity* **45**, 483-496 (2016).

20. McCoy, L.E. *et al.* Holes in the glycan shield of the native HIV envelope are a target of trimer-elicited neutralizing antibodies. *Cell Rep* **16**, 2327-2338 (2016).

21. de Taeye, S.W. *et al.* Immunogenicity of stabilized HIV-1 envelope trimers with reduced exposure of non-neutralizing epitopes. *Cell* **163**, 1702-1715 (2015).

22. van Gils, M.J. *et al.* An HIV-1 antibody from an elite neutralizer implicates the fusion peptide as a site of vulnerability. *Nat Microbiol* **2**, 16199 (2016).

23. Li, M. *et al.* Genetic and neutralization properties of subtype C human immunodeficiency virus type 1 molecular env clones from acute and early heterosexually acquired infections in Southern Africa. *J Virol* **80**, 11776-11790 (2006).

24. Sliepen, K. *et al.* Structure and immunogenicity of a stabilized HIV-1 envelope trimer based on a group-M consensus sequence. *Nat Commun* **10**, 2355 (2019).

25. Rutten, L. *et al.* A universal approach to optimize the folding and stability of prefusion-closed HIV-1 envelope trimers. *Cell Rep* **23**, 584-595 (2018).

26. deCamp, A. *et al.* Global panel of HIV-1 Env reference strains for standardized assessments of vaccine-elicited neutralizing antibodies. *J Virol* **88**, 2489-2507 (2014).

27. Brochet, X., Lefranc, M.P. & Giudicelli, V. IMGT/V-QUEST: The highly customized and integrated system for IG and TR standardized V-J and V-D-J sequence analysis. *Nucleic Acids Res* **36**, W503-508 (2008).

28. Giudicelli, V., Brochet, X. & Lefranc, M.P. IMGT/V-QUEST: IMGT standardized analysis of the immunoglobulin (IG) and T cell receptor (TR) nucleotide sequences. *Cold Spring Harb Protoc* **2011**, 695-715 (2011).

29. Wu, T.T. & Kabat, E.A. An analysis of the sequences of the variable regions of Bence Jones proteins and myeloma light chains and their implications for antibody complementarity. *J Exp Med* **132**, 211-250 (1970).

30. Joyce, M.G. *et al.* Soluble prefusion closed DS-SOSIP.664-Env trimers of diverse HIV-1 strains. *Cell Rep* **21**, 2992-3002 (2017).

31. Punjani, A., Rubinstein, J.L., Fleet, D.J. & Brubaker, M.A. cryoSPARC: Algorithms for rapid unsupervised cryo-EM structure determination. *Nat Methods* **14**, 290-296 (2017).

32. Wang, H. *et al.* Cryo-EM structure of a CD4-bound open HIV-1 envelope trimer reveals structural rearrangements of the gp120 V1V2 loop. *Proc Natl Acad Sci U S A* **113**, E7151-E7158 (2016).

33. Scheres, S.H. RELION: Implementation of a Bayesian approach to cryo-EM structure determination. *J Struct Biol* **180**, 519-530 (2012).

34. Xu, K. *et al.* Epitope-based vaccine design yields fusion peptide-directed antibodies that neutralize diverse strains of HIV-1. *Nat Med* **24**, 857-867 (2018).

35. Henderson, R. *et al.* Disruption of the HIV-1 Envelope allosteric network blocks CD4-induced rearrangements. *Nat Commun* **11** (2020).

36. Young, G. *et al.* Quantitative mass imaging of single biological macromolecules. *Science* **360**, 423-427 (2018).

37. Soltermann, F. *et al.* Quantifying protein-protein interactions by molecular counting with mass photometry. *Angew Chem Int Ed Engl* **59**, 10774-10779 (2020).

38. Wang, H., Barnes, C.O., Yang, Z., Nussenzweig, M.C. & Bjorkman, P.J. Partially open HIV-1 envelope structures exhibit conformational changes relevant for coreceptor binding and fusion. *Cell Host Microbe* **24**, 579-592 e574 (2018).

39. Sok, D. *et al.* A prominent site of antibody vulnerability on HIV envelope incorporates a motif associated with CCR5 binding and its camouflaging glycans. *Immunity* **45**, 31-45 (2016).

40. Montefiori, D.C. Evaluating neutralizing antibodies against HIV, SIV, and SHIV in luciferase reporter gene assays. *Curr Protoc Immunol* **Chapter 12**, Unit 12.11 (2005).

41. Montefiori, D.C. Measuring HIV neutralization in a luciferase reporter gene assay. *Methods Mol Biol* **485**, 395-405 (2009).

42. Shingai, M. *et al.* Passive transfer of modest titers of potent and broadly neutralizing anti-HIV monoclonal antibodies block SHIV infection in macaques. *J Exp Med* **211**, 2061-2074 (2014).

43. Jiang, X. *et al.* Conserved structural elements in the V3 crown of HIV-1 gp120. *Nat Struct Mol Biol* **17**, 955-961 (2010).

44. Gristick, H.B. *et al.* Natively glycosylated HIV-1 Env structure reveals new mode for antibody recognition of the CD4-binding site. *Nat Struct Mol Biol* **23**, 906-915 (2016).

45. Stewart-Jones, G.B.E. *et al.* Trimeric HIV-1-Env structures define glycan shields from clades A, B, and G. *Cell* **165**, 813-826 (2016).

46. Webb, N.E., Montefiori, D.C. & Lee, B. Dose-response curve slope helps predict therapeutic potency and breadth of HIV broadly neutralizing antibodies. *Nat Commun* **6**, 8443 (2015).

47. Gorny, M.K. *et al.* Cross-clade neutralizing activity of human anti-V3 monoclonal antibodies derived from the cells of individuals infected with non-B clades of human immunodeficiency virus type 1. *J Virol* **80**, 6865-6872 (2006).

48. Pugach, P. *et al.* A native-like SOSIP.664 trimer based on an HIV-1 subtype B env gene. *J Virol* **89**, 3380-3395 (2015).

49. Stadtmueller, B.M. *et al.* DEER spectroscopy measurements reveal multiple conformations of HIV-1 SOSIP Envelopes that show similarities with Envelopes on native virions. *Immunity* (2018).

50. Julien, J.P. *et al.* Design and structure of two HIV-1 clade C SOSIP.664 trimers that increase the arsenal of native-like Env immunogens. *Proc Natl Acad Sci U S A* **112**, 11947-11952 (2015).

51. Bianchi, M. *et al.* Electron-microscopy-based epitope mapping defines specificities of polyclonal antibodies elicited during HIV-1 BG505 envelope trimer immunization. *Immunity* **49**, 288-300 e288 (2018).

52. Kwon, Y.D. *et al.* Crystal structure, conformational fixation and entry-related interactions of mature ligand-free HIV-1 Env. *Nat Struct Mol Biol* **22**, 522-531 (2015).

53. Guenaga, J. *et al.* Well-ordered trimeric HIV-1 subtype B and C soluble spike mimetics generated by negative selection display native-like properties. *PLoS Pathog* **11**, e1004570 (2015).

54. Hoffmann, M.A.G. *et al.* ESCRT recruitment to SARS-CoV-2 spike induces virus-like particles that improve mRNA vaccines. *Cell* **186**, 2380-2391 e2389 (2023).

55. Yang, L. *et al.* Structure-guided redesign improves NFL HIV Env trimer integrity and identifies an inter-protomer disulfide permitting post-expression cleavage. *Front Immunol* **9**, 1631 (2018).

56. Turner, H.L. *et al.* Disassembly of HIV envelope glycoprotein trimer immunogens is driven by antibodies elicited via immunization. *Sci Adv* **7** (2021).

57. Schaefer-Babajew, D. *et al.* Antibody feedback regulates immune memory after SARS-CoV-2 mRNA vaccination. *Nature* **613**, 735-742 (2023).

58. Tas, J.M.J. *et al.* Antibodies from primary humoral responses modulate the recruitment of naive B cells during secondary responses. *Immunity* **55**, 1856-1871 e1856 (2022).

59. Schiepers, A. *et al.* Molecular fate-mapping of serum antibody responses to repeat immunization. *Nature* **615**, 482-489 (2023).

60. Heyman, B. Regulation of antibody responses via antibodies, complement, and Fc receptors. *Annu Rev Immunol* **18**, 709-737 (2000).

61. McNamara, H.A. *et al.* Antibody feedback limits the expansion of B cell responses to malaria vaccination but drives diversification of the humoral response. *Cell Host Microbe* **28**, 572-585 e577 (2020).

62. Hodge, E.A. *et al.* Structural dynamics reveal isolate-specific differences at neutralization epitopes on HIV Env. *iScience* **25** (2022).

63. Lee, J.H. *et al.* Antibodies to a conformational epitope on gp41 neutralize HIV-1 by destabilizing the Env spike. *Nat Commun* **6**, 8167 (2015).

64. Wang, H. *et al.* Asymmetric recognition of HIV-1 Envelope trimer by V1V2 loop-targeting antibodies. *eLife* **6** (2017).

65. Mastronarde, D.N. Automated electron microscope tomography using robust prediction of specimen movements. *J Struct Biol* **152**, 36-51 (2005).

66. Bepler, T. *et al.* Positive-unlabeled convolutional neural networks for particle picking in cryo-electron micrographs. *Nat Methods* **16**, 1153-1160 (2019).

67. Punjani, A., Zhang, H. & Fleet, D.J. Non-uniform refinement: Adaptive regularization improves single-particle cryo-EM reconstruction. *Nat Methods* **17**, 1214-1221 (2020).

68. Pettersen, E.F. *et al.* UCSF ChimeraX: Structure visualization for researchers, educators, and developers. *Protein Sci* **30**, 70-82 (2021).

69. Roark, R.S. *et al.* Recapitulation of HIV-1 Env-antibody coevolution in macaques leading to neutralization breadth. *Science* **371**, eabd2638 (2021).

Supplemental material

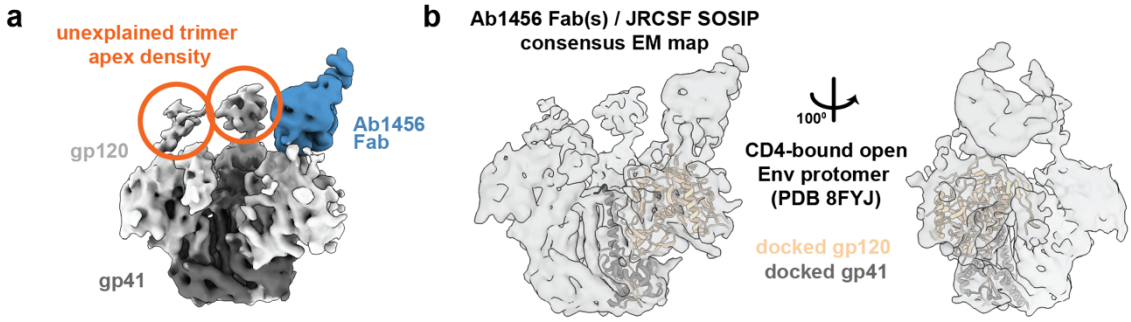

Supplementary Figure 1: Analysis of Ab1456 Fab(s)/JRCSF SOSIP consensus map. a, Unexplained density present at the trimer apex of the consensus EM map. **b**, Consensus EM density of the Ab1456/JRCSF structure including a cartoon representation of docked coordinates of protomer A gp120 and gp41 from an Env heterotrimer (HT2) bound by two copies of soluble CD4 (PDB 8FYJ).

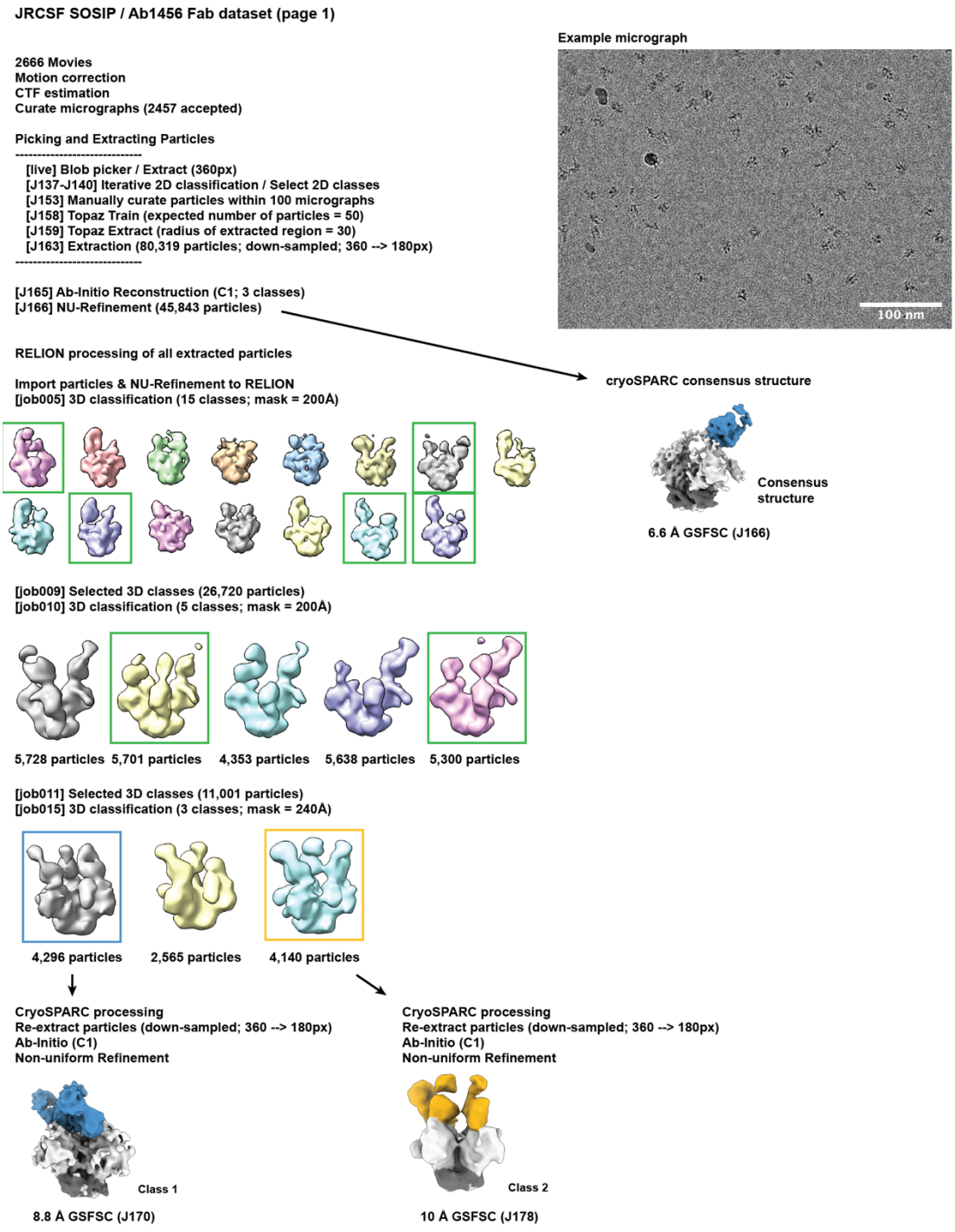

Supplementary Figure 2 (page 1 of 3): Data processing of the Ab1456 Fab/JRCSF SOSIP dataset.

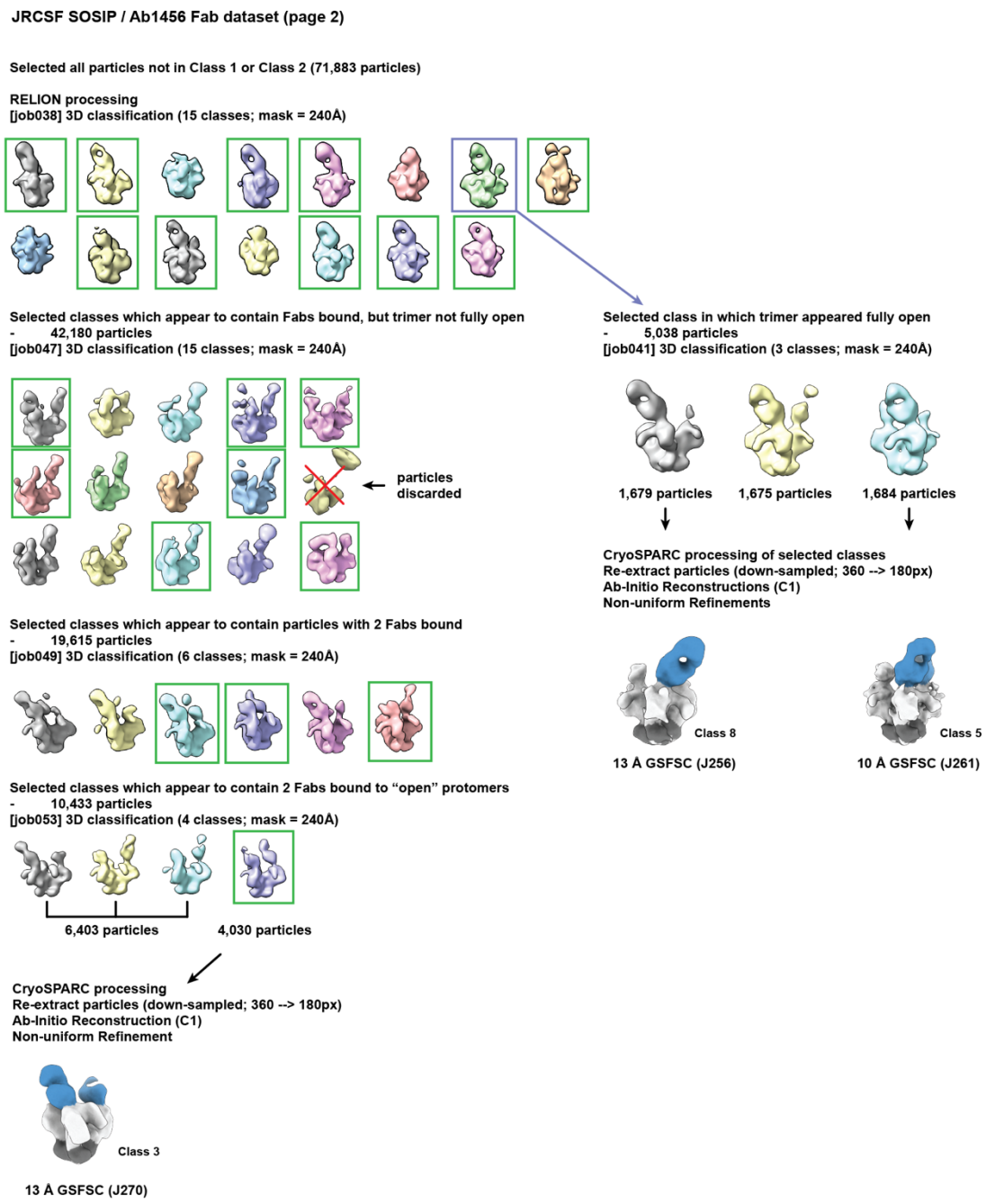

Supplementary Figure 2 (page 2 of 3): Data processing of the Ab1456 Fab/JRCSF SOSIP dataset.

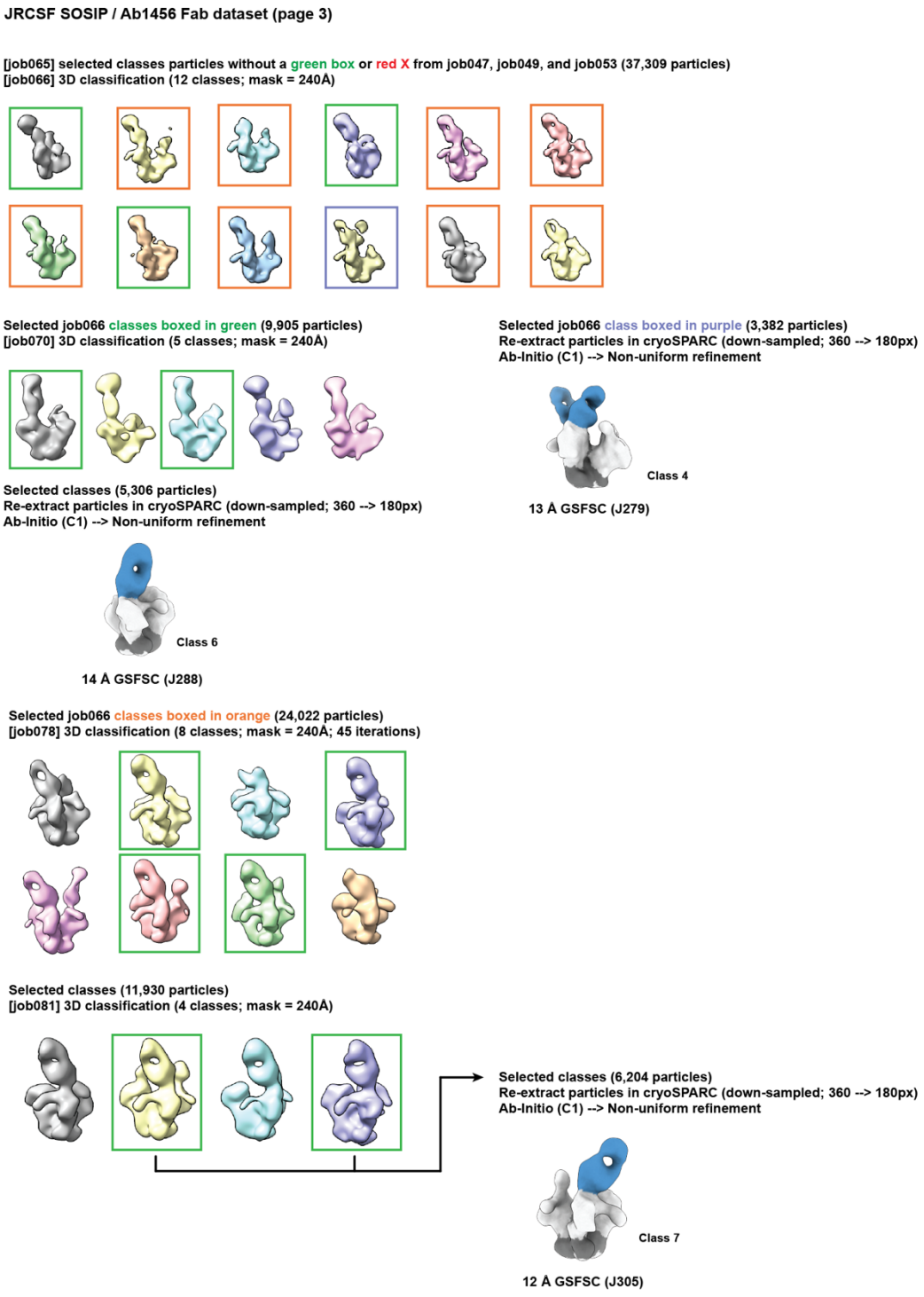

Supplementary Figure 2 (page 3 of 3): Data processing of the Ab1456 Fab/JRCSF SOSIP dataset.

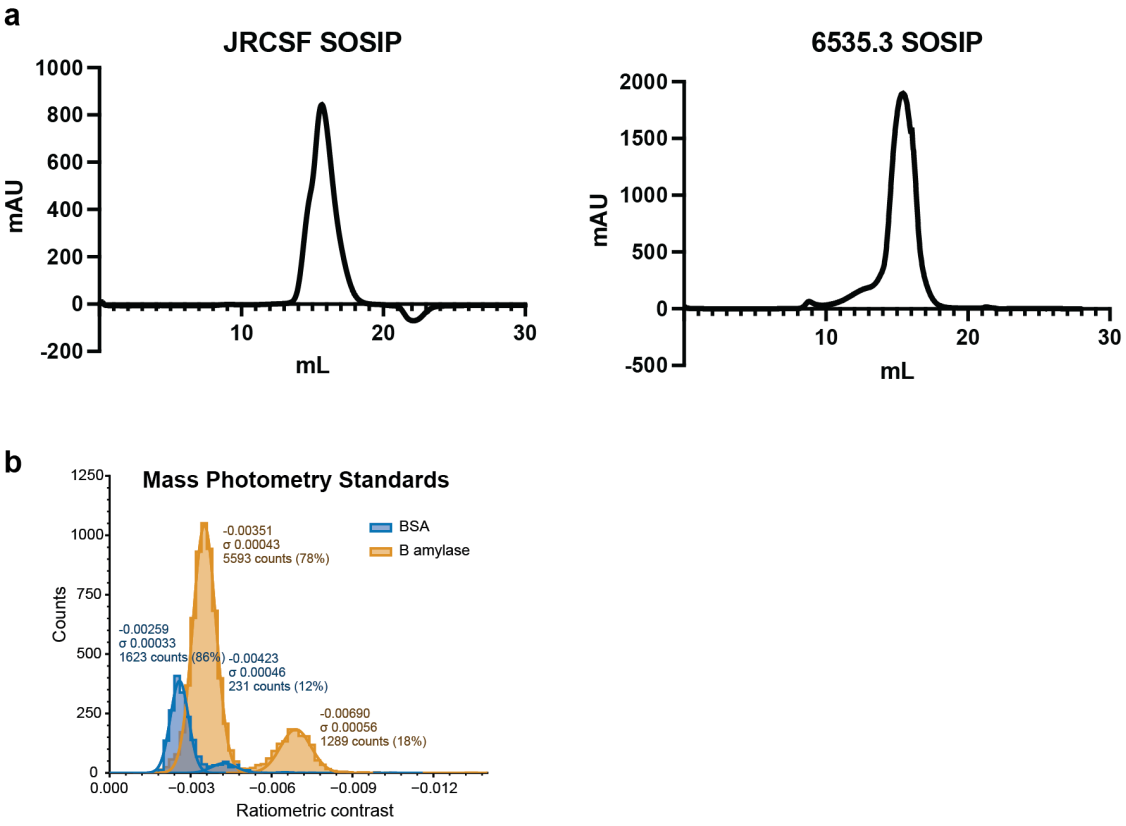

Supplementary Figure 3: Characterization of JRCSF and 6535.3 SOSIP Envs. a, SEC profiles for the purification of JRCSF SOSIP (left) and 6535.3 SOSIP (right). **b**, Experimental histograms for the mass standards used in mass photometry experiments of SOSIP Envs and Fab-SOSIP complexes.

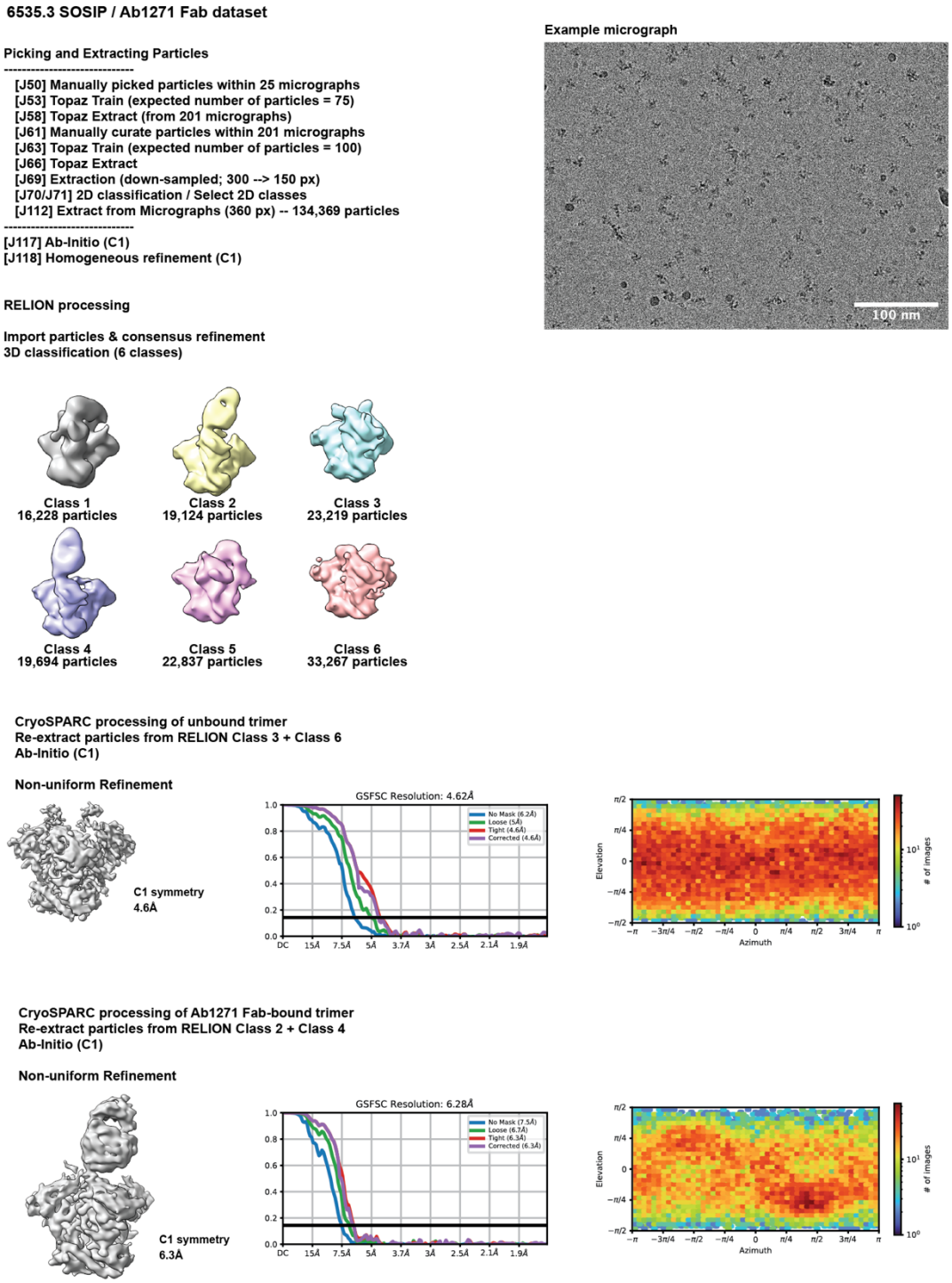

Supplementary Figure 4: Data processing of the Ab1271 Fab/6535.3 SOSIP dataset.

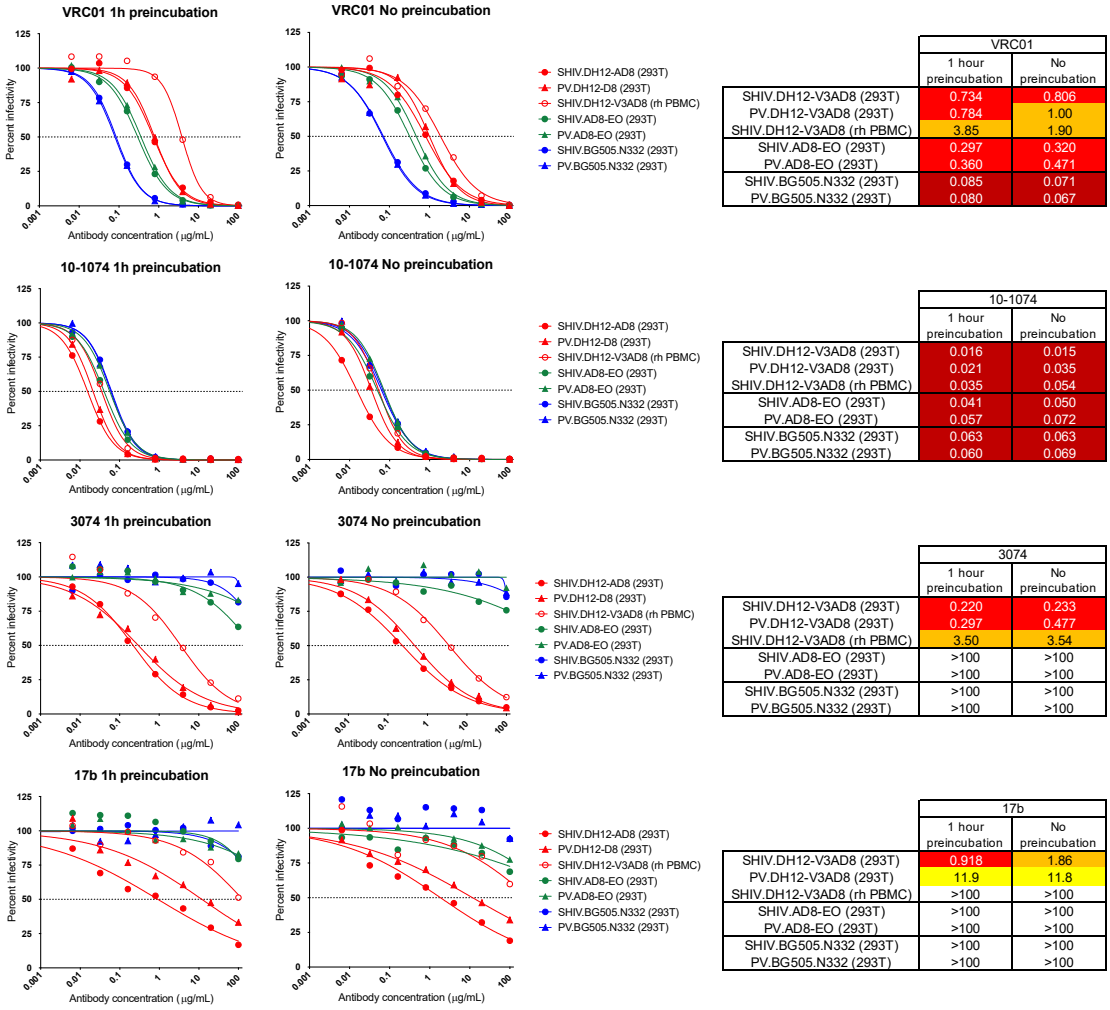

	VRC01	
	1 hour preincubation	No preincubation
SHIV.DH12-V3AD8 (293T)	0.734	0.806
PV.DH12-V3AD8 (293T)	0.784	1.00
SHIV.DH12-V3AD8 (rh PBMC)	3.85	1.90
SHIV.AD8-EO (293T)	0.297	0.320
PV.AD8-EO (293T)	0.360	0.471
SHIV.BG505.N332 (293T)	0.085	0.071
PV.BG505.N332 (293T)	0.080	0.067

	10-1074	
	1 hour preincubation	No preincubation
SHIV.DH12-V3AD8 (293T)	0.016	0.015
PV.DH12-V3AD8 (293T)	0.021	0.035
SHIV.DH12-V3AD8 (rh PBMC)	0.035	0.054
SHIV.AD8-EO (293T)	0.041	0.050
PV.AD8-EO (293T)	0.057	0.072
SHIV.BG505.N332 (293T)	0.063	0.063
PV.BG505.N332 (293T)	0.060	0.069

	3074	
	1 hour preincubation	No preincubation
SHIV.DH12-V3AD8 (293T)	0.220	0.233
PV.DH12-V3AD8 (293T)	0.297	0.477
SHIV.DH12-V3AD8 (rh PBMC)	3.50	3.54
SHIV.AD8-EO (293T)	>100	>100
PV.AD8-EO (293T)	>100	>100
SHIV.BG505.N332 (293T)	>100	>100
PV.BG505.N332 (293T)	>100	>100

	17b	
	1 hour preincubation	No preincubation
SHIV.DH12-V3AD8 (293T)	0.918	1.86
PV.DH12-V3AD8 (293T)	11.9	11.8
SHIV.DH12-V3AD8 (rh PBMC)	>100	>100
SHIV.AD8-EO (293T)	>100	>100
PV.AD8-EO (293T)	>100	>100
SHIV.BG505.N332 (293T)	>100	>100
PV.BG505.N332 (293T)	>100	>100

Supplementary Figure 5: Omission of the antibody-virus preincubation step does not affect the potency of bNAbs or antibodies recognizing non-closed Env trimers. The sensitivity of viruses expressing the DH12-V3AD8 (red), AD8-EO (green) and BG505.N332 (blue) Envs to neutralization by VRC01, 10-1074, 3074, and 17b in a standard TZMbl assay including a 1 hour antibody and virus preincubation step[40, 41] and a modified assay with no preincubation are shown. Neutralization curves for the indicated mAbs are shown on the left (dashed lines indicate 50% reduction in virus infectivity), with the corresponding 50% inhibitory concentrations (IC_{50}) in µg/mL shown on the right (coloring indicates relative neutralization potency). Pseudoviruses (PV) as well as replication-competent SHIVs derived either by HEK293T transfection (293T) or following propagation in rhesus macaque PBMC (rh PBMC) were tested. Note that similar to Ab1456 (Fig. 4a), the slopes of the neutralization curves for the linear V3 mAb 3074 and the CD4-induced mAb 17b are more shallow slopes than slopes of the CD4bs bNAb VRC01[45] and the V3 glycan bNAb 10-1074[44].

	Ab1456 Fab / JRCSF SOSIP	Ab1271 Fab / 6535.3 SOSIP
Data collection conditions		
Microscope	Titan Krios	Titan Krios
Voltage (kV)	300	300
Camera	Gatan K3 6k x 4k	Gatan K3 6k x 4k
Energy filter slit width (eV)	10	10
Magnification	105,000x	105,000x
Frames per movie	40	40
Recording mode	counting	counting
Dose rate (e^-/pixel/s)	25	26
Total electron dose ($e^-/Å^2$)	60	60
Defocus range (μm)	-1 to -3	-1 to -3
Pixel size (Å)	0.416 (super resolution)	0.416 (super resolution)
Micrographs collected	2664	2898
Micrographs used	2456	2756
Total extracted particles	80,319	134,369

	Consensus	Class 1	Class 2	Class 3	Class 4	Class 5	Class 6	Class 7	Class 8	Unbound 6535.3 SOSIP	Ab1271 Fab-bound 6535.3 SOSIP
EMD	**45944**	**45945**	**45946**	**45947**	**45948**	**45949**	**45950**	**45951**	**45952**	**45942**	**45943**
Particles in class	45,843	4296	4140	4030	3382	1684	5306	6204	1679	56,486	38,818
Symmetry	C1	C1	C1	C1	C1	C1	C1	C1	C1	C1	C1
Map resolution (Å)	6.6	8.8	10	13	13	10	14	12	13	4.6	6.3
FSC Threshold	0.143	0.143	0.143	0.143	0.143	0.143	0.143	0.143	0.143	0.143	0.143

Supplementary Table 1: EM data collection and processing statistics.

Chapter 4

PROFILING OF HIV-1 ELITE NEUTRALIZER COHORT REVEALS A CD4BS BNAB FOR HIV-1 PREVENTION AND THERAPY

Gieselmann, L.*, **DeLaitsch, A.T.*,** Rohde, M., Gruell, H., Kreer, C., Ercanoglu, M.S., Gristick, H.B., Schommers, P., Ahmadov, E., Radford, C., Mazzolini, A., Zhang, L., West, A.P., Worczinski, J., Momot, A., Reichwein, M.L., Knüfer, J., Stumpf, R., Mkhize, N.N., Kaldine, H., Bhebhe, S., Deshpande, S., Giovannoni, F., Stefanutti, E., Benigni, F., Havenar-Daughton, C., Corti, D., Kroidl, A., Adhikari, A., Nanfack, A.J., Ambada, G.E., Duerr, R., Maganga, L., William, W., Ntinginya, N.E., Wolf, T., Geldmacher, C., Hoelscher, M., Lehmann, C., Moore, P.L., Mora, T., Walczak, A.M., Gilbert, P.B., Doria-Rose, N.A., Huang, Y., Bloom, J.D., Seaman, M.S., Bjorkman, P.J., and Klein, F. Profiling of HIV-1 elite neutralizer cohort reveals a CD4bs bnAb for HIV-1 prevention and therapy. *Nat Immunol* 1-14 (2025). doi:10.1038/s41590-025-02286-5

**** Equal Contributions***

The following describes the structural characterizations of new CD4 binding site-targeting broadly neutralizing antibodies that were identified from a single elite neutralizer. This work is part of a large collaboration involving Florian Klein's lab and many other labs, and the complete manuscript is published with the doi:10.1038/s41590-025-02286-5. Included in this thesis is the abstract and introduction from the published manuscript, followed by a brief summary of experiments to add necessary context to the structural characterizations of these antibodies, which is the portion of the project I led at Caltech. The structural characterizations of these antibodies are presented in detail after the summary section.

Abstract: Administration of HIV-1 neutralizing antibodies can suppress viremia and prevent infection in vivo. However, clinical use is challenged by envelope diversity and rapid viral escape. Here, we performed single B cell profiling of 32 top HIV-1 elite neutralizers to identify broadly neutralizing antibodies with highest antiviral activity. From 831 expressed monoclonal antibodies, we identified 04_A06, a V_H1-2-encoded broadly neutralizing antibody to the CD4 binding site with remarkable breadth and potency against multiclade pseudovirus panels (geometric mean half-maximal inhibitory concentration = 0.059 μg ml^{-1}, breadth = 98.5%, 332 strains). Moreover, 04_A06 was not susceptible to classic CD4 binding site escape variants and maintained full viral suppression in HIV-1-infected humanized mice. Structural analyses revealed an unusually long 11-amino-acid heavy chain insertion that facilitates interprotomer contacts with highly conserved residues on the adjacent gp120 protomer. Finally, 04_A06 demonstrated high activity against contemporaneously circulating viruses from the Antibody-Mediated Prevention trials (geometric mean half-maximal inhibitory concentration = 0.082 μg ml^{-1}, breadth = 98.4%, 191 virus strains), and in silico modeling for 04_A06LS predicted prevention efficacy of >93%. Thus, 04_A06 will provide unique opportunities for effective treatment and prevention of HIV-1 infection.

Introduction

Broadly neutralizing antibodies (bnAbs), capable of neutralizing diverse HIV-1 strains and subtypes, represent promising tools for immunotherapy and prevention[1]. bnAbs target conserved epitopes on the HIV-1 Env trimer, including the CD4 binding site (CD4bs), glycan-dependent sites at the V3 base and V2 region, the gp120–gp41 interface, the membrane-proximal external region, the fusion peptide and the silent face[2]. The highly conserved CD4bs is critical for virus engagement of host cells. Given its pivotal role in the viral lifecycle, many bnAbs to the CD4bs display high levels of antiviral activity, and viral evasion may entail substantial fitness costs[3]. Therefore, bnAbs to the CD4bs are prime targets for clinical evaluation and vaccine development[4].

bnAbs to the CD4bs are categorized by genetic and structural features into VRC01-class (for example, VRC01, 3BNC117, N6, N49P7 and $VRC07_{523\text{-}LS}$)[5, 6, 7, 8, 9] and non-VRC01-class (for example, CH103, 8ANC131 and 1-18)[10, 11]. VRC01-class members, encoded by the immunoglobulin heavy chain gene segment *IGHV1-2*, include a five-residue light chain complementary-determining region 3 (CDRL3) and are characterized by high somatic hypermutation[8, 12]. Although bnAbs can reduce viremia, delay viral rebound and prevent infection with sensitive viruses, clinical trials have highlighted limitations, such as HIV-1 Env diversity and pre-existing and de novo resistance[1, 13], impeding clinical applicability. Therefore, identification of bnAbs with enhanced potency and breadth and restricted viral escape pathways remains critical.

Most bnAbs in clinical testing were isolated from a few HIV-1 elite neutralizers[6, 7, 9, 10, 11]. However, as both elite neutralizers and bnAb lineages within these individuals are rare, using large-scale screening can support discovery of new bnAbs with promising clinical potential. Here, we combined microscale antibody production with direct functional testing[14] to perform detailed single-cell profiling of the largest cohort of top HIV-1 elite neutralizers studied to date (32 individuals). We

identified 04_A06, a highly broad and potent bnAb to the CD4bs, from one of three genetically divergent B cell clones with overlapping CD4bs specificity. 04_A06 contains an 11-amino-acid insertion in the framework region heavy chain 1 (FWRH1) that contacts highly conserved Env residues (>99%), providing a structural explanation for its remarkable antiviral activity. This insertion also allowed 04_A06 to overcome classic viral CD4bs escape and to achieve full suppression of viremia in HIV-1YU2-infected humanized mice. Finally, based on high neutralizing activity of 04_A06 against transmitted viruses from two Antibody-Mediated Prevention (AMP) trials[13], modeling predicted a 93% prevention efficacy (PE) for an extended half-life variant, supporting 04_A06 as a promising candidate for treatment and prevention.

The following summary section is intended to provide context to the structural work presented in this thesis and does not encompass all aspects of the research. For the complete manuscript, figures, methods, and associated data, please see doi:10.1038/s41590-025-02286-5.

Summary

Serum samples from an international cohort of 2,354 people living with HIV-1 (PLWH) were first ranked according to neutralization activity against a 12-strain HIV-1 global pseudovirus panel[15, 16]. From 32 identified elite neutralizers within this cohort, blood samples were collected for the isolation of new bnAbs via single B-cell sorting using GFP-labeled $BG505_{SOSIP.664}$ and $YU2_{gp140}$ baits. Of 2,255 paired heavy and light chain antibodies sequences identified, a representative 831 were expressed and tested for neutralizing activity against a screening panel of six HIV-1 pseudoviruses.

Among tested monoclonal antibodies, those derived from individual EN02, a female living with HIV-1 clade C in Tanzania, exhibited the highest levels of breadth and mean neutralization potency against the HIV-1 pseudovirus screening panel[16]. Neutralization fingerprinting of purified serum IgG revealed VRC01-like activity, suggesting neutralization to be predominantly mediated by antibodies to the CD4bs. Indeed, most neutralizing antibodies (nAbs) isolated from donor EN02 were encoded by V_H1-2*07 paired with V_K1-33*01, and most contained a 5-amino-acid CDRL3, a hallmark of V_H1-2-encoded bnAbs to the CD4bs[8]. Isolated heavy chain sequences of nAbs varied in length, position and/or sequence of insertions within the heavy chain framework region 1 (FWRH1) or 3 (FWRH3), as well as in lengths and/or sequences of the heavy chain complementarity determining region 3 (CDRH3). Some antibodies lacked amino acid insertions, whereas others displayed six- and four-amino-acid insertions in the FWRH1 and FWRH3, respectively, or a 10- or 11-amino acid insertion in the FWRH1, suggesting parallel B cell evolution from distinct B cell progenitors.

V_H1-2-derived nAbs from expanded B-cell clones were tested for $BG505_{SOSIP.664}$ binding and neutralizing activity against the HIV-1 global pseudovirus panel[15]. Additionally, nAbs were tested for neutralizing activity against wild-type (WT) YU2 pseudovirus and YU2 pseudoviruses containing common CD4bs escape mutations (e.g., introduction of a potentially *N*-linked glycosylation site at position 279 on gp120). nAbs from clone 9, a clone containing either a 10- or 11-amino acid FWRH1 insertion were the most broad and potent and also neutralized all escape mutants tested. nAbs from clone 11, a clone containing both a 6-amino acid FWRH1 insertion and a 4-amino acid FWRH3 insertion, were also able to neutralize some of the CD4bs escape mutants, whereas monoclonal antibodies belonging to clone 7, a clone without insertions, were unable to neutralize the escape mutants. Transfer of the 11-amino acid insertion from 04_A06 (a monoclonal antibody from clone 9) to 05_B08 (a monoclonal antibody from clone 7 that lacks insertions) or VRC07 enabled these antibodies to overcome VRC01-class escape variants in vitro, highlighting a role for this insertion in resilience to CD4bs escape mutations.

Monoclonal antibodies from each of the three clones (04_A06 from clone 9, 01_D03 from clone 11, and 05_B08 from clone 7) were tested against a 119-strain psuedovirus panel[17] as well as a 208-strain panel[18]. 04_A06 was also tested against a 100-strain clade C panel[19]. Using a cutoff of 10 μg ml^{-1}, 04_A06 neutralized 98.5% of pseudovirus strains (332/337 strains) with a geometric mean IC_{50} of 0.059 μg ml^{-1}; meanwhile, against tested pseudovirus strains, 01_D03 exhibited 92.2% breadth, whereas 05_B08 exhibited 53.9% breadth. 04_A06 also achieved greater neutralization breadth (77%) and potency (GeoMean IC_{50} = 0.12 μg ml^{-1}) when tested against 35 VRC01-resistant virus strains than the near-pan-neutralizing bnAb 1-18 (ref. [10]) and N6 (ref. [7]), which neutralized 57% and 60% of strains, respectively. However, neither 04_A06 nor other CD4bs bnAbs tested were able to neutralize psuedoviruses derived from plasma single-genome sequencing (SGS) *env* sequences of donor EN02, which contained rare amino acid residues or insertions.

Additional experiments demonstrated that 04_A06 restricts viral escape and fully suppresses viremia in vivo. For example, 04_A06 was tested using deep mutational scanning (DMS) performed in a Env_{BF520} background[20, 21], and escape mutants were more readily identified for comparator CD4bs bnAbs $N6_{LS}$, $VRC07_{523\text{-}LS}$, 3BNC117, and 1-18 than for 04_A06. Additionally, when administered to HIV-1_{YU2}-infected humanized mice, 04_A06 fully suppressed viremia in 19 out of 19 mice without viral rebound until week 12. In contrast, VRC01 or VRC07 administration led to viral rebound within three weeks of treatment initiation, while N49P7 or N6 administration led to viral rebound occurring in some of the mice (six of seven for N49P7; three of six for N6), which occurred between two and four weeks after treatment initiation. 04_A06 was also able to fully suppress VRC01-resistant variants in vivo, as demonstrated by an experiment in which HIV-1_{YU2}-infected humanized mice were first administered VRC01, followed by the addition of 04_A06 at week four, after viral rebound had occurred in response to VRC01. Complete suppression of viremia was observed in all VRC01-pretreated animals that received 04_A06.

Results

Antibody insertions enable new CD4bs bnAbs to bind adjacent protomer

To elucidate mechanisms of Env recognition, we determined single-particle cryo-electron microscopy (cryo-EM) structures of a $BG505_{SOSIP.664}$ trimer[22] unbound (2.9 Å) and in complex with representative Fabs from each expanded B cell clone: 04_A06 (3.8 Å), 01_D03 (3.2 Å) and 05_B08 (3.3 Å; Fig. 1a, Extended Data Figs. 1 and 2a and Supplementary Table 1). The 04_A06 complex also included a Fab from PGDM1400, a broader and more potent variant of the V_1V_2 bnAb PGT145 (ref. [23]), and structures both with and without bound PGDM1400 were determined (Extended Data Fig. 1). All three bnAbs to the CD4bs exhibited canonical gp120 contacts made by CD4 and CD4-mimetic bnAbs[12, 24, 25] (Fig. 1b and Extended Data Fig. 2b). In each structure, R71 of the heavy chain

contacts D368 of gp120 (Fig. 1b and Extended Data Fig. 2b), a feature typical of VRC01-class antibodies and a hallmark of CD4-mimetic bnAbs[12]. Additionally, the V_H1-2-encoded S54 of the heavy chain is mutated to R54 in 04_A06 and Y54 in 01_D03, which insert into a hydrophobic gp120 cavity analogous to CD4 residue F43 (ref. [26]; Fig. 1b and Extended Data Fig. 2b). These interactions are similar to the interactions made by heavy chain R54 of the V_H1-2-encoded, non-VRC01-class bnAb IOMA[25] and heavy chain Y54 of the VRC01-class bnAb N6[7] (Fig. 1b and Extended Data Fig. 2b). Additionally, the V_H1-2-encoded heavy chain N58 is mutated to K58 in 04_A06 and IOMA (Fig. 1b and Extended Data Fig. 2b), mimicking the interaction of CD4 K35 with Env residues N280 and R456 of gp120. Although 04_A06 features a five-amino-acid-long CDRL3 characteristic of VRC01-class bnAbs, it also shares key somatic hypermutations and structural determinants with IOMA shaping recognition of the CD4bs (Fig. 1b and Extended Data Fig. 2b). Thus, 04_A06 possesses features representative of both VRC01-class and IOMA-like bnAbs to the CD4bs.

The presence and length of insertions in the three representative bnAbs correlated with the formation of interprotomer contacts (Fig. 1a). 04_A06 and 01_D03, but not 05_B08, contacted the adjacent gp120 protomer (Fig. 1a), a feature seen in other potent bnAbs such as 1-18 (ref. [10]) and 3BNC117 (ref. [27]). Contacts between 04_A06 and the adjacent protomer were mediated exclusively via a protruding CDRH1 in 04_A06, a consequence of the 11-residue FWRH1 insertion (Fig. 1a), which also contacted the primary protomer (Extended Data Fig. 2c). On the adjacent protomer, 04_A06 interacted with gp120 K207 (99.6% conserved; www.hiv.lanl.gov and West et al.[28]) and formed a potential electrostatic interaction with heavy chain D26 (Fig. 1a). D26 is also positioned adjacent to gp120 R304 (93.5% conserved), whereas residues within the tip of the 04_A06 CDRH1 (heavy chain Y31–Y35C) are in close proximity to residues H66 and H72 on gp120 (99.9% and 96.2% conserved, respectively; Fig. 1a). Together, these residues could form interactions that permit tolerance to structural variability within the CD4bs on the primary Env protomer (for example, the addition of a

potential N-linked glycosylation site at gp120 N279). The extended CDRH1 of the CD4bs bnAb 1-18 also contacts gp120 K207 on the adjacent protomer but mainly interacts with less conserved V3 residues[10], whereas the CDRH1 of 04_A06 extends toward a more conserved gp120 region (Fig. 1c), likely contributing further to 04_A06's enhanced neutralization profile. In contrast to the CDRH1-mediated interprotomer contacts of 04_A06, antibody 01_D03, with its 6-residue FWRH1 insertion, 4-residue FWRH3 insertion, and 20-residue CDRH3, contacts the adjacent protomer with each of its heavy chain CDRs and makes potential electrostatic interactions with gp120 K207 and E64 (99.6% and 99.7% conserved; Fig. 1a). In the 01_D03-complexed Env structure, but not in the unbound BG505 SOSIP structure, EM density was observed for residues 57–65 of gp120 on the adjacent protomer (Extended Data Fig. 2d), suggesting that this normally disordered loop becomes stabilized after antibody binding.

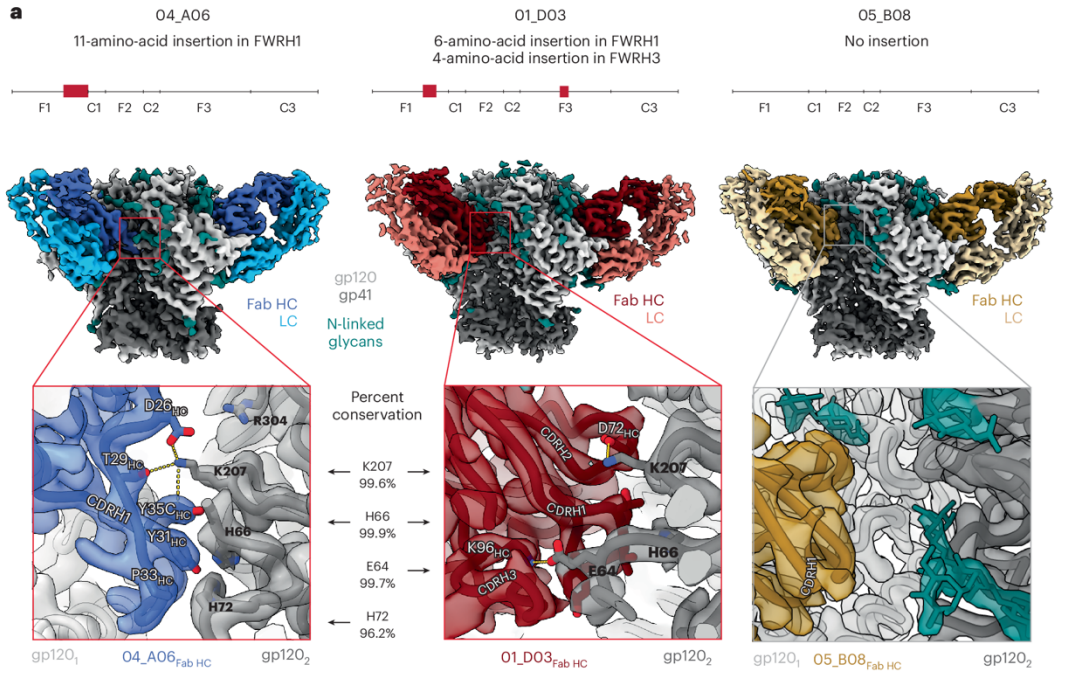

bnAb	04_A06	01_D03	05_B08	3BNC117	VRC01
PDB	8ULU (this study)	8ULS (this study)	8UKI (this study)	5V8M	6V8X
Breadth	98.5% (332 strains)	92.2% (245 strains)	53.9% (245 strains)	82.3% (209 strains)	83.3% (209 strains)
Insertions	11-aa FWRH1	6-aa FWRH1 + 4-aa FWRH3	None	4-aa FWRH3	None
gp120$_1$ BSA (Å^2)	1,310	1,130	1,140	1,100	1,030
gp120$_2$ BSA (Å^2)	180	330	5	160	0
Total BSA (Å^2)	1,490	1,460	1,140	1,260	1,040

Figure 1: Insertions facilitate adjacent protomer binding of new CD4bs bnAbs. a, Schematics illustrating the position and length of FWRH1 and/or FWRH3 insertions of 04_A06 (left), 01_D03 (middle) and 05_B08 (right; top), EM maps showing side views of 04_A06, 01_D03 and 05_B08 bnAb Fabs in complex with $BG505_{SOSIP.664}$ Env trimers (middle) and insets illustrating a close-up of bnAb interactions with the adjacent gp120 protomer ($gp120_2$; bottom); HC, heavy chain; LC, light chain. **b,** Canonical interactions of CD4 and bnAbs to the CD4bs (04_A06, IOMA and VRC01) with Env gp120 D368, the F43 pocket and gp120 N280/R456. **c,** Interactions between the CDRH1s of 04_A06 (blue cartoon representation) and 1-18 (red cartoon representation) with the secondary ($gp120_2$) Env protomer, shown as a surface colored by percent conservation. The inset (top right) shows the Env trimer–04_A06 complex as a surface representation for orientation. **d,** Crystal structure of unbound 04_A06 Fab (bottom) and inset highlighting the 04_A06 CDRH1, with electron density contoured at 1.5σ (top). **e,** Molecular surface representation showing the surface area buried by VRC01-class bnAbs (04_A06, 01_D03, 05_08, 3BNC117 and VRC01) on primary ($gp120_1$) or secondary ($gp120_2$) Env protomers (top). Listing of Protein Data Bank (PDB) accession codes, breadth (%), heavy chain insertion length and position, buried surface area (BSA) on $gp120_1$ and $gp120_2$ as well as total BSA for VRC01-class bnAbs (bottom).

To determine whether the conformation of the extended CDRH1 of 04_A06 is preorganized for binding, we solved a 1.75-Å crystal structure of unbound 04_A06 Fab (Fig. 1d and Supplementary Table 2). The structure, which does not appear to be influenced by crystal contacts (Extended Data Fig. 2e), revealed a well-ordered antibody combining site and CDRH1 that resembled the conformation of the combining site in the Env-bound Fab (root mean square deviation (r.m.s.d.) = 0.64 Å; 235 Cα atoms), consistent with a lock-and-key mechanism of binding[29] (Fig. 1d and Extended Data Fig. 2f). This is in contrast to the induced fit mechanism of binding by the extended CDRH1 of VRC–CH31, which is unresolved in crystal structures in complex with gp120 (ref. [30]) but becomes partially ordered in a VRC–CH31–SOSIP Env structure, where it is stabilized by interactions with the adjacent protomer[31]. The preorganized antibody combining site of 04_A06 likely leads to a more favorable interaction with Env due to a lower entropic cost of binding.

In addition to contacting highly conserved residues, the insertions and interprotomer contacts of 04_A06 and 01_D03 contribute to an increased amount of surface area buried on Env by antibody

binding. These insertions enable 04_A06 and 01_D03 to bury more surface area on Env than 05_B08 or other VRC01-class bnAbs (Fig. 1e), presenting another possible mechanism contributing to breadth, potency and resistance to escape[10]. Consistent with this and in common with 04_A06, 01_D03 exhibited greater potency and breadth than 3BNC117 and VRC01 (GeoMean IC50/IC80 = 0.052/0.187 μg ml^{-1}, breadth = 92%/88%; 245 strains; Fig. 1e).

Our 04_A06 complex structure also included PGDM1400 (Extended Data Fig. 3a). The PGDM1400 Fab binds asymmetrically to the trimer apex with a stoichiometry of one Fab per trimer (Extended Data Fig. 3b). Its 34-residue CDRH3 is inserted down the trimer symmetry axis and contacts protein residues and the gp120 N160 N-glycan of all three protomers, resulting in a well-resolved glycan density for the core pentasaccharide of each N160 glycan and additional glycans in some cases (Extended Data Fig. 3c). Mass spectrometry analysis reported that the gp120 N160 glycan is underprocessed, containing a mixture of high-mannose, hybrid and complex-type N-glycans[32]. In our structure, density was not observed for a core fucose, a component of complex-type N-glycans[25], nor could clear density be discerned much beyond the core pentasaccharide (Extended Data Fig. 3c), the latter a likely consequence of limited resolution, glycan compositional heterogeneity and/or glycan flexibility. However, a surface electrostatic calculation revealed electropositive patches that could accommodate, or interact with, negatively charged sialic acid residues on complex-type glycans[33] (Extended Data Fig. 3c), particularly for surfaces on PGDM1400 that interact with the N160 glycan 2 and N160 glycan 3 relative to analogous interactions with PGT145 (ref. [27]; Extended Data Fig. 3c,d). Additionally, PGDM1400 appears to stabilize the core pentasaccharide of the N160 glycan 3 (Extended Data Fig. 3c,d), whereas this glycan was proposed to be inhibitory to the binding of PGT145 (ref. [27]). The ability to accommodate and/or interact with the three gp120 N160 glycans on an Env trimer, whether or not processed beyond high-mannose carbohydrates, likely contributed to the enhanced breadth and potency of PGDM1400. Our structure recapitulates key molecular

interactions between PGDM1400 and Env recently reported[34], such as the interaction between gp120 K169 and heavy chain Tys100F, electrostatic interactions between an Asp-Asp-Asp motif at the tip of the PGDM1400 CDRH3 with gp120 R166 of all three protomers and extensive glycan density at gp120 N160 on all protomers.

Discussion

Structural analysis of 04_A06 revealed mechanisms that contributed to the breadth and potency of the antibody. Most notably, 04_A06 uses an 11-amino-acid insertion in FWRH1 that contacts gp120 K207, H66 and H72, highly conserved residues on the adjacent gp120. Pseudoviruses containing substitutions at these residues exhibit decreased or completely abrogated infectivity[31], suggesting that these residues are functionally important and that escape mutations at these sites are likely associated with fitness costs. Engrafting the FWRH1 insertion from 04_A06 to VRC07 restored neutralizing activity against VRC01-class-resistant viruses in vitro, supporting the functional relevance of these contacts for restriction of viral escape. To our knowledge, among the antibodies identified to date, only 04_A06 contacts this conserved surface on HIV-1 Env, a region that is sterically difficult for antibody access. In addition, an unliganded 04_A06 Fab structure showed that its FWRH1 insertion is preorganized for binding, despite potential flexibility arising from it extending away from the antibody combining site, suggesting no entropic penalties for reorganizing the FWRH1 insertion after Env binding. Beyond these heavy chain features, 04_A06 diverges from canonical V_H1-2-encoded bnAbs to the CD4bs in light chain architecture. Unlike VRC01 or VRC07, which exhibit a shortened CDRL1 to accommodate the gp120 N276 glycan, 04_A06 lacks such a deletion, highlighting alternative structural solutions for effective CD4bs engagement. In addition to 04_A06, we identified and structurally characterized 01_D03 and 05_B08, two phylogenetically distinct VRC01-class bnAbs also isolated from donor EN02. Like 04_A06, 01_D03 contacts the adjacent protomer, likely through its FWRH1 and FWRH3 insertions. The four-residue DASG FWRH3 insertion is situated in

the same position as a WDFD insertion identified in the 3BNC60/3BNC117 bnAb family, which arose in a different individual[11, 35]. Analysis of clonal relatives of 3BNC60/3BNC117 revealed a correlation between the presence of this insertion and potent neutralizing activity, and its removal from 3BNC60 reduced its ability to neutralize diverse viruses[35], further highlighting the potential importance of antibody insertions for antiviral activity.

Methods

Cloning and production of monoclonal antibodies for cryo-EM studies

Heavy chain variable regions of antibodies 04_A06, 05_B08 and 01_D03 were subcloned into a mammalian Fab expression vector containing a C-terminal hexahistidine tag and coexpressed with corresponding light chains in Expi293F cells (Thermo Fisher). Fabs were purified from culture supernatants by Ni-NTA affinity chromatography (GE Life Sciences), buffer exchanged into TBS (20 mM Tris (pH 8.0) and 150 mM NaCl) using Amicon 10-kDa concentrators (Millipore) and further purified by size-exclusion chromatography (SEC) on a Superdex-200 16/60 column equilibrated in TBS. Fractions corresponding to the Fab peak were pooled, concentrated with Amicon 10-kDa concentrators and stored at 4 °C.

Expression and purification of $BG505_{SOSIP}$ trimer

$BG505_{SOSIP.664}$ for cryo-EM was expressed by transient co-transfection with a furin-encoding plasmid in Expi293F cells (Thermo Fisher) as previously described[36]. Proteins were purified from supernatants by 2G12 (04_A06/PGDM1400 complex) or PGT145 (01_D03, 05_B08 and unbound structure) immunoaffinity chromatography, dialyzed into TBS and concentrated. SEC was performed on a Superose-6 Increase column (PGT145 preps) or sequentially on a Superdex-200 16/60 and Superose-6 Increase 10/300 GL column (2G12 preps) in TBS. Fractions were stored individually at 4 °C.

Cryo-EM sample preparation

The 04_A06–PGDM1400–BG505 complex was assembled at a 3.6:1.2:1 molar ratio (Fab:Fab:trimer), incubated overnight at room temperature, purified on a Superose-6 Increase 10/300 GL column and concentrated to ~2.5 mg ml^{-1} in TBS (Amicon 10-kDa, Millipore) 1 day before vitrification. The 01_D03–BG505 and 05_B08–BG505 complexes were prepared at a 3.6:1 molar ratio (Fab:trimer), incubated overnight in TBS at room temperature and concentrated to ~4.2 mg ml^{-1} and ~4.4 mg ml^{-1}, respectively, without further SEC. Unbound BG505 was concentrated to ~4.0 mg ml^{-1}.

Octyl-maltoside fluorinated solution was added to each sample for a final concentration of 0.02% (wt/vol) immediately preceding the addition of 3 µl to a Quantifoil R1.2/1.3 Cu 300-mesh grid (04_A06–PGDM1400 complex) or a Quantifoil R1.2/1.3 Holey Carbon Film 300-mesh gold grid (01_D03 and 05_B08 complexes and unbound BG505; Electron Microscopy Services) that had been glow discharged for 1 min at 20 mA using a PELCO easiGLOW (Ted Pella). Grids were blotted for 3 s with Whatman No. 1 filter paper and plunge-frozen in liquid ethane using a Mark IV Vitrobot (Thermo Fisher) operating at room temperature and 100% humidity.

Cryo-EM data collection and processing

Data were collected on a 300-keV Titan Krios transmission electron microscope (Thermo Fisher Scientific) equipped with a GIF Quantum energy filter and a K3 6,000 × 4,000 direct electron detector (Gatan) operating in counting mode. Data collection was performed using SerialEM v4.0.13 (04_A06 and unbound BG505) or v4.1.0beta[37] (01_D03 and 05_B08) at a nominal magnification of ×105,000 (super-resolution = 0.416 Å per pixel) and a defocus range of –1.0 to –3.0 µm. Movies were recorded using a 3 × 3 beam image shift pattern with one (04_A06/PGDM1400 dataset), two (01_D03 and

05_B08 datasets) or three shots (unbound BG505 dataset) per hole. For the 04_A06 and 01_D03 datasets, motion correction, contrast transfer function estimation, particle picking and binned particle extraction were performed using cryoSPARC Live (v3 and v4, respectively) before processing in cryoSPARC[38]. For the 05_B08 and unbound BG505 datasets, all processing was performed in cryoSPARCv4. Particles were picked using blob picker or Topaz[39] and extracted from micrographs. For the 04_A06–PGDM1400–BG505 dataset, a model was built into the map containing PGDM1400, and after verifying that this model (minus PGDM1400 and the N160 glycans) fit well into the C3 symmetric map that lacked PGDM1400, particle subtraction and local refinement (with applied C3 symmetry) were performed to obtain a higher-resolution view of the 04_A06–BG505 interface. To create a mask for particle subtraction, the 'molmap' command in ChimeraX was applied to a model of the PGDM1400 Fab and gp120 N160 glycans that was built into the EM density. The mask was imported into cryoSPARC[38], and a soft padding was applied (threshold = 0.1; soft padding width = 10 voxels). A mask for local refinement was similarly created using a model of BG505 and the 04_A06 V_HV_L (threshold = 0.05, dilation radius = 5; soft padding width = 10).

Structure modeling and refinement

The following coordinates were docked into the corresponding densities of the EM maps using ChimeraX[40] to generate starting models: BG505 (PDB: 6UDJ), PGDM1400 (PDB: 4RQQ) and the 04_A06 Fab crystal structure (PDB: 8UKI; this study). Sequence-corrected models for the 01_D03 and 05_B08 V_HV_L domains were built into the corresponding densities in Coot[41] using the 04_A06 Fab crystal structure as a starting model. Models were refined through iterative rounds of Phenix real space refine and Coot. N-Glycans were built using tools in Coot[41] and verified as 'OK' by Privateer[42]. Modeling of side chains should be considered approximate, owing to the intermediate resolution of the EM structures. Antibody residues were numbered according to Kabat.

X-ray crystallography

Crystallization screens for the 04_A06 Fab were performed using sitting drop vapor diffusion at room temperature by mixing 0.2 µl of Fab (4.1 mg ml^{-1}) with 0.2 µl of reservoir solution (Hampton Research) using a TTP Labtech Mosquito automatic microliter pipetting robot. 04_A06 Fab crystals were obtained in 8% (vol/vol) Tacsimate (pH 7.0) and 20% (wt/vol) polyethylene glycol 3350. Crystals were looped and cryopreserved in reservoir solution supplemented stepwise with 5–20% glycerol and cryopreserved in liquid nitrogen. A 1.75-Å structure of 04_A06 Fab was solved using a dataset collected at 100 K and a 1-Å wavelength on Beamline 12-2 at the Stanford Synchrotron Radiation Lightsource with an Eiger X 16M (Dectris) detector, which was indexed and integrated with iMosflm v7.4 and then merged with AIMLESS in the CCP4 software package v7.1.018.

The structure was determined by molecular replacement in Phaser with the coordinates of the VRC01 Fab (PDB: 3NGB), using C_H–C_L and V_H–V_L (with truncated CDR loops) as separate search models. Coordinates were refined using PHENIX v1.20.1-4487129 with individual B factors and TLS restraints[43]. Manual rebuilding was performed iteratively with Coot v0.9.8.8131 (ref. [44]). A total of 99.1% of residues were in the favored regions of the Ramachandran plot, and 0.9% were in the allowed region (Supplementary Table 2).

Structural analyses

Figures were prepared using UCSF ChimeraX[33] and PyMOL (Schrödinger). Buried surface area was calculated using PDBePISA v1.52 (ref. [45]) with a 1.4-Å probe. The r.m.s.d. values were calculated in PyMOL (Schrödinger), and electrostatic surfaces were calculated in UCSF ChimeraX[33]. Owing to the intermediate resolution and minor differences in modeling of identical copies of chains within a trimer, a general cutoff of ≤6.0 Å was used to define potential interactions.

Data availability

Cryo-EM maps and models have been deposited in the Electron Microscopy Data Bank and PDB under accession codes EMD-46649 and 9D8V (unbound BG505), EMD-42363 and 8ULR (05_B08–BG505v2), EMD-42364 and 8ULS (01_D03–BG505), EMD-42365 and 8ULT (04_A06–BG505) and EMD-42366 and 8ULU (04_A06–PGDM1400–BG505). Coordinates for the 04_A06 Fab crystal structure have been deposited to the PDB under accession code 8UKI.

Acknowledgements (original publication)

We thank all study participants for supporting our research by blood donation; members of the laboratories of F.K., P.J.B. and J.D.B. for their support and inspiring discussions; X. Shi (Tsinghua University), T. Zhou (VRC) and L. Zhang (Tsinghua University) for sharing and providing the plasmids encoding CD4bs-resistant pseudovirus strains; A. Schmitt (University of Cologne) and T. Bresser (University of Cologne) for lab management and assistance and S. Chen (Caltech) and the Caltech Cryo-EM Center and J. Vielmetter (Caltech) and the Caltech Protein Expression Center for experimental support. A.T.D. was supported by an NSF Graduate Research Fellowship. We thank the Cologne Center for Genomics for sequencing and library preparation support and the staff of the Animal Care Facility Weyertal at the University of Cologne. The panel of global HIV-1 pseudoviruses was obtained through the NIH AIDS Reagent Program. This work was funded by grants from the German Center of Infection Research (DZIF) to F.K., the German Research Foundation CRC1279 and CRC1310, European Research Council (ERC) ERC-stG639961 and COVIM: NaFoUniMed-Covid19 to F.K. This work was also supported, in whole or in part, by the Bill and Melinda Gates Foundation (INV-002143, to F.K. and P.J.B.; INV-036842, M.S.S.). Under the grant conditions of the Foundation, a Creative Commons Attribution 4.0 Generic License has already been assigned to the Author Accepted Manuscript version that might arise from this submission. Research reported in this publication was also supported by the National Institute of

Allergy and Infectious Diseases of the National Institutes of Health under award numbers P01AI100148 and 1U54AI170856 to P.J.B. and R01AI140891 and U01AI169385 to J.D.B. The content is solely the responsibility of the authors and does not necessarily represent the official views of the National Institutes of Health. P.L.M is supported by the South African Research Chairs Initiative of the Department of Science and Innovation and the National Research Foundation (98341). This study was supported in part by the Bill and Melinda Gates Foundation's Collaboration for AIDS Vaccine Discovery (1032144) to P.L.M. This work was also supported by the European Research Council COG 724208 and ANR-19-CE45-0018 'RESPREP' from the Agence Nationale de la Recherche to A.M.W. P.S. is supported by the Emmy Noether Programme of the German Research Foundation (495793173). BnAb 04_A06 has been exclusively licensed to Vir Biotechnology. The funders had no role in study design, data collection and analysis, decision to publish or preparation of the manuscript.

Contributions (original publication)

Conceptualization: L.G., A.T.D., H.B.G., C.K., H.G., P.J.B. and F.K. Methodology: L.G., C.K., H.G., A.T.D., H.B.G., C.R., J.D.B, A. Mazzolini, A.M.W., T.M., M.S.S., P.J.B. and F.K. Formal analysis: L.G., A.T.D., C.K., H.B.G., A.P.W., M.R., P.S., H.G., M.S.E., E.A., J.W., A. Momot, M.L.R., J.K., R.S., S.D., F.G., E.S., F.B., C.H.-D., D.C., C.R., N.A.D.-R., M.S.S., N.N.M., L.Z., H.K., S.B., P.S., A. Mazzolini, A.M.W., L.Z. and T.M. Investigation: L.G., A.T.D., H.B.G., C.R., M.R., M.S.E., E.A., J.W., A. Momot, M.L.R., J.K., R.S., S.D., F.G., E.S., F.B., C.H.-D., D.C., N.D., J.D.B., M.S.S., P.L.M., T.M., A.M.W., P.B.G., N.A.D.-R., Y.H., P.J.B. and F.K. Resources: A.K., A.A., A.J.N., G.E.A., R.D., P.S., L.M., W.W., N.E.N., T.W., C.G., M.H. and C.L. Writing, original draft: L.G., A.T.D., H.B.G., C.R., C.K., H.G., A. Mazzolini, P.J.B. and F.K. Writing, reviewing and editing: all authors. Supervision: H.B.G., H.G., P.J.B. and F.K. Funding acquisition: M.S.S., J.D.B., P.L.M., A.M.W., F.K. and P.J.B.

Supplementary Figures and Tables

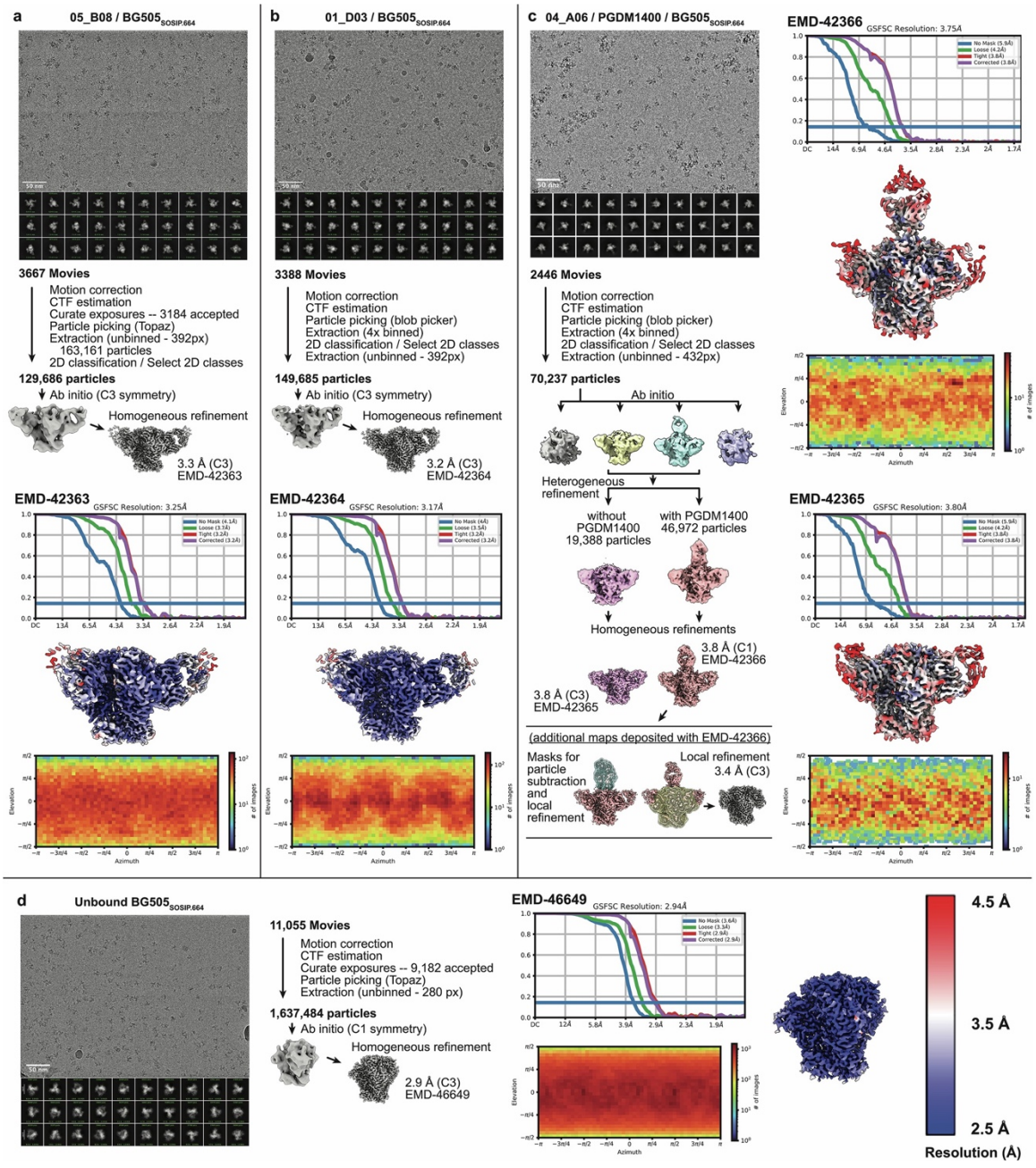

Extended Data Fig. 1: Cryo-EM data collection and processing.
Representative micrographs, two-dimensional class averages, workflows, gold-standard Fourier shell correlation (GSFSC) curves, final density maps colored by local resolution, and particle orientation distributions for **a,** 05_B08 Fab / BG505$_{SOSIP.664}$, **b,** 01_D03 Fab / BG505$_{SOSIP.664}$, **c,** 04_A06 Fab / PGDM1400 Fab / BG505$_{SOSIP.664}$, and **d,** unbound BG505$_{SOSIP.664}$ datasets.

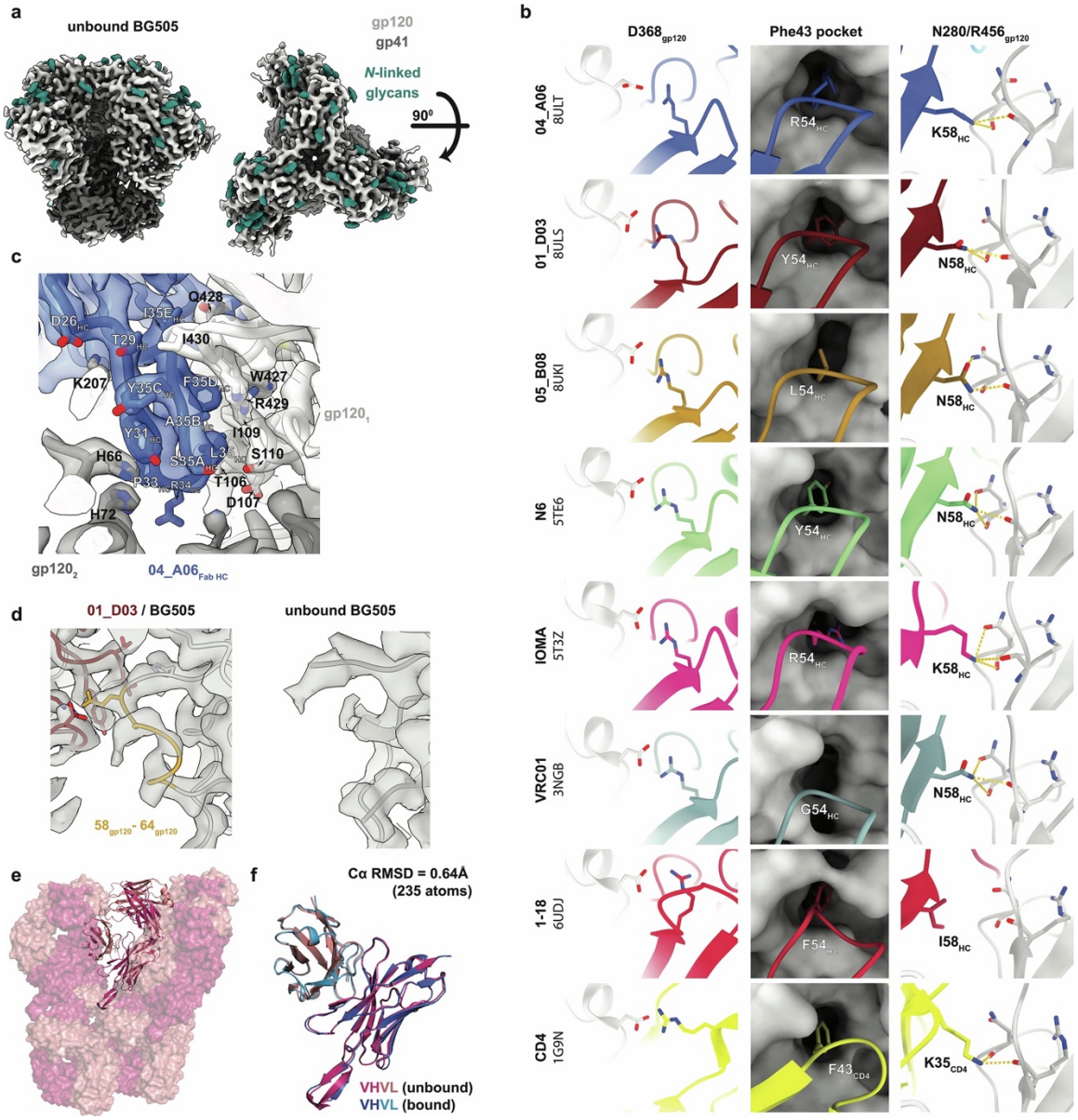

Extended Data Fig. 2: Structural analysis of CD4bs antibodies from EN02 with other CD4bs antibodies and unbound BG505.

a, EM density of unbound $BG505_{SOSIP.664}$ structure showing side and top views. **b,** Canonical interactions of CD4 and CD4bs bnAbs with Env: $D368_{gp120}$, Phe43 pocket, and $N280_{gp120}$ / $R456_{gp120}$. **c,** Close up view of 04_A06's CDRH1 interactions (blue) with the primary gp120 ($gp120_1$). **d,** EM density for gp120 residues 58-64 on the adjacent protomer ($gp120_2$) as observed in complex with 01_D03 Fab compared to unbound $BG505_{SOSIP.664}$. **e,** Crystal packing environment of 04_A06 Fab. **f,** Overlay of V_H-V_L domains in bound (from Fab-SOSIP cryo-EM structure) and unbound (from Fab crystal structure) structures.

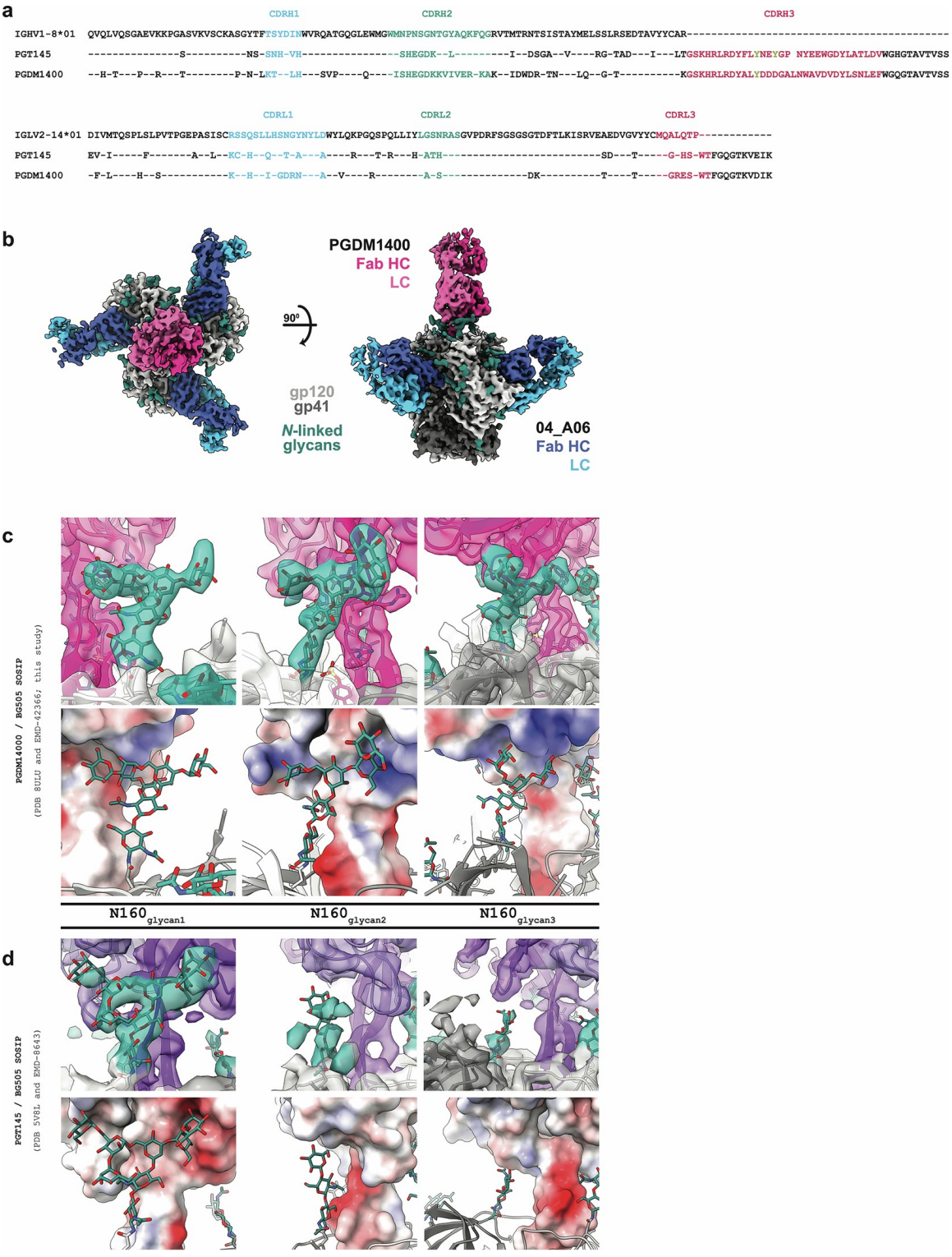

Extended Data Fig. 3: Structural analyses of PGDM1400.

a, Amino acid sequence alignment of heavy and light chain V gene-encoded regions from bNAbs PGT145 and PGDM1400. Sulfated tyrosine residues located in the CDRH3 are indicated by a green "Y". **b,** Structure overview showing EM density of $BG505_{SOSIP.664}$ in complex with 04_A06 and PGDM1400 Fabs. EM density for N160 glycans (top) and a Fab electrostatic surface calculation (bottom) for PGDM1400 **(c)** and PGT145 **(d)**. Glycans labeled as glycan 1,2, and 3 correspond to the $N160_{gp120}$ glycans from each of the three Env protomers[27].

Cryo-EM data collection and refinement

	BG505 SOSIPv2	05_B08 Fab / BG505 SOSIPv2	01_D03 Fab / BG505 SOSIPv2	04_A06 Fab / PGDM1400 Fab / BG505 SOSIPv2	
Data collection conditions					
Microscope	Titan Krios	Titan Krios	Titan Krios	Titan Krios	
Voltage (kV)	300	300	300	300	
Detector	Gatan K3	Gatan K3	Gatan K3	Gatan K3	
Magnification	105,000x	105,000x	105,000x	105,000x	
Pixel size (Å)	0.832	0.832	0.832	0.832	
Recording mode	counting	counting	counting	counting	
Defocus range (μm)	1.0 - 3.0	1.0 - 3.0	1.0 - 3.0	1.0 - 3.0	
Electron exposure ($e^-/Å^2$)	60	60	45	60	
Exposure rate (e^-/pixel/s)	22.5	20.7	17.9	22.9	
Energy filter slit width (eV)	10	10	10	10	
Frames per movie	40	40	40	40	
Movies collected	11,055	3,667	3,388	2,446	
				Class 1 (without PGDM1400)	Class 2 (with PGDM1400)
PDB	**9D8V**	**8ULR**	**8ULS**	**8ULT**	**8ULU**
EMD	**EMD-46649**	**EMD-42363**	**EMD-42364**	**EMD-42365**	**EMD-42366**
Refined particles	1,637,484	149,685	129,686	19,388	46,972
Symmetry imposed	C3	C3	C3	C3	C1
Map Resolution (Å)					
FSC threshold (0.143)	2.9	3.3	3.2	3.8	3.8
Refinement and Validation					
Initial models used	6UDJ	6UDJ, 8UKI	6UDJ, 8UKI	6UDJ, 8UKI	6UDJ, 8UKI, 4RQQ
Model composition					
Non-hydrogen atoms	14,219	19,837	20,959	19,757	22,029
Protein residues	1692	2349	2463	2406	2649
Ligands	64	101	119	70	102
Average B-factors ($Å^2$)					
Protein	69.5	53.2	52.8	108.8	97.4
Ligands	73.6	86.6	86.0	119.7	113.8
R.m.s. deviations					
Bond lengths (Å)	0.004	0.003	0.005	0.004	0.006
Bond angles (°)	0.537	0.562	1.087	0.626	1.036
Validation					
MolProbity score	1.5	1.9	1.8	1.7	2.1
Clashscore (all atom)	9.7	10.0	9.4	10.1	15.1
Poor rotamers (%)	0	0.24	0.52	0	0.57
Ramachandran plot					
Favored (%)	98.1	95.0	95.8	96.7	93.5
Allowed (%)	1.9	5.0	4.1	3.3	6.1
Disallowed (%)	0	0	0.1	0	0.1

Supplementary Table 1: Cryo-EM data collection and refinement statistics.

X-ray data collection for 04_A06 Fab crystals (PDB 8UKI)

Space group	P 1 2_1 1
Cell dimensions	
a, b, c (Å)	42.7, 133.3, 43.4
α, β, γ (°)	90, 111, 90
Resolution (Å)	39.8–1.65 (1.68–1.65)[a]
R_{merge}	0.12 (0.71)
R_{pim}	0.08 (0.45)
$I/\sigma(I)$	7.7 (1.8)
$CC_{1/2}$	0.99 (0.82)
Completeness (%)	97 (96)
Redundancy	6.6 (6.1)
Refinement	
Resolution (Å)	39.8–1.75
No. reflections	43,821
R_{work} / R_{free}	0.170 / 0.205
No. atoms	
Protein	3,239
Ligand/ion	456
B factors (Å^2)	
Protein	17.2
Ligand/ion	27
R.m.s. deviations	
Bond lengths (Å)	0.006
Bond angles (°)	0.9

[a] Values in parentheses are for the highest-resolution shell.

Supplementary Table 2: X-ray data collection and refinement statistics.

References

1. Caskey, M. Broadly neutralizing antibodies for the treatment and prevention of HIV infection. *Curr Opin HIV AIDS* **15**, 49-55 (2020).

2. Sok, D. & Burton, D.R. Recent progress in broadly neutralizing antibodies to HIV. *Nat Immunol* **19**, 1179-1188 (2018).

3. Lynch, R.M. *et al.* HIV-1 fitness cost associated with escape from the VRC01 class of CD4 binding site neutralizing antibodies. *J Virol* **89**, 4201-4213 (2015).

4. Haynes, B.F. *et al.* Strategies for HIV-1 vaccines that induce broadly neutralizing antibodies. *Nat Rev Immunol* **23**, 142-158 (2023).

5. Rudicell, R.S. *et al.* Enhanced potency of a broadly neutralizing HIV-1 antibody in vitro improves protection against lentiviral infection in vivo. *J Virol* **88**, 12669-12682 (2014).

6. Sajadi, M.M. *et al.* Identification of near-pan-neutralizing antibodies against HIV-1 by deconvolution of plasma humoral responses. *Cell* **173**, 1783-1795.e1714 (2018).

7. Huang, J. *et al.* Identification of a CD4-binding-site antibody to HIV that evolved near-pan neutralization breadth. *Immunity* **45**, 1108-1121 (2016).

8. Zhou, T. *et al.* Structural basis for broad and potent neutralization of HIV-1 by antibody VRC01. *Science* **329**, 811-817 (2010).

9. Wu, X. *et al.* Rational design of envelope identifies broadly neutralizing human monoclonal antibodies to HIV-1. *Science* **329**, 856-861 (2010).

10. Schommers, P. *et al.* Restriction of HIV-1 escape by a highly broad and potent neutralizing antibody. *Cell* **180**, 471-489.e422 (2020).

11. Scheid, J.F. *et al.* Sequence and structural convergence of broad and potent HIV antibodies that mimic CD4 binding. *Science* **333**, 1633-1637 (2011).

12. West, A.P., Diskin, R., Nussenzweig, M.C. & Bjorkman, P.J. Structural basis for germ-line gene usage of a potent class of antibodies targeting the CD4-binding site of HIV-1 gp120. *Proc Natl Acad Sci U S A* **109**, E2083-E2090 (2012).

13. Corey, L. *et al.* Two randomized trials of neutralizing antibodies to prevent HIV-1 acquisition. *New Engl J Med* **384**, 1003-1014 (2021).

14. Gieselmann, L. *et al.* Profiling of HIV-1 elite neutralizer cohort reveals a CD4bs bnAb for HIV-1 prevention and therapy. *Nat Immunol* 1-14 (2025).

15. deCamp, A. *et al.* Global panel of HIV-1 Env reference strains for standardized assessments of vaccine-elicited neutralizing antibodies. *J Virol* **88**, 2489-2507 (2014).

16. Schommers, P. *et al.* Dynamics and durability of HIV-1 neutralization are determined by viral replication. *Nat Med* **29**, 2763-2774 (2023).

17. Seaman, M.S. *et al.* Tiered categorization of a diverse panel of HIV-1 Env pseudoviruses for assessment of neutralizing antibodies. *J Virol* **84**, 1439-1452 (2010).

18. Doria-Rose, N.A. *et al.* HIV-1 neutralization coverage is improved by combining monoclonal antibodies that target independent epitopes. *J Virol* **86**, 3393-3397 (2012).

19. Hraber, P. *et al.* Panels of HIV-1 subtype C Env reference strains for standardized neutralization assessments. *J Virol* **91** (2017).

20. Dadonaite, B. *et al.* A pseudovirus system enables deep mutational scanning of the full SARS-CoV-2 spike. *Cell* **186**, 1263-1278 e1220 (2023).

21. Radford, C.E. *et al.* Mapping the neutralizing specificity of human anti-HIV serum by deep mutational scanning. *Cell Host Microbe* **31**, 1200-1215 e1209 (2023).

22. Sanders, R.W. *et al.* A next-generation cleaved, soluble HIV-1 Env trimer, BG505 SOSIP.664 gp140, expresses multiple epitopes for broadly neutralizing but not non-neutralizing antibodies. *PLoS Pathog* **9**, e1003618 (2013).

23. Sok, D. *et al.* Recombinant HIV envelope trimer selects for quaternary-dependent antibodies targeting the trimer apex. *Proc Natl Acad Sci U S A* **111**, 17624-17629 (2014).

24. Zhou, T. *et al.* Structural repertoire of HIV-1-neutralizing antibodies targeting the CD4 supersite in 14 donors. *Cell* **161**, 1280-1292 (2015).

25. Gristick, H.B. *et al.* Natively glycosylated HIV-1 Env structure reveals new mode for antibody recognition of the CD4-binding site. *Nat Struct Mol Biol* **23**, 906-915 (2016).

26. Kwong, P.D. *et al.* Structures of HIV-1 gp120 envelope glycoproteins from laboratory-adapted and primary isolates. *Structure* **8**, 1329-1339 (2000).

27. Lee, J.H. *et al.* A broadly neutralizing antibody targets the dynamic HIV envelope trimer apex via a long, rigidified, and anionic β-hairpin structure. *Immunity* **46**, 690-702 (2017).

28. West, A.P., Jr. *et al.* Computational analysis of anti-HIV-1 antibody neutralization panel data to identify potential functional epitope residues. *Proc Natl Acad Sci U S A* **110**, 10598-10603 (2013).

29. Wilson, I.A. & Stanfield, R.L. 50 Years of structural immunology. *J Biol Chem* **296**, 100745 (2021).

30. Zhou, T. *et al.* Multidonor analysis reveals structural elements, genetic determinants, and maturation pathway for HIV-1 neutralization by VRC01-class antibodies. *Immunity* **39**, 245-258 (2013).

31. Liu, Q. *et al.* Improvement of antibody functionality by structure-guided paratope engraftment. *Nat Commun* **10**, 721 (2019).

32. Behrens, A.J. *et al.* Composition and antigenic effects of individual glycan sites of a trimeric HIV-1 envelope glycoprotein. *Cell Rep* **14**, 2695-2706 (2016).

33. Goddard, T.D. *et al.* UCSF ChimeraX: Meeting modern challenges in visualization and analysis. *Protein Sci* **27**, 14-25 (2018).

34. Mason, R.D. *et al.* Structural development of the HIV-1 apex-directed PGT145-PGDM1400 antibody lineage. *Cell Rep* **44**, 115223 (2025).

35. Klein, F. *et al.* Somatic mutations of the immunoglobulin framework are generally required for broad and potent HIV-1 neutralization. *Cell* **153**, 126-138 (2013).

36. Gristick, H.B. *et al.* CD4 binding site immunogens elicit heterologous anti–HIV-1 neutralizing antibodies in transgenic and wild-type animals. *Sci Immunol* **8**, eade6364 (2023).

37. Mastronarde, D.N. Automated electron microscope tomography using robust prediction of specimen movements. *J Struct Biol* **152**, 36-51 (2005).

38. Punjani, A., Rubinstein, J.L., Fleet, D.J. & Brubaker, M.A. cryoSPARC: Algorithms for rapid unsupervised cryo-EM structure determination. *Nat Methods* **14**, 290-296 (2017).

39. Bepler, T., Kelley, K., Noble, A.J. & Berger, B. Topaz-Denoise: General deep denoising models for cryoEM and cryoET. *Nat Commun* **11**, 5208 (2020).

40. Pettersen, E.F. *et al.* UCSF ChimeraX: Structure visualization for researchers, educators, and developers. *Protein Sci* **30**, 70-82 (2021).

41. Emsley, P. & Crispin, M. Structural analysis of glycoproteins: Building N-linked glycans with Coot. *Acta Crystallogr D Struct Biol* **74**, 256-263 (2018).

42. Agirre, J. *et al.* Privateer: Software for the conformational validation of carbohydrate structures. *Nat Struct Mol Biol* **22**, 833-834 (2015).

43. Winn, M.D., Isupov, M.N. & Murshudov, G.N. Use of TLS parameters to model anisotropic displacements in macromolecular refinement. *Acta Crystallogr D Biol Crystallogr* **57**, 122-133 (2001).

44. Emsley, P., Lohkamp, B., Scott, W.G. & Cowtan, K. Features and development of Coot. *Acta Crystallogr D Biol Crystallogr* **66**, 486-501 (2010).

45. Krissinel, E. & Henrick, K. Inference of macromolecular assemblies from crystalline state. *J Mol Biol* **372**, 774-797 (2007).

Chapter 5

IDENTIFICATION OF A BROAD AND POTENT V3 GLYCAN SITE BNAB TARGETING AN N332 GLYCAN-INDEPENDENT EPITOPE

Gieselmann, L.*, **DeLaitsch, A.T.*,** Rohde, M.*, Radford, C., Worczinski, J., Momot, A., Ahmadov, E., Burger, J.A., Havenar-Daughton, C., Deshpande, S., Giovannoni, F., Corti, D., Kreer, C., Ercanoglu, M.S., Schommers, P., Georgiev, I.S., West, A.P., Knüfer, J., Stumpf, R., Kroidl, A., Geldmacher, C., Maganga, L., Williams, W., Ntinginya, N.E., Hoelscher, M., Yang, Z., Wei, Q., Renfrow, M., Green, T.J., Novak, J., van Gils, M.J., Gristick, H.B., Gruell, H., Bloom, J.D., Seaman, M.S., Bjorkman, P.J., Klein, F. Identification of a broad and potent V3 glycan site bNAb targeting an N332 glycan-independent epitope. *Nat Immunol* (2025; accepted in principle). (bioRxiv doi: 10.1101/2025.09.05.674437)

**** Equal Contributions***

The following describes structural, biophysical, and functional characterizations of a new V3 glycan site broadly neutralizing antibody identified from an elite neutralizer. This work is part of a large collaboration involving Florian Klein's lab and many other labs, and the complete manuscript is published with the doi: 10.1101/2025.09.05.674437. Included in this thesis is the abstract and introduction from the manuscript, followed by a brief summary of experiments to add necessary context to the portions of the project that I led at Caltech. The results sections included in this thesis present work that I led, as well as neutralization data with viruses produced in the presence of kifunensine, conducted by collaborators at the Amsterdam University Medical Center, and site-specific mass-spectrometry, conducted by collaborators at the University of Alabama at Birmingham. Relevant methods sections and discussion related to the work I led are presented after the results.

Abstract: Broadly neutralizing antibodies (bnAbs) against HIV-1 can suppress viremia in vivo and inform vaccine development. Here, we characterized 007, a V3 glycan site bnAb exhibiting high levels of antiviral activity against multiclade pseudovirus panels[1, 2, 3] (GeoMean IC_{50} = 0.012 μg/mL, breadth = 69%, 217 virus strains) by targeting an $N332_{gp120}$ glycan-independent V3 epitope, a site of Env vulnerability to which only weakly neutralizing antibodies had previously been identified. Functional analyses demonstrated distinct binding and neutralization profiles compared to classical V3 glycan site bnAbs. A 007 Fab-Env cryo-EM structure revealed contacts with the V3 ^{324}GD/NIR^{327} motif and interactions with $N156_{gp120}$ and $N301_{gp120}$ glycans. In contrast to classical V3 bnAbs, 007 binding to Env does not depend on the $N332_{gp120}$ glycan, rendering it resistant to common escape mutations. Structures of 007 IgG-Env trimer complexes showed two Env trimers crosslinked by three bivalent IgGs, and bivalent 007 IgG was up to ~300-fold more potent than monovalent 007 IgG heterodimer, suggesting a role for avidity in potent neutralization. Finally, in HIV-1_{ADA}-infected humanized mice, 007 caused transient decline of viremia and overcame classical V3 escape mutations, highlighting 007's potential for HIV-1 prevention, therapy, functional cure, and vaccine design.

Introduction

Broadly neutralizing antibodies (bnAbs) targeting the HIV-1 envelope protein (Env) inform vaccine design, hold potential for therapy and prevention, and advance efforts toward achieving a functional cure[4, 5, 6, 7, 8, 9]. However, clinical trials have underscored the stringent requirements for enhanced antiviral activity that will be critical to counteract virus Env diversity and emergence of escape. Combined application of bnAbs with complementary neutralization coverage offers an opportunity to overcome these challenges[10, 11, 12, 13, 14]. Thus, the discovery of new bnAbs demonstrating distinct binding modes, neutralizing profiles, and viral escape pathways remains essential to facilitate successful clinical application of bnAbs.

On the HIV-1 Env trimer, bnAbs recognize highly conserved epitopes essential for viral entry[15, 16, 17, 18, 19, 20]. One such epitope is the V3 glycan site located at the base of the V3 loop. This epitope includes the $N332_{gp120}$ glycan, the ^{324}GD/NIR^{327} motif, and N-linked glycans in the vicinity ($N133_{gp120}$, $N137_{gp120}$, $N156_{gp120}$, and $N301_{gp120}$)[21, 22, 23]. However, some V3 glycan site bnAbs are also known to exhibit promiscuity in their glycan recognition and/or accommodation, allowing tolerance to shifts in N-glycan composition and configuration. For example, while bnAbs such as 10-1074, BG18, PGT124, and DH270 are highly dependent on the presence of the $N332_{gp120}$ glycan, others like PGT121, PGT128 and PGT130 can compensate for the loss of the $N332_{gp120}$ glycan by targeting alternative glycans within the high-mannose patch[24, 25, 26, 27, 28, 29]. Recently, a neutralizing antibody (nAb), EPTC112, that lacks contacts with the $N332_{gp120}$ glycan and instead targets a previously undescribed $N332_{gp120}$ glycan-independent V3 epitope extending to glycans of the V1 loop was reported[30]. However, EPTC112 displayed low levels of breadth (25%, cut-off <10μg/mL, 129 virus strains)[31] and potency (GeoMean IC_{50} against all strains = 3.7 μg/mL)[31], limiting its applicability for vaccine design, prevention and immunotherapy.

Anti-HIV-1 bnAbs neutralize the virus through multiple mechanisms including blocking of receptor binding, hindering membrane fusion, and accelerating decay of Env trimers[15]. As with antibodies to other antigens[32], IgG bivalency could enhance the breadth and potency of HIV-1 bnAbs by permitting the binding of adjacent Envs on the surface of the virus (inter-spike crosslinking) or by simultaneously engaging with multiple protomers of the same Env (intra-spike crosslinking)[33, 34]. However, HIV-1 bnAb IgGs are usually not known to utilize bivalent binding, a likely consequence of the relatively few Envs coating the surface of the virus and the positioning of conserved bNAb epitopes preventing inter- and intra-Env crosslinking, respectively[33]. Thus, the discovery of naturally occurring bnAbs that utilize avidity presents an opportunity for optimizing prevention and immunotherapy, as well as for informing vaccine design.

Here, we report on the identification and detailed characterization of the new anti-HIV-1 bnAb 007 targeting an $N332_{gp120}$ glycan-independent V3 epitope on Env. Cryo-EM analyses revealed a distinct binding mode compared to canonical V3 glycan site bnAbs that depends on the $N301_{gp120}$ and $N156_{gp120}$ glycans. Bivalent 007 IgG was more potent than its monovalent forms, and a structure of 007 IgG in complex with SOSIP trimers revealed a stable dimer of Env trimers linked by IgGs. Moreover, 007 displayed high levels of antiviral activity and exhibited a different neutralization profile compared to V3 reference bnAbs against extended multiclade panels. In HIV-1_{ADA}-infected humanized mice, 007 achieved transient decline of viremia and overcame V3 escape mutations. In conclusion, our findings suggest the $N332_{gp120}$-independent V3 epitope as a viable target for vaccine design and expand the armamentarium of bnAbs available for clinical use.

The following summary section is intended to provide context to the work presented in this thesis and does not encompass all aspects of the research. For the complete manuscript, figures, methods, and associated data, please see doi: 10.1101/2025.09.05.674437.

Summary

From the same international cohort of 2,354 people living with HIV-1 described in Chapter 4, donor EN01, an individual from southern Tanzania, was identified as the top elite neutralizer. Purified serum IgG from donor EN01 neutralized 100% of a 12-strain global HIV-1 pseudovirus panel with high potency (mean neutralization of 99% at 300 μg/ml)[3, 35]. Single B-cells were sorted from peripheral blood mononuclear cells (PBMCs) using GFP-labeled $BG505_{SOSIP.664}$ and sequenced, with 189 heavy chain and 100 light chain sequences successfully amplified from donor EN01. Of these, a representative 48 monoclonal antibodies were produced and evaluated for neutralizing activity against the 12-strain global panel. Members of clone 17 neutralized all strains on this panel, with the monoclonal antibody 007 being the most potent member of the clone (GeoMean IC_{50}/IC_{80} = 0.008/0.069 μg/mL). 007 and other members of clone 17 are encoded by V_H4-34*01/02 and V_K1-12*01 gene segments and have 22-residue CDRH3 lengths. 007 was not reactive to Hep-2 cells, a test for autoreactivity[36], yet displayed a less favorable pharmacokinetic profile than bnAbs 10-1074 or 3BNC117. Notably, the neutralization activity of 007 contributes to, but does not fully account for the donor's serum IgG neutralizing activity, as suggested by a moderate correlation between the neutralization profiles of 007 and purified serum IgGs from donor EN01 across a panel of 40 pseudoviruses (Pearson r = 0.54).

Initial attempts to delineate the epitope of 007 were ambiguous, as both competition binding assays as well as neutralization profiles (tested against an f61 fingerprint panel[37], a 119 strain panel[1], and a panel of mutants known to abrogate activity of various bnAbs) were inconsistent with reference

bnAbs of known epitope specificities. Cryo-EM analyses, described in detail below, revealed that 007 targets a V3 epitope that includes the N156 and N301 glycans on gp120, but does not include the N332 glycan, a glycan important for the binding and neutralization of many other V3 bnAbs[21, 22, 23]. The epitope and glycan-dependencies resembled that of the recently described antibody EPTC112[30], but 007 displayed much greater breadth and potency than EPTC112.

When tested against a 119-strain strain pseudovirus panel[1], 007 demonstrated desirable breadth and potency that far exceeded that of EPTC112, the recently identified antibody of the same epitope class[30]. 007 maintained high neutralization coverage against viruses lacking the $N332_{gp120}$ glycan (breadth = 71%) but was unable to neutralize any of the viruses on the panel that lacked a PNGS at either position 156 or 301 on gp120, consistent with glycan dependencies observed by EM analysis. Interestingly, when a subset of 46 10-1074-resistent strains were evaluated, 007 exhibited 65% breadth, whereas other V3 bnAbs tested exhibited between 0-26% breadth. Conversely, other V3 glycan site bNAbs exhibited up to 62% breadth against a subset of 40 007-resistent pseudoviruses, suggesting functional complementarity between 007 and other V3 glycan site bnAbs. Additionally, *in* silico modeling of 007 and 10-1074 combination predicted complementary neutralizing activity with a combined breadth of 86.2% and GeoMean IC_{50} of 0.011 μg/mL. Furthermore, 007 demonstrated high neutralization activity against a 100-strain clade C panel[2] (GeoMean IC_{50}/IC_{80} = 0.01/0.03 μg/mL; breadth = 68%/49%).

Deep mutational scanning (DMS) experiments performed using HIV-1 Envs from TRO.11 (Clade B) and BF520.W14M.C2 (Clade A) demonstrated distinct escape pathways for 007 compared to other V3 bnAbs. Different escape pathways were also observed *in vivo*, as demonstrated by single genome sequencing of plasma virus in HIV-1_{ADA}-infected humanized mice that were treated with either 10-1074 or 007 IgG. After viral rebound, viruses from 10-1074-treated mice contained mutations

abrogating the PNGS at $N332_{gp120}$, whereas viruses from 007-treaded mice contained mutations at 303_{gp120} (abrogating the $N301_{gp120}$ PNGS) and at 322_{gp120}. Notably, all generated escape variants from 10-1074 monotherapy retained *in vitro* sensitivity to 007, and vice versa. Finally, treatment with a combination of both 007 and 10-1074 resulted in prolonged suppression of viremia, with viral rebound occurring 42 days after treatment initiation.

Results

007 targets an $N332_{gp120}$ glycan-independent V3 epitope on Env

To elucidate the binding mode of 007, we performed single-particle cryo-EM analysis of the antibody Fab in complex with a soluble BG505 Env trimer, which included SOSIP stabilizing mutations[38] and an engineered disulfide ($I201C_{gp120}$-$A433C_{gp120}$) designed to prevent trimer opening (BG505-DS)[39, 40]. Fab was added in a greater than 3-fold molar excess to SOSIP trimer, and Fab-Env complexes were then isolated by size-exclusion chromatography (SEC). Structural analysis revealed four trimer classes with either 0, 1, 2, or 3 bound Fabs, with the most populated class being a 3.0 Å single Fab-bound trimer (Fig. 1a, Extended Data Fig. 1, Supplementary Table 1). Comparison of the 007 binding pose to poses of V3 glycan site bnAbs showed a distinct mode of binding, most closely resembling the V3 glycan site bnAb PGT128 (Fig. 1b).

The structure revealed 007 is framed by N-linked glycans attached to $N156_{gp120}$ and $N301_{gp120}$, but does not contact the glycan at $N332_{gp120}$, which is important for binding of many V3 glycan bNAbs[26, 41, 42] (Fig. 1c,d). Antibody contacts with protein portions of Env are mediated exclusively by a 22-residue CDRH3 which extends outward to contact the conserved ^{324}GD/NIR^{327} motif on Env (Fig. 1c,e). Within this region, $F100E_{HC}$ contacts $G324_{gp120}$, and $E100D_{HC}$ at the tip of the CDRH3 is in close proximity to $R327_{gp120}$ (Fig. 1e). Other V3 bnAbs possess negatively-charged glutamate residues within their CDRH3s that may form electrostatic contacts with the positively-charged

$R327_{gp120}$ ($E100I_{HC}$ in 10-1074[41], PGT122[42], and PGT124[43] and $E100G_{HC}$ in BG18[26]). In addition, $K99_{HC}$ of 007 forms an electrostatic interaction with $D322_{gp120}$ ($D321(1)_{gp120}$ in some numbering nomenclatures) within V3 (Fig. 1e), a residue that is a negatively-charged Asp or Glu in >70% of sequences (www.hiv.lanl.gov and ref. [44]). The CDRH3 is also positioned near the gp120 V1 loop, which is located adjacent to V3, thereby allowing 007 $L100A_{HC}$ and $L100F_{HC}$ to contact $R151_{gp120}$ within V1 (Extended Data Fig. 3a). Interestingly, in gp120 protomers bound by 007, but not in unbound gp120s, a portion of the V1 loop is disordered (Extended Data Fig. 3b) suggesting that 007 binding destabilizes the V1 loop.

The V1/V3 epitope of 007 resembles that of the recently described bnAb EPTC112[30] (Extended Data Fig. 2a, b). Both antibodies depend on the $N156_{gp120}$ and $N301_{gp120}$ glycans, but not the $N332_{gp120}$ glycan, and both contact the ^{324}GD/NIR^{327} motif on Env. However, 007 exhibits greater breadth and is more potent (GeoMean IC_{50}/IC_{80} = 0.01/0.03 vs. 0.32/0.29 μg/mL, breadth = 66/53% vs 27/14%, 110 or 105 virus strains) than EPTC112. Structurally, EPTC112 contacts extend only to $D325_{gp120}$ of the ^{324}GD/NIR^{327} motif, whereas 007 interacts with the entirety of the motif (Fig. 1e,f). More extensive contact with the ^{324}GD/NIR^{327} motif and better accommodation of the $N156_{gp120}$ and $N301_{gp120}$ glycans could contribute to the enhanced neutralization properties of 007 compared with EPTC112.

N-glycans comprise much of the 007 epitope (Fig. 1c,d). The FWRH1/CDRH1 of 007 contains a glycine-rich stretch of amino acids (GVHGVGLGGSGWG; $G23_{HC}$ – $G35_{HC}$), which wrap around the core pentasaccharide of the $N156_{gp120}$ glycan (Extended Data Fig. 3c). Five of these glycine residues arose from somatic hypermutation (Fig. 1c), but only one is an improbable mutation, as defined by the ARMADiLLO web server[45]. A similar mechanism of glycan accommodation is utilized by the VRC01-class CD4-binding site bnAbs, which either acquire deletions or glycine substitutions in

CDRL1 to accommodate the $N276_{gp120}$ glycan[46]. In addition, the 007 CDRH2 packs against the $N301_{gp120}$ glycan (Extended Data Fig. 3c). Although extensive EM density was observed for both glycans, density corresponding to a core fucose, a component of complex-type glycans, was not observed, and more density was seen for the $N156_{gp120}$ glycan (8 monosaccharide subunits modelled) than the $N301_{gp120}$ glycan (6 monosaccharide subunits modelled) (Fig. 1g). In contrast, for unbound protomers, relatively little EM density was observed at these positions (0-2 monosaccharide subunits modelled), as is typically the case for glycans not stabilized by interactions with an antibody. A caveat of these observations is that single-particle cryo-EM analysis of glycans is limited due to their compositional and conformational heterogeneity[47].

To evaluate the role of N-glycan processing in 007 neutralization, we expanded our neutralization analysis to include pseudoviruses produced in the presence of kifunensine, an inhibitor that prevents processing of high-mannose N-glycans to complex-type carbohydrates[48]. In contrast to other V3-targeting bnAbs, but in common with EPTC112[30], 007 did not neutralize kifunensine-treated viruses (Supplementary Table 2), implying that the Man-9 (i.e., Man9(GlcNAc)2) high-mannose glycan trimming by mannosidase I is required for potent neutralization. We also performed site-specific N-glycan analysis using quantitative mass spectrometry profiling to determine the specific glycoforms enriched in 007-bound BG505 SOSIPs compared to total BG505 SOSIPs. The potential N-linked glycosylation site (PNGS) at $N301_{gp120}$ in 007-bound BG505 showed an increase in Man-5 high-mannose glycans compared to the same site in the total BG505 sample (Fig. 2h), consistent with EM density and neutralization data (Fig. 2g and Supplementary Table 2). Unambiguous glycoform identification at position $N156_{gp120}$ was not possible, however, as both $N156_{gp120}$ and $N160_{gp120}$ PNGSs resided on the same glycopeptide (Extended Data Fig. 4).

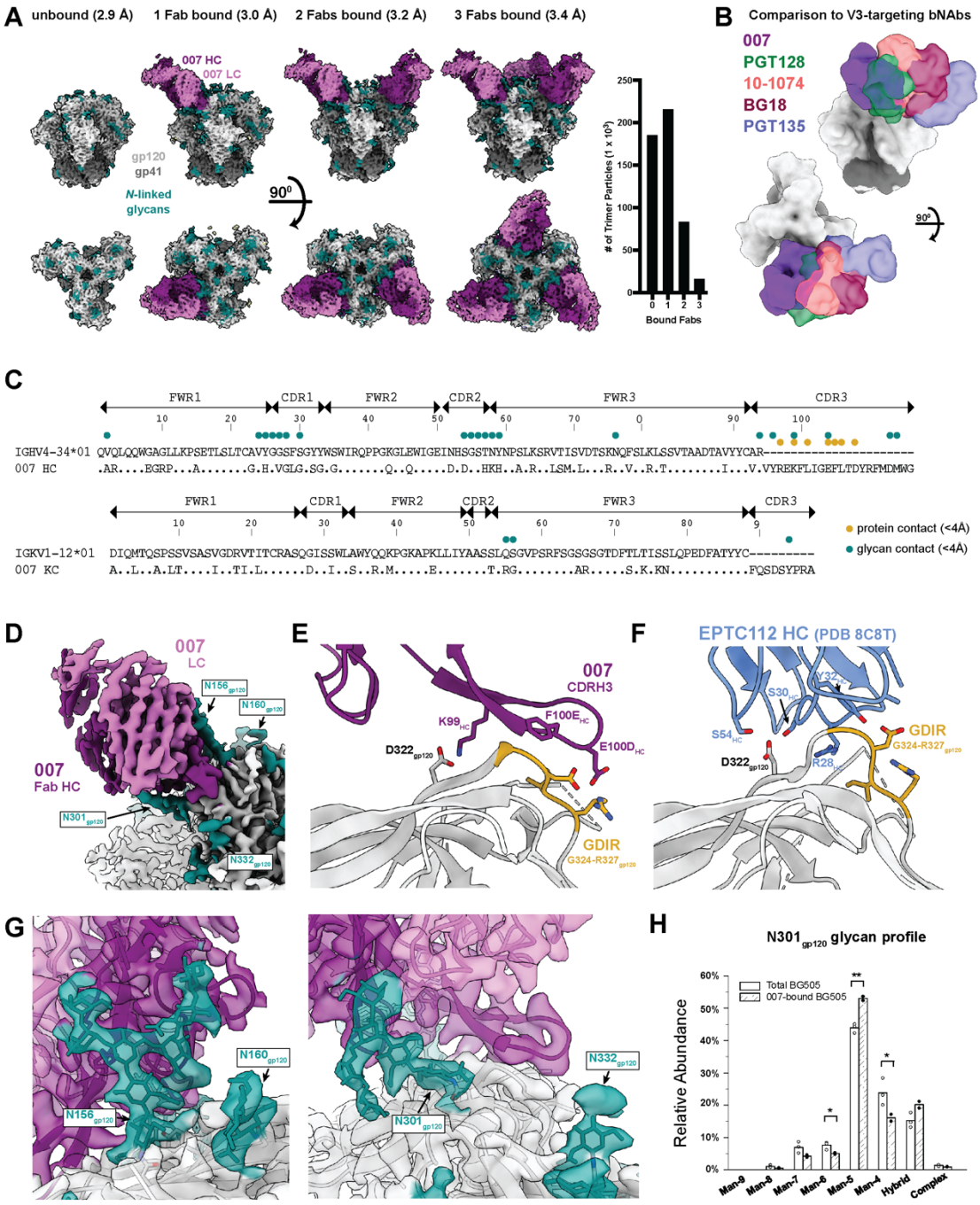

Figure 1: 007 recognizes an N332$_{gp120}$ glycan-independent V3 epitope.

a, (left) Overviews of the four structural classes identified of SOSIP trimers with 0-, 1-, 2-, or 3-bound 007 Fabs per trimer. (right) The number of particles used in each of the final reconstructions. **b,** Overlay of 007 with V3-targeting bNAbs (PDB codes 5C7K, 5T3Z, 6CH7, 4JM2). **c,** Alignment of 007 VH and VL to their predicted germline V gene segments. 007 residues within 4Å of protein or

glycan components on Env are indicated by colored circles. **d,** Structure overview, highlighting proximal glycans. **e,** Protein contacts between 007 and Env. **f,** Protein contacts between EPTC112 and Env (PDB code 8C8T). **g,** EM density highlighting the $N156_{gp120}$ (left) and $N301_{gp120}$ (right) glycans. **h,** Comparison of glycoform abundance between total BG505 SOSIP and 007-bound SOSIP at $N301_{gp120}$ determined by LC-MS/MS, with asterisks denoting level of significance (* denotes $0.01 < P \leq 0.05$, ** denotes $P \leq 0.01$).

007 bivalency is required for potent neutralization

The observation of sub-stoichiometric trimer binding by a bnAb Fab could result from a weak monovalent binding interaction, which is unexpected for a potent bnAb such as 007. Using a surface plasmon resonance (SPR)-based assay, we confirmed that the binding affinities of 007 Fab were weak for the BG505 (7.5 μM) and BG505-DS (5.7 μM) SOSIPs, in contrast to the V3 bnAb Fabs 10-1074 and PGT135, which exhibited affinities in the low nanomolar range (Extended Data Fig. 5a). The neutralization experiments differ from the structural characterizations and SPR binding experiments, however, in that bivalent IgGs were used for neutralization assays, whereas monovalent Fabs were used for the EM and SPR analyses. Bivalent IgG binding could compensate for a weak Fab-antigen binding affinity; however, HIV-1 bnAb IgGs generally do not utilize avidity due to the relatively few Env trimers coating the virus and the positioning of conserved bnAb epitopes on Env, thus limiting inter- and intra-spike crosslinking, respectively[33]. To evaluate potential contributions of avidity in neutralization, molar neutralization ratios (MNRs) [IC_{50} Fab (nM)/IC_{50} IgG (nM)] can be calculated. We note that viruses with densely-packed spikes can exhibit MNRs over 1000, whereas MNRs for anti-HIV-1 bnAbs tend to be low[33]. Notable exceptions include V3 bnAbs PGT128[49] and EPTC112[30], which target similar Env epitopes as 007 (Fig. 2b and Extended Data Fig. 2a) and were reported to be ~30 to 2000-fold more potent when formatted as an IgG than as a Fab against viruses tested. Although the mechanism underlying the enhanced IgG potencies was not reported, it was speculated to result from inter-spike crosslinking between adjacent Env trimers on the virion surface.

To investigate the possibility that 007 IgG utilizes avidity during neutralization of pseudovirions, we repeated in vitro neutralization assays to compare the neutralization potency of the monovalent 007 Fab to bivalent IgG1 and bivalent IgG3 forms of 007. To control for steric effects that may impact IgG neutralization due to the increased mass of an IgG compared to a Fab (~150kDa for an IgG1 versus ~50kDa for a Fab), we also created a bispecific 007 IgG1[50] in which one Fab arm was replaced with the anti-CD3 antibody OKT3[51], which does not recognize HIV-1 Env. We found bivalent IgG1 and bivalent IgG3 forms of 007 had similar potencies, with a mean IgG1/IgG3 MNR of 0.82 across viruses tested (Fig. 2a,b, Supplementary Table 3). Additionally, the monovalent 007 Fab and monovalent 007/OKT3 bispecific IgG1 had similar potencies, with a mean Fab/bispecific IgG1 MNR of 1.6 across viruses tested. However, against all viruses tested, the bivalent forms of 007 were more potent than monovalent forms, consistent with avidity effects that enhanced neutralization: bispecific IgG1/bivalent IgG1 MNRs ranged from 4.0 to 250 across the 26 viruses for which MNRs were derived (Fig. 2a,b, Supplementary Table 3). Such variation is expected since enhancements due to avidity depend on multiple factors including the dissociation rate of a Fab for an Env antigen[33], which is expected to vary for different viral strains. Notably, viruses that were less potently neutralized by monovalent forms of 007 benefitted more from antibody bivalency than viruses that were more potently neutralized by monovalent forms of 007 (Extended Data Fig. 5b,c).

A possible mechanism for IgG avidity effects is through intra-spike crosslinking (i.e., both Fab arms on a bivalent IgG engage with epitopes on a trimeric Env), which has been previously inferred from Fab-trimer structures for other viral pathogens: e.g., as described for anti-SARS-CoV-2 antibodies[52, 53, 54], a measured distance < ~65Å between the C-termini of adjacent Fab heavy chains raises the possibility for intra-spike crosslinking by an IgG, as this would permit the C-termini of two Fab heavy chains to come together to form the N-terminus of the IgG Fc region. In our structure of BG505-DS SOSIP with two copies of 007 Fab, the measured distance between the C-termini of adjacent Fab

heavy chains, ~120 Å, was ~2-fold greater than this distance cutoff (Fig. 2c), suggesting that intra-spike crosslinking by 007 IgG interacting with the closed BG505 Env trimer in our structure would not be possible. However, one must also consider different structural states of the antigen that may be targeted. For example, double electron-electron resonance (DEER) spectroscopy demonstrated that unliganded SOSIP Env trimers can sample open states that can be recognized by neutralizing antibodies, such as the occluded-open Env trimer state in which the gp120 protomers are outwardly rotated but the V1/V2 loop is not displaced to the sides of the Env trimer[55]. Docking the 007 Fab-gp120 coordinates onto the gp120s of an occluded-open Env placed the C-termini of adjacent Fabs within 65 Å (Fig. 2c). Therefore, one possibility to account for the apparent involvement of avidity effects in 007 interactions with Env trimers is that the 007 IgG binds bivalently to an occluded-open or other altered Env conformation that was not observed in our 007 Fab-SOSIP complex structures.

In the context of SARS-CoV-2 spike trimers, structural studies of IgGs interacting with stabilized trimers revealed intra-spike crosslinking[56, 57]. Thus, in an attempt to investigate bivalent IgG interactions with Env trimer structurally, we incubated BG505 SOSIP with 007 IgG1 and imaged by cryo-EM (Extended Data Fig. 6, Supplementary Table 1). Rather than observing intra-spike crosslinking, the most populated structural class of 007 IgG-BG505 complexes contained "trimer-dimers" in which two SOSIP Envs were crosslinked by Fabs from three IgG molecules (Fig. 2d). This assembly exhibited D3 symmetry, with the apexes of two Env trimers facing each other and separated by ~70Å. Density for the Fc region of the IgG was not resolved, an expected consequence of flexibility at the IgG hinge region[58]. However, the distance between the C-termini of the closest Fabs on the opposing Env trimers was 13 Å (Fig. 2d), consistent with these densities originating from a single IgG. In addition to the trimer-dimer structural class, trimer classes with 0, 1, or 2 copies of bound 007 IgG were also observed (Fig. 2d). In these structures, the unbound Fab and Fc of each IgG

were unresolved, leading to EM densities closely matching the densities of the Fab-SOSIP complexes (Fig. 2d, 1a).

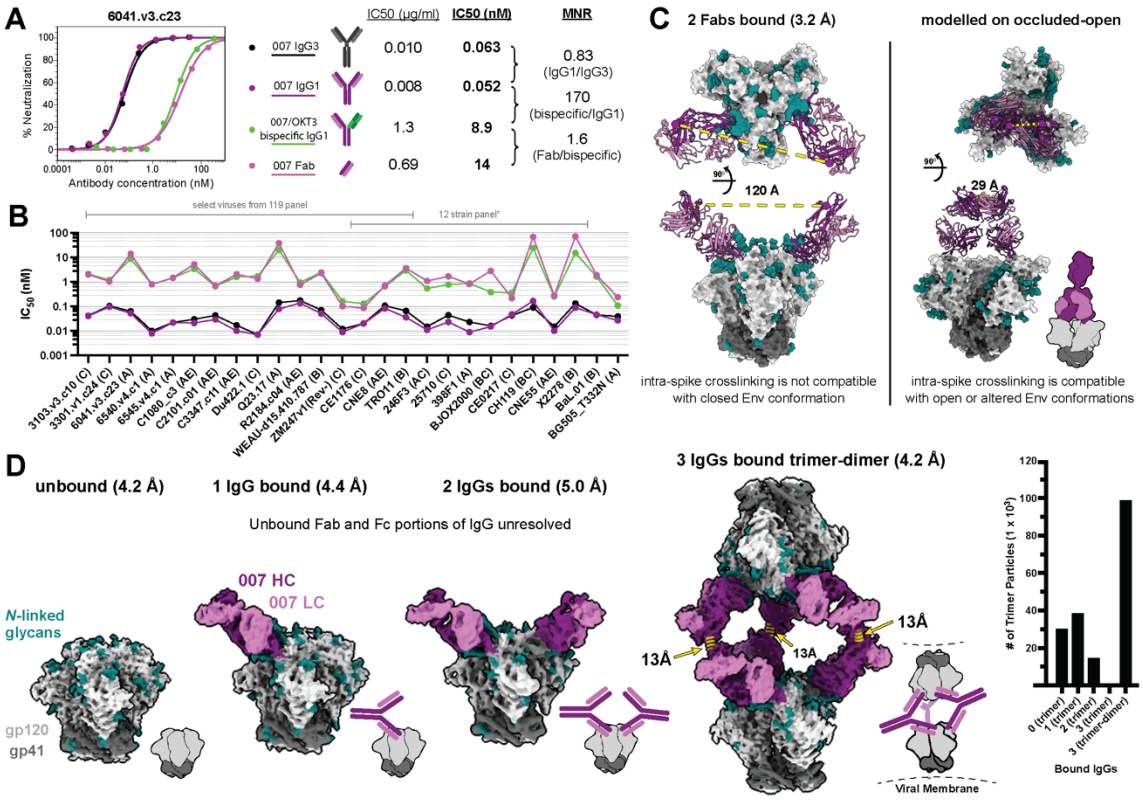

Figure 2: Potent neutralizing activity requires 007 bivalency.
a, Neutralization curves against strain 6041.v3.c23 (left) used to calculated molar neutralization ratios (MNRs) comparing the IC_{50} values for the IgG1, IgG3, bispecific IgG1, and Fab forms of 007 (right). **b,** Molar IC_{50} values for IgG1, IgG3, bispecific IgG1, and Fab forms of 007 against a panel of HIV-1 strains. Clades are indicated in parentheses. *X1632 is not shown with the remainder of the 12-strain panel due to incomplete pseudovirus neutralization. IC_{50} values and calculated MNRs are in Supplementary Table 3. **c,** Distance measurements between the C-termini of the Fab heavy chains on the experimentally determined 2 Fab-bound trimer structure (left) compared to a structure in which 007 Fab was modelled onto an occluded-open trimer conformation (PDB code 5VN8). A schematic showing a 007 IgG-bound occluded-open trimer is shown for clarity. **d,** (left) Four structural classes identified after complexing 007 IgG with BG505 SOSIP. Schematics are included for clarity. Dashed line (yellow) indicates the distance measurements between C-termini of Fab regions in 007 IgG-bound trimer-dimer structure. (right) The number of particles used in each of the final reconstructions.

The number of particles in the trimer-dimer class were multiplied by two, as each particle contained two SOSIP trimers.

The observed trimer-dimer structure would be compatible with Envs attached to separate virions (Fig. 2d), thus raising the possibility that the 007 IgG neutralizes at least in part by aggregating virions. However, the extent to which enhanced pseudovirus neutralization by 007 IgG can be attributed to viral aggregation, intra-spike crosslinking, or another mechanism such as inter-spike crosslinking[30, 49], heteroligation[59], or by enhancing gp120 shedding[57] warrants further investigation.

Discussion

Structural analysis of the 007 Fab in complex with a SOSIP Env trimer revealed sub-stoichiometric Fab binding, a surprising finding for a potent bnAb. Interestingly, EPTC112, which recognizes a similar epitope, also lacked full Fab occupancy in its structure, with only two Fabs per trimer modeled[30]. Similar to results with EPTC112[30], in vitro neutralization assays for 007 demonstrated IgG bivalency enhanced neutralization potencies. Based on our 007 Fab-SOSIP structures, we hypothesized that intra-spike bivalent IgG binding could occur on open forms of an Env trimer. However, when SOSIP-IgG complexes were analyzed by cryo-EM, a trimer-dimer of closed Env-IgG complexes was observed, a configuration that could occur if IgGs link Envs trimers on two separate virions. Analogous structures linking two SARS-CoV-2 spike trimers by IgGs were postulated to enhance neutralization by aggregating virions[32], and cryo-electron tomography of nAbs incubated with SARS-CoV-2 demonstrated inter-virion bivalent binding of IgGs[60]. It should be noted that the SOSIP Env trimers we used for structure determinations contained specific mutations ($I559P_{gp41}$, $A501C_{gp120}$, $T605C_{gp41}$) that decrease the sampling of alternative Env conformations[61], whereas neutralization assays use membrane-bound Env trimers lacking these mutations. Further studies of 007 IgG in complex with HIV-1 virions or virus-like particles displaying native Env trimers

could elucidate its mechanism of bivalent neutralization. In summary, the favorable neutralization properties and distinct viral escape profile position 007 as a promising investigational candidate for HIV-1 therapy, functional cure, and prevention. Our findings further emphasize the $N332_{gp120}$ glycan-independent V3 epitope as a compelling target for vaccine development.

Methods

Cloning and production of monoclonal antibodies

The heavy and light chain V gene regions of mAbs were synthesized as eBlocks gene fragments (IDT), incorporating complementary overhangs pre-configured for cloning into expression vectors (IgG1, IgG3, Igλ, Igκ). Cloning was performed using Sequence- and Ligation-Independent Cloning (SLIC) with T4 DNA polymerase (New England Biolabs) and chemically competent Escherichia coli DH5α, following established protocols[62, 63, 64, 65, 66]. Positive transformants were identified through Sanger sequencing, after which confirmed bacterial colonies were expanded in LB medium. Plasmid DNA was subsequently extracted using the NucleoBond Xtra Midi kit (Macherey-Nagel).

007 and 10-1074 IgGs used for structural studies, mass spectrometry, and molar neutralization ratio assays were expressed via transient co-transfection of Expi293F cells with heavy and light chain plasmids. IgG1 antibodies were purified from cell culture supernatant using MabSelect™ SuRe (Cytiva), concentrated, and SEC purified on a Superdex 200 column (Cytiva). 007 IgG3 was purified by diluting the Expi293F cell culture supernatant 5-fold in PBS (pH 7.0) and loading over a HiTrap Protein G HP column (Cytiva). The column was washed in PBS (pH 7.0) and IgG3 was eluted in 0.1M glycine, 150mM NaCl (pH 2.7) into 2M Tris (pH 8.0). The IgG3 sample was then concentrated and SEC purified on a Superdex 200 column (Cytiva). SEC fractions corresponding to IgG were combined and concentrated.

To produce Fabs, the heavy chain variable region of 007 was subcloned into a mammalian expression vector containing the CH1 domain and a C-terminal 6xHis tag. 10-1074 plasmids were cloned as previously described[41]. Fab heavy and light chain plasmids were used to transiently co-transfect Expi293F cells (Thermo Fisher) and Fabs were purified from culture supernatant by immobilized metal affinity chromatography (IMAC) using a HisTrap HP column (Cytiva). Fabs were concentrated and buffer exchanged into TBS (20mM Tris pH 8.0, 150mM NaCl) using Amicon 10 kDa spin concentrators (Millipore) and further purified by size exclusion chromatography (SEC) on a Superdex 200 column (Cytiva) equilibrated with TBS. SEC fractions corresponding to Fab were combined and concentrated.

To produce bispecific IgGs comprising a 007 arm and an anti-CD3 OKT3 arm[51], mutations were introduced into the respective IgG1-LS[67] constant regions (E357Q and S364K in 007_{HC} and Q295E, L368D, K370S, N384D, Q418E, N421D in $OKT3_{HC}$) to promote heavy chain heterodimerization and facilitate downstream purification[50], and the CH1 and CL domains of the OKT3 antibody were domain swapped to promote correct heavy and light chain pairing of both Fab arms[68]. Heavy and light chain plasmids were mixed in equal amounts (50 μg of each of the four plasmids per 200mL transfection culture) and used to transiently co-transfect Expi293F cells (Thermo Fisher). IgGs were purified from cell culture supernatant using a MabSelect™ SuRe (Cytiva) affinity column and were concentrated and buffer exchanged into 50mM Tris, pH 8.7 using 10 kDa Amicon spin concentrators (Millipore). Bispecific IgGs were purified by anion exchange chromatography using a HiTrap Q column (Cytiva) and eluted with a NaCl gradient. Fractions corresponding to the bispecific IgG were combined and concentrated before SEC purification using a Superdex 200 column (Cytiva) equilibrated in TBS.

Expression and purification of BG505 SOSIP trimers

BG505[38] and BG505-DS[39, 40] SOSIPs used for cryo-EM, mass spectrometry, and SPR experiments were expressed via transient co-transfection of Expi293F cells with a plasmid encoding soluble furin. Briefly, SOSIPs were purified from cell culture supernatant by either PGT145 or 2G12 immunoaffinity chromatography, dialyzed in TBS, concentrated to <2 mL, and purified by SEC on a Superose 6 Increase column (Cytiva). SEC fractions corresponding to trimeric SOSIPs were combined and concentrated.

Generation of HIV-1 pseudoviruses

HIV-1 pseudoviruses were produced in HEK293T cells by co-transfection with pSG3Δenv and the respective HIV-1 Env plasmids as previously described[1, 2, 37, 69]. Kifunensine-treated pseudoviruses were produced under presence of 5 μg/ml Kifunensine. Supernatants containing Kifunensine-treated pseudoviruses were harvested 3 days after transfection and stored at -80°C.

Molar neutralization ratio (MNR) assays

Pseudovirus neutralization assays were conducted using TZM-bl reporter cells as above and as previously described[70, 71]. IgGs, bispecifics, and Fabs were evaluated in duplicate with an eight-point, five-fold dilution series starting at a top concentration of 2, 5, or 50 μg/mL. 007 antibodies were expressed and purified within 3 weeks of neutralization assays. The dilution at which 50% of virus was neutralized (IC_{50}) is reported in μg/mL and molar concentrations in Supplementary Table 3. MNRs were calculated as the ratio of molar IC_{50} values for different formats of the antibody.

Cryo-EM sample preparation

007 Fab was incubated in a 3.4:1 molar ratio of Fab to BG505-DS SOSIP trimer[39, 40] and incubated overnight at room temperature. SOSIP trimers and Fab-SOSIP complexes were purified from

unbound Fabs on a Superose 6 10/300 Increase column (Cytiva) operating in TBS and concentrated using a 30 kDa spin concentrator to ~3.4 mg/mL immediately prior to vitrification. 007 IgG1 was added to BG505 SOSIP at a 1:1 molar ratio of IgG to BG505 SOSIP trimer, with a total protein concentration of ~2.6 mg/mL and vitrified after incubating for ~38 hours at room temperature.

Octyl-maltoside, fluorinated solution (Anatrace) was added to 0.02% (w/v) final concentration for each sample immediately before addition of 3 µL to a Quantifoil R1.2/1.3 Cu 300 mesh grid (Electron Microscopy Sciences) that had been glow discharged for 1 min at 20 mA using a PELCO easiGlow™ (Ted Pella). Grids were blotted for 3-4s with Whatman No. 1 filter paper and vitrified in liquid ethane using a Mark IV Vitrobot (Thermo Fisher) operating at 22°C and 100% humidity.

Cryo-EM data collection and processing

Data for the 007 Fab-SOSIP sample were collected on a 300 keV Titan Krios transmission electron microscope (Thermo Fisher) equipped with a Gatan BioQuantum Energy Filter and a K3 6k x 4k direct electron detector, and data for the 007 IgG1-SOSIP sample were collected on a 200 keV Talos Arctica (Thermo Fisher) equipped with a Gatan K3 6k x 4k direct electron detector. 40-frame movies were collected in SerialEM[72]. 007 Fab-SOSIP movies were recorded in super-resolution (0.416 Å per pixel) using a 3x3 beam image shift pattern with 3 shots per hole and 007 IgG-SOSIP movies were recorded in super-resolution (0.72 Å per pixel) with a 3x3 beam image shift pattern and 1 shot per hole.

Data collection and processing details are included in Supplementary Table 1 and Extended Data Figs. 1 and 6. Motion correction, CTF estimation, particle picking, and particle extraction were performed in cryoSPARC Live v4[73]. Extracted particles were subject to 2D classification in cryoSPARC[73] and particles from select 2D classes processed by 3D classification in RELION

v4.0.1[74, 75]. Particles from select 3D classes were re-extracted in cryoSPARC and subject to ab initio reconstruction and non-uniform refinement[73, 76]. Particles underwent reference-based motion correction and were subject to a final round of non-uniform refinements[76].

Model building and refinement

Initial coordinates for the 1 Fab-bound trimer structure were generated by docking individual protein chains from reference structures [PDB 5BZD (V_H), 7PS3 (V_L), and 6UDJ (BG505)] into the corresponding EM density in ChimeraX[77, 78]. The initial model was sequence corrected in Coot[79] and underwent iterative rounds of refinement in Phenix[80] and Coot[79]. Glycans were built in Coot[81] and glycan geometries evaluated in Privateer[82]. Coordinates for the 1 Fab-bound trimer aided in generating trimer structures with 0, 2, or 3-bound Fabs, as well as the 3 IgG-bound trimer-dimer structure. To facilitate measurements between the C-termini of the Fab heavy chains, the Fab CHCL domains from PDB 8UKI were docked into the corresponding densities in the 2 Fab-bound trimer structure and the 3 IgG-bound trimer-dimer structure. Antibodies were numbered according to Kabat.

Structural analyses

Figures were prepared using UCSF ChimeraX v1.9[77, 78]. 007 Fab-Env interactions were evaluated using the 1 Fab-bound trimer structure. Distance measurements between C-termini of Fab HCs were taken from the alpha carbon of R222 in either the 2 Fab-bound trimer structure or the 3 IgG-bound trimer-dimer structure. Coordinates for a 007-bound gp120 were aligned to two gp120 chains in a b12-bound trimer structure (PDB 5VN8)[83] to model the analogous distance on an occluded open conformation of the trimer. The distance between trimer apexes reported for the trimer-dimer structure was measured between residues N188 on opposing trimers.

Surface plasmon resonance (SPR)

SPR measurements were performed on a Biacore T200 (GE Healthcare) at 25 °C in HBSEP+ (10mM Hepes, 150mM NaCl, 3mM EDTA, 0.005% Tween-20) (GE Healthcare) running buffer. BG505 and BG505-DS SOSIPs were directly immobilized on a CM5 chip (GE Healthcare) to ~500 resonance units (RUs) using primary amine chemistry. Fab samples were injected over the flow cells at increasing concentrations (3-fold dilution series with a top concentration of 10 μM or 1 μM) at a flow rate of 60 μL/min for 60 s and allowed to dissociate for 300 s. Regeneration of flow cells was achieved by injecting one pulse of 10 mM glycine pH 2.0 at a flow rate of 90 μL/min. All samples were performed in duplicate and a representative sensorgram is plotted in Extended Data Fig 5a. Kinetic constants and affinities were derived using the Biacore T200 Evaluation Software (v2.0) with a 1:1 binding model.

Data availability

Cryo-EM maps and models have been deposited in the Electron Microscopy Data Bank (EMDB) and Protein Data Bank with accession codes: EMD-70018 and PDB ID 9O2Q (007-BG505v2, 0 Fabs bound), EMD-70019 and PDB ID 9O2R (007-BG505v2, 1 Fab bound), EMD-70020 and PDB ID 9O2S (007-BG505v2, 2 Fabs bound), EMD-70021 and PDB ID 9O2T (007-BG505v2, 3 Fabs bound), EMD-70022 and PDB ID 9O2U (007-BG505v2, IgG crosslinked trimer-dimer).

Acknowledgements (original publication)

We thank all study participants for supporting our research by blood donation; members of the Klein, Bjorkman, and Bloom Labs for their support and inspiring discussions; we thank Svea Rose for helpful discussions; Anna Schmitt and Tina Bresser for lab management and assistance; We thank the staff of the Animal Care Facility Weyertal at the University of Cologne. We thank Songye Chen and the Beckman Institute Resourse Center for Transmission Electron Microscopy at Caltech as well

as Jost Vielmetter and the Caltech Protein Expression Center. We thank Priyanthi Gnanapragasam for help conducting MNR neutralization assays. A.T.D. was supported by an NSF Graduate Research Fellowship. The panel of global HIV-1 pseudoviruses was obtained through the NIH AIDS Reagent Program. This work was funded by grants from the German Center of Infection Research (DZIF) to F.K., the German Research Foundation (DFG) CRC1279 and CRC1310, European Research Council (ERC) ERC-stG639961, and COVIM: NaFoUniMed-Covid19 to F. K.. This work was also supported, in whole or in part, by the Bill & Melinda Gates Foundation (grant INV-002143) to F.K. and P.J.B. and (grant INV-036842) to M.S.S.. Under the grant conditions of the Foundation, a Creative Commons Attribution 4.0 Generic License has already been assigned to the Author Accepted Manuscript version that might arise from this submission. Research reported in this publication was also supported by the National Institute of Allergy and Infectious Diseases of the National Institutes of Health under award number P01AI100148 and 1U54AI170856 to P.J.B., and R01AI140891 and U01AI169385 to J.D.B., Z.Y., Q.W., M.B.R., T.J.G., and J.N. are supported in part by a grant from National Institutes of Health AI162236 and research-acceleration funds from the University of Alabama at Birmingham (JN). The content is solely the responsibility of the authors and does not necessarily represent the official views of the National Institutes of Health. P.F.S. is supported by the Emmy Noether Programme of the German Research Foundation (DFG; project no. 495793173). bnAb 007 has been exclusively licensed to Vir Biotechnology.

Contributions (original publication)

Conceptualization – L.G., A.T.D., M.R., F.K., P.J.B., H.B.G.; Methodology – L.G., C.K., H. Gruell., A.T.D., H.B.G., C.R., J.D.B, Z.Y., Q.W., M.B.R., T.J.G., J.N. and P.F.S; Formal analysis – L.G., A.T.D., M.R., C.K., H.B.G., A.P.W., C.R., M.S., J.W., A.M. and P.F.S; Investigation – L.G., A.T.D., M.R. F.K., P.J.B., H.B.G., C.H.D., S.D., F.G., D.C., C.R., M.S., Z.Y., Q.W., M.B.R., T.J.G., J.N. and J.D.B.; Resources – H. Gruell., P.F.S.; Writing original draft - L.G., A.T.D., M.R., H.B.G., C.R.,

C.H.D., F.K., P.J.B., H. Gruell, and F.K.; Writing reviewing and editing – all authors; Supervision – F.K., P.J.B., H.B.G., and H. Gruell.; Funding acquisition – F.K., P.J.B.

Supplementary Figures and Tables

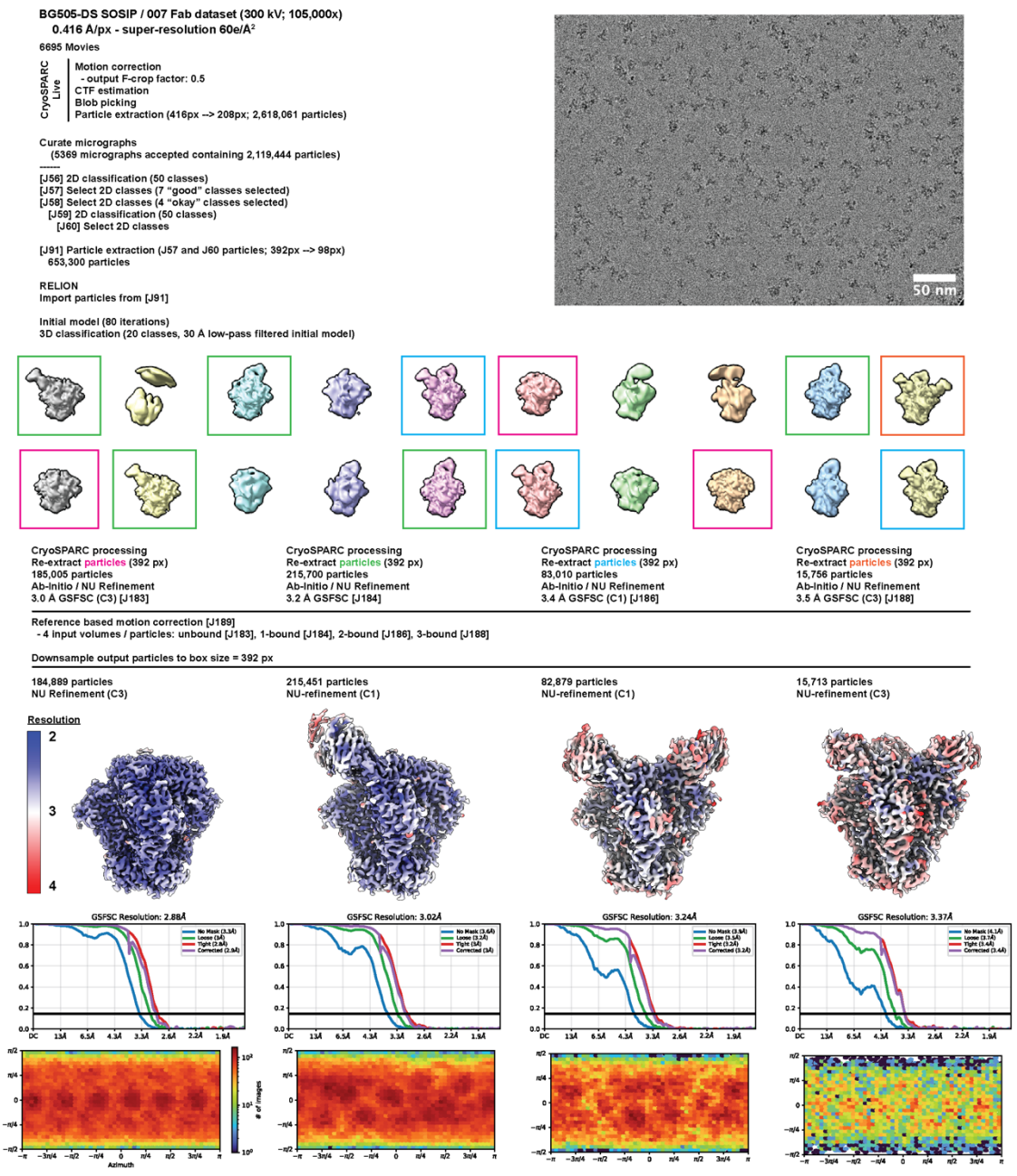

Extended Data Fig. 1: Data collection and processing for 007 Fab / BG505-DS complexes. **a,** Example micrograph, data processing workflow, final densities colored by local resolution, gold-standard Fourier shell correlations (GSFSC), and particle orientation distribution plots.

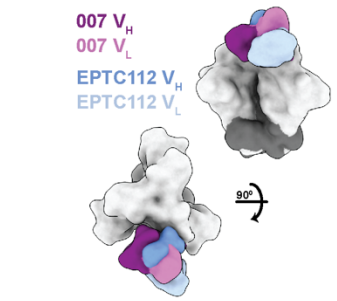

B

V_H-V_L volume overlap calculations

	007	PGT128	10-1074	BG18	PGT135	EPTC112
007	1	0.4	0.21	0.01	0	0.39
PGT128	0.4	1	0.36	0.08	0	0.45
10-1074	0.21	0.36	1	0.36	0.1	0.22
BG18	0.01	0.08	0.36	1	0.33	0
PGT135	0	0	0.1	0.33	1	0
EPTC112	0.39	0.45	0.22	0	0	1

Extended Data Fig. 2: V_H-V_L overlays between 007, EPTC112, and other V3 bnAbs.
a, Overlay of 007 V_H-V_L with EPTC112 V_H-V_L (PDB code 8C8T). **b,** V_H-V_L volume overlap between V3 bnAbs. To calculate volume overlap, coordinates (PDB codes 5C7K, 5T3Z, 6CH7, 4JM2) were aligned on gp120 and depicted as solvent-excluded surfaces in ChimeraX[77, 78]. The overlap volume between two antibodies was calculated as the sum of the two V_HV_L volumes minus the volume enclosed by the merged V_H-V_L surfaces. The Dice similarity coefficient is reported.

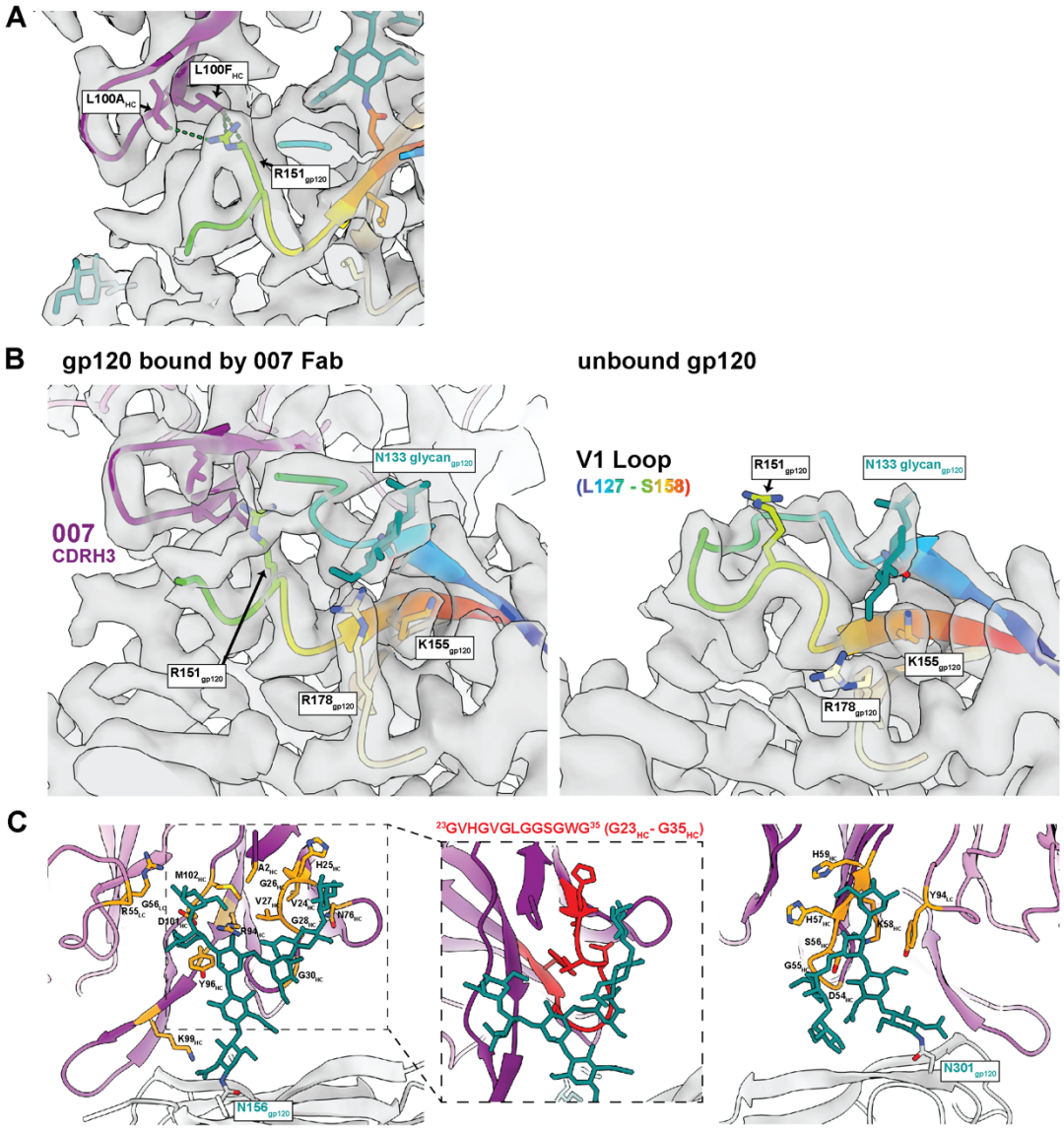

Extended Data Fig. 3: Interactions of 007 with the V1 loop and N-glycans on Env.
a, Contacts between the V1 residue R151$_{gp120}$ and 007. Contacts on 007 within 4Å of R151$_{gp120}$ are shown by green dotted lines. **b,** Differences in the V1 loop on gp120 between a protomer bound by 007 Fab (left) and an unbound protomer (right). **c,** Contacts between 007 and the N156$_{gp120}$ glycan (left) or the N301$_{gp120}$ glycan (right). 007 residues within 4Å of modelled glycans are colored orange. Inset (middle) highlights the interactions between a glycine-rich motif in 007, colored red, and the N156$_{gp120}$ glycan.

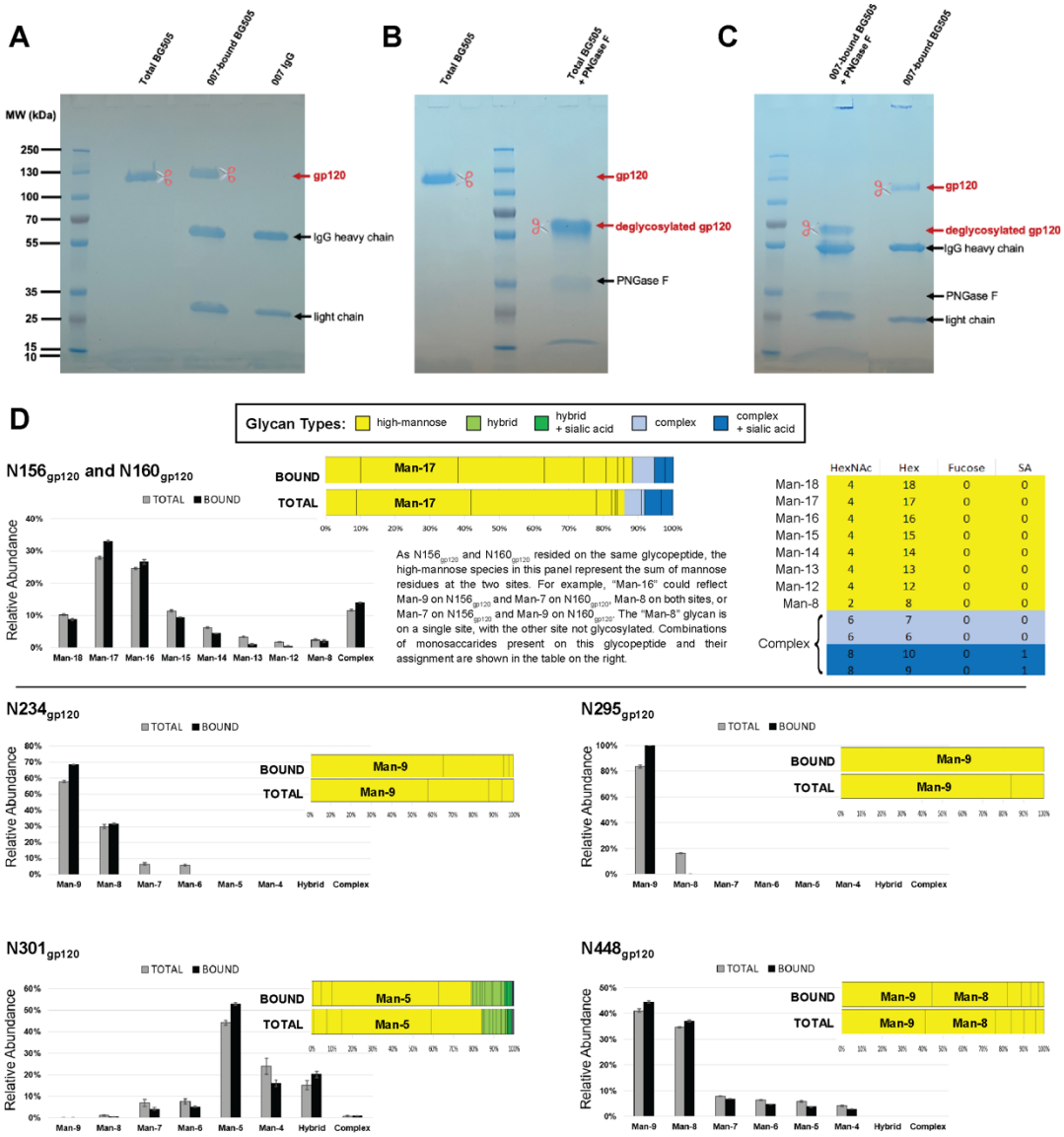

Extended Data Fig. 4: N-glycan analysis by quantitative mass spectrometry.
Electrophoretic separation of gp120 Env subunit using SDS-PAGE under denaturing and reducing conditions, stained with Coomassie G-250 **(a-c)**: **a,** Total BG505, 007_{IgG}-bound BG505, and 007_{IgG} control; **b,** Total BG505 with and without PNGase F treatment; **c,** 007_{IgG}-bound BG505 with and without PNGase F treatment. The shift in mobility of PNGase F-treated samples in **(b-c)** indicates removal of N-glycans from gp120. Arrows mark gp120, deglycosylated gp120, IgG heavy and light chains, and PNGase F. Scissors and red text mark gp120 bands that were excised and stored for LC-MS analyses. **d,** Comparison of glycoform abundance in total unliganded BG505 and 007-bound BG505 at $N156_{gp120}/N160_{gp120}$, $N234_{gp120}$, $N295_{gp120}$, $N301_{gp120}$, and $N448_{gp120}$. Data are presented as a side-by-side bar graph, where different high-mannose glycoforms are differentiated, but hybrid and complex-type glycans are presented as single groups. Error bars represent the standard deviations of replicate measurements (three for total BG505 and two for bound BG505). For visualization

purposes, data are also presented as a stacked bar with individual glycoforms separated by a vertical line, and the most prevalent glycoform(s) labelled.

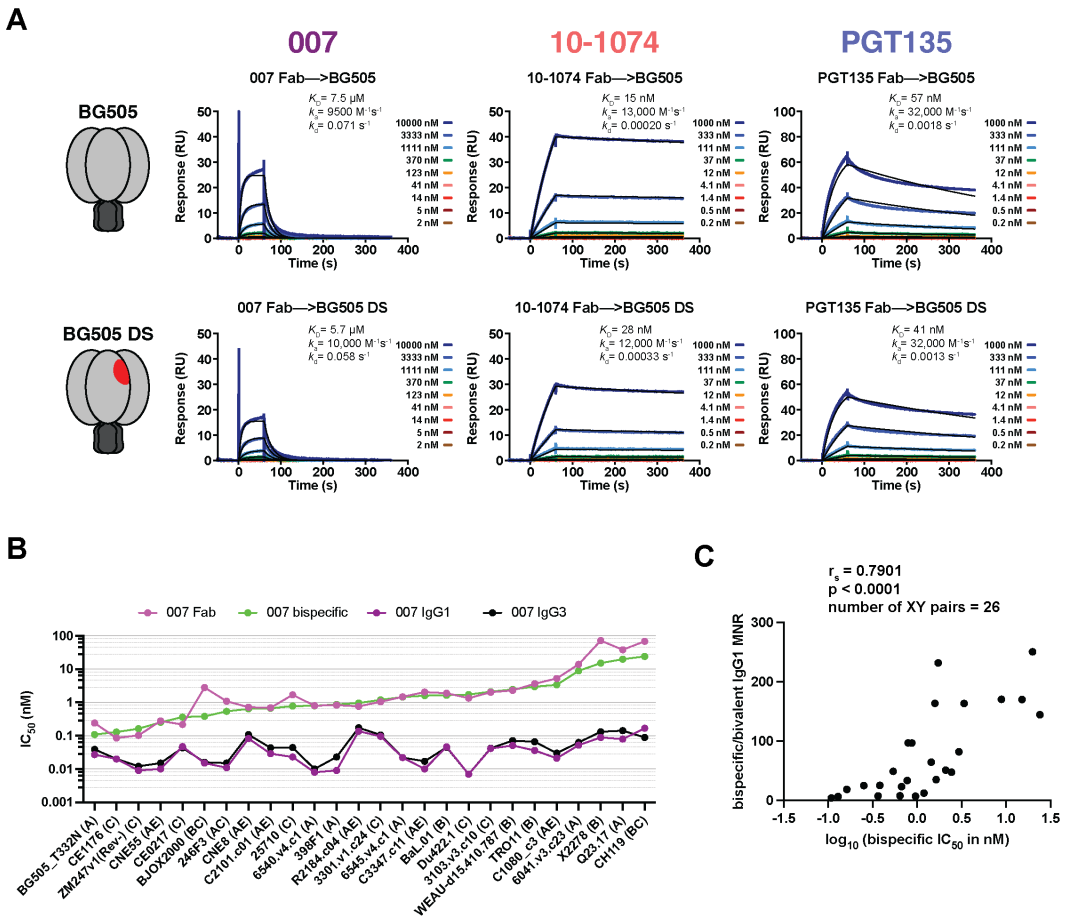

Extended Data Fig. 5: Binding and neutralization data for 007.

a, V3 bnAb Fabs were injected over BG505 (top) or BG505-DS (bottom) SOSIP trimers, and a 1:1 binding model was used to fit the experimental data and derive kinetic constants. Experimental data are shown by colored lines and predicted values are shown by black lines. A representative SPR sensorgram of duplicate experiments is shown. **b,** Molar IC_{50} values for IgG1, IgG3, bispecific IgG1, and Fab forms of 007 against a panel of HIV-1 pseudoviruses. The data are the same as in Figure 3b, but rearranged in order of decreasing potency (i.e., increasing IC_{50} values) of the 007 bispecific IgG1 to highlight the positive correlation between decreasing monovalent potencies and increasing bispecific / bivalent IgG1 MNRs. **c,** A plot showing the positive correlation between the 007 bispecific IC_{50} values and the bispecific / bivalent IgG1 MNRs. The Spearman correlation coefficient (r_s) and p-value are included next to the plot.

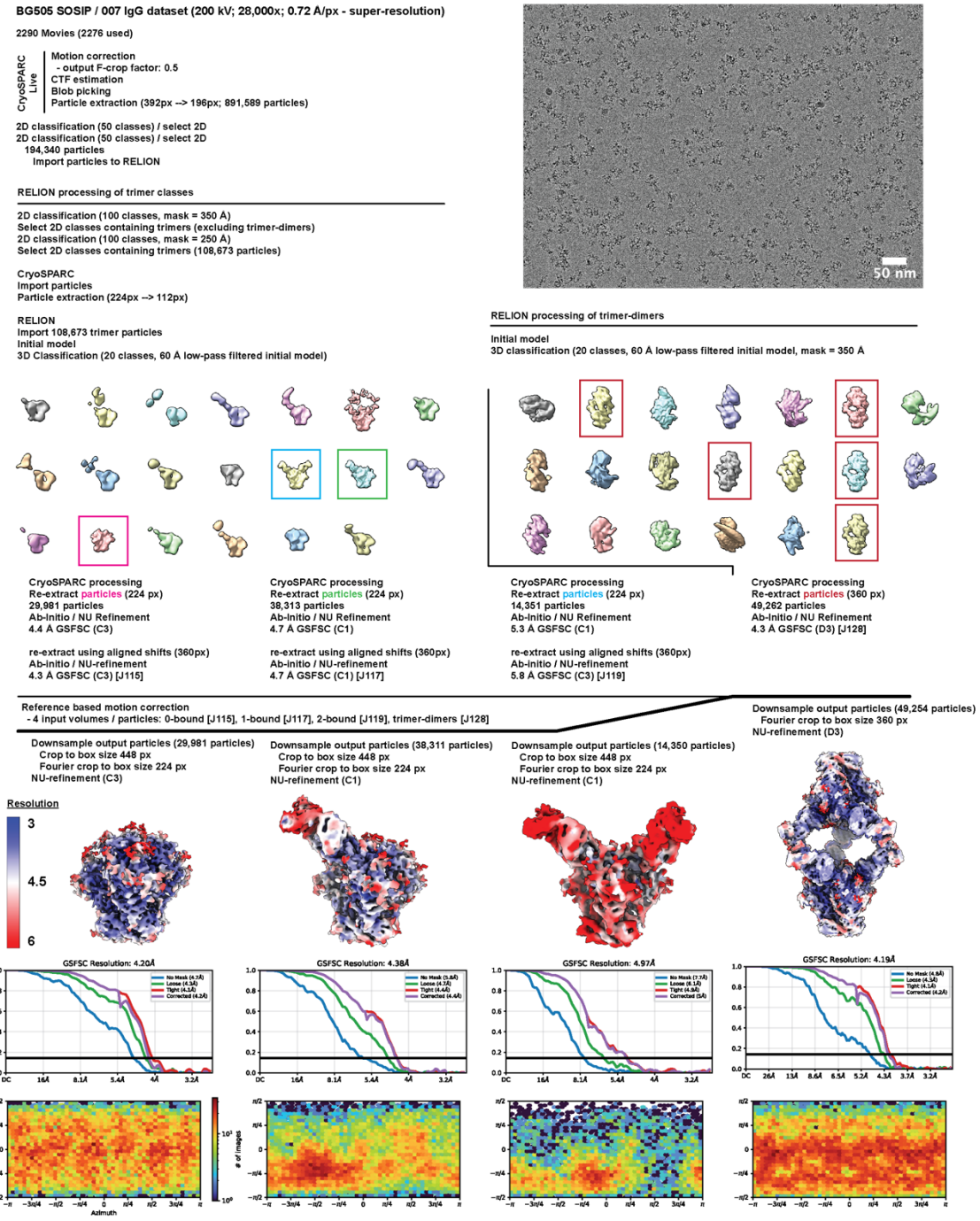

Extended Data Fig. 6: Data collection and processing for 007 IgG / BG505 complexes.
Example micrograph, data processing workflow, final densities colored by local resolution, gold-standard Fourier shell correlations (GSFSC), and particle orientation distribution plots.

	007 Fab / BG505-DS SOSIP				007 IgG1 / BG505 SOSIP
Data collection conditions					
Microscope	Titan Krios				Talos Arctica
Voltage (kV)	300				200
Detector	Gatan K3				Gatan K3
Magnification	105,000x				28,000x
Super-resolution pixel size (Å)	0.416				0.72
Recording mode	counting				counting
Defocus range (μm)	1-3 μm				1-3 μm
Electron exposure ($e^-/Å^2$)	60				45
Exposure rate (e^-/pixel/s)	22				19
Energy filter slit width (eV)	10				none
Frames per movie	40				30
Movies collected	6,695				2,290
PDB	**0 Fabs bound 9O2Q**	**1 Fab bound 9O2R**	**2 Fabs bound 9O2S**	**3 Fabs bound 9O2T**	**IgG crosslinked trimer-dimer 9O2U**
EMD	**EMD-70018**	**EMD-70019**	**EMD-70020**	**EMD-70021**	**EMD-70022**
Refined particles	184,889	215,451	82,879	15,713	49,254
Symmetry imposed	C3	C1	C1	C3	D3
Map Resolution (Å)					
Unmasked at 0.143 FSC	3.3	3.6	3.9	4.1	4.8
Masked at 0.143 FSC	2.9	3.0	3.2	3.4	4.2
Model Refinement and Validation					
Initial models used	6UDJ	6UDJ, 5BZD, 7PS3	6UDJ, 5BZD, 7PS3, 8UKI	6UDJ, 5BZD, 7PS3	6UDJ, 5BZD, 7PS3, 8UKI
Model composition					
Non-hydrogen atoms	14,010	15,902	20,686	19,686	48,054
Protein residues	1665	1897	2523	2361	5904
Ligands	60	70	80	90	180
Average B-factors ($Å^2$)					
Protein	28.2	69.9	67.2	80.4	68.7
Ligands	43.8	82.6	80.6	79.1	79.1
R.m.s. deviations					
Bond lengths (Å)	0.004	0.006	0.01	0.006	0.006
Bond angles (°)	0.943	1.038	1.222	1.111	1.146
Validation					
MolProbity score	1.5	1.6	1.5	1.7	2
Clashscore (all atom)	7.1	6.8	6.5	7.98	18.8
Rotamer outliers (%)	0	0.3	0.2	0.2	0.2
CaBLAM outliers (%)	2.6	2.4	2	2.6	2
Ramachandran plot					
Favored (%)	97.4	96.7	96.9	96.1	96.7
Allowed (%)	2.7	3.3	3	3.9	3.2
Disallowed (%)	0	0.0	0.1	0	0
CC (mask)	0.87	0.85	0.71	0.82	0.58

Supplementary Table 1: Cryo-EM data collection and refinement statistics.

Virus	007		10-1074		PGT121		PGT128		BG18	
	wildtype	+kif	wildtype	+kif	wildtype	+kif	wildtype	+kif	wildtype	+kif
398F1	0.004	>1	0.009	0.004	0.009	0.007	0.004	0.004	0.004	0.004
25710-2.43	0.006	>1	0.044	0.019	0.011	0.020	0.010	0.004	0.004	0.004
CNE8	0.005	>1	>1	>1	>1	>1	0.005	0.004	>1	>1
TRO.11	0.002	>1	0.011	0.006	0.005	0.004	0.006	0.004	0.004	0.004
X2278	0.005	>1	0.020	0.006	0.013	0.007	0.005	0.004	0.004	0.004
BJOX002000.03.2	0.004	>1	0.009	0.006	0.015	0.009	0.010	0.004	0.005	0.004
X1632-S2-B10	0.090	>1	>1	>1	>1	>1	>1	>1	>1	>1
Ce1176_A3	0.004	>1	0.021	0.008	0.012	0.012	0.010	0.004	0.004	0.004
CH119.10	0.007	>1	0.014	0.006	0.014	0.005	0.014	0.004	0.007	0.004
Ce703010217_B6	0.004	>1	0.006	0.004	0.005	0.003	0.027	0.004	>1	0.004
GeoMean IC_{50} (μg/ml)	0.006	>1	0.014	0.007	0.010	0.007	0.009	0.004	0.005	0.004
Breadth (%)	100	0	80	80	80	80	90	90	70	80

IC_{50} (μg/ml)	Breadth (%)
<0.01	>95
0.01-0.1	90-95
0.1-1.0	80-90
1.0-10.0	70-80
>10	50-70
	<50

Supplementary Table 2: Neutralizing activity against viral glycovariants.

007

Virus	Clade	IgG3 IC50 (µg/ml)	IgG3 IC50 (nM)**	IgG1 IC50 (µg/ml)	IgG1 IC50 (nM)**	bispecific IC50 (µg/ml)	bispecific IC50 (nM)**	Fab IC50 (µg/ml)	Fab IC50 (nM)**	IgG1 / IgG3 MNR	bispecific IgG1 / bivalent IgG1 MNR	Fab / bispecific IgG1 MNR
246F3	AC	0.002	0.015	0.002	0.011	0.079	0.539	0.054	1.087	0.73	49	2.0
25710	C	0.007	0.044	0.003	0.023	0.114	0.775	0.083	1.683	0.52	34	2.2
3103.v3.c10	C	0.007	0.042	0.006	0.041	0.309	2.103	0.100	2.015	0.99	51	1.0
3301.v1.c24	C	0.017	0.105	0.014	0.096	0.176	1.197	0.052	1.043	0.92	12	0.9
398F1	A	0.004	0.023	0.001	0.009	0.128	0.872	0.041	0.827	0.39	97	0.9
6041.v3.c23	A	0.010	0.063	0.008	0.052	1.309	8.893	0.691	13.966	0.83	171	1.6
6540.v4.c1	A	0.002	0.010	0.001	0.008	0.117	0.794	0.039	0.795	0.85	97	1.0
6545.v4.c1	A	0.003	0.022	0.003	0.022	0.212	1.440	0.073	1.474	1.01	65	1.0
BaL.01	B	0.007	0.045	0.007	0.046	0.241	1.637	0.094	1.898	1.04	35	1.2
BG505_T332N	A	0.006	0.039	0.004	0.027	0.016	0.108	0.012	0.240	0.69	4	2.2
BJOX2000	BC	0.003	0.016	0.002	0.015	0.056	0.381	0.139	2.810	0.94	25	7.4
C1080_c3	AE	0.005	0.030	0.003	0.021	0.497	3.376	0.260	5.257	0.69	164	1.6
C2101.c01	AE	0.007	0.043	0.004	0.029	0.098	0.668	0.034	0.690	0.66	23	1.0
C3347.c11	AE	0.003	0.017	0.001	0.010	0.233	1.586	0.101	2.043	0.57	164	1.3
CE0217	C	0.007	0.043	0.007	0.047	0.054	0.364	0.011	0.217	1.09	8	0.6
CE1176	C	0.003	0.020	0.003	0.020	0.019	0.129	0.004	0.085	1.00	6	0.7
CH119	BC	0.014	0.089	0.025	0.167	3.552	24.136	3.403	68.741	1.88	145	2.8
CNE55	AE	0.002	0.015	0.001	0.010	0.037	0.252	0.014	0.277	0.67	25	1.1
CNE8	AE	0.017	0.107	0.012	0.082	0.094	0.642	0.036	0.720	0.77	8	1.1
Du422.1	C	0.001	0.007	0.001	0.007	0.254	1.727	0.066	1.342	1.00	232	0.8
Q23.17	A	0.022	0.142	0.012	0.079	2.933	19.935	1.887	38.120	0.56	251	1.9
R2184.c04	AE	0.028	0.174	0.020	0.136	0.142	0.962	0.038	0.762	0.78	7	0.8
TRO11	B	0.010	0.066	0.005	0.036	0.435	2.957	0.179	3.619	0.55	82	1.2
WEAU-d15.410.787	B	0.011	0.071	0.008	0.051	0.360	2.444	0.113	2.291	0.72	48	0.9
X1632*	G	n.d.	n.d.	n.d.	n.d.	n.d.	n.d.	n.d.	n.d.	n.d.	n.d.	n.d.
X2278	B	0.021	0.132	0.013	0.089	2.232	15.169	3.553	71.778	0.67	170	4.7
ZM247v1(Rev-)	C	0.002	0.012	0.001	0.009	0.024	0.162	0.009	0.102	0.74	19	0.6
									Mean MNR -->	0.82	n.d.	1.6

*Virus strain X1632 was incompletely neutralized by 007
**Color coding according to (IC50 µg/ml) of the respective IgG/Fab
n.d = not determined

10-1074

Virus	Clade	IgG IC50 (µg/ml)	IgG IC50 (nM)**	Fab IC50 (µg/ml)	Fab IC50 (nM)**	Fab/IgG MNR
246F3	AC	>50	>340	>50	>1000	n.d.
25710	C	0.0290	0.200	0.0620	1.300	6
398F1	A	0.0048	0.032	0.0110	0.220	7
BG505_T332N	A	0.0110	0.078	0.0300	0.600	8
BJOX2000	BC	0.0059	0.040	0.0071	0.140	4
CE0217	C	<0.00064	<0.004	<0.00064	<0.013	n.d.
CE1176	C	<0.00064	<0.004	<0.00064	<0.013	n.d.
CH119	BC	<0.00064	<0.004	<0.00064	<0.013	n.d.
CNE8	AE	>50	>340	>50	>1000	n.d.
CNE55	AE	>50	>340	>50	>1000	n.d.
TRO11	B	<0.00064	<0.004	<0.00064	<0.013	n.d.
X1632	G	>50	>340	>50	>1000	n.d.
X2278	B	0.0140	0.095	0.0330	0.680	7

IC50 (µg/ml)
<0.01
0.01-0.1
0.1-1.0
1.0-10.0
>10

Supplementary Table 3: Molar neutralization ratio assays.

References

1. Seaman, M.S. *et al.* Tiered categorization of a diverse panel of HIV-1 Env pseudoviruses for assessment of neutralizing antibodies. *J Virol* **84**, 1439-1452 (2010).

2. Hraber, P. *et al.* Panels of HIV-1 subtype C Env reference strains for standardized neutralization assessments. *J Virol* **91** (2017).

3. deCamp, A. *et al.* Global panel of HIV-1 Env reference strains for standardized assessments of vaccine-elicited neutralizing antibodies. *J Virol* **88**, 2489-2507 (2014).

4. Walker, L.M. & Burton, D.R. Passive immunotherapy of viral infections: 'super-antibodies' enter the fray. *Nat Rev Immunol* **18**, 297-308 (2018).

5. Walsh, S.R. & Seaman, M.S. Broadly neutralizing antibodies for HIV-1 prevention. *Front Immunol* **12**, 712122 (2021).

6. Caskey, M., Klein, F. & Nussenzweig, M.C. Broadly neutralizing anti-HIV-1 monoclonal antibodies in the clinic. *Nat Med* **25**, 547-553 (2019).

7. Gruell, H. & Schommers, P. Broadly neutralizing antibodies against HIV-1 and concepts for application. *Curr Opin Virol* **54**, 101211 (2022).

8. Schriek, A.I., Aldon, Y.L.T., van Gils, M.J. & de Taeye, S.W. Next-generation bNAbs for HIV-1 cure strategies. *Antiviral Res* **222**, 105788 (2024).

9. Grobben, M., Stuart, R.A. & van Gils, M.J. The potential of engineered antibodies for HIV-1 therapy and cure. *Curr Opin Virol* **38**, 70-80 (2019).

10. Julg, B. *et al.* Safety and antiviral activity of triple combination broadly neutralizing monoclonal antibody therapy against HIV-1: A phase 1 clinical trial. *Nat Med* **28**, 1288-1296 (2022).

11. Wagh, K. & Seaman, M.S. Divide and conquer: Broadly neutralizing antibody combinations for improved HIV-1 viral coverage. *Curr Opin Hiv Aids* **18**, 164-170 (2023).

12. Bar-On, Y. *et al.* Safety and antiviral activity of combination HIV-1 broadly neutralizing antibodies in viremic individuals. *Nat Med* **24**, 1701-1707 (2018).

13. Julg, B. *et al.* Safety and antiviral effect of a triple combination of HIV-1 broadly neutralizing antibodies: A phase 1/2a trial. *Nat Med* **30**, 3534-3543 (2024).

14. Wagh, K. *et al.* Optimal combinations of broadly neutralizing antibodies for prevention and treatment of HIV-1 clade C infection. *PLoS Pathog* **12**, e1005520 (2016).

15. Burton, D.R. & Hangartner, L. Broadly neutralizing antibodies to HIV and their role in vaccine design. *Annu Rev Immunol* **34**, 635-659 (2016).

16. Kwong, P.D. & Mascola, J.R. HIV-1 Vaccines based on antibody identification, B cell ontogeny, and epitope structure. *Immunity* **48**, 855-871 (2018).

17. Sok, D. & Burton, D.R. Recent progress in broadly neutralizing antibodies to HIV. *Nat Immunol* **19**, 1179-1188 (2018).

18. Ward, A.B. & Wilson, I.A. The HIV-1 envelope glycoprotein structure: Nailing down a moving target. *Immunol Rev* **275**, 21-32 (2017).

19. Wibmer, C.K., Moore, P.L. & Morris, L. HIV broadly neutralizing antibody targets. *Curr Opin Hiv Aids* **10**, 135-143 (2015).

20. Gama, L. & Koup, R.A. New-generation high-potency and designer antibodies: Role in HIV-1 treatment. *Annu Rev Med* **69**, 409-419 (2018).

21. Moyo, T., Kitchin, D. & Moore, P.L. Targeting the N332-supersite of the HIV-1 envelope for vaccine design. *Expert Opin Ther Targets* **24**, 499-509 (2020).

22. Kong, L. *et al.* Supersite of immune vulnerability on the glycosylated face of HIV-1 envelope glycoprotein gp120. *Nat Struct Mol Biol* **20**, 796-803 (2013).

23. Daniels, C.N. & Saunders, K.O. Antibody responses to the HIV-1 envelope high mannose patch. *Adv Immunol* **143**, 11-73 (2019).

24. Mouquet, H. *et al.* Complex-type N-glycan recognition by potent broadly neutralizing HIV antibodies. *Proc Natl Acad Sci U S A* **109**, E3268-E3277 (2012).

25. Freund, N.T. *et al.* Coexistence of potent HIV-1 broadly neutralizing antibodies and antibody-sensitive viruses in a viremic controller. *Sci Transl Med* **9** (2017).

26. Barnes, C.O. *et al.* Structural characterization of a highly-potent V3-glycan broadly neutralizing antibody bound to natively-glycosylated HIV-1 envelope. *Nat Commun* **9**, 1251 (2018).

27. Krumm, S.A. *et al.* Mechanisms of escape from the PGT128 family of anti-HIV broadly neutralizing antibodies. *Retrovirology* **13**, 8 (2016).

28. Walker, L.M. *et al.* Broad neutralization coverage of HIV by multiple highly potent antibodies. *Nature* **477**, 466-470 (2011).

29. Bonsignori, M. *et al.* Staged induction of HIV-1 glycan-dependent broadly neutralizing antibodies. *Sci Transl Med* **9** (2017).

30. Molinos-Albert, L.M. *et al.* Anti-V1/V3-glycan broadly HIV-1 neutralizing antibodies in a post-treatment controller. *Cell Host Microbe* (2023).

31. Yoon, H. *et al.* CATNAP: A tool to compile, analyze and tally neutralizing antibody panels. *Nucleic Acids Res* **43**, W213-219 (2015).

32. Nan, X. *et al.* Exploring distinct modes of inter-spike cross-linking for enhanced neutralization by SARS-CoV-2 antibodies. *Nat Commun* **15**, 10578 (2024).

33. Klein, J.S. & Bjorkman, P.J. Few and far between: How HIV may be evading antibody avidity. *PLOS Pathog* **6**, e1000908 (2010).

34. Cavacini, L.A., Emes, C.L., Power, J., Duval, M. & Posner, M.R. Effect of antibody valency on interaction with cell-surface expressed HIV-1 and viral neutralization. *J Immunol* **152**, 2538-2545 (1994).

35. Schommers, P. *et al.* Dynamics and durability of HIV-1 neutralization are determined by viral replication. *Nat Med* **29**, 2763-2774 (2023).

36. Yang, G. *et al.* Identification of autoantigens recognized by the 2F5 and 4E10 broadly neutralizing HIV-1 antibodies. *J Exp Med* **210**, 241-256 (2013).

37. Doria-Rose, N.A. *et al.* Mapping polyclonal HIV-1 antibody responses via next-generation neutralization fingerprinting. *PLoS Pathog* **13**, e1006148 (2017).

38. Sanders, R.W. *et al.* A next-generation cleaved, soluble HIV-1 Env trimer, BG505 SOSIP.664 gp140, expresses multiple epitopes for broadly neutralizing but not non-neutralizing antibodies. *PLoS Pathog* **9**, e1003618 (2013).

39. Kwon, Y.D. *et al.* Crystal structure, conformational fixation and entry-related interactions of mature ligand-free HIV-1 Env. *Nat Struct Mol Biol* **22**, 522-531 (2015).

40. Guenaga, J. *et al.* Structure-guided redesign increases the propensity of HIV Env to generate highly stable soluble trimers. *J Virol* **90**, 2806-2817 (2015).

41. Gristick, H.B. *et al.* Natively glycosylated HIV-1 Env structure reveals new mode for antibody recognition of the CD4-binding site. *Nat Struct Mol Biol* **23**, 906-915 (2016).

42. Pancera, M. *et al.* Structure and immune recognition of trimeric pre-fusion HIV-1 Env. *Nature* **514**, 455-461 (2014).

43. Garces, F. *et al.* Structural evolution of glycan recognition by a family of potent HIV antibodies. *Cell* **159**, 69-79 (2014).

44. West, A.P., Jr. *et al.* Computational analysis of anti-HIV-1 antibody neutralization panel data to identify potential functional epitope residues. *Proc Natl Acad Sci U S A* **110**, 10598-10603 (2013).

45. Martin Beem, J.S., Venkatayogi, S., Haynes, B.F. & Wiehe, K. ARMADiLLO: A web server for analyzing antibody mutation probabilities. *Nucleic Acids Res* **51**, W51-W56 (2023).

46. West, A.P., Diskin, R., Nussenzweig, M.C. & Bjorkman, P.J. Structural basis for germ-line gene usage of a potent class of antibodies targeting the CD4-binding site of HIV-1 gp120. *Proc Natl Acad Sci U S A* **109**, E2083-E2090 (2012).

47. Lee, J.H., de Val, N., Lyumkis, D. & Ward, A.B. Model building and refinement of a natively glycosylated HIV-1 Env protein by high-resolution cryoelectron microscopy. *Structure* **23**, 1943-1951 (2015).

48. Gristick, H.B., Wang, H. & Bjorkman, P.J. X-ray and EM structures of a natively glycosylated HIV-1 envelope trimer. *Acta Crystallogr D Struct Biol* **73**, 822-828 (2017).

49. Pejchal, R. *et al.* A potent and broad neutralizing antibody recognizes and penetrates the HIV glycan shield. *Science* **334**, 1097-1103 (2011).

50. Moore, G.L. *et al.* A robust heterodimeric Fc platform engineered for efficient development of bispecific antibodies of multiple formats. *Methods* **154**, 38-50 (2019).

51. Kjer-Nielsen, L. *et al.* Crystal structure of the human T cell receptor CD3εγ heterodimer complexed to the therapeutic mAb OKT3. *Proc Natl Acad Sci U S A* **101**, 7675-7680 (2004).

52. Jette, C.A. *et al.* Broad cross-reactivity across sarbecoviruses exhibited by a subset of COVID-19 donor-derived neutralizing antibodies. *Cell Reports* **36**, 109760 (2021).

53. Barnes, C.O. *et al.* SARS-CoV-2 neutralizing antibody structures inform therapeutic strategies. *Nature* **588**, 682-687 (2020).

54. Fan, C. *et al.* Neutralizing monoclonal antibodies elicited by mosaic RBD nanoparticles bind conserved sarbecovirus epitopes. *Immunity* **55**, 2419-2435 e2410 (2022).

55. Yang, Z. *et al.* Neutralizing antibodies induced in immunized macaques recognize the CD4-binding site on an occluded-open HIV-1 envelope trimer. *Nat Commun* **13**, 732 (2022).

56. Callaway, H.M. *et al.* Bivalent intra-spike binding provides durability against emergent Omicron lineages: Results from a global consortium. *Cell Rep* **42**, 112014 (2023).

57. Yan, R. *et al.* Structural basis for bivalent binding and inhibition of SARS-CoV-2 infection by human potent neutralizing antibodies. *Cell Res* **31**, 517-525 (2021).

58. Saphire, E.O. *et al.* Contrasting IgG structures reveal extreme asymmetry and flexibility. *J Mol Biol* **319**, 9-18 (2002).

59. Mouquet, H. *et al.* Polyreactivity increases the apparent affinity of anti-HIV antibodies by heteroligation. *Nature* **467**, 591-595 (2010).

60. Yao, H. *et al.* Cryo-ET of IgG bivalent binding on SARS-CoV-2 provides structural basis for antibody avidity. *bioRxiv*, 2025.2002.2028.640788 (2025).

61. Torrents de la Peña, A. *et al.* Similarities and differences between native HIV-1 envelope glycoprotein trimers and stabilized soluble trimer mimetics. *PLOS Pathog* **15**, e1007920 (2019).

62. Tiller, T. *et al.* Efficient generation of monoclonal antibodies from single human B cells by single cell RT-PCR and expression vector cloning. *J Immunol Methods* **329**, 112-124 (2008).

63. Schommers, P. *et al.* Restriction of HIV-1 escape by a highly broad and potent neutralizing antibody. *Cell* **180**, 471-489.e422 (2020).

64. Kreer, C. *et al.* Longitudinal isolation of potent near-germline SARS-CoV-2-neutralizing antibodies from COVID-19 patients. *Cell* **182**, 843-854 e812 (2020).

65. Gieselmann, L. *et al.* Effective high-throughput isolation of fully human antibodies targeting infectious pathogens. *Nat Protoc* **16**, 3639-3671 (2021).

66. von Boehmer, L. *et al.* Sequencing and cloning of antigen-specific antibodies from mouse memory B cells. *Nat Protoc* **11**, 1908-1923 (2016).

67. Zalevsky, J. *et al.* Enhanced antibody half-life improves in vivo activity. *Nat Biotechnol* **28**, 157-159 (2010).

68. Schaefer, W. *et al.* Immunoglobulin domain crossover as a generic approach for the production of bispecific IgG antibodies. *Proc Natl Acad Sci U S A* **108**, 11187-11192 (2011).

69. Sarzotti-Kelsoe, M. *et al.* Optimization and validation of the TZM-bl assay for standardized assessments of neutralizing antibodies against HIV-1. *J Immunol Methods* **409**, 131-146 (2014).

70. Montefiori, D.C. Evaluating neutralizing antibodies against HIV, SIV, and SHIV in luciferase reporter gene assays. *Curr Protoc Immunol* **64**, 12.11.11-12.11.17 (2004).

71. Montefiori, D.C. Measuring HIV neutralization in a luciferase reporter gene assay. *Methods Mol Biol* **485**, 395-405 (2009).

72. Mastronarde, D.N. Automated electron microscope tomography using robust prediction of specimen movements. *J Struct Biol* **152**, 36-51 (2005).

73. Punjani, A., Rubinstein, J.L., Fleet, D.J. & Brubaker, M.A. cryoSPARC: Algorithms for rapid unsupervised cryo-EM structure determination. *Nat Methods* **14**, 290-296 (2017).

74. Scheres, S.H. RELION: Implementation of a Bayesian approach to cryo-EM structure determination. *J Struct Biol* **180**, 519-530 (2012).

75. Kimanius, D., Dong, L., Sharov, G., Nakane, T. & Scheres, S.H.W. New tools for automated cryo-EM single-particle analysis in RELION-4.0. *Biochem J* **478**, 4169-4185 (2021).

76. Punjani, A., Zhang, H. & Fleet, D.J. Non-uniform refinement: Adaptive regularization improves single-particle cryo-EM reconstruction. *Nat Methods* **17**, 1214-1221 (2020).

77. Meng, E.C. *et al.* UCSF ChimeraX: Tools for structure building and analysis. *Protein Sci* **32**, e4792 (2023).

78. Pettersen, E.F. *et al.* UCSF ChimeraX: Structure visualization for researchers, educators, and developers. *Protein Sci* **30**, 70-82 (2021).

79. Emsley, P., Lohkamp, B., Scott, W.G. & Cowtan, K. Features and development of Coot. *Acta Crystallogr D Biol Crystallogr* **66**, 486-501 (2010).

80. Afonine, P.V. *et al.* Real-space refinement in PHENIX for cryo-EM and crystallography. *Acta Crystallogr D Struct Biol* **74**, 531-544 (2018).

81. Emsley, P. & Crispin, M. Structural analysis of glycoproteins: Building N-linked glycans with Coot. *Acta Crystallogr D Struct Biol* **74**, 256-263 (2018).

82. Agirre, J. *et al.* Privateer: Software for the conformational validation of carbohydrate structures. *Nat Struct Mol Biol* **22**, 833-834 (2015).

83. Ozorowski, G. *et al.* Open and closed structures reveal allostery and pliability in the HIV-1 envelope spike. *Nature* **547**, 360-363 (2017).